MARTIN MARIETTA

DEFINITION OF PROMINENT THERMAL MECHANISMS ASSOCIATED WITH THE BUOYANCY-INDUCED TRANSPORT OF HAFNIUM-CARBIDE WITHIN A SOLIDIFYING URANIUM-HAFNIUM ALLOY

Michael J. Taylor
Gail Mackiewicz-Ludtka

DEFINITION OF PROMINENT THERMAL MECHANISMS ASSOCIATED WITH THE BUOYANCY-INDUCED TRANSPORT OF HAFNIUM-CARBIDE WITHIN A SOLIDIFYING URANIUM-HAFNIUM ALLOY

Michael J. Taylor

Computing and Telecommunications Division
at
Oak Ridge K-25 Site
Post Office Box 2003
Oak Ridge, Tennessee 37831-7039

Gail Mackiewicz-Ludtka

Y-12 Development Division
Oak Ridge Y-12 Plant
Post Office Box 2009
Oak Ridge, Tennessee 37831-7039

CONTENTS

LIST OF FIGURES

iv

LIST OF FIGURES (continued)

NOMENCLATURE

A   =   overall heat transfer surface area, m^2 or macroscopic surface area of contact joint, m^2

a   =   dimensionless accommodation coefficient

B   =   contact joint dimensionless gap number

β =   volume coefficient of expansion. $°C^{-1}$

C   =   contact joint dimensionless constriction number

C_p =   specific heat, J/kg$-°C$

D   =   diameter, m

δ =   current penetration depth, cm or contact joint gap thickness, m

ϵ =   dimensionless surface emissivity

η =   dimensionless constant in viscosity formula $\mu = \eta \rho VLm$

f =   frequency, Hz

G   =   mass velocity, kg/s$-m^2$

g   =   gravitational constant, 9.8 m/s^2

γ =   dimensionless ratio of specific heats

Γ =   dimensionless magnetic field radial direction attenuation

H_o =   magnetic field strength, amp-turns/m

h   =   heat transfer coefficient, W/$m^2-°C$

I   =   coil current, amps

K   =   contact joint dimensionless conductivity number

$k_{g,0}$ =   thermal conductivity of gas in contact joint at zero contact pressure, W/m$-°C$

k   =   thermal conductivity, W/m$-°C$

L   =   length, m

L_m =   mean free path of gas molecule, m

ℓ =   rms surface roughness, μm

M   =   dimensionless independent function used to calculate Bessel function or Meyer hardness, Pa

μ =   dynamic viscosity, mNs/m^2 or magnetic permeability, H/m

N   =   coil turns

P   =   induced power, W/m^3 or pressure in contact joint, Pa

Pr   =   dimensionless Prandtl number

NOMENCLATURE (continued)

Re   =   dimensionless Reynolds number

r   =   radius, m

ρ =   density, kg/m^3 or electrical resistivity, $\mu\Omega$/cm

σ =   Stefan-Boltzmann constant, 5.67×10^{-8} W/m^2–K^4

T   =   temperature, °C

Tm   =   temperature of contact joint, K

ΔT   =   temperature difference, °C

θ =   phase angle, radians

Δt   =   incremental time, s

U   =   contact joint dimensionless conductance number

u   =   contact joint conductance, W/m^2–°C

V   =   volume, m^3

W   =   classical magnetic field dimensionless penetration function

w   =   magnetic field angular frequency, Hz

ξ =   magnetic field dimensionless axial direction attenuation

subscripts

avg   =   average value

conv   =   forced convection heat transfer

f   =   fluid

h   =   horizontal orientation

i   =   interior

m   =   material

nc   =   natural convection heat transfer

r   =   radiation heat transfer

v   =   vertical orientation

ABSTRACT

Increased environmental concerns over the handling of uranium wastes have generated interest in using existing uranium stockpiles as feed materials. One obstacle to extensive recycling is that it causes an accumulation of carbon that can degrade as-cast mechanical properties. A program was begun to develop a casting procedure capable of reducing the carbon content in components made from recycled uranium to levels comparable with virgin feed stock. Trace amounts of hafnium are added to form low-density hafnium-carbide, which floats to the top of the casting. This procedure effectively relocates the carbon, where it can be removed at a later time. Developing this procedure requires modeling carbide transport within solidifying uranium, and this necessitates solving a coupled, nonlinear *fluid dynamics, heat transfer*, and *solution thermodynamics* problem. Because of the large number of technical and numerical uncertainties associated with this calculation, it was necessary to initially study the problem elements separately and the *heat transfer* facet was addressed first. The steady-state and transient thermal performance of a laboratory-scale casting assembly was characterized to identify those mechanisms that have a prominent influence on modeling uranium melt solidification. The analysis showed that (1) at least first-order accurate definitions for all thermal mechanisms were required to obtain meaningful agreement with experimental data; (2) prominent mechanisms were thermal contact resistances, liquid uranium natural convection, and internal heat generation; and (3) accurately modeling assembly geometry and enclosure radiation heat transfer would also improve agreement. It was recommended that a second-generation thermal model should be constructed which would include each of these elements.

INTRODUCTION

BACKGROUND AND GENERAL PROBLEM STATEMENT

The Oak Ridge Y-12 Plant produces uranium (U) castings using carbon (C) molds as a part of its production activities. In response to increased environmental concerns over the handling and storage of uranium wastes, the use of recycled uranium as a feed material is becoming increasingly attractive. One obstacle to extensive recycling is that repeated casting causes an accumulation of unacceptable carbon levels—on the order of hundreds of parts per million (ppm). This additional carbon results in an increased number of carbide inclusions that have a deleterious effect on as-cast mechanical properties. In CY 1985 the Materials Engineering Department of the Y-12 Development Division began a program to develop a casting procedure capable of reducing the carbon content in recycled uranium products to levels comparable with virgin feed stock. The procedure chosen for development takes advantage of two characteristics of carbon chemistry: it can easily form compounds with certain elements, and these compounds are less dense than liquid uranium. Conceptually, trace amounts of an alloying element are added to the uranium to combine with the carbon, forming a relatively low-density compound. Buoyancy forces would then tend to transport this compound toward the top of the casting. This procedure effectively relocates the carbon contaminants, where, after solidification, they can be removed and the remainder of the billet used as needed.[1] After a study of the reaction kinetics of several candidate elements, hafnium (Hf) was chosen for its large free energy of formation and relatively low density, 12.6 g/cm^3 for HfC compared with 17.7 g/cm^3 for uranium.

Developing an optimum uranium-hafnium (U-Hf) composition and production-scale casting assembly design requires predicting carbide motion within solidifying uranium. This transport is controlled by buoyancy forces that result from uranium-hafnium-carbide (U/HfC) and thermally induced density differences. Fluid convective currents, in turn, are dependent on heat transfer out of the casting assembly. Predicting carbide transport then requires solving three coupled, nonlinear problems: a *fluid dynamics* calculation to define pouring, carbide transport, and solidification; a *heat transfer* calculation to define the transport of thermal energy away from the fluid; and a *solution thermodynamics* calculation to define carbide formation. These calculations require a considerable numerical analysis effort, with as many computational uncertainties as there are HfC formation and transport unknowns. Accordingly, an integrated experimental-numerical execution sequence was implemented so both elements could mature simultaneously. The current focus of this joint effort are laboratory-scale casting experiments designed to quantify basic system performance. Uranium billets are produced to define macroscopic carbide behavior, and casting assembly temperature data are supplied to support numerical studies that are currently aimed at defining thermal-hydraulic cause and effect. The focus of this report is the numerical studies.

The macroscopic objective of these studies is to characterize the thermal, hydraulic, and metallurgical behavior of a U-Hf alloy and its U/HfC component as it melts then solidifies within a carbon casting assembly. Modeling tasks will be defined to support this goal within the context of a research and development (R&D) environment:

1. coordinating with experimental studies to characterize carbide transport as a function of prominent thermal, hydraulic, and metallurgical mechanisms for a given casting assembly geometry;

2. providing guidance for scale-up of assembly geometry where the recommendations have been constrained by the current level of technical uncertainties; and

3. repeating the *analyses/scale-up* sequence until the uncertainties have been reduced to an acceptable level and a mature production-scale technology exists.

CASTING SYSTEM DESCRIPTION

Experimental studies are conducted using a laboratory-scale vacuum-induction casting system located in the Y-12 Development Foundry. It consists of a casting assembly, a water-cooled induction heater, a vacuum-caster, which is a type of pressure vessel that permits the casting process to take place under evacuated conditions, as well as process control and data recording instrumentation.

The casting assembly is designed to mold approximately 18 kg of U-Hf alloy into a rectangular billet 3.97 cm thick, 13 cm wide, and 18.73 cm long. It consists of five components: a crucible, upper end cap, two bookmold halves, and a lower end cap. The crucible contains the liquid uranium prior to pour, the end caps restrain the bookmold halves, and the bookmold contains the uranium as it solidifies. Scale drawings (dimensions in millimeters) of the crucible, bookmold, and a nominal end cap are shown in Figs. 1, 2, 3, and 4 respectively. The individual components are shown in Fig. 5, and the assembled pieces are shown in Fig. 6. All components are fabricated in-house from ATJ grade graphite, and those surfaces that might come in contact with liquid uranium are coated with yttrium-oxide. In addition, three platinum − 90% platinum-/10% rhodium thermocouples with aluminum-oxide (Al_2O_3) insulating sheaths are installed along the height of one of the bookmold halves. They are positioned halfway into the width and thickness of the piece at distances of 5.08 cm, 11.75 cm, and 18.42 cm from the top of the bookmold. Figure 6 illustrates this thermocouple configuration. As Fig. 6 also shows, the components are assembled by simply stacking them; no mechanical fasteners or other external constraints are used. From a numerical analysis uncertainty perspective, there are two noteworthy aspects of the stacking process.

1. The radial clearances between the bookmold and endcaps are such that a great deal of mechanical force is required to seat the bookmold. This results in larger contact pressures and, conceptually, smaller thermal contact resistances in the radial direction than in the axial direction.

2. The radial clearances between the crucible and the Al_2O_3 shield are such that there is the possibility of direct contact between the components at high temperatures. Even though there is no question that radiation exchange is the only heat transfer mechanism between the assembly and shield below the crucible, there is considerable uncertainty as to the mechanism(s) and their magnitude between the crucible and the shield.

The induction heater is a 15-kW, 10,000-Hz, digitally controlled, solid-state (i.e., silicon controlled rectifier (SCR) based invertor) unit originally manufactured by Industrial Electric Heating, Inc. It is designed to deliver a constant power level to the casting assembly and consists of four basic subsystems: a high-frequency power supply, an isolation transformer, work coil, and the casting assembly. Electrically, these components function as a series of transformer windings, with the heating coil and casting assembly comprising the final pair. The primary winding of the isolation transformer is placed across the high-frequency power supply, and the secondary is the work coil. The work coil, in turn, represents the primary of the heating coil, and the casting assembly functions as the secondary, once it is placed inside the heating coil. This basic design

3
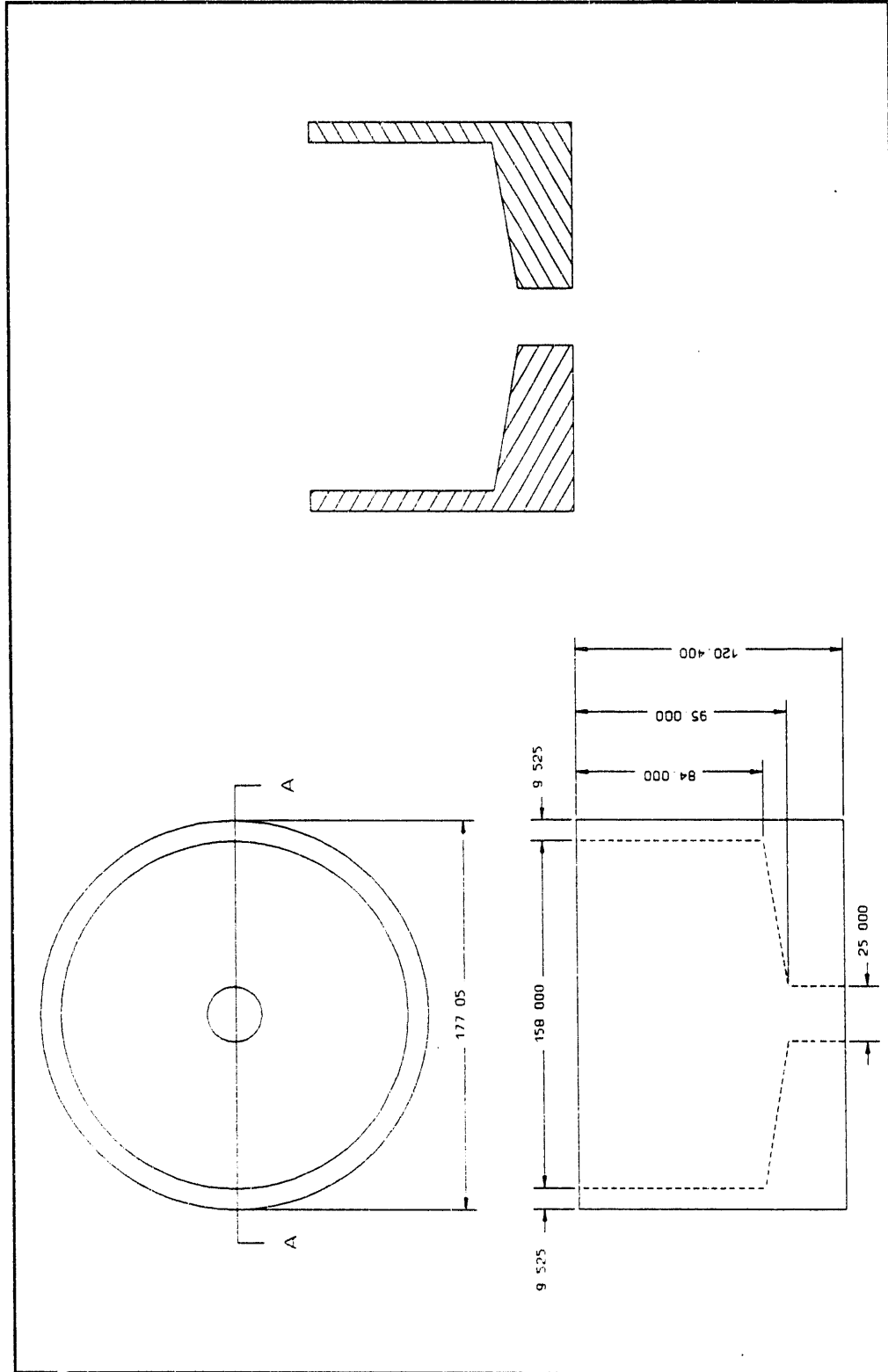
Fig. 1. Engineering drawings showing top, front, and cross-sectional views of the crucible with dimensions in millimeters.
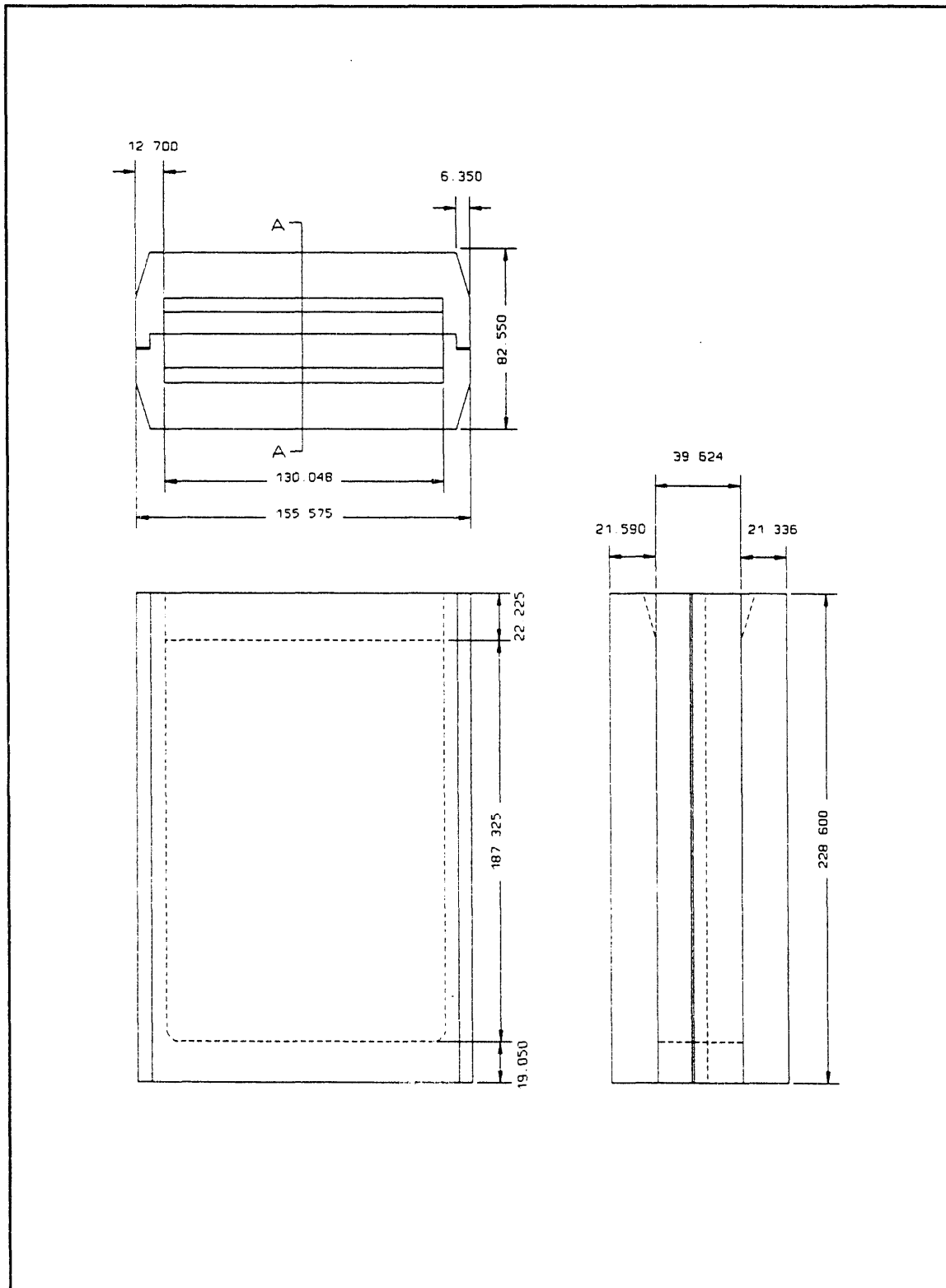
Fig. 2. Engineering drawing showing the top, front, and side views of the assembled bookmold with dimensions in millimeters.

CROSS SECTION "B-B"
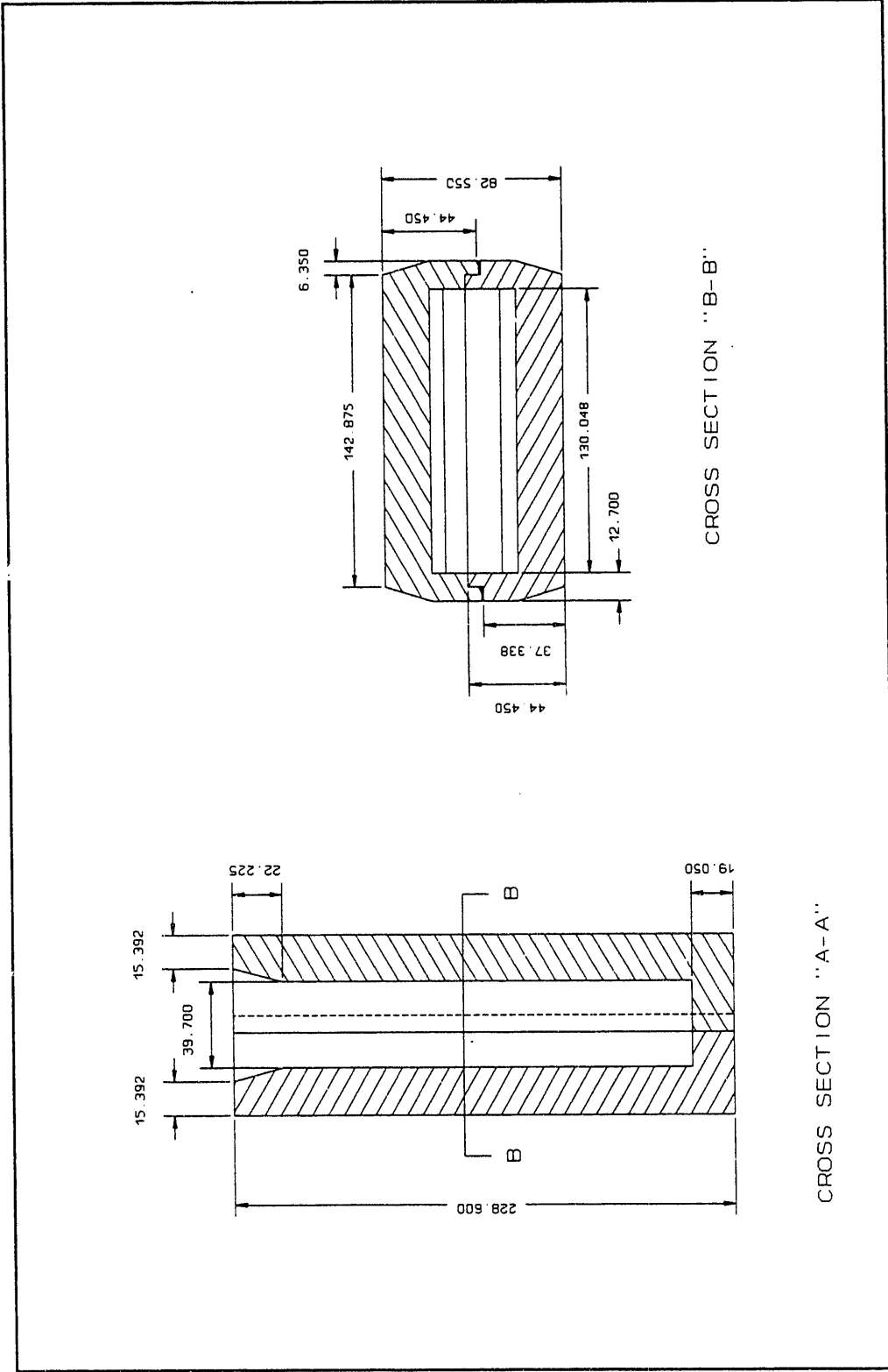
CROSS SECTION "A-A"

Fig. 3. Engineering drawing showing the top and side cross-sectional views of assembled bookmold with dimensions in millimeters.
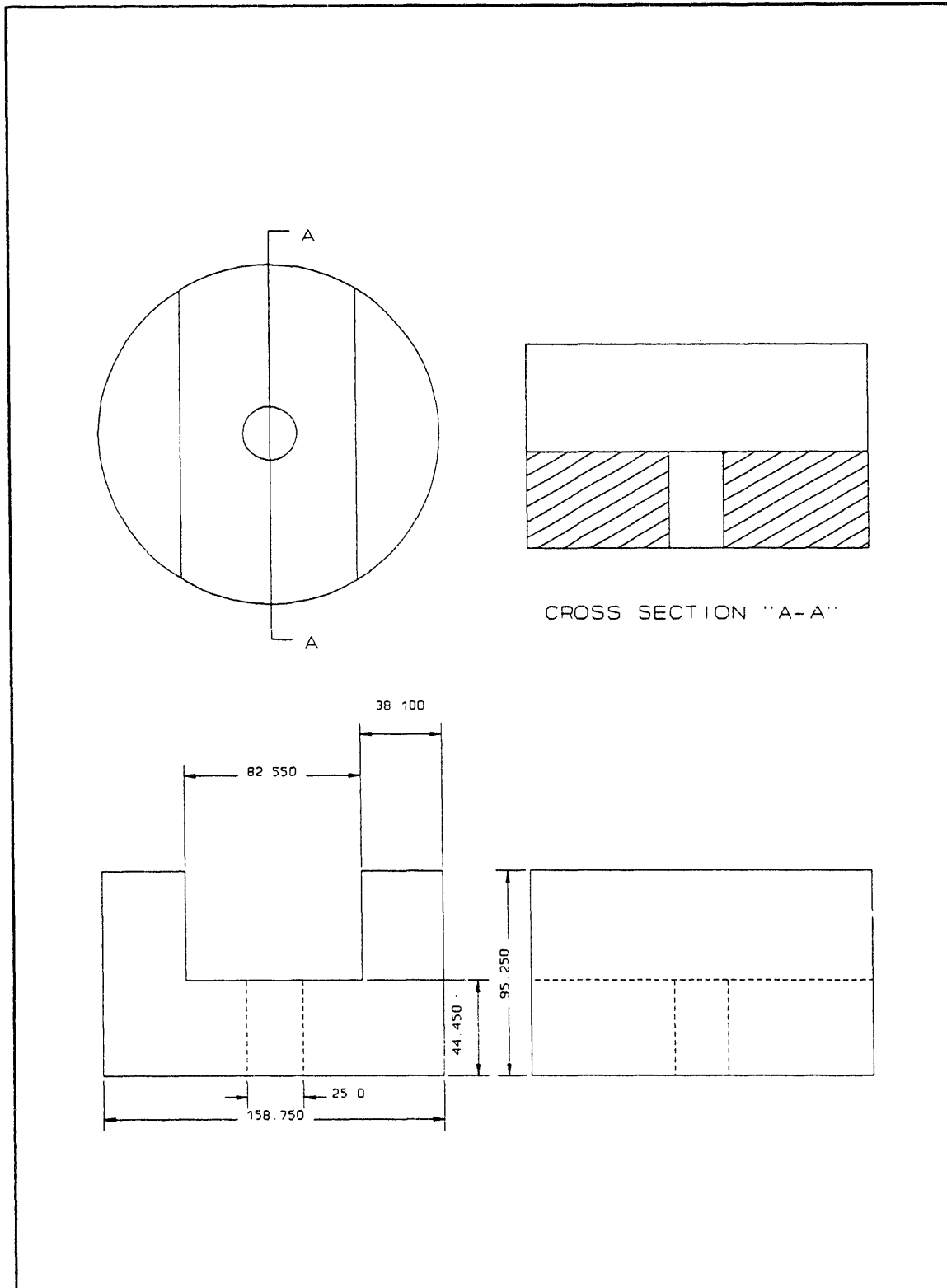
CROSS SECTION "A-A"

Fig. 4. Engineering drawing showing the top, front, side and cross-sectional views of typical end cap with dimensions in millimeters.
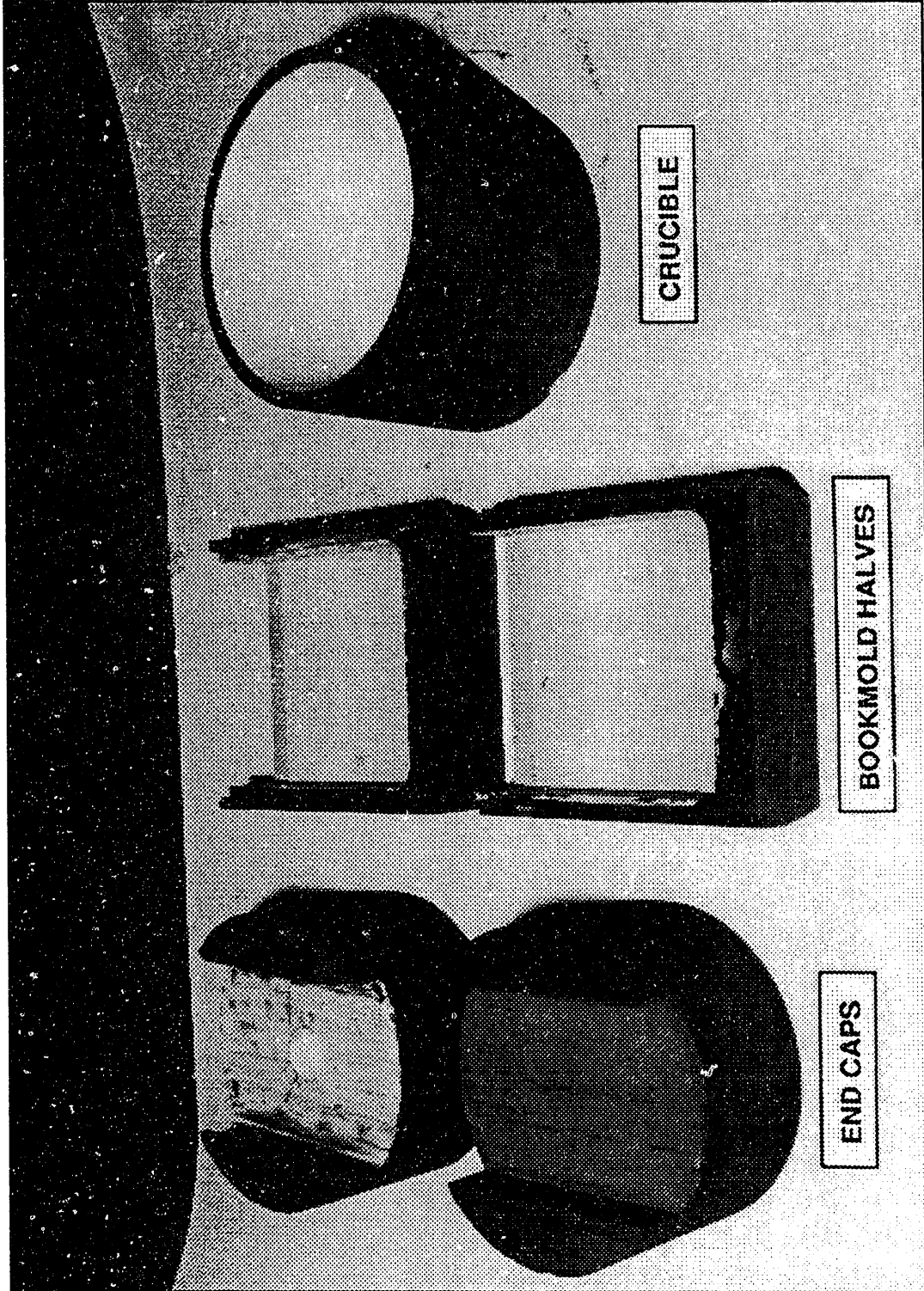
Fig. 5. Unassembled casting assembly components showing yttrium-oxide coatings.
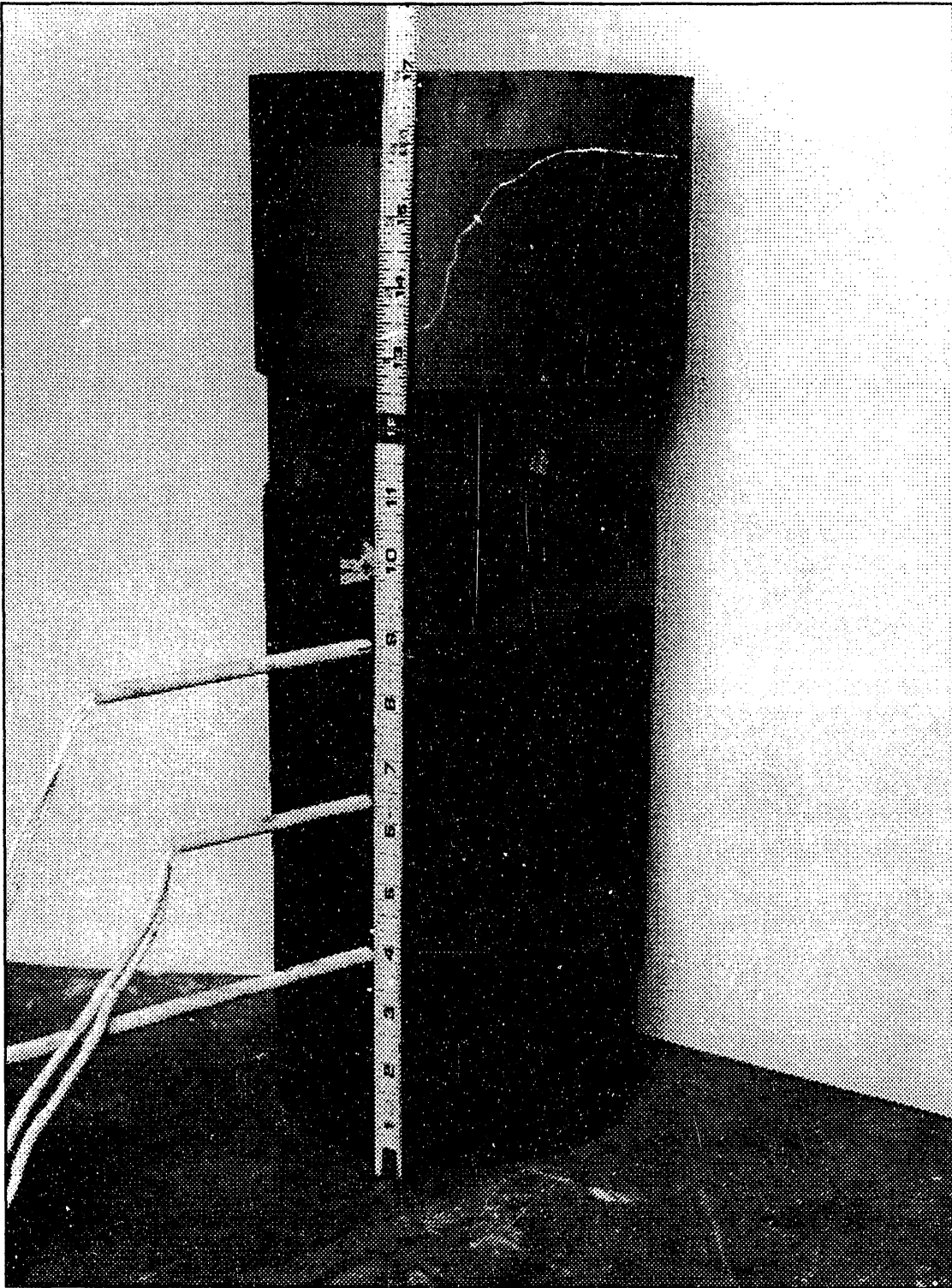
Fig. 6. Assembled casting assembly components showing thermocouple placement.

is illustrated schematically in Fig. 7. Within the context of this problem the induction heater is divided mechanically into two sections: the heating coil primary winding located inside the vacuum-caster, and the remainder of the system located outside the caster in separate enclosures. The heating coil is formed from twelve turns of a single, small-diameter copper tube and is physically supported and electrically insulated by three nonconducting members. It has a mean radius of 10.75 cm, is 23.5 cm high, and is elevated 44.5 cm from the bottom of the caster. Figure 8 illustrates this configuration. The copper tube is hollow to permit the flow of cooling water and has an inner diameter (ID) and wall thickness of 1.5875 cm and 0.1651 cm respectively. Cooling water from the plant process water system (i.e., cooled across a direct contact, forced draft cooling tower) enters at the bottom and exits at the top of the coil. The water is not pumped locally but rather is supplied from and returned to the ultimate heat sink via an extensive interbuilding piping network. Accordingly, the flow rate is a function of the hydraulic load on the entire network and can therefore vary between experiments, as well as during an individual run. This variability is an uncertainty that must also be addressed in the numerical studies.
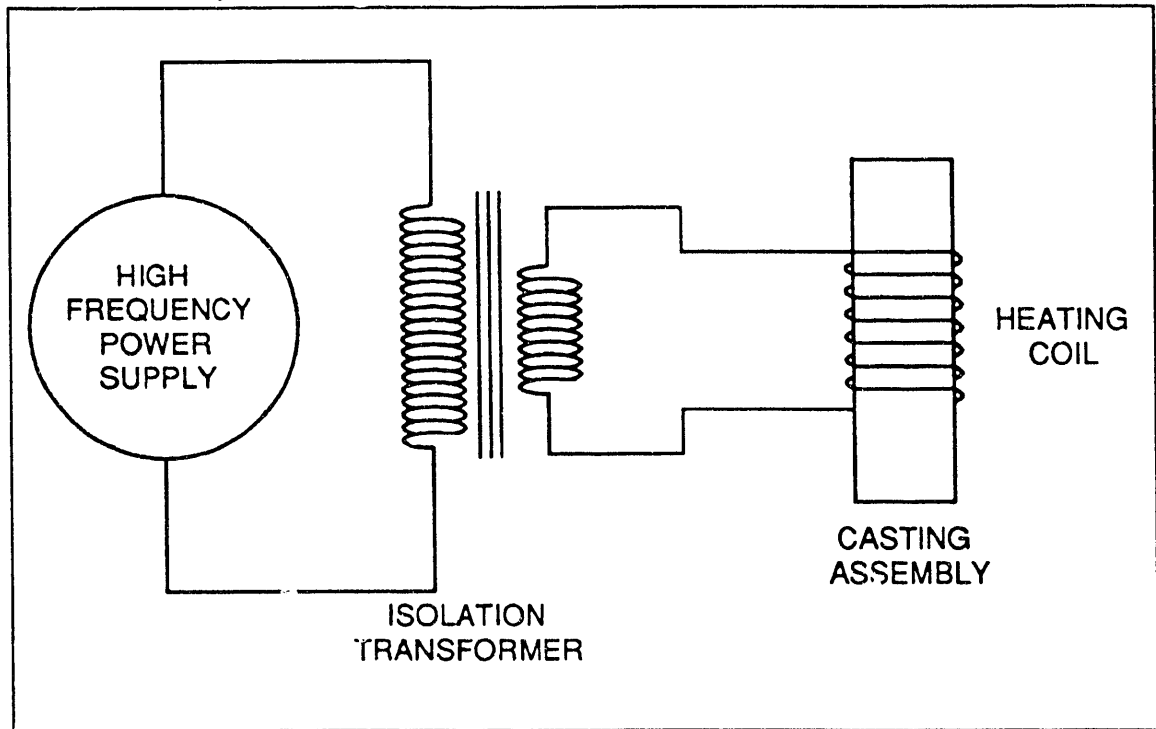
Fig. 7. Schematic illustration of induction heater design.

The vacuum-caster consists of a pressure vessel, two vacuum pumping systems, and associated piping and valves. It was originally designed, procured, and fabricated in-house. The pressure vessel is cylindrical in shape, constructed from 0.953-cm-thick carbon steel, and has an inner diameter and height of 116.0 and 106.5 cm respectively. It is divided into two sections: a fixed bottom half and a hinged top to facilitate loading and unloading of the casting assembly. Figure 9 shows the exterior of the vessel. The vessels's interior contains a pour rod, rod linkage, and the primary winding of the induction heater. Figure 8 also shows the rod and its linkage. Two pumping systems are required to achieve the high vacuums needed for casting of uranium alloys. The first system is a DUO-SEAL model 1398 roughing pump designed to reduce the pressure inside the vessel from atmospheric to approximately 50 μm Hg. The second system
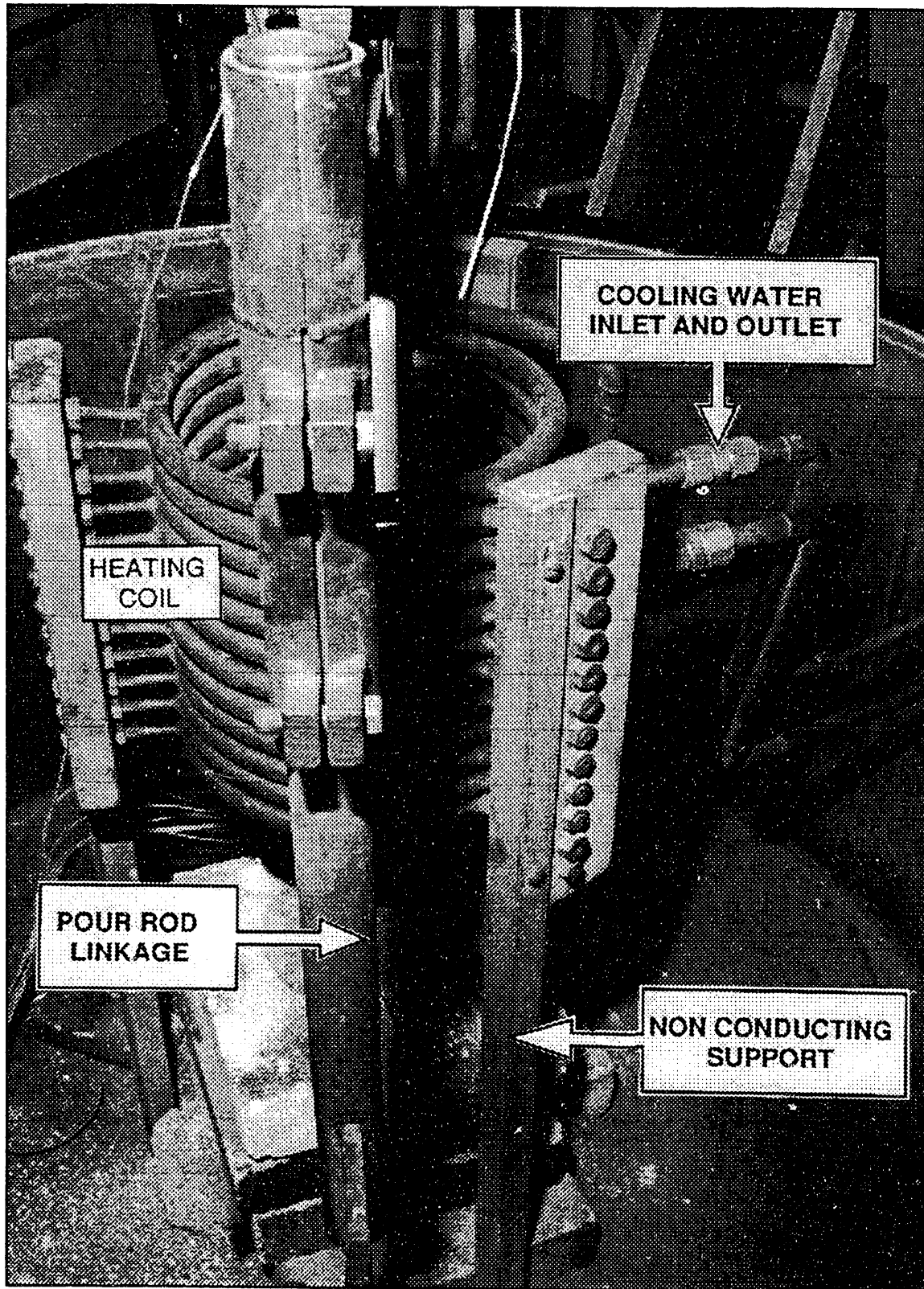
Fig. 8. Interior of vacuum-caster pressure vessel.
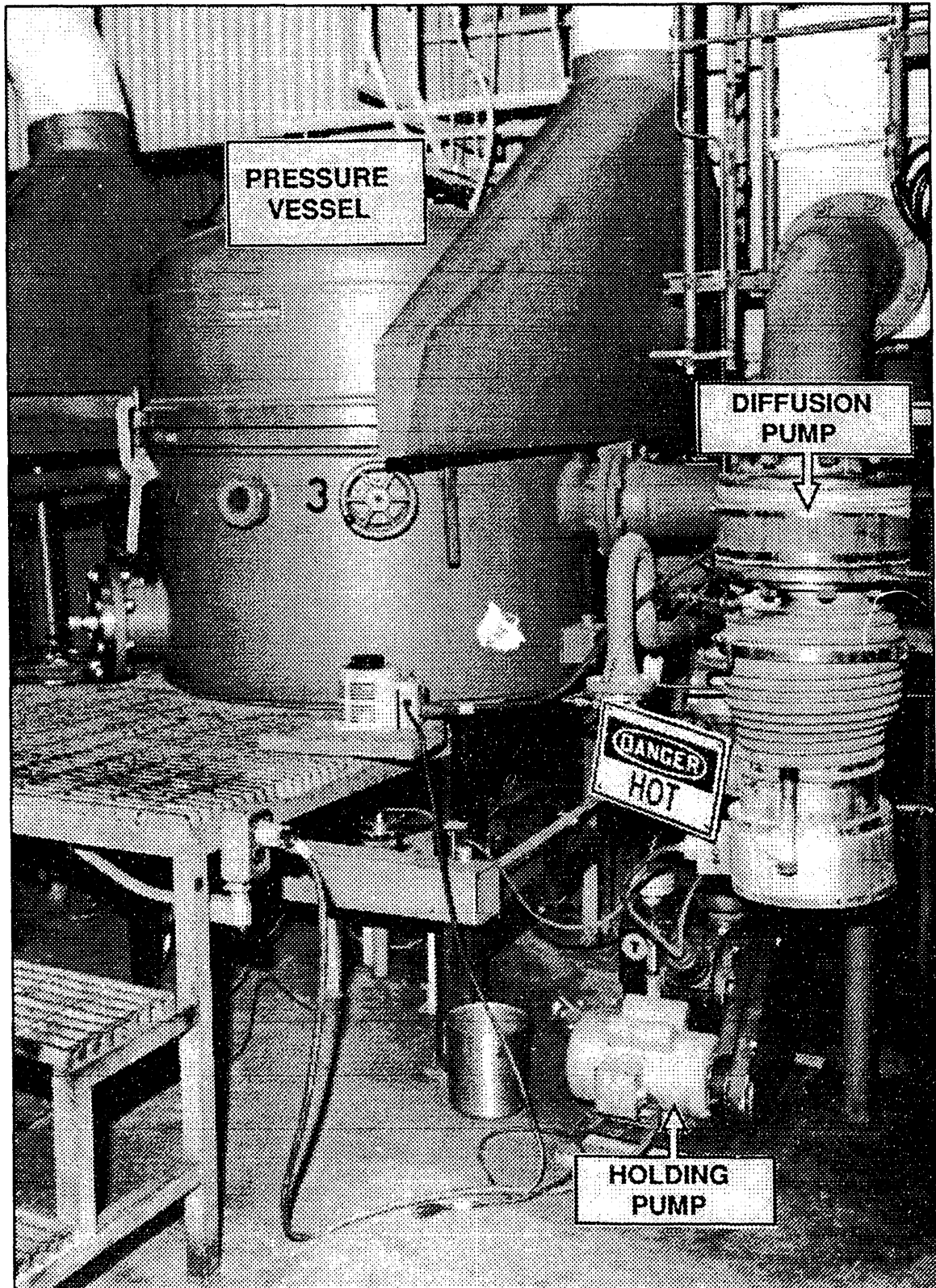
Fig. 9. Exterior of pressure vessel showing diffusion and holding pumps.

consists of a VARIAN diffusion pump and a DUO-SEAL model 1397 holding pump connected in series. They further reduce the pressure to the desired operating level of about 5 μm Hg. Figure 9 also shows the location of the diffusion and holding pumps.

During an experiment the casting assembly is positioned inside the heating coil, as shown in Fig. 10. Sufficient firebrick is placed under the assembly to elevate it 25.50 cm from the bottom of the caster. The assembly is mechanically, electrically, and thermally insulated from the heating coil by a ceramic shield constructed from 96% pure Al_2O_3. It has an ID of 17.78 cm, a wall thickness of 0.95 cm, and is 32.5 cm high. As shown in Fig. 10, the shield is positioned vertically via small pieces of firebrick such that it is elevated 12.5 cm from the bottom of the casting assembly. The relative position of the casting assembly, the Al_2O_3 shield, and the heating coil is critical for the proper preheating of the bookmold, and for establishing and maintaining the directional solidification required for acceptable castings. The uranium melt temperature in the crucible is measured using a single platinum − 90% platinum/10% rhodium thermocouple that has been inserted in an Al_2O_3 thermowell. The thermowell is secured to the side of the crucible, rests on the bottom of the crucible, is 20.32 cm long, and has an ID and wall thickness of 0.6350 cm and 0.15876 cm respectively.

Within the context of this problem, the casting system has two sets of instrumentation; one to control and monitor the operation of the heating coil, and one to record pertinent process temperatures and pressures. Analog displays are provided with the induction heater to show frequency and voltage across the heating coil primary winding, as well as kilowatts, voltage, and current across the primary winding of the isolation transformer. Uranium melt and bookmold temperatures are recorded using a multichannel TOKOGAWA strip chart recorder. Pressure inside the caster is measured using a TELEDYNE-type DV6M *vacuum gage tube* pressure transmitter and is displayed on a HASTINGS analog vacuum gage calibrated in μm Hg. During the time period covered by this report there were no provisions for measuring heating-coil current, cooling-water flow rates, cooling-water inlet and outlet temperatures, or pressure-vessel wall temperatures.

A typical casting experiment has two phases: a heat-up phase in which the recycled uranium and hafnium are melted together in the crucible and a solidification phase where the alloy is poured into the bookmold and allowed to freeze. A nominal experiment proceeds as follows.

1. The casting assembly, Al_2O_3 shield, and firebrick are positioned in the caster, as shown in Fig. 10. Approximately 18 kg of recycled uranium containing 200 to 225 ppm carbon is placed in the crucible along with some number of pre-alloyed uranium-hafnium *buttons*. The thermowell with its thermocouple are secured to the crucible wall, the pour rod is seated in the crucible, and an Al_2O_3 cover is placed on top of the crucible.

2. The caster is secured and the roughing pump started. When the pressure has dropped to approximately 50 μm Hg, the roughing pump is valved out and the diffusion and holding pumps started and continue to run for the remainder of the experiment. When the pressure reaches 5 μm Hg, the cooling water and power to the heating coil are turned on.

3. Coil power is manually increased at a rate to minimize the caster's instantaneous pressure rise due to assembly outgasing. Once the uranium has reached the target melt temperature, coil power is gradually reduced until the system has reached steady-state. These conditions are held for approximately 30 min, at which time the pour rod is removed and the uranium alloy is drained into the bookmold and allowed to freeze. The induction heater continues to run for some few seconds after the pour and is then turned
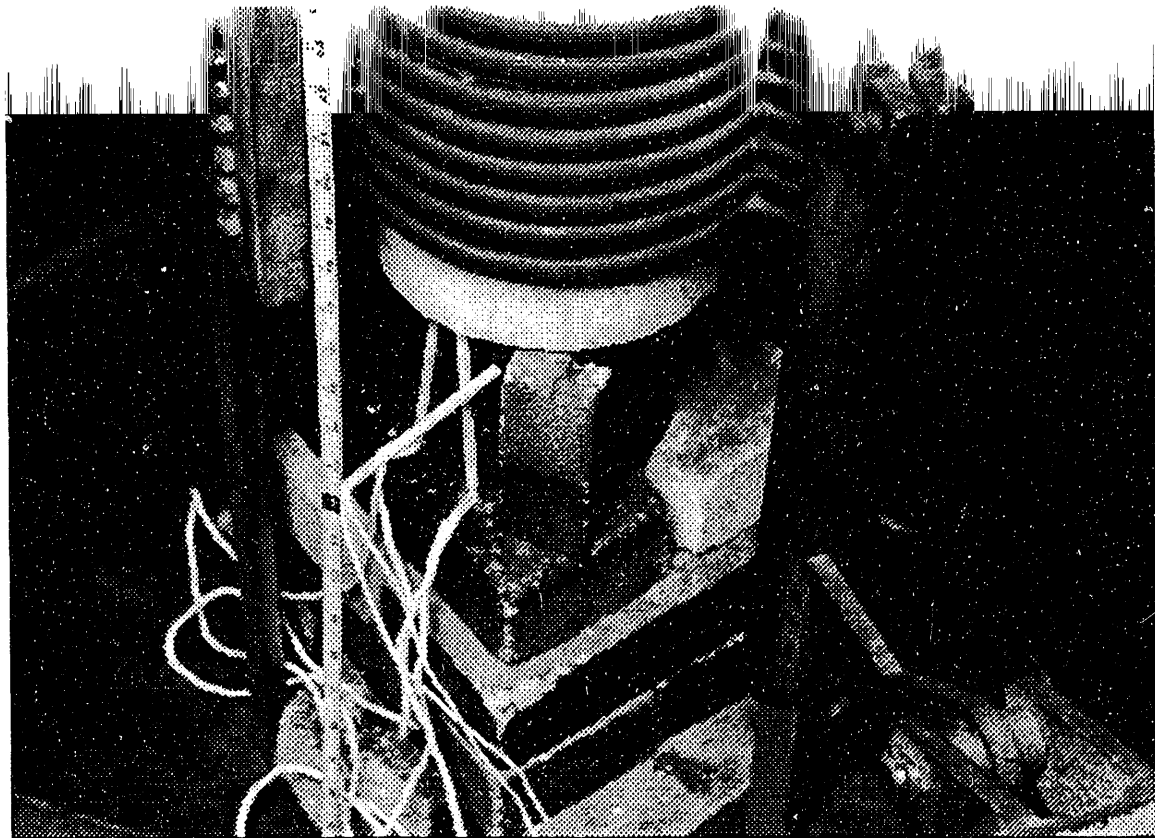
Fig. 10. Interior of pressure vessel showing casting assembly and Al_2O_3 shield positioned inside heating coil.

off. The cooling water continues to run for the remainder of the experiment. During the melting phase the operators record time, melt temperature, isolation transformer primary coil power, and caster pressure. Beginning at the pour and continuing for several hours, the TOKOGAWA recorder prints out the three bookmold temperatures.

4.   After the casting has completely solidified, the caster is backfilled with argon to a pressure of approximately 10 in. Hg vacuum and allowed to cool for an extended time period. The caster is then filled with argon to atmospheric pressure, opened up, and the casting removed for metallurgical examination.

5.   The casting assembly is completely disassembled; any remaining yttrium-oxide is grit-blasted off, fresh oxide is applied, and the components are stored until the next run.

A typical set of experimental temperature data are shown in Fig. 11. These data represent the transient response of the casting assembly during the solidification phase and were taken with the three thermocouples located in the bookmold vertical wall. The experiment utilized the casting assembly and vacuum-caster described above, was designated as Run No. 892, had a uranium target melt temperature of 1375°C, a caster internal pressure of 6 μm Hg, and a total charge weight of 18,019.9 g.
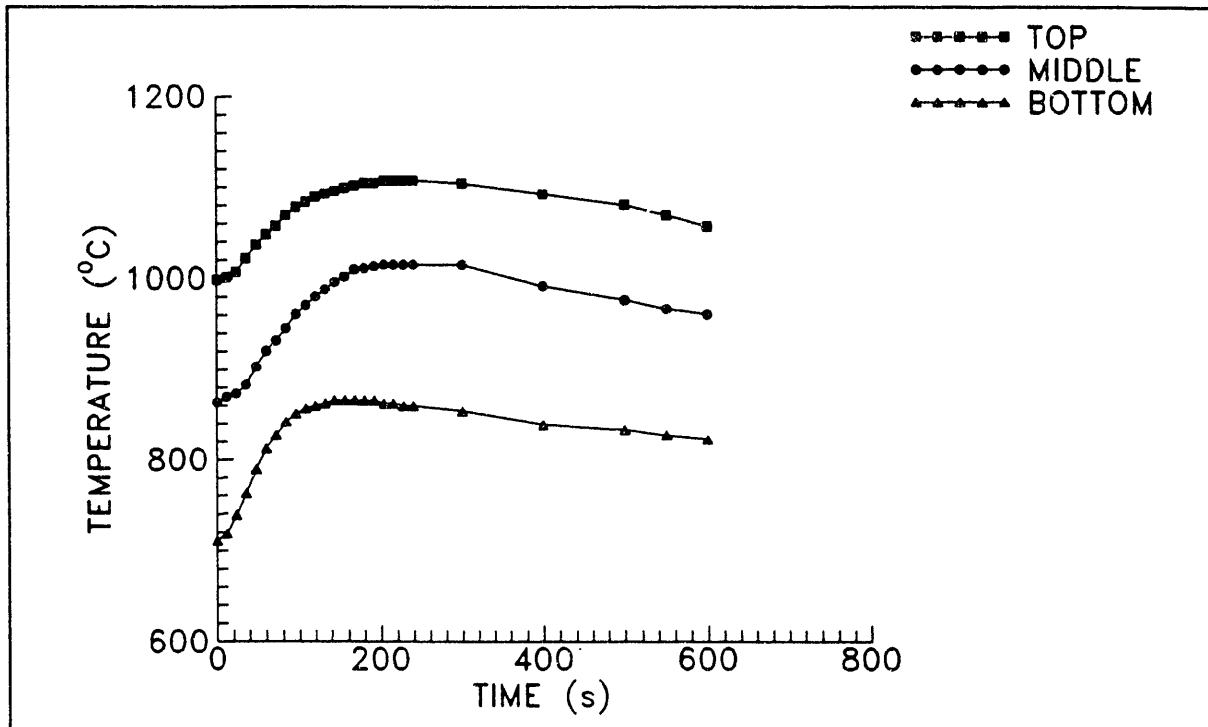
Fig. 11. Typical experimental temperature data showing transient response of casting assembly during solidification.

DETAILED PROBLEM STATEMENT

As explained, predicting carbide transport will ultimately require a coupled *fluid dynamics*, *heat transfer*, and *solution thermodynamics* calculation. Formulating a tractable solution procedure requires consideration of several technical and programmatic issues, primarily the scope of the

problem and the relative immaturity of the numerical studies. The scope of the problem is extensive. No fewer than 14 thermal-hydraulic mechanisms must be considered to some degree:

1. Three-dimensional transient heat conduction with temperature-dependent material properties.
2. Nonuniform internal heat generation in portions of the casting assembly resulting from operation of the induction heater. Because the current penetration depth into liquid uranium at 10,000 Hz is very small and the material properties of Al_2O_3 do not support significant eddy currents, only the carbon components are heated internally.
3. *In-vacuo* contact resistances between bare and coated assembly components, as well as between the assembly and Al_2O_3 shield, the Al_2O_3 shield and copper coils, and the assembly and the firebrick.
4. Radiation heat transfer between individual assembly components, from some components to the Al_2O_3 shield and pressure-vessel wall, from the liquid uranium to the crucible and bookmold walls, from the Al_2O_3 shield to the copper coils and pressure-vessel wall, and from the exterior of the copper coils to the pressure-vessel wall.
5. *Enclosure* natural convection heat transfer between the liquid uranium and the crucible and bookmold walls.
6. *Enclosure* buoyancy-driven fluid flow and carbide transport within the liquid uranium during melting and solidification.
7. *Interfacial* heat transfer between solidified uranium and the bookmold.
8. *Free surface*, momentum-driven fluid flow during the pour.
9. Multiphase, nonequilibrium, *solution thermodynamics* in the uranium during melting and solidification.
10. Solid-liquid, liquid-solid, and solid-solid phase-change heat transfer in the uranium alloy.
11. Forced convection heat transfer from the interior of the heater coils to the cooling water.
12. A hydraulic *manifold* controlling the heating coil's cooling-water instantaneous flow rate.
13. Low-pressure, *enclosure* natural convection heat transfer from casting assembly components during the extended cooling period.
14. Natural convection heat transfer from the exterior of the pressure vessel.

As is generally the case during the initial phases of an R&D effort that seeks to define cause and effect, the problem contains a large number of uncertainties. These include but are not limited to the following examples:

1. Is carbide formation complete prior to the pour or does it continue during solidification? If so, is it affected by the uranium solid-liquid interface?
2. Are buoyancy forces resulting from U/HfC density differences the same magnitude as those resulting from fluid-mold temperature differences, or is one so dominant as to permit the other to be neglected?
3. Does the complete casting assembly have to be modeled to ensure the proper thermal mass and inertia, or can some components be simplified and/or eliminated?
4. Which of the 14 individual mechanisms has a prominent effect on carbide transport and must therefore be accurately modeled? Furthermore, what level of accuracy is required for these critical mechanisms?
5. Is a computational fluid dynamics (CFD) computer program needed to quantify the thermal aspects of pouring and solidification, or would a strictly heat-conduction solid-liquid approximation be adequate?

A programmatic consideration is that the systematic reduction of technical uncertainties and the evolution of numerical tools must complement each other. In the beginning when uncertainties are great, tools should be correspondingly simple. As technical uncertainties are reduced, tools must be improved to take advantage of the more accurate information. This balance is required because it is computationally and economically inefficient to construct a mathematical model with capabilities that cannot be utilized because inputs and/or system behavior are so uncertain as to preclude any meaningful results. As it concerns this problem, the *uncertainty reduction/tool evolution* process is extremely unbalanced. No numerical tools are available, yet there are considerable experimental data that define bookmold thermal response and macroscopic HfC behavior. Thus, any model constructed for this problem, even if it is the initial effort, must be of sufficient rigor to accommodate the existing data. An additional facet of numerical model construction is that it can be nonuniform and iterative. Nonuniform because each problem element can have uncertainties that vary in number and complexity and, therefore, require different amounts of modeling effort to reach the same level of sophistication. For this problem the distribution of uncertainties is extremely skewed: the *heat transfer* facet has the greatest number. Also, because of the design of the casting system, the uncertainties must be defined before meaningful solidification results can be obtained. The *reduction/evolution* process can become iterative when large numbers of nontrivial uncertainties exist. Under these conditions it is often necessary to make simplifying assumptions to begin the analysis. If these are shown to be incorrect, the calculations must often be repeated. These circumstances put a burden on the investigator to coordinate model construction iterations to ensure that study goals are obtained with a minimum number of iterations. As it concerns this problem, the complete lack of numerical models, the large number of thermal uncertainties, and the need to construct a model capable of accommodating existing experimental data mean that more than one iteration will be required for the thermal facet.

No single computer program is available to solve the coupled *thermal-hydraulic-thermodynamic* problem. Separate heat conduction and CFD codes are available, but (from the perspective of this problem) each has serious limitations. Existing conduction programs can only model the liquid-solid uranium as a conducting region with temperature-dependent material properties. Including the effects of momentum-dominated pouring or buoyancy-driven flow is beyond the capabilities of even the most sophisticated conduction program. Similarly, commercially available CFD codes have limited conjugate heat transfer capabilities. They can calculate conduction heat transfer within a containment vessel, but generally cannot accommodate complicated vessel geometries nor multiple, nonlinear heat transfer paths. An additional consideration is that even though there are at least two heat conduction programs readily available within Energy Systems, there are no CFD codes with sufficient capabilities to model the pouring operation. With respect to U/Hf and U/Hf/C solution thermodynamics within a carbon containment vessel at the temperatures and species concentrations applicable to this problem, no computer programs are available at all.

Ultimately, the large number of uncertainties and the need to systematically quantify them completely dominate the problem definition effort. Accordingly, the individual problem elements will initially be studied separately, and the *heat transfer* facet will be defined first because of its central importance to the overall solution and the availability of numerical tools. Furthermore, the study will be divided into two phases — each focused on the current laboratory-scale casting system. The first uses an existing stand-alone conduction program, contains idealized uranium regions, and casting assembly geometry considerations are minimized to permit maximum effort toward defining cause and effect. The second-phase will also use a stand-alone conduction model, accurately model the previously defined mechanisms, and iterate with a stand-alone CFD code

to further quantify the prominent mechanisms, examine the effect of casting assembly design on carbide transport, and begin the study of the *fluid dynamics* problem. The macroscopic objective of the first-phase study then is to generate the analytical experience and technical data required to construct and efficiently execute the second-phase thermal model. This goal will be achieved by completing three subtasks:

1. construction of a base-case thermal model of the current laboratory-scale casting assembly;
2. sensitivity studies to identify those thermal mechanisms that have a prominent effect on the simulation of the bookmold thermal response; and
3. abbreviated studies to define a physical model that is as simple as possible, yet not so emaciated as to introduce unacceptable errors into the analysis.

The remainder of this report documents the conduct and results of the first-phase study.

DEVELOPMENT OF THE BASE-CASE MODEL

The HEATING 7.1 (ref. 2) heat conduction program was selected to conduct the first-phase studies because of its availability and low operating cost. The following macroscopic design criteria were established.

1. Because HEATING cannot accommodate mixed geometries within a single problem and since the focus of the study is the rectangular uranium region within the bookmold, a cartesian coordinate system will be used. Although the crucible, end caps, shield, and coils are cylindrical, this approximation is considered acceptable for the first-phase effort.

2. The physical model will include all major casting system components, including the insulated thermocouple junctions. The pressure vessel will not be explicitly modeled, its influence will be included using radiation heat transfer to and from a black body.

3. The thermal model will include all apparent mechanisms: conduction, temperature-dependent material properties, internal heat generation, forced and natural convection heat transfer, radiation heat transfer, thermal contact resistances, and interfacial gap conductance between the solidified uranium and bookmold. In keeping with the scope of the first-phase study, carbide formation, buoyancy-induced transport, and CFD considerations will not be included.

4. Each transient solidification analysis will require a steady-state calculation to define initial conditions (i.e. the temperature distribution in the system just prior to the pour).

5. Uranium regions will be approximated as simply conducting phase change materials with temperature dependent properties. In all cases properties of unalloyed uranium will be used.

6. The solidification analysis will begin with a uniform temperature within the solidifying uranium and the undisturbed steady-state temperature distribution within the casting assembly. That is, the effects of the pour will not be considered.

7. The only direct indication of model accuracy is a comparison between calculated and measured bookmold temperatures. This comparison then will determine the prominence of individual mechanisms.

As explained, the large number of uncertainties dictated an iterative numerical study. An initial model was conducted to qualitatively identify prominent thermal mechanisms, and a second effort actually constructed and executed the base-case model. The first iteration considered only a portion of the casting assembly and used measured temperatures as boundary conditions to produce a numerical *testbed* with fewer uncertainties than a complete model would have had. This method allowed maximum effort toward defining thermal-hydraulic cause and effect. The second iteration used this information and a complete geometry to identify the prominent mechanisms.

FIRST ITERATION

The initial modeling effort consisted of two separate tasks, each designed to bound the thermal problem.[3,4] The first was a scoping study to qualitatively define the prominent heat conduction paths. It was executed using a simplified 1-D geometry and it quickly showed that a more detailed model was required to generate meaningful results. The goal of the second task then was to define, construct, and execute the more rigorous model. It consisted of a 3-D,

18

quarter-symmetric, cartesian coordinate approximation of the bookmold, upper and lower end caps, firebrick base, and that portion of the Al_2O_3 shield below the top of the upper end cap Also, gaps were included to simulate contact resistances between the bookmold and lower end cap, as well as melt shrinkage between the uranium melt and bookmold. Figure 12 shows a scale drawing of the discretized casting assembly geometry; the material regions have been shaded for clarity. Figure 13 is a schematic illustration of the bookmold/end-cap portion of the discretized geometry with some nominal dimensions in millimeters. For simplicity, the firebrick base is not shown in either figure. This geometry was input to HEATING, with the following initial and boundary conditions:

1. one-dimensional radiation heat transfer from assembly exterior surfaces to the pressure-vessel wall,
2. temperature-dependent material properties for solid uranium and carbon,
3. initial temperature conditions for the entire model extrapolated from three experimental measurements, and
4. a constant temperature boundary condition for the top of the upper end cap that had been derived from experimental data.

A series of sensitivity studies were conducted whose purpose, like the earlier 1-D examinations, was to qualitatively identify prominent thermal mechanisms. Ranges of likely values were specified for the above conditions and their effect on model accuracy (i.e., agreement with experimental temperature data) noted. The analyses established that the primary heat conduction path out of the uranium is in the radial direction and that model accuracy is quite sensitive to initial temperature conditions, boundary temperatures, temperature-dependent physical properties, and radiation heat transfer as applied to boundary conditions, contact resistances, and melt shrinkage. Figure 14 illustrates the best agreement obtained during the studies. It shows experimental and calculated temperatures at the three thermocouple locations in the bookmold vertical wall as a function of time. The primary observation is that model agreement is quite good at the uppermost location but steadily worsens toward the bottom location. This behavior is consistent with the structure of the model. The upper portion has a specified temperature boundary condition defined from experimental data. The boundary conditions for the middle and lower portions of the model are calculated using assumptions about initial temperatures and the magnitude of the radiation heat transfer coefficient. It is quite reasonable then to expect greater uncertainties, and therefore poorer agreement, in the middle and lower portions of the model.

SECOND ITERATION

The second iteration consisted of two parts: developing a complete physical model and defining those first-order accurate analytical relationships required to simulate the mechanisms identified in the initial effort. The resulting physical model contains a 3-D, quarter-symmetric, cartesian approximation of the firebrick base, lower and upper end caps, bookmold, crucible and its top, Al_2O_3 shield, induction heater coils, and the three insulated thermocouple junctions. The approximated assembly components are shown in Figs. 15—20. They show scale drawings (dimensions in millimeters) of, respectively, the upper and lower end caps, the bookmold, the crucible, the pair of flat plates used to represent the Al_2O_3 shield, and one pair of the plates used to represent the heater coils. The complete physical model is shown in Fig. 21, and the individual material regions have been shaded for clarity. There are three noteworthy features of the model: gaps between components, flat plates representing the heating coils, and dual uranium regions.
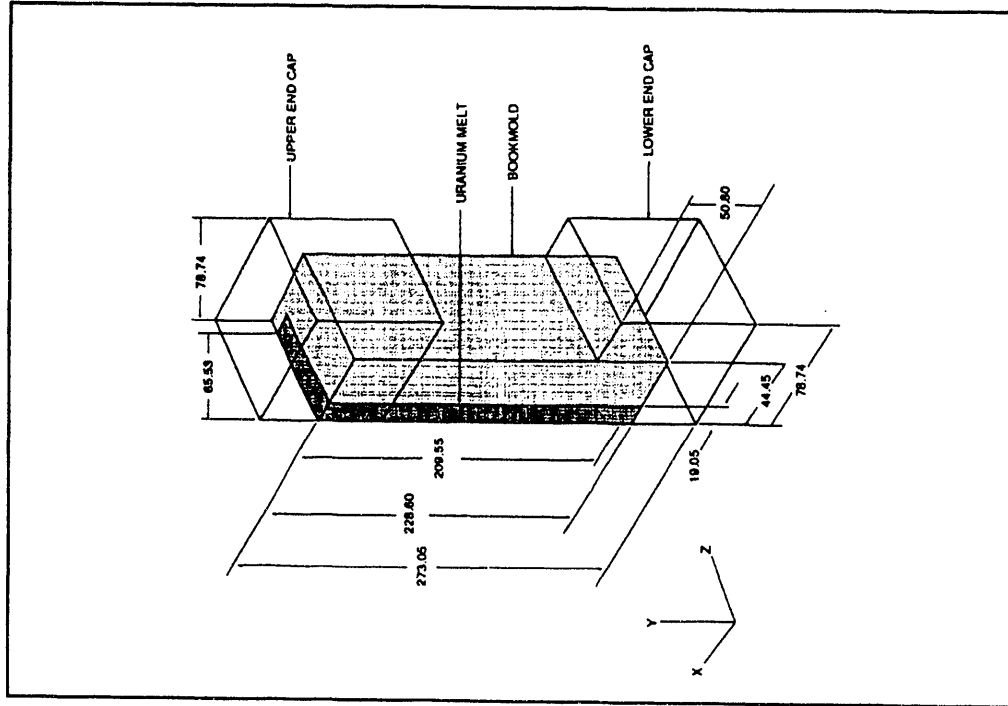
Fig. 13. Schematic illustration of bookmold/end-cap portion of discretized casting assembly geometry with dimensions in millimeters.
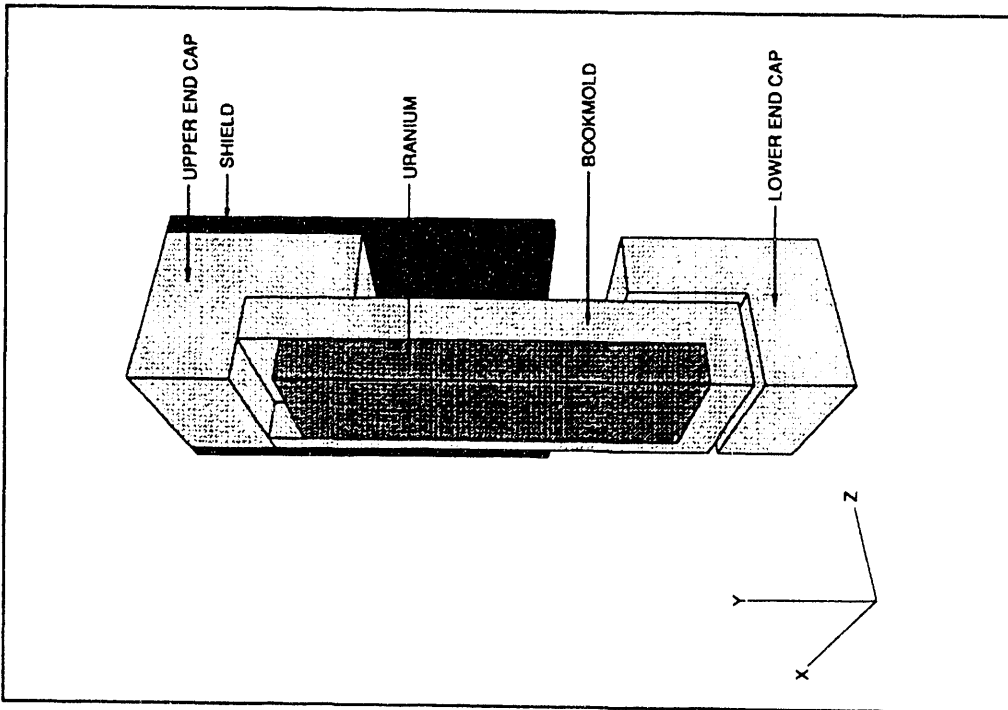
Fig. 12. Discretized geometry used to represent casting assembly during the initial model construction effort.

21
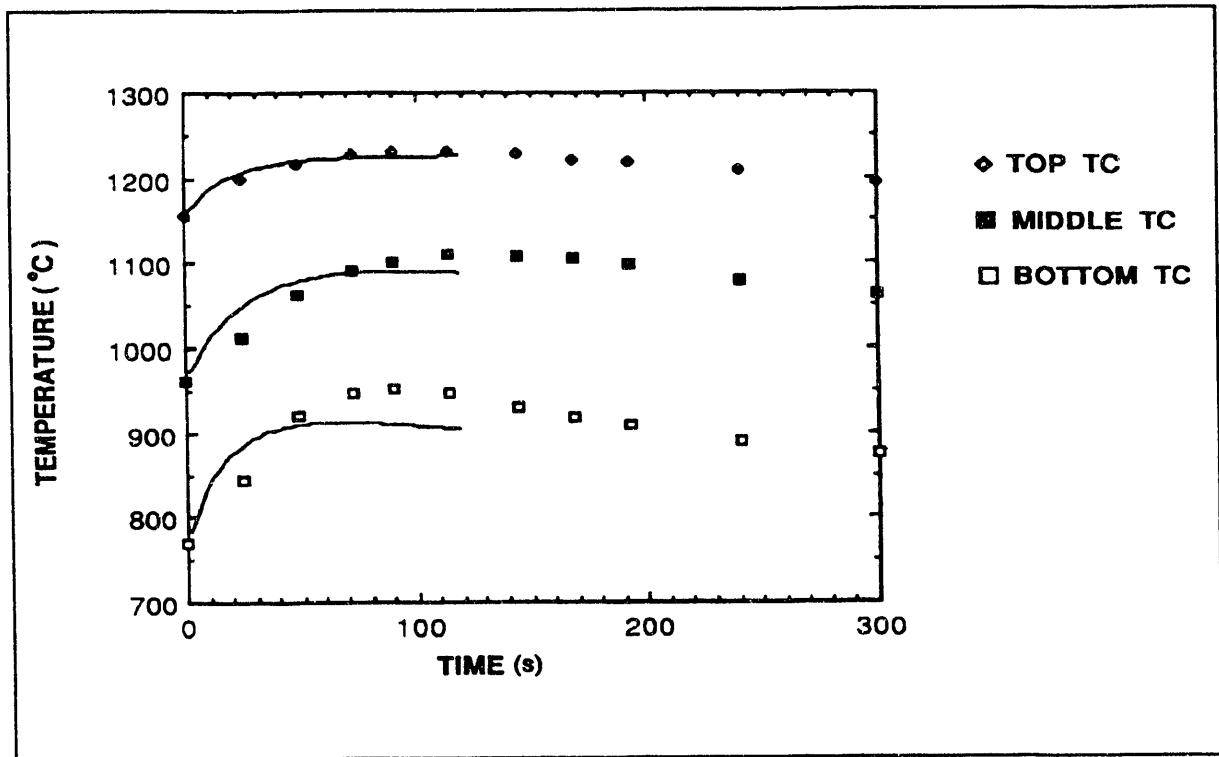
Fig. 14. Comparison of calculated and experimental bookmold temperatures for the first iteration.
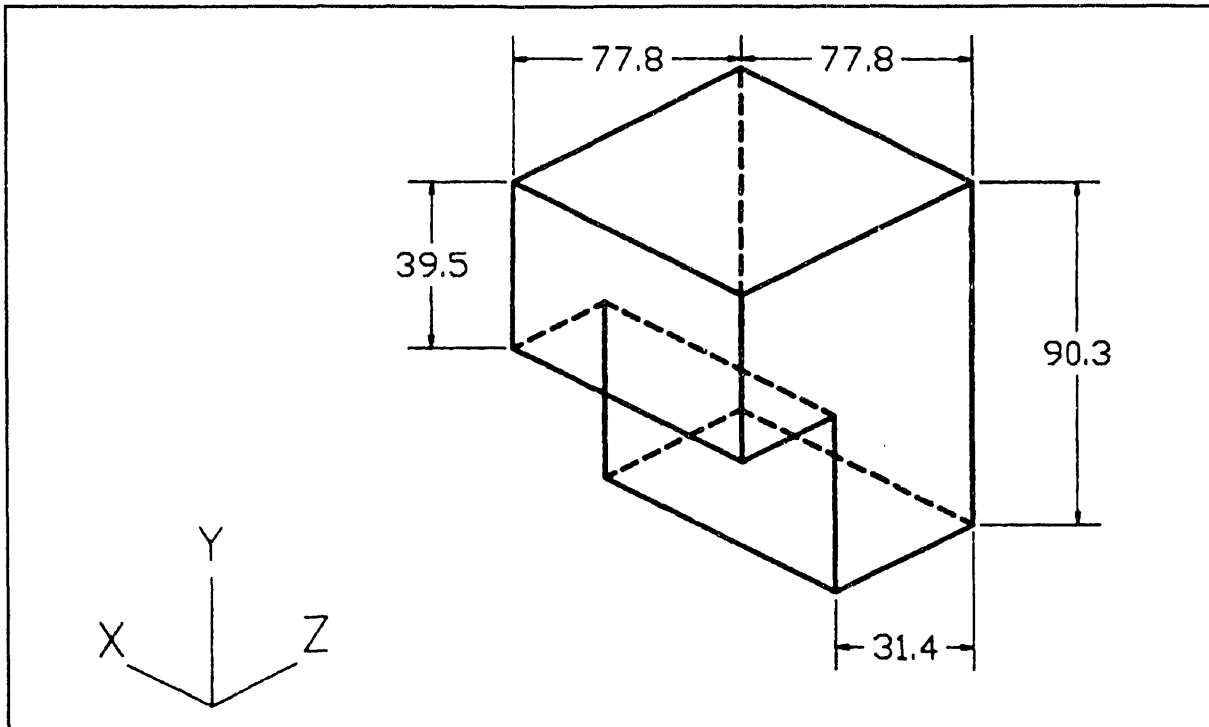
Fig. 15. Engineering drawing of the approximated upper end cap with dimensions in millimeters.
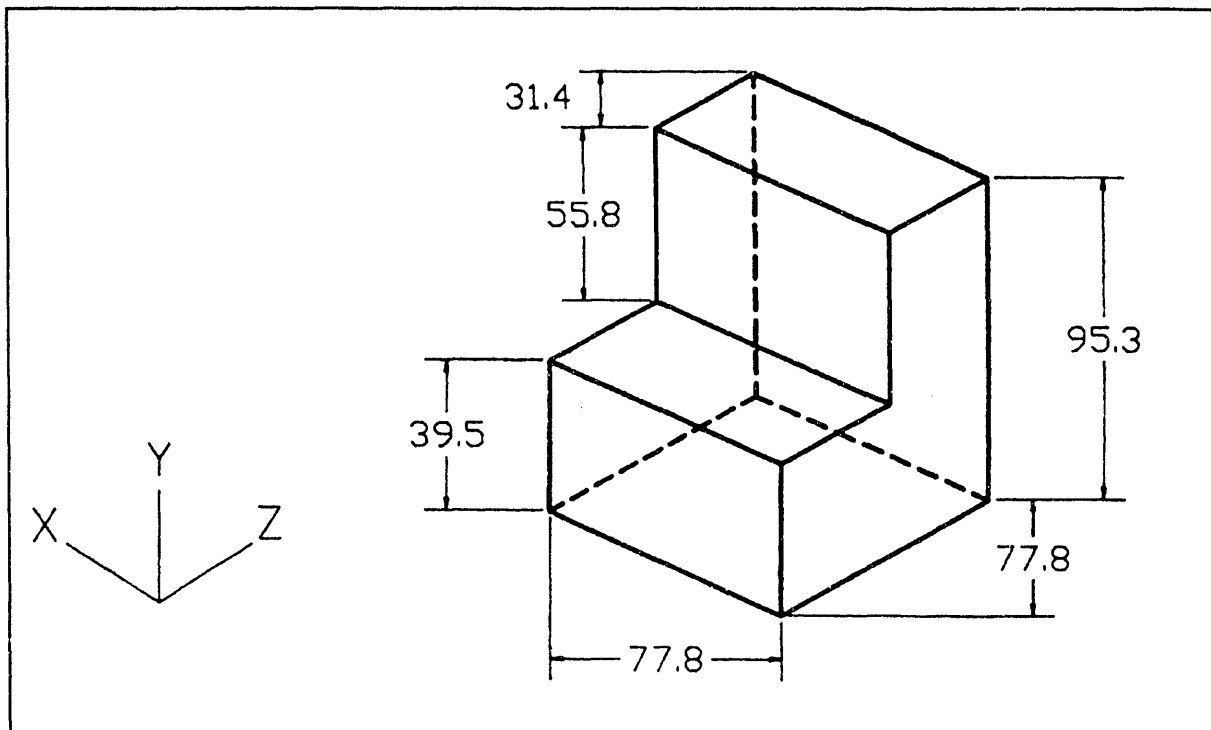
Fig. 16. Engineering drawing of the approximated lower end cap with dimensions in millimeters.
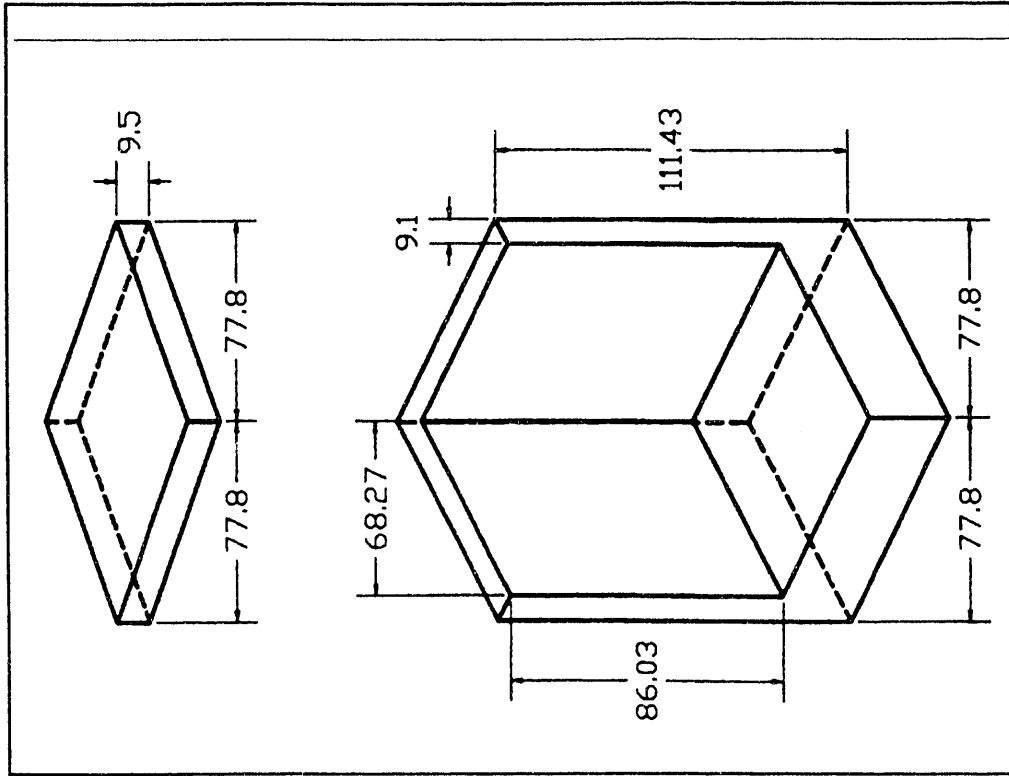
Fig. 18. Engineering drawing of the approximated crucible and its top with dimensions in millimeters.
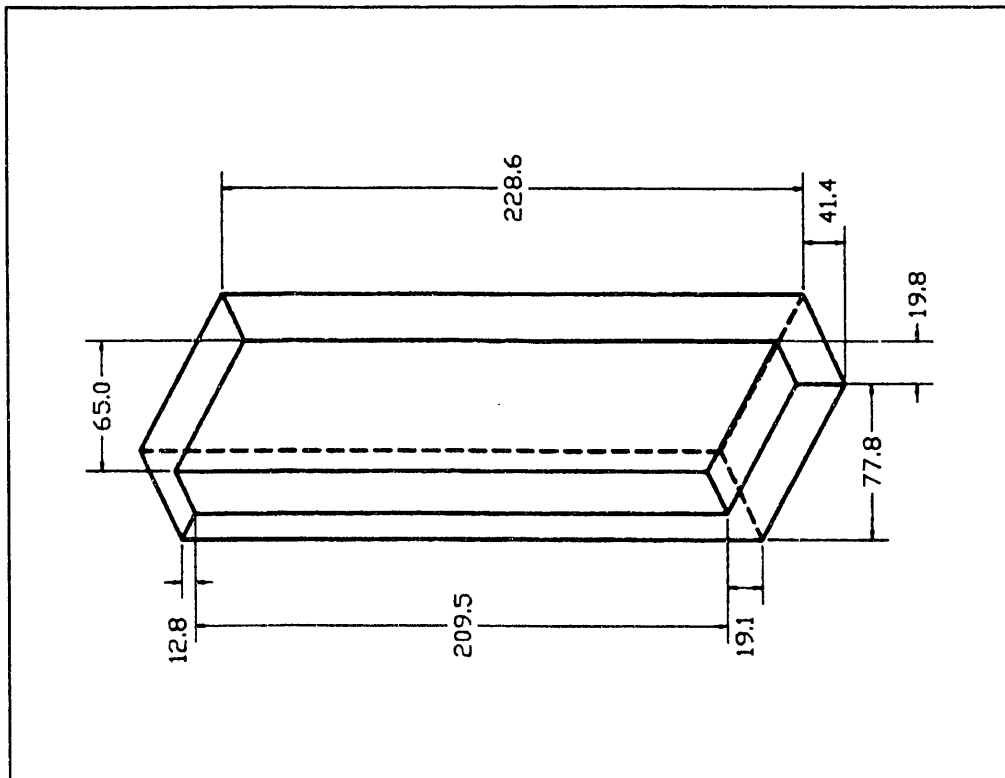
Fig. 17. Engineering drawing of the approximated book-mold with dimensions in millimeters.
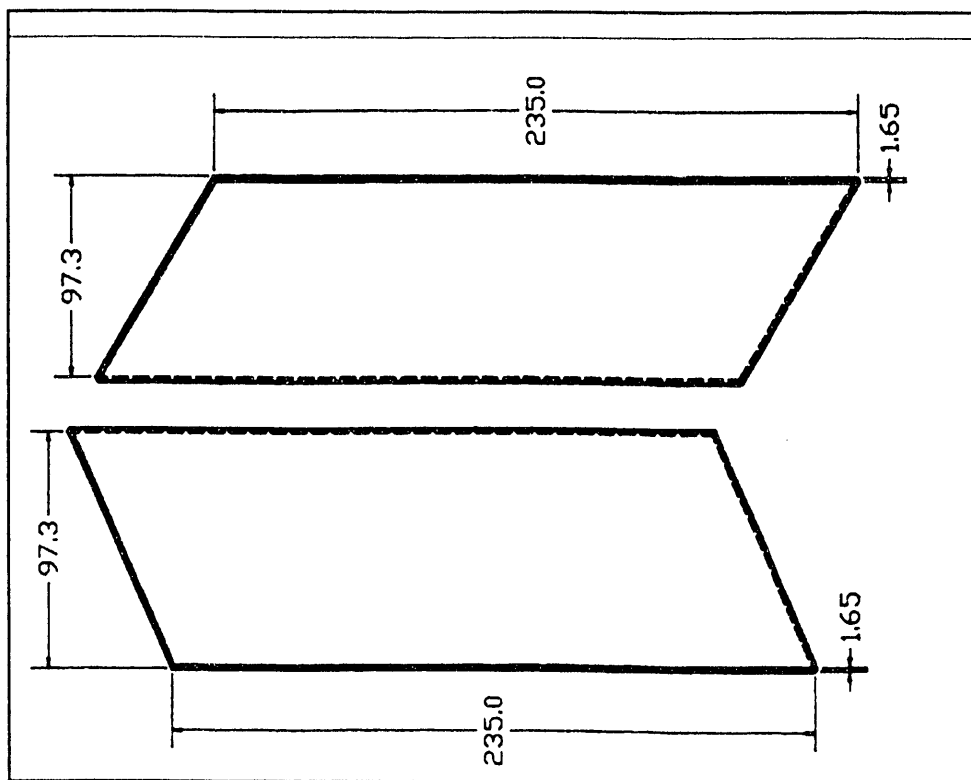
Fig. 20. Engineering drawing of one pair of plates used to approximate the induction heater coils with dimensions in millimeters.
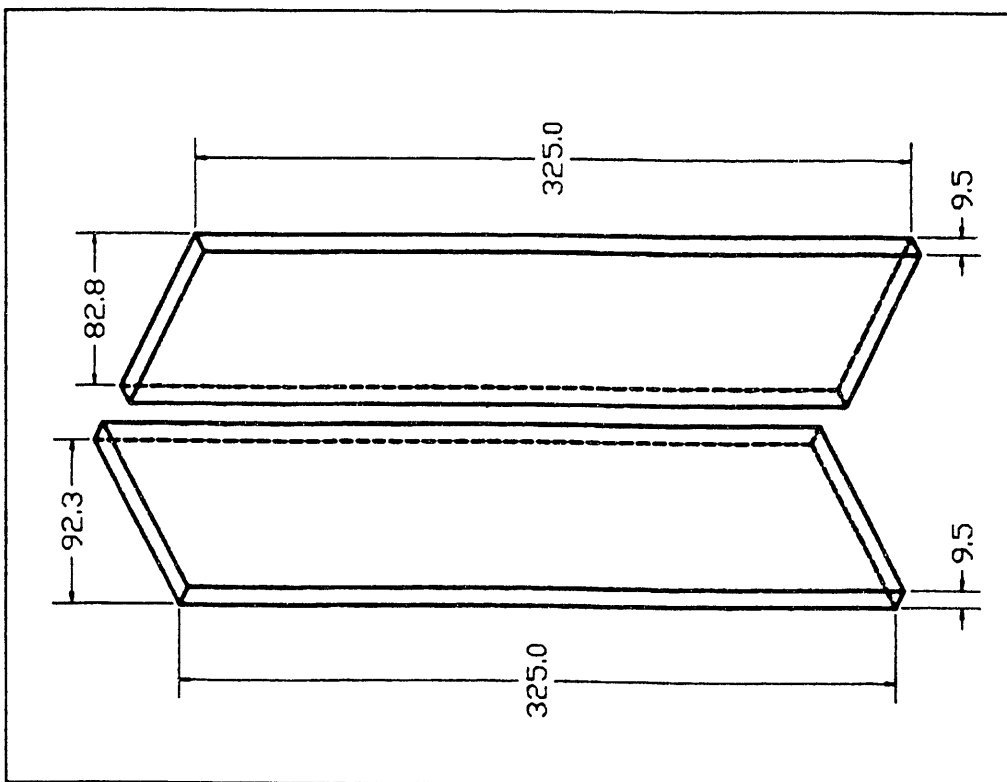
Fig. 19. Engineering drawing of the approximated Al_2O_3 shield with dimensions in millimeters.
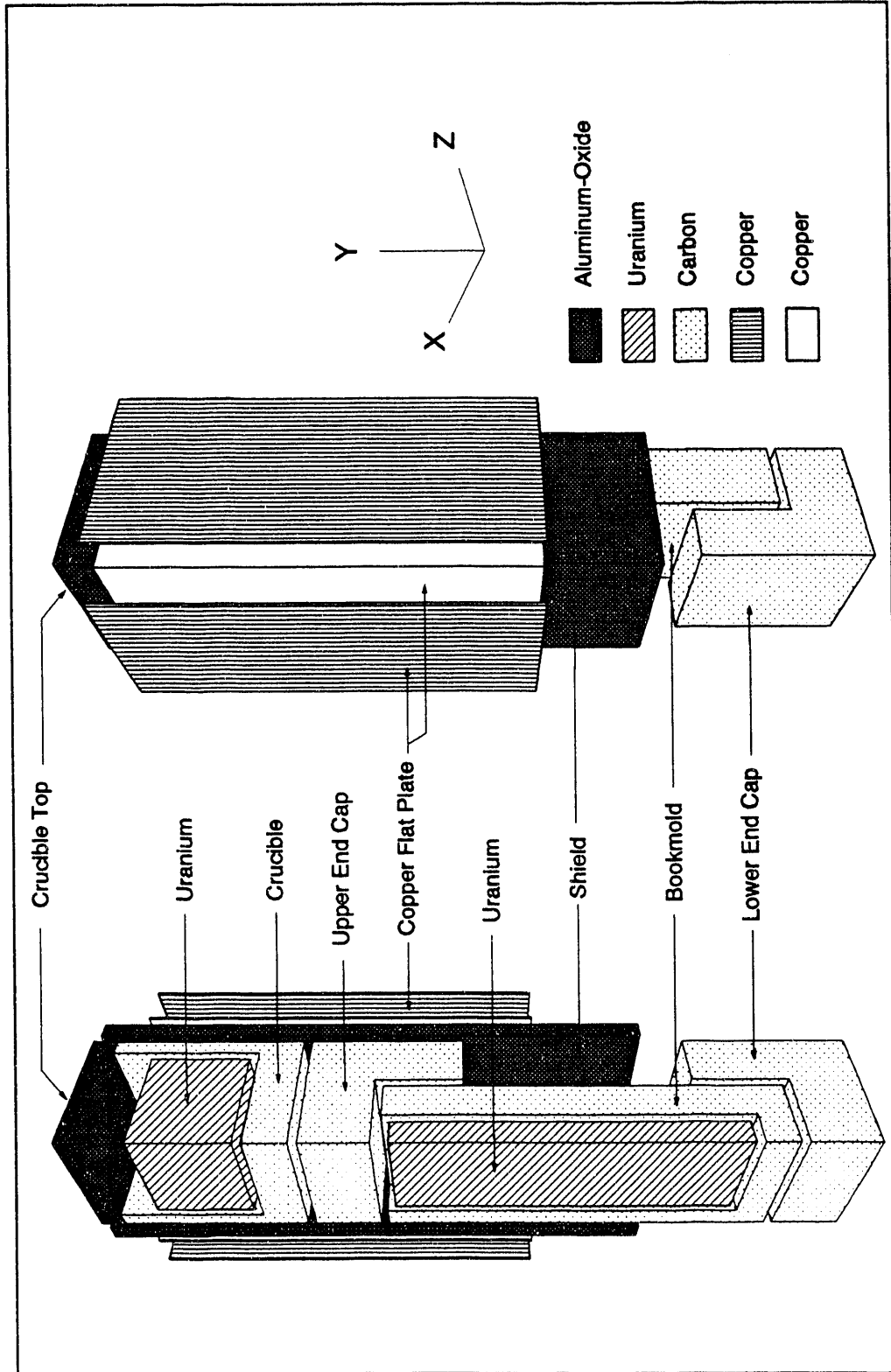
Fig. 21. Complete casting assembly physical model.

1. An exact representation of the heating coils was not possible, and to have approximated them as lengths of square tubes would have been cumbersome. A simplified 2-D (R&Θ) transient study showed that temperatures and heat fluxes were uniformly distributed around the coil's inner surface. Because the coils are also closely spaced, it seemed reasonable to represent them as a flat plate with a thickness equal to that of an actual coil. Because the height of a single plate was limited to the actual height of the coils, two thermally connected plates were required to give the correct heat transfer surface area.

2. To transfer steady-state temperatures to the transient input file, both input files must have the same number of phase-change regions. Accordingly, dual uranium regions were incorporated. The bookmold region is thermally isolated during the steady-state analysis, and the crucible region is similarly isolated during the transient calculation.

3. A system of uniform size gaps were placed between casting assembly components to include the effects of contact resistances, sliding fits, melt shrinkage, and fluid thermal boundary layers. These were placed between the bookmold and lower and upper end caps, the lower end cap and the firebrick, the upper end cap and crucible, the crucible walls and top, the end caps and the Al_2O_3 shield, the shield and the copper flat plate, and the uranium regions and the crucible and bookmold walls. Gap regions are a capability within HEATING that permit one to specify a heat transfer rate independent of the gap's thickness. Thus, the same size gap can be made to represent a radiation heat transfer mechanism as well as a much larger forced convection coefficient. This system is also illustrated in Fig. 21. Each narrow space between components represents a gap.

With the physical model specified, the required material properties, first-order accurate analytical relationships, and boundary conditions needed to simulate the thermal mechanisms were defined.

To solve the transient heat conduction equation, HEATING requires values for the density (ρ), specific heat (C_p), and thermal conductivity (k_m) of each material comprising the casting assembly. In addition, the latent heats of transformation and fusion are required for uranium. Although some of these data had been defined during the first iteration, they were all redefined[5,6,7,8,9,10,11,12,13] for consistency and are summarized below.

1. The densities of each material are constant or vary only a few percent over the temperature range of interest. For this reason and because HEATING does not conserve mass, constant values were specified for each material. These were 1730, 240, 2000, 8954, 18400, 17050, and 21791 kg/m³ for carbon, Al_2O_3, firebrick, copper, solid and liquid uranium, and platinum respectively.

2. The thermal conductivities of all materials except firebrick are temperature dependent. A value of 1.04 W/m−°C was specified for firebrick, and the values defined for the other materials are summarized in Fig. 22.

3. The specific heats of firebrick and liquid uranium are essentially constant and values of 960 and 198.4 J/kg−°C were specified respectively. The remaining materials are temperature dependent, and these data are summarized in Fig. 23.

4. The latent heats of transformation and their corresponding temperatures for unalloyed uranium are −20.1 kJ/kg at 661°C and −12.3kJ/kg at 769°C. The latent heat of fusion is 38.72 kJ/kg at 1133°C.

27
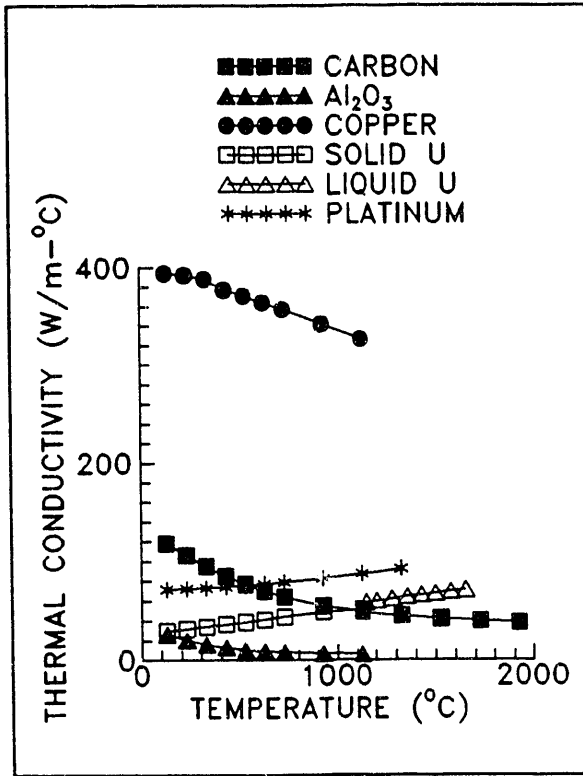
Fig. 22. Thermal conductivity data for carbon, Al_2O_3, copper, solid and liquid uranium, and platinum.
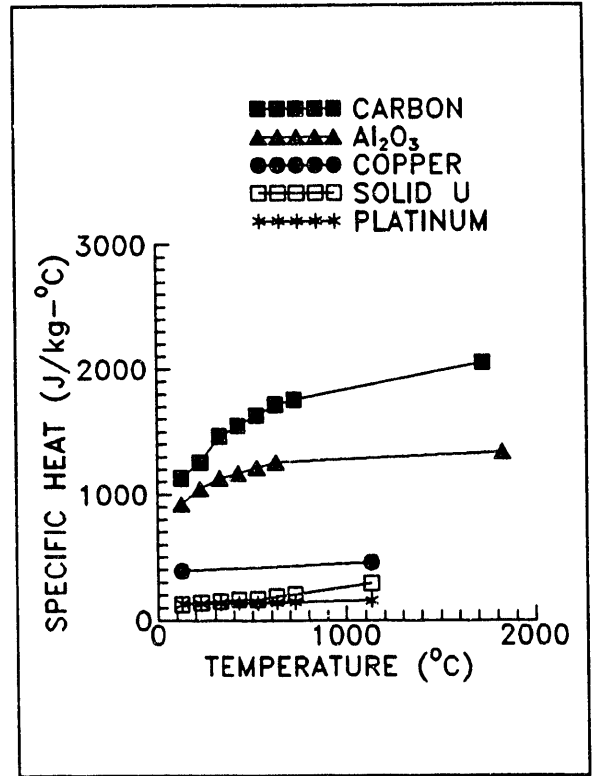
Fig. 23. Specific heat data for carbon, Al_2O_3, copper, solid uranium, and platinum.

Two additional liquid uranium properties are required to calculate natural convection heat transfer coefficients: viscosity (μ), and the volume coefficient of expansion (β). In addition, the dimensionless modulus Prandtl number Pr, is also required. A literature survey produced several sets of experimental data for uranium viscosity and these were evaluated to define a consistent set of values. Eventually, the results of Ofte[14,15] were adopted, and these data are summarized in Fig. 24.

The Prandtl number of a fluid is defined as

$$Pr = \frac{\mu C_p}{k_f} . \qquad (1)$$
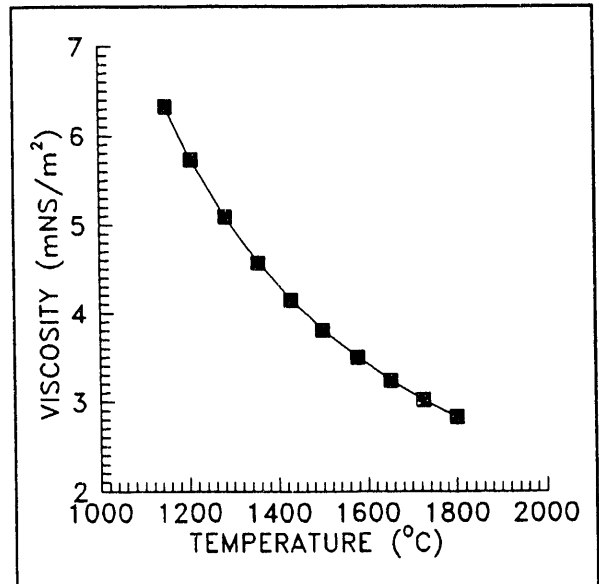
Fig. 24. Viscosity data for liquid uranium.

The viscosity data shown in Fig. 24 and the previously defined specific heat and thermal

conductivity were used to calculate the liquid uranium Prandtl number. These data are summarized in Fig. 25.

The volume coefficient of expansion is defined as

$$\beta = \left(\frac{1}{\rho}\right)\left(\frac{\partial \rho}{\partial T}\right)_P . \tag{2}$$

Liquid density data from Mulford[12] were used to evaluate Eq. (2), and the resulting values are summarized in Fig. 26. Because the coefficient does not vary much over the temperature range of interest, a constant value of 1.0×10^{-4} is used for all natural convection calculations.
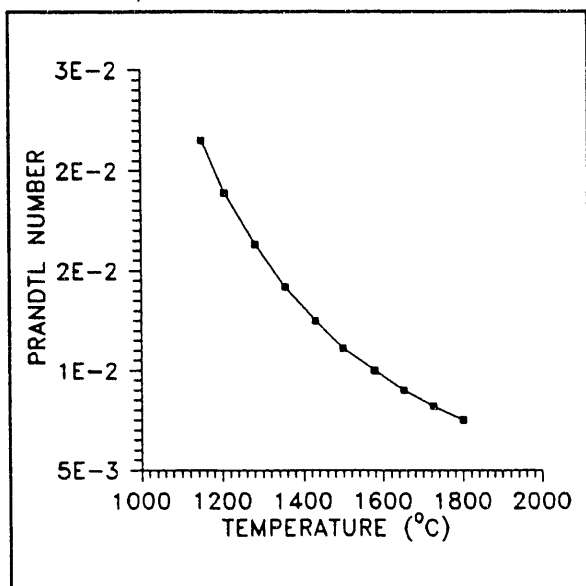
Fig. 25. Prandtl number for liquid uranium.
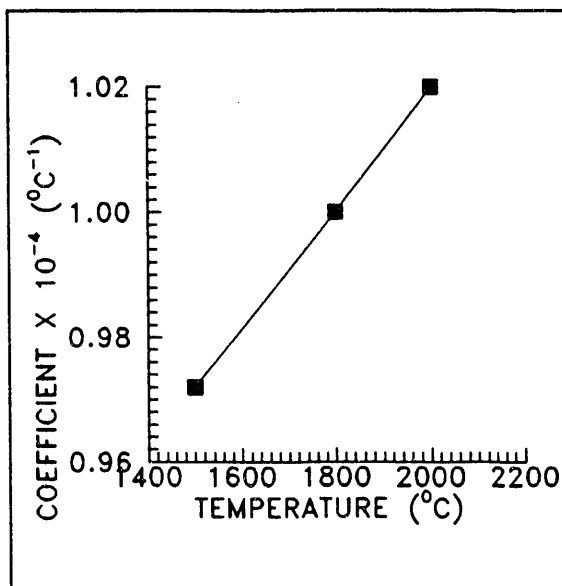
Fig. 26. Volume coefficient of expansion for liquid uranium.

Surface emissivities for each material were also defined. Constant values of 0.80 (ref. 16) 0.75 (ref. 10) and 0.37 (ref. 17) were specified for carbon, firebrick, and liquid uranium respectively. The emissivities of Al_2O_3 and copper are temperature dependent, and the available data are summarized in Figs. 27 and 28. These show the range of values given in the literature.[18,19] Average values were interpolated and/or extrapolated for use in the calculations. All the Al_2O_3 data, but only the STABLY OXIDIZED AT 1033 K copper data are used.

Radiation heat transfer occurs from exterior assembly surfaces to the pressure-vessel wall, between closely spaced components and the Al_2O_3 shield, as well as within the enclosures defined by the crucible interior and its top, the interior of the bookmold and the upper end cap, and the exterior of the bookmold, the upper and lower end caps, and the Al_2O_3 shield. With the exception of the enclosures, each of these mechanisms can be simulated to an acceptable degree of accuracy using a simple 1-D heat transfer coefficient. To accurately model enclosure radiation heat transfer, however, requires the use of exchange factors. These terms are a function of geometry and material surface emissivities and to calculate them for a discretized geometry with temperature dependent emissivities and two planes of symmetry is an extremely labor intensive and computationally demanding task. For these reasons and because
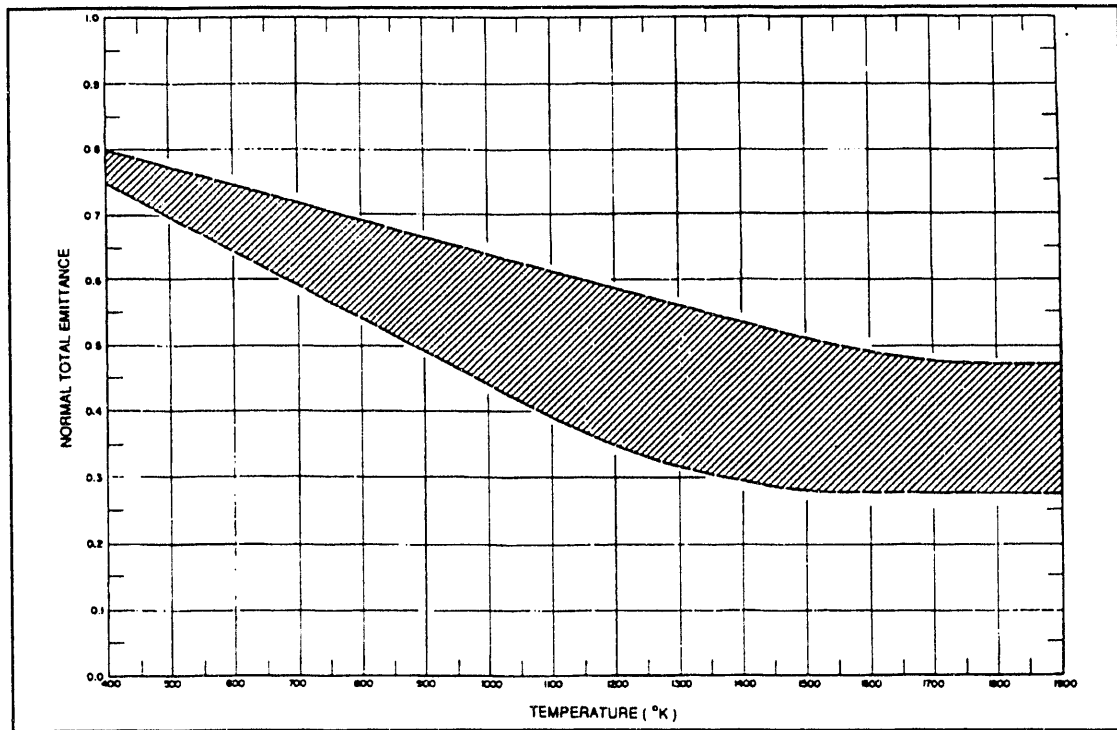
Fig. 27. Temperature-dependent normal total emittance for Al₂O₃.
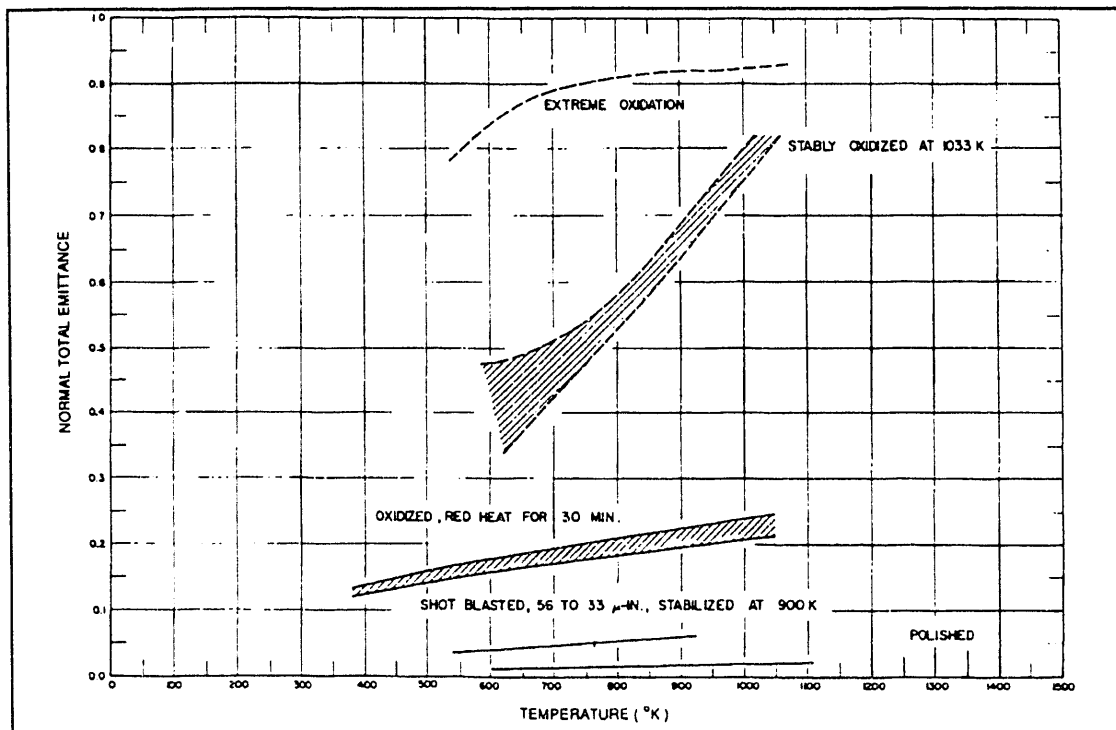
Fig. 28. Temperature-dependent normal total emittance for copper.

1.   the goal of the first-phase studies is to identify prominent mechanisms, and it is already known[20] that an accurate representation of radiation heat transfer effects is important in correctly modeling uranium solidification;

2.   exchange factors are geometry dependent, and it was felt the cartesian approximation would introduce considerable error; and

3.   necessary software was not currently available for the IBM RS/6000 computer,

it was decided that a rigorous treatment of enclosure radiation would be left for the second-phase effort. For the current studies the following relationship[10] is used to calculate 1-D radiant energy exchange between any two directly opposing, gray, diffuse surfaces:

$$h_r = \frac{\sigma}{\left(\dfrac{1}{\epsilon_1}\right) + \left(\dfrac{A_1}{A_2}\right)\left(\dfrac{1}{\epsilon_2} - 1\right)} \ , \tag{3}$$

where the subscripts 1 and 2 refer to the surfaces with the smaller and larger surface areas respectively. For radiation to a black body, Eq. (3) reduces to the product of the emissivity and the Stefan-Boltzmann constant:

$$h_r = \epsilon \sigma \ . \tag{4}$$

Thermal boundary layers resulting from buoyancy-induced fluid motion occur at all uranium-carbon boundaries, and accurately calculating the associated heat transfer coefficients is nontrivial. In external free convection, the ambient fluid is considered to be infinite, isothermal, and unaffected by the resulting buoyancy-driven flow. This assumption considerably simplifies any analysis because it permits one to independently specify conditions outside the boundary layer. In the crucible and bookmold *enclosures*, however, the flows between adjacent surfaces (i.e., the horizontal bottom and vertical walls) are coupled to each other and to the thermally stratified core region formed by the individual boundary layers. Furthermore, these interacting boundary layers cause regions of stagnant flow at those locations where surface orientations change. Consequently, pressure and buoyancy force terms must be retained in the governing equations. As previously explained, it is not possible to include these effects within the HEATING program. Also, there are no analytical relationships directly applicable to the crucible and bookmold configurations, and defining such relationships via a separate numerical study is beyond the scope of the first-phase studies. It was decided reasonable results could be obtained by applying heat transfer coefficients to each surface in the enclosure, where the value of the coefficient had been calculated using empirical correlations appropriate for external natural convection from that surface's orientation. These are an upward-facing horizontal flat plate for the bottoms of the enclosures and a vertical flat plate for the vertical walls. For external, steady-state, laminar flow over an isothermal, upward-facing flat plate in an infinite region of quiescent fluid, the average heat transfer coefficient is calculated[10] using

$$h_{nc,h} = (0.54)\left(\frac{k_f}{L_h}\right)\left(\frac{g\beta \, \Delta T L_h^3 \rho^2 C_p}{\mu k_m}\right)^{0.25} \ . \tag{5}$$

For these same conditions the average heat transfer coefficient for a vertical flat plate is calculated[10] using

$$h_{nc,v} = \frac{(0.67)\left(\frac{k_f}{L_v}\right)\left(\frac{g\beta \Delta T L_v^3 \rho^2 C_p}{\mu k_m}\right)^{0.25}}{\left(1 + \left(\frac{0.492}{Pr}\right)^{0.562}\right)^{0.444}} .$$ (6)

The induction heater induces a current in the crucible, upper end cap, and parts of the bookmold. The shield material is essentially transparent to the magnetic field, and field penetration (and therefore induced current) into the uranium at the coil frequency of 10^4 Hz is extremely small, on the order of 0.25 cm.[21] There are three basic options for calculating induced energy: an algebraic relationship for average (i.e., integrated over volume) power induced in a complete workpiece of extremely simple geometry, an algebraic relationship for energy induced at a particular X, Y, and Z location in an extremely simple geometry, and a numerical solution of the governing differential equations for an arbitrary geometry. A numerical solution was beyond the scope of the first-phase studies, and it was not possible to define a consistent set of relationships for energy induced at a point within the time allowed for model construction. Accordingly, a total average power approach was adopted with some slight modifications. An average power is calculated for a cylindrical workpiece, multiplied by the volume of interest (i.e., the volume of a particular assembly component) to get total power induced in the piece, and then 86% of this amount is uniformly applied across one *skin depth*. The average power induced in a cylindrical workpiece contained within a multiturn induction coil is calculated[22] using

$$P_{avg} = \mu \omega H_o^2 W(\xi) \Gamma^2 \zeta ,$$ (7)

where H_o is the strength of the magnetic field at the surface of a coil and at its axial centerline, and is defined as

$$H_o = \frac{NI}{2L} ,$$ (8)

$W(\xi)$ is the classical[23] power dissipation function and is defined as

$$W(\xi) = \frac{2}{\xi} \frac{M_1(\xi)}{M_0(\xi)} \cos(\theta_1 - \theta_2 - 0.5\pi) ,$$ (9)

and ξ is an evaluation parameter defined as

$$\xi = \frac{2r}{\delta} ,$$ (10)

where r is the workpiece outer radius, and δ is that distance where the induced power has dropped to 14% of its surface value (i.e., 1 *skin depth*). For the S. I. system of units, δ is defined as

$$\delta = 5.03 \sqrt{\frac{\rho}{\mu f}} \ . \tag{11}$$

The Γ and ζ terms in Eq. (7) represent magnetic field radial and axial attenuation respectively. The relationship used by Lavers and Biringer[22] to define axial attenuation was incompatible with the need to approximate induced energy at a point. Consequently Γ and ζ were dropped, and the generic field attenuation data[24] shown in Fig. 29 were used instead. This figure shows the ratio of field strength at a coil's surface and axial centerline to field strength at the surface of an arbitrary workpiece with a radius and length not equal to that of the coil. Although none of the data shown in Fig. 29 exactly matches the casting assembly geometry, Curve 6 is close and is used in the calculations.
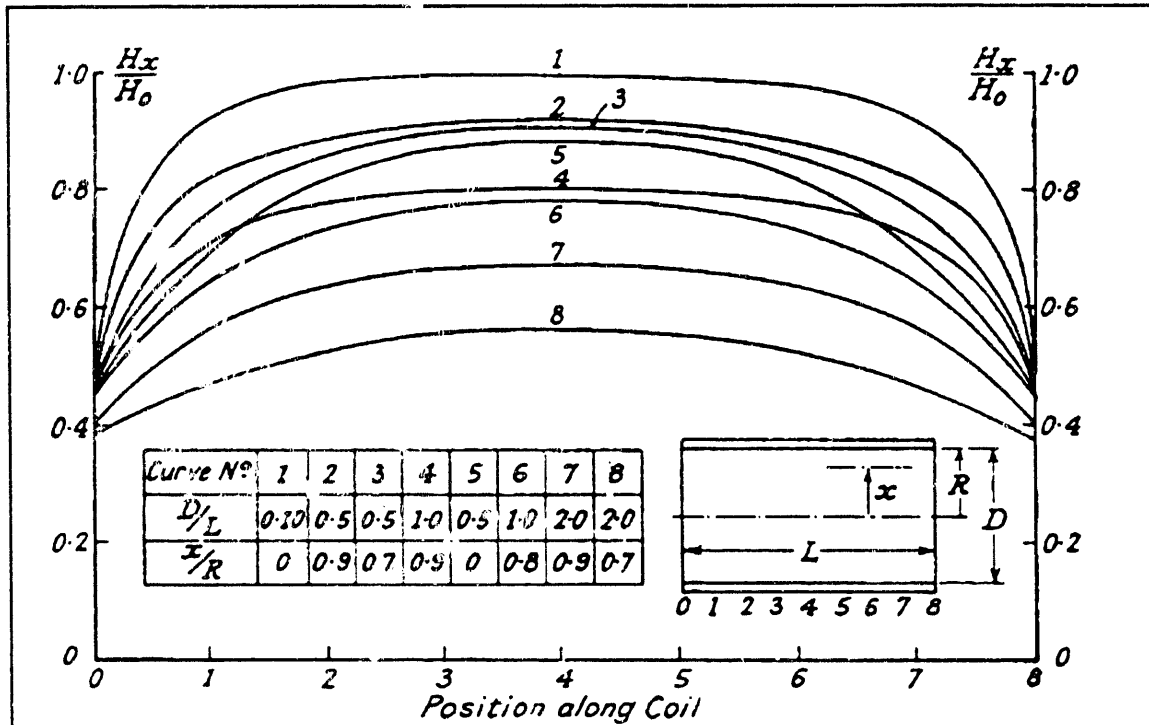
Fig. 29. Generic magnetic field radial and axial attenuation for short coils.

Forced convective heat transfer occurs from the interior of the coil to the cooling water. For turbulent flow in a constant cross-section circular tube with constant fluid properties and neglecting strong temperature gradients across the boundary layer, the heat transfer coefficient is calculated[10] using

$$h_{conv} = 0.023 \left(\frac{k_f}{D_i}\right) Re^{0.8} Pr^{0.40} \ , \tag{12}$$

where Re is the fluid Reynolds number and is defined as

$$Re = \frac{GD_i}{\mu} \quad and \quad G = \frac{\dot{m}}{A_{cs}} \ . \tag{13}$$

Thermal contact resistances occur at those locations where components touch and result from less-than-perfect mechanical contact. One-dimensional analytical relationships abound to calculate these terms, but selecting a particular equation requires a great deal of information about the material properties and surface characteristics of the individual components. Since most of this information was not available at the beginning of the numerical studies and could not be defined within the time allowed for model construction, it was decided initially to use a constant resistance appropriate for metal-to-metal contact in a vacuum and then define model agreement sensitivity to changes in the value. In this way a range of appropriate values (i.e., values that improved thermocouple agreement) would be available for use in selecting the most suitable analytical relationship for the second-phase study. Accordingly, a constant value of 2000 W/m^2–°C is utilized[25] for the base-case model.

An additional thermal resistance required is for the interfacial conductance between solidified uranium and the bookmold. Such terms are extremely system dependent, and no experimental data were available to make the required definition. It was decided to use the value from Rollett and Lewis,[20] which gave good model agreement for that particular uranium solidification analysis. Accordingly, a value of 0.5 W/m^2–°C is utilized for the base-case model.

The final relationship defined for the base-case model was included to mitigate some of the negative effects of the cartesian approximation. When a cartesian approximation of cylindrical geometries is used, it is often necessary to adjust the total heat capacities and surface conductances of the individual material regions. The total heat capacity is defined as the product of the density and specific heat: the goal is to make this product for a particular model volume equal to the product for the actual volume, that is

$$\left(\rho C_p\right)_{model} \left(Volume\right)_{model} = \left(\rho C_p\right)_{actual} \left(Volume\right)_{actual} \ . \tag{14}$$

If one chooses to adjust the heat capacity by modifying only the density (i.e., $Cp_{actual} = Cp_{model}$) then Eq. (14) can be rearranged to give

$$\rho_{model} = \rho_{actual} \left(\frac{Volume_{actual}}{Volume_{model}}\right) \ . \tag{15}$$

The material densities of all approximated cylindrical regions are adjusted using Eq. (15). The total conductance associated with a material's surface is defined as the product of the heat transfer coefficient and heat transfer surface area. As before, the goal is to equate the actual and modeled products. The modeled heat transfer coefficients are, therefore, defined as the product of the actual coefficient and the ratio of actual-to-modeled surface areas, that is,

$$h_{model} = h_{actual} \left(\frac{Surface\, Area_{actual}}{Surface\, Area_{model}} \right) . \tag{16}$$

At this point all the information needed to specify the base-case thermal model was available, and two HEATING input files were constructed: one to calculate the steady-state temperature distributions in the casting assembly prior to pour, and one that would use these distributions as initial conditions for the transient solidification analysis. A strictly numerical consideration that had to be addressed at this point was the choice of solution procedures. For the steady-state solution there are three options within the HEATING program: direct solve, successive overrelaxation, and conjugate gradient. The direct solution is not implemented for 3-D problems and there was concern that the conjugate gradient would be slow to converge given the problem's size, complexity, and highly nonlinear nature. Thus, the successive overrelaxation procedure was used. Choices for the transient solution procedure are more limited. For problems involving phase-change materials, HEATING must use an explicit time-integration procedure that is stable only so long as the time step meets certain criteria that are functions of discretized geometry and material properties. For a 3-D geometry the maximum time step for an interior node is defined as

$$\Delta t \leq \left[\frac{\displaystyle\sum_{i=1}^{8} Cp_i \rho_i V_i}{\displaystyle\sum_{m=1}^{6} \sum_{n=1}^{4} \frac{1}{L_m} k_{m,n} A_{m,n}} \right] , \tag{17}$$

where the numerator represents the sum of the heat capacities for the eight material volumes surrounding a particular node and the denominator represents the sum of the conductances between a particular node and its six neighbor nodes. A time step is calculated for each node in the problem using Eq. (17), and the minimum value in the set is used for the calculations. The time step limitation defined in Eq. (17) can, for some geometries and material properties, result in execution times (and therefore costs) becoming so great that the explicit procedure becomes impracticable. For these circumstances HEATING has the option of the Levy modification to the explicit procedure. The modification results in a stable solution procedure for any size time step so long as the discretized heat conduction equation for temperature at the $n + 1$ time step is defined as

$$T^{n+1} = T^n + \frac{1}{1+Z} \left\{ \frac{\Delta t}{C} \left[P^n + K_{l,m} \left(T_{l,m}^n - T^n \right) \right] + Z \left[T^n - T^{n-1} \right] \right\} , \tag{18}$$

where

$$Z = \begin{cases} 0 & , \dfrac{\Delta t}{(\Delta t_{max})} \leq 1 \\[4mm] 0.5 \left[\dfrac{\Delta t}{(\Delta t_{max})} - 1 \right] & , \dfrac{\Delta t}{(\Delta t_{max})} > 1 \end{cases} , \tag{19}$$

and Δt is the maximum step size defined in Eq. (17). Because it was felt that the geometry discretization used in the problem would result in very small time steps, the Levy modified explicit solution procedure was used for all transient calculations.

To summarize, the base-case steady-state and transient HEATING models have the following structure:

1. A 3-D, quarter-symmetric cartesian approximation of the complete experimental system; the heater coils, firebrick base, and three Al_2O_3 insulated platinum thermocouple junctions. In addition two uranium regions are also included: one inside the crucible and one inside the bookmold. Their dimensions were defined using the data from Run No. 892.

2. A successive overrelaxation solution procedure for the steady-state calculation and an explicit solution procedure with Levy's modification for the transient calculations.

3. S.I. units; watts (W), joules (J), meters (m), kilograms (kg), seconds (s), and temperature (°C). Specific properties were thermal conductivity in $W/m-°C$, specific heat in $J/kg-°C$, density in kg/m^3, heats of transformation and fusion in $J/kg-°C$, internal heat generation in W/m^3, fluid viscosity in $mN-s/m^2$, Stefan-Boltzmann as $5.67 \times 10^{-8} W/m^2-K^4$, and heat transfer coefficients in $W/m^2-°C$.

4. Temperature-dependent material properties, except for density where constant (with respect to (wrt) temperature) average values are used. In addition, two solid-solid and one solid-liquid phase changes are included for uranium. During steady-state analyses the uranium in the crucible is treated as a simply conducting phase-change region with liquid properties. During the transient calculation the uranium in the bookmold is treated as a simply conducting phase-change region with temperature dependent properties; i.e., liquid for those portions above melting temperature and solid for those below the melting temperature.

5. Adjusted heat capacities for those assembly components approximated with the cartesian geometry. The actual densities were adjusted using Eq. (15), and the specific heats were not modified. Components, actual densities, volume ratios, and adjusted densities are the following:

    a. carbon end caps: 1730 kg/m^3, 1.11, and 1920.3 kg/m^3;
    b. copper plates: 8954 kg/m^3, 2.12, and 18990 kg/m^3;
    c. Al_2O_3 shield: 240 kg/m^3, 3.38, and 811.2 kg/m^3;
    d. Al_2O_3 thermocouple insulation: 240 kg/m^3, 1.57, 376.8 kg/m^3; and
    e. platinum thermocouple junctions: 21791 kg/m^3, 1.57, 34212 kg/m^3.

6. Induction heater modeled with a modified total average power scheme.

    a. 0.86% of the total average induced power for a cylindrical workpiece is calculated and uniformly applied across one current penetration depth to the crucible, upper end cap, and upper part of the bookmold. The actual value is calculated at run time within a user-supplied subroutine* that reads the coil current from the HEATING input file, determines the axial location of the current node of

---

* User-supplied subroutines are a HEATING option that allow the user to override default procedures for calculating such terms as boundary temperatures, heat transfer coefficients, and/or internal heat generation.

interest, calculates a corresponding[†] value for the magnetic field intensity using a coil power frequency of 10,000 Hz and the information in Fig. 29, and then calculates a value for the heat generation rate using Eq. (7). In addition, the rate for the upper end cap is adjusted by the ratio of actual region volume to modeled volume: 1.11.

b. No internal heat generation in the Al_2O_3 shield, firebrick base, uranium, lower part of the bookmold, or lower end cap.

c. Coil cooling-water flow rate constant wrt time and equal to 7 gpm.[26]

d. Steady-state cooling-water temperature rise constant wrt time and equal to 6°C.[26]

e. Transient cooling-water temperature rise constant wrt time and equal to 1°C.[26]

f. Cooling-water inlet temperature constant wrt time and equal to 24°C.[26]

g. Pressure-vessel wall temperature constant wrt time and equal to 43°C.[26]

h. Internal heat generation for the copper plates calculated using a simple I^2R relationship and actual value equal to 4.938×10^1 w/m³ × I, where I is coil current. A user-supplied subroutine reads the HEATING input file for the coil current and then calculates a value for heat generation.

i. Internal heat generation at the base-case values for the first 15 s of the solidification transient.

7. Contact resistances using a constant (wrt temperature) coefficient of 2000 W/m²–°C and are applied between the crucible and crucible top, upper end cap and crucible, upper end cap and bookmold in both the vertical and horizontal orientations, lower end cap and bookmold in both the vertical and horizontal orientations, and lower end cap and firebrick.

8. *External* natural convection heat transfer from the following surfaces.

a. Crucible bottom and walls to liquid uranium during a steady state. Horizontal and vertical values calculated using Eqs. (5) and (6) and actual values are vertical h = 4.258×10^3 W/m²–°C and horizontal h = 1.415×10^4 W/m²–°C.

b. Bookmold bottom and walls to liquid uranium during transient so long as the fluid temperature at a node is above the melting point. Horizontal and vertical values calculated using Eqs. (5) and (6) and actual values are vertical h = 1.5778×10^4 W/m²–°C and horizontal h = 1.595×10^4 W/m²–°C.

9. Constant wrt temperature heat transfer coefficient applied across the gap separating the solidified uranium and bookmold vertical and horizontal walls when the fluid temperature drops below the melting point. Actual value used is 0.5×10^3 W/m²–°C. A user-supplied subroutine stores all the node pairs at the three uranium-carbon interfaces, determines the pair of nodes containing the current node of interest, and then assigns a value for the gap conductance based on the temperature of the node on the uranium side of the gap. For a node temperature above the melting point, a natural convection coefficient is used; below the melt temperature, the constant coefficient is used.

10. Forced convection heat transfer between interior surfaces of the copper flat plates and cooling water using Eq. (12) and actual value is h = 1.2931×10^4 W/m²–°C.

11. One-dimensional radiation heat transfer using Eqs. (3) and (4) applied at the following locations.

[†] Field attenuation was calculated using a single radial spacing, when in fact, there are three.

a. Between the top of the crucible uranium region and the bottom of the crucible top during steady state; nominal h = 1.889 × 10^{-8} W/m^2–°C and is a function of Al$_2$O$_3$ temperature. A user-supplied subroutine identifies a typical temperature in the crucible top, calculates a value for Al$_2$O$_3$ emissivity, and then calculates the coefficient.

b. Between the top of the bookmold uranium region and the bottom of the upper end cap during the transient analysis; nominal h = 1.920 × 10^{-8} W/m^2–°C and is constant wrt temperature.

c. From the upper surface of the crucible top to the pressure vessel wall; nominal h = 4.366 × 10^{-8} W/m^2–°C and is a function of Al$_2$O$_3$ temperature.

d. Between the crucible exterior walls and the Al$_2$O$_3$ shield; nominal h = 3.661 × 10^{-8} W/m^2–°C and is a function of Al$_2$O$_3$ temperature. The same user-supplied subroutine described above in *(a)* is used to determine shield temperature and calculate a value for the coefficient.

e. Between the Al$_2$O$_3$ shield and the first copper plate; nominal h = 1.797 × 10^{-8} W/m^2–°C and is a function of both Al$_2$O$_3$ and copper temperatures. A user-supplied subroutine determines the temperatures of the current copper and Al$_2$O$_3$ nodes of interest, calculates values for their emissivities, and then calculates the coefficient.

f. From the nonobstructed (i.e., above and below heater coils) portion of the Al$_2$O$_3$ shield to the pressure vessel wall; nominal h = 4.366 × 10^{-8} W/m^2–°C and is a function of Al$_2$O$_3$ temperature.

g. With respect to the Y/Z plane of the model shown in Fig. 21, a nominal, constant coefficient of 4.536 × 10^{-8} W/m^2–°C is applied to the following surfaces using a boundary temperature that is the average of the Al$_2$O$_3$ and pressure vessel wall temperatures:

- lower Y surface of that portion of the upper end cap directly facing the lower end cap,
- upper Y surface of that portion of the lower end cap directly facing the upper end cap,
- upper Z surface of the bookmold wall in the elevation between the top of the lower end cap and the lower edge of the Al$_2$O$_3$ shield, and
- upper Z surface of that portion of the lower end cap facing the pressure vessel wall.

A user-supplied subroutine receives the pressure-vessel wall temperature, calculates the average temperature of a subset of shield nodes, and then defines the average of the two values as the boundary temperature.

h. With respect to the Y/X plane of the model shown in Fig. 21, the same constant coefficient is applied to that portion of the bookmold wall below the Al$_2$O$_3$ shield, as well as the upper face of the lower end cap. The boundary temperature for these two locations is a weighted percentage of pressure vessel wall and Al$_2$O$_3$ temperatures: specifically, 75% of the pressure-vessel wall and 25% of the Al$_2$O$_3$. The same user-supplied subroutine described above determines the average temperature of a collection of Al$_2$O$_3$ nodes and then calculates the boundary temperature.

i.   From the bottom of the crucible to a boundary temperature defined from a nominal node in the bottom of the crucible top during the solidification analysis, from the lower surface of the crucible top to a boundary temperature defined from a nominal node in the bottom of the crucible during the solidification analysis, from the bottom of the bookmold to a boundary temperature defined from a nominal node in the lower surface of the upper end cap during the steady-state analysis, and from the lower surface of the upper end cap to a boundary temperature defined using a nominal node in the bottom of the bookmold during the steady-state analysis. These circuitous boundary conditions are required because the dual uranium regions preclude the use of straightforward *surface to surface* boundary conditions. A user-supplied subroutine defines the temperatures at the nominal nodes and then calculates the heat transfer coefficient.

j.   From the outer surface of the second copper plate to the pressure-vessel wall; nominal $h = 1.985 \times 10^{-8}$ W/m^2–°C and is a function of copper temperature. Also, from the firebrick base to the pressure-vessel wall; actual $h = 4.252 \times 10^{-8}$ W/m^2–°C and is constant wrt temperature.

12.   Adjusted surface conductances; the actual heat transfer coefficients were modified using Eq. (16). The locations, actual values, area surface ratios, and adjusted values are

a.   vertical crucible walls facing the uranium: 4.258×10^3 W/m^2–°C, 0.99, 4.215×10^3 W/m^2–°C;

b.   horizontal crucible walls facing the uranium: 1.415×10^4 W/m^2–°C, 1.01, 1.557×10^4 W/m^2–°C;

c.   vertical crucible walls facing the Al$_2$O$_3$ shield: 3.661×10^{-8} W/m^2–°C, 1.01, 3.698×10^{-8} W/m^2–°C;

d.   uranium surface facing the Al$_2$O$_3$ cover: 1.889×10^{-8} W/m^2–°C, 1.01 1.908×10^{-8} W/m^2–°C;

e.   upper end cap facing the Al$_2$O$_3$ shield: 3.661×10^{-8} W/m^2–°C, 0.807, 2.95×10^{-8} W/m^2–°C;

f.   lower end cap facing the pressure-vessel wall: 4.536×10^{-8} W/m^2–°C, 0.807, 3.66×10^{-8} W/m^2–°C;

g.   Al$_2$O$_3$ shield facing the copper plates: 1.797×10^{-8} W/m^2–°C, 1.78, 3.2×10^{-8} W/m^2–°C; and

h.   Al$_2$O$_3$ shield facing the pressure-vessel wall: 4.366×10^{-8} W/m^2–°C, 1.78, 7.78×10^{-8} W/m^2–°C.

The steady-state and transient models were then run to define a base-case transient response. The steady-state model was executed with a series of values for the coil current until the target uranium melt temperature of 1375°C had been calculated in the crucible. The resulting casting assembly 3-D temperature distribution was then used as initial conditions for the solidification transient. The transient analysis was limited to approximately 100 s of problem time to conserve computing resources. The size and complexity of the models, combined with the explicit solution procedure constraint, resulted in 40 h of RS/6000-320 machine time being needed to simulate 100 s of problem time. The results are shown in Fig. 30, and listings of the input files and user-supplied subroutines are included in Appendix A. As Fig. 30 indicates, the base-case model predicts the actual bookmold thermal response to within ±10%. Considering the relatively crude relationships used to model the thermal mechanisms, the many assumptions that had to be made concerning induction heater operation, and the detrimental influence of the cartesian

approximation on internal heat generation, region volumes and surface areas, this level of agreement is quite satisfactory.
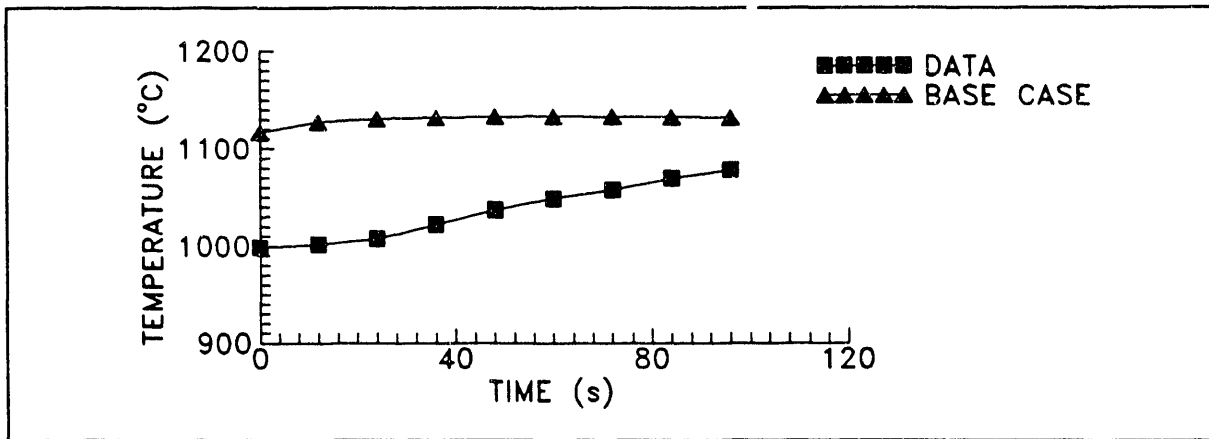
(a) top thermocouple
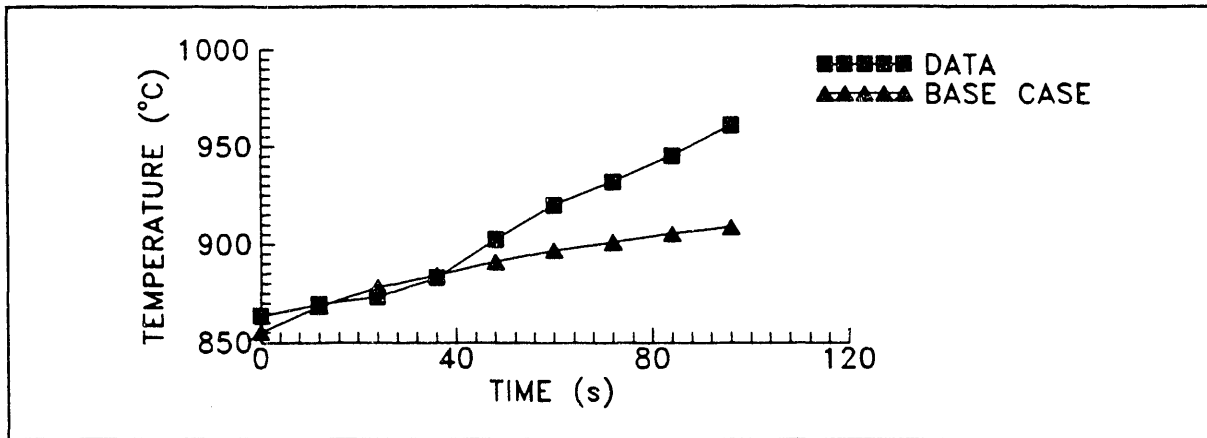
(b) middle thermocouple
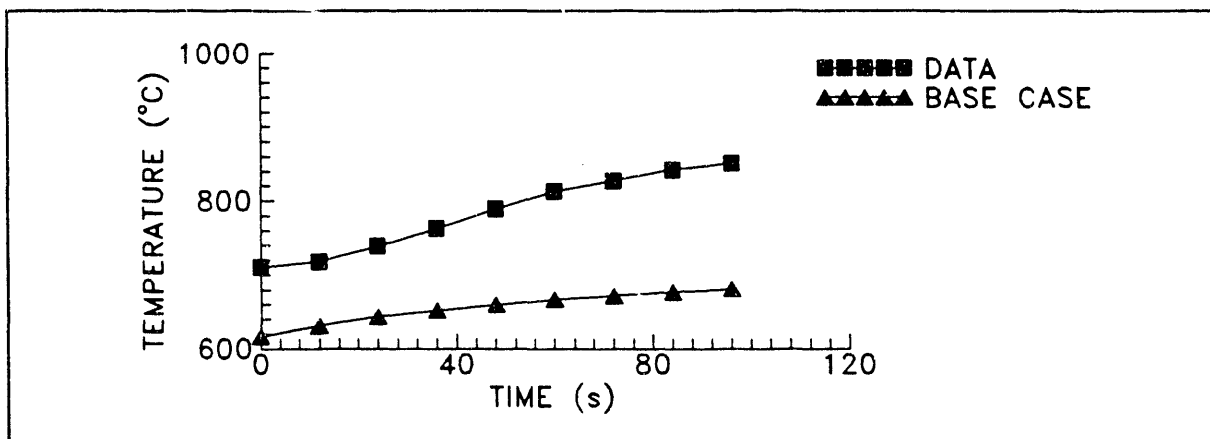
(c) bottom thermocouple

Fig. 30. Base-case HEATING model thermocouple agreement.

SENSITIVITY STUDIES

Twenty-one scenarios were examined to characterize the sensitivity of base-case thermocouple agreement. Even though the focus of the studies is the solidifying uranium region, the only direct measure of model performance is a comparison with experimental bookmold temperatures. For each scenario the variable of interest was changed from its base-case value, and a series of steady-state runs were made to determine the coil current that gave a uranium melt temperature of 1375°C in the crucible. The resulting casting assembly temperature distribution was then used as initial conditions for a 100-s transient solidification analysis. Each case is described in Table 1, and the results are summarized graphically in Figs. 31–41. Each figure shows typical experimental data (Run No. 892), base-case response, and study results at the three thermocouple locations. Also, the fraction of base-case current required to obtain the desired melt temperature is summarized in Table 1.

The most significant macroscopic observation is that the slopes of the transient responses closely match the experimental data. This match represents a considerable improvement from an earlier second-iteration study[27] that utilized a simplified thermal model. Typical (i.e., all thermocouple locations and variable values examined) results from the earlier study are shown in Fig. 42. This figure summarizes model agreement for the middle thermocouple for various values of pressure-vessel wall temperature, cooling-water temperature, cooling-water flow rate, and thermal contact resistance. As these data show, agreement is uniformly poor in both the absolute value of temperatures at a point and the slopes of the temperature transients. Therefore, all the thermal mechanisms must be included in the numerical model to some degree to obtain meaningful thermocouple agreement. This result was expected, but prudence dictated the effort to ensure that the more rigorous (and expensive) model was necessary.

As it concerns the prominence of individual mechanisms, these most current results indicate that model agreement is unaffected or only slightly sensitive to nominal changes in vertical thermal contact resistances between casting assembly components, heating coil cooling-water flow rates, pressure-vessel interior wall temperatures, enclosure radiation heat transfer, interfacial gap conductances between solidified uranium and the bookmold, magnetic field axial direction attenuation, and induced power distribution. With the exception of enclosure radiation, gap conductance, and power induced distribution, these results appear reasonable. Specific results and their implication on the structure of the second-phase thermal model are discussed below.

1. Pressure-vessel wall temperatures and cooling-water outlet temperatures resulting from changes in cooling-water flow rate represent sink temperatures for the solidifying uranium. Given that the uranium temperatures are quite large in comparison to all the sink temperatures examined in this study, one would not expect the overall temperature difference, and therefore model response, to change significantly. Accordingly, pressure-vessel wall and cooling-water temperatures should be included in the second-phase model, but only macroscopically. Each should be implemented as a constant (wrt time) value boundary temperature.

41

Table 1. Summary of variable values used in the sensitivity studies

Case	Description	Coil Current
1	Thermal contact resistance for all gaps decreased by 5.	1.29
2	Thermal contact resistance for all gaps increased by 5.	1.43
3	Thermal contact resistance for those gaps with a vertical orientation increased by 5.0.	1.41
4	Thermal contact resistance for those gaps with a vertical orientation increased by 10.0.	1.41
5	Heating coil cooling-water flow rate decreased by 30%.	1.41
6	Heating coil cooling-water flow rate increased by 30%.	1.41
7	Pressure vessel interior wall temperature decreased by 50%.	1.41
8	Pressure vessel interior wall temperature increased by 50%.	1.41
9	Natural convection heat transfer coefficients decreased by 50%.	1.41
10	Natural convection heat transfer coefficients increased by 50%.	1.41
11	Enclosure radiation approximation removed.	1.36
12	Interfacial gap conductance made equal to base-case natural convection coefficient.	1.41
13	Interfacial gap conductance made equal to base-case contact resistance.	1.36
14	Magnetic field axial direction attenuation decreased by 10%.	1.48
15	Magnetic field axial direction attenuation increased by 10%.	1.33
16	No internal heat generation during solidification transient.	1.41
17	Radiation heat transfer coefficient between crucible walls and Al_2O_3 insulating shield increased by 100.	1.58
18	Radiation heat transfer coefficient between crucible walls and Al_2O_3 insulating shield increased by 1000.	1.56
19	Heating coil estimated current decreased by 10%.	1.55
20	Heating coil estimated current increased by 10%	1.27
21	Distribution of induced power changed to an exponentially decaying rate applied across one current penetration depth.	1.18
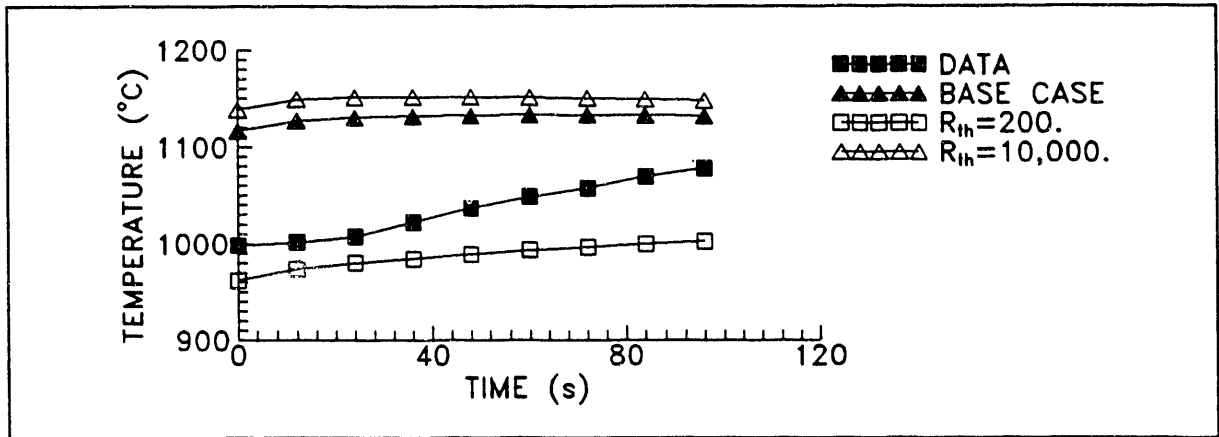
(a) top thermocouple location
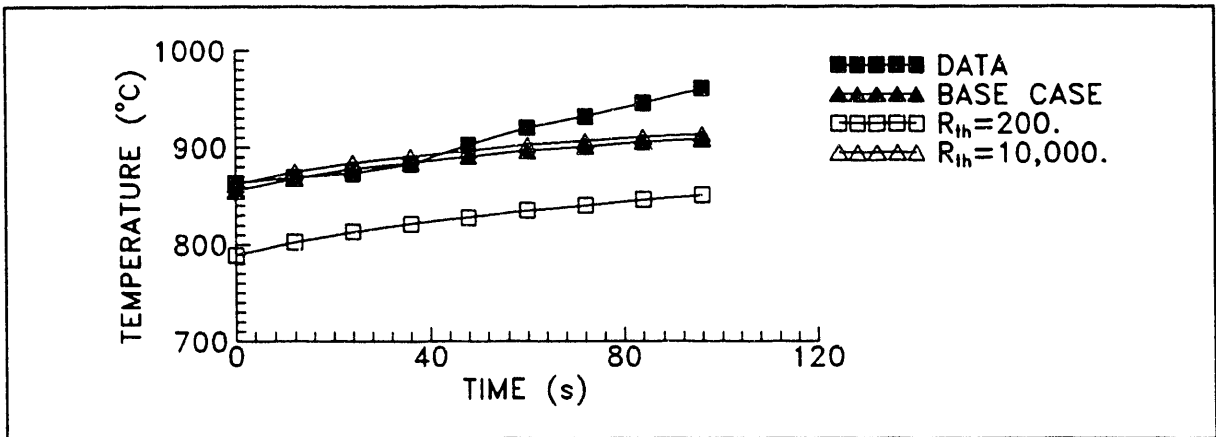
(b) middle thermocouple location

(c) bottom thermocouple location

Fig. 31. Model agreement for the cases where the vertical and horizontal thermal contact resistances (Rth) were increased and decreased by a factor of 5.
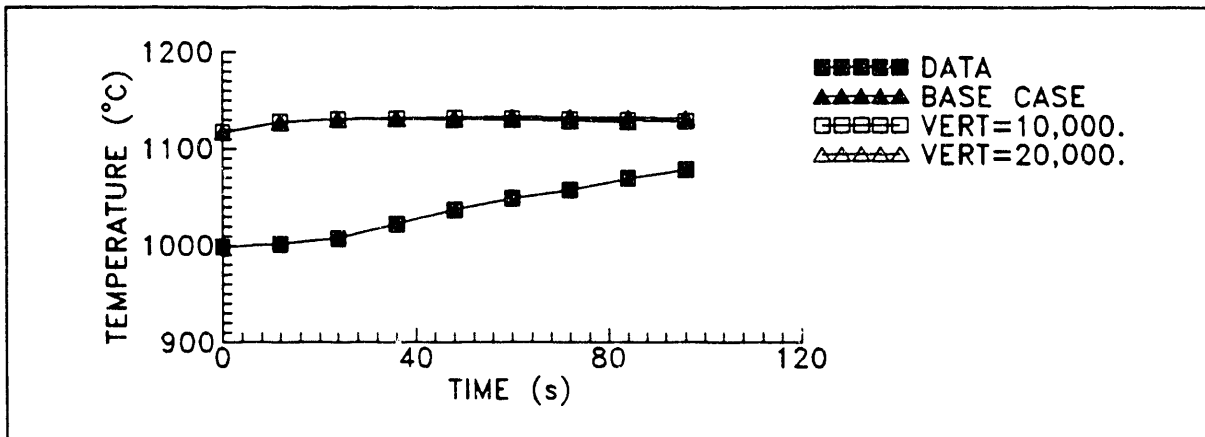
(a) top thermocouple location
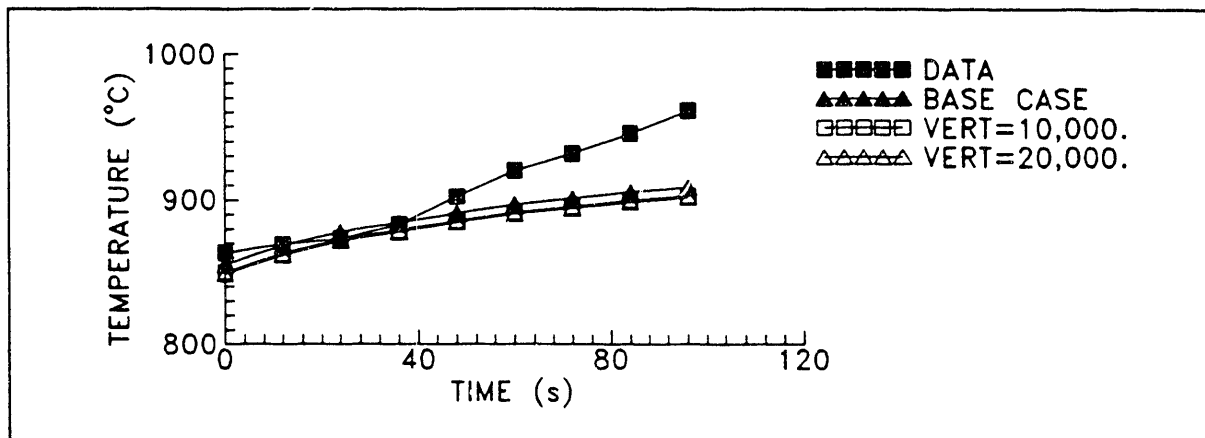
(b) middle thermocouple location
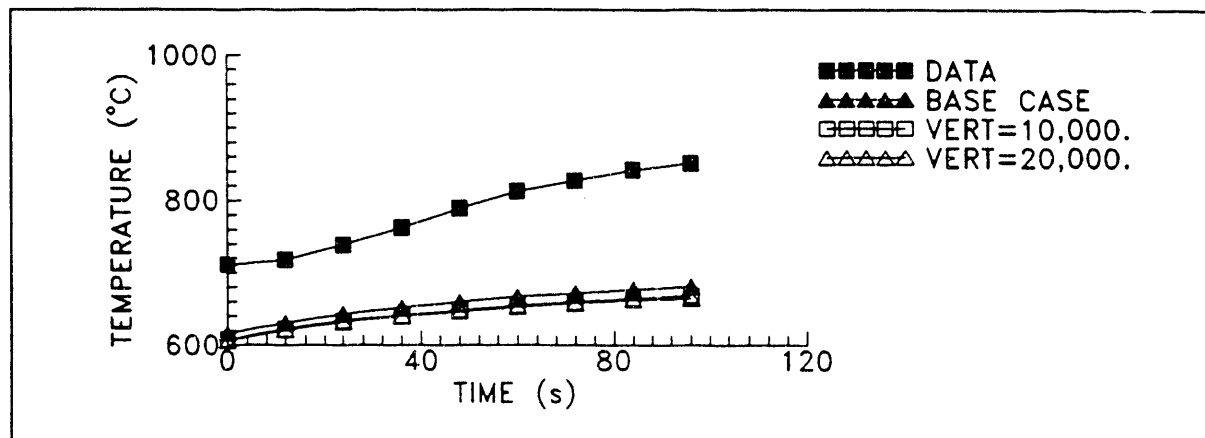
(c) bottom thermocouple location

Fig. 32. Model agreement for the cases where the vertical thermal contact resistances were increased by factors of 5 and 10.
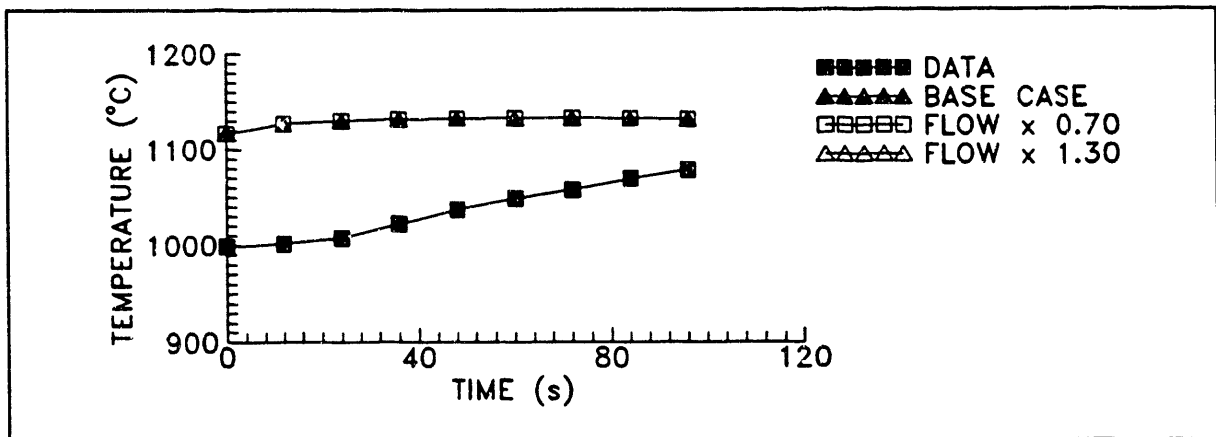
(a) top thermocouple location
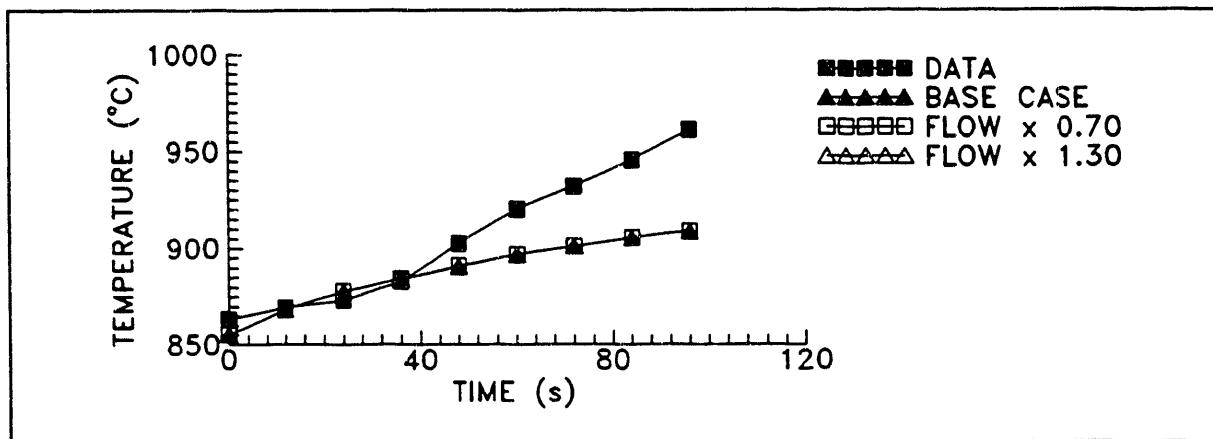
(b) middle thermocouple location
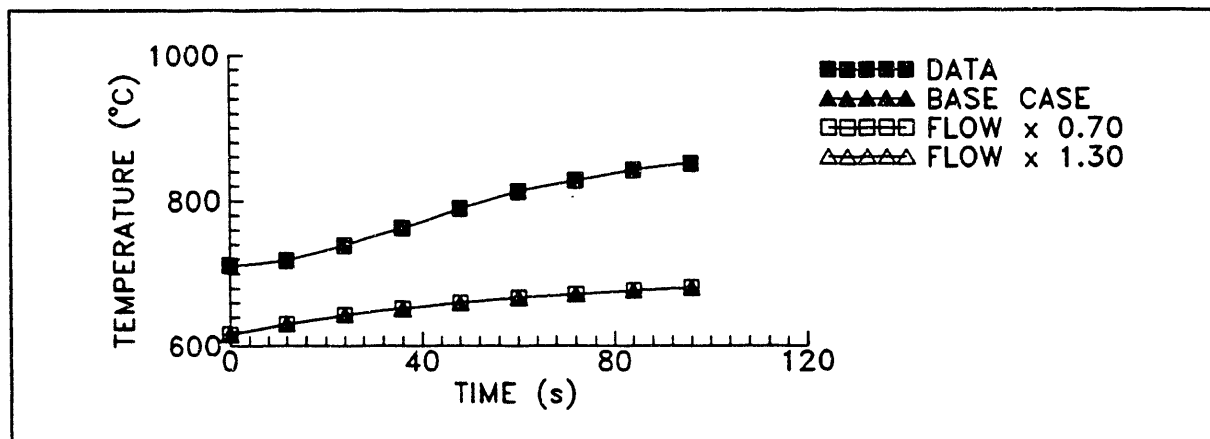
(c) bottom thermocouple location

Fig. 33. Model agreement for the cases where the heating coil cooling-water flow rate was varied by ±30%.
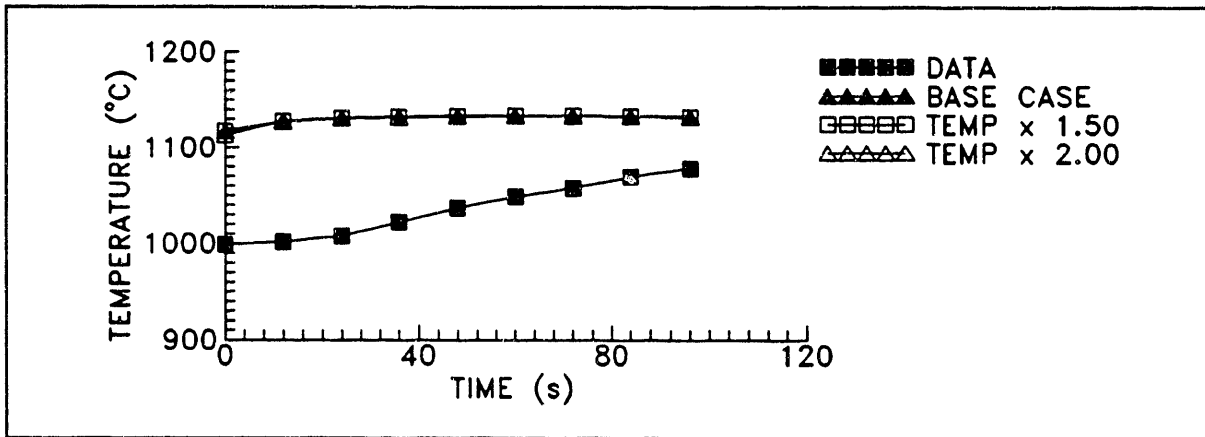
46

(a) top thermocouple location
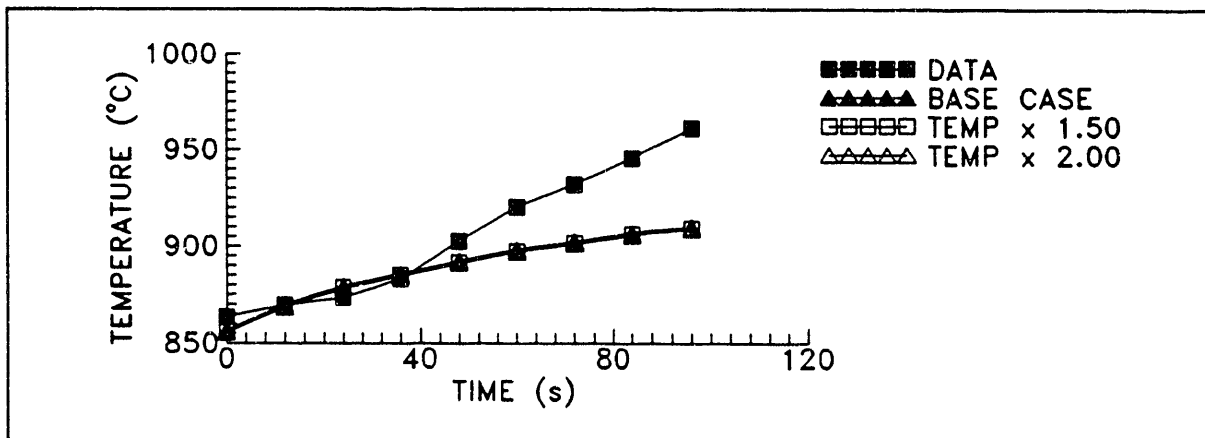
(b) middle thermocouple location
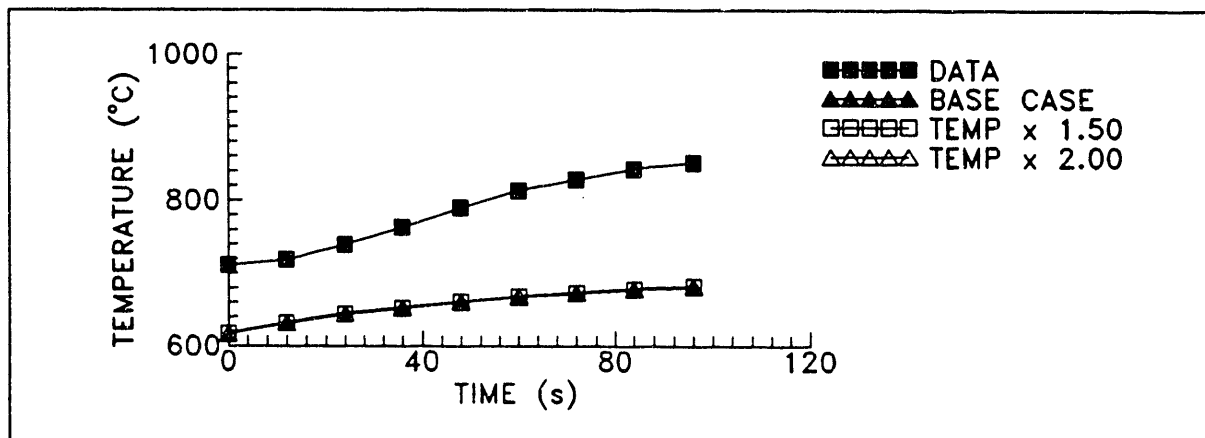
(c) bottom thermocouple location

Fig. 34. Model agreement for the cases where the pressure-vessel wall temperature was varied by ±50%.
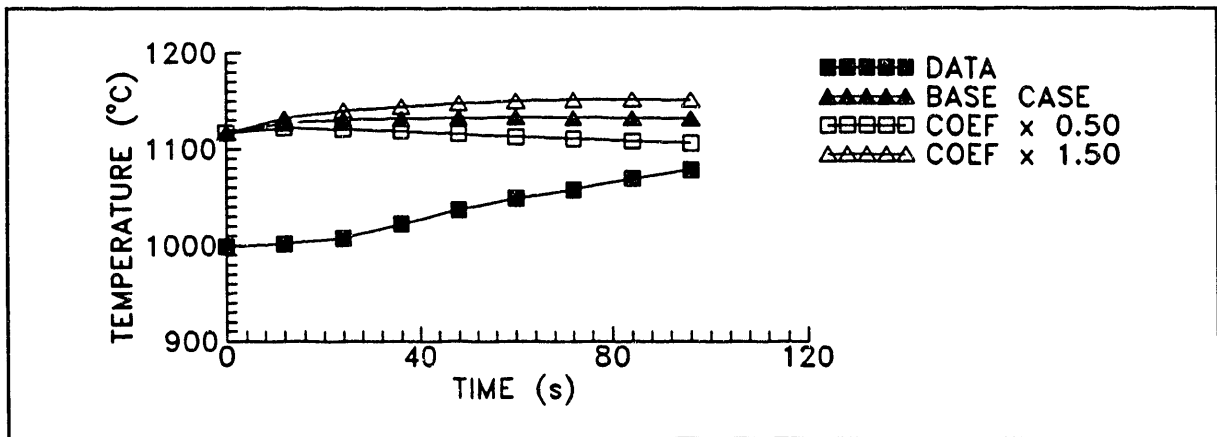
(a) top thermocouple location
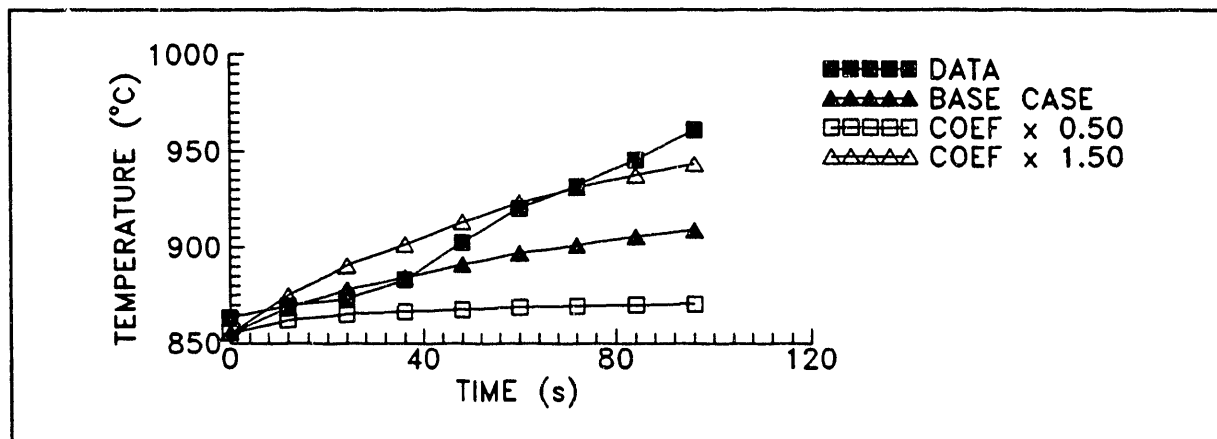
(b) middle thermocouple location
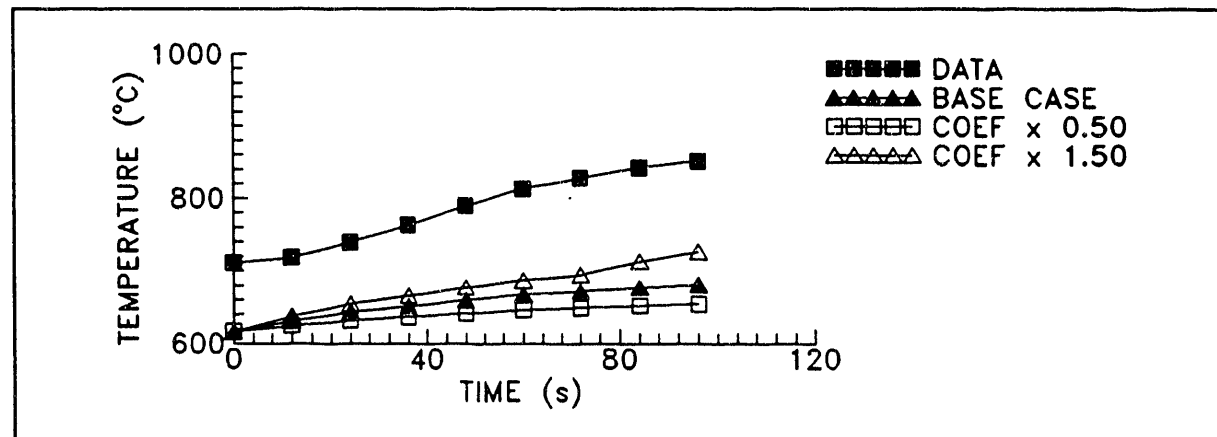
(c) bottom thermocouple location

Fig. 35. Model agreement for the cases where the liquid uranium natural convection heat transfer coefficients were varied by ±50%.
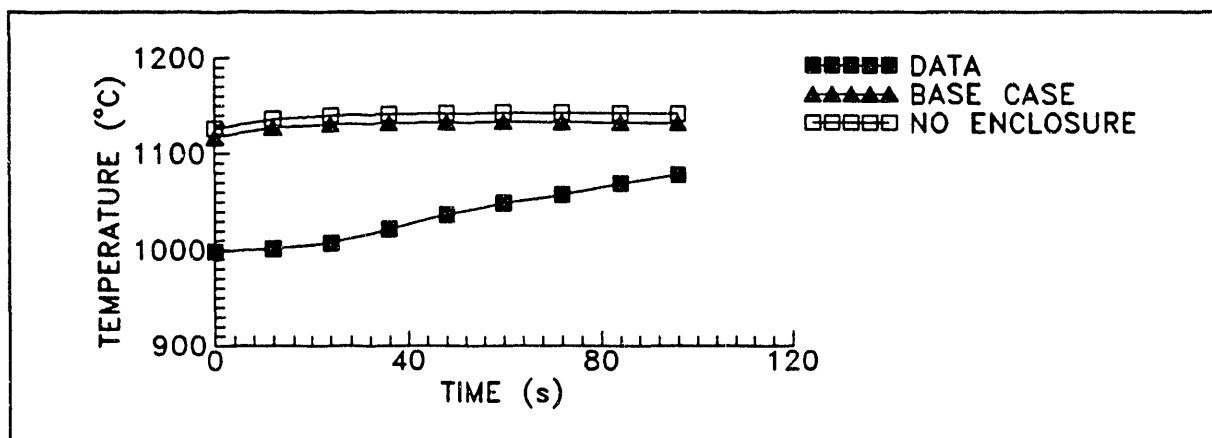
(a) top thermocouple location
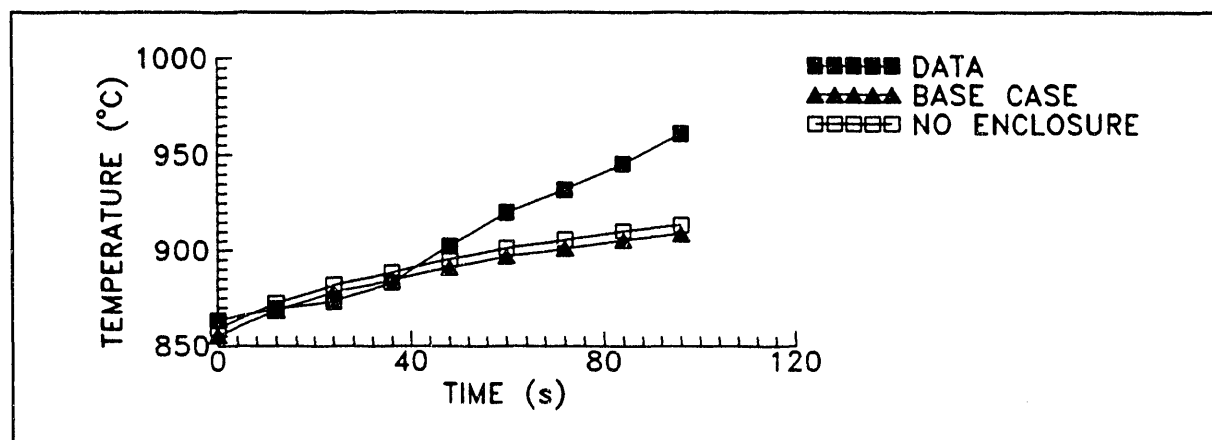
(b) middle thermocouple location
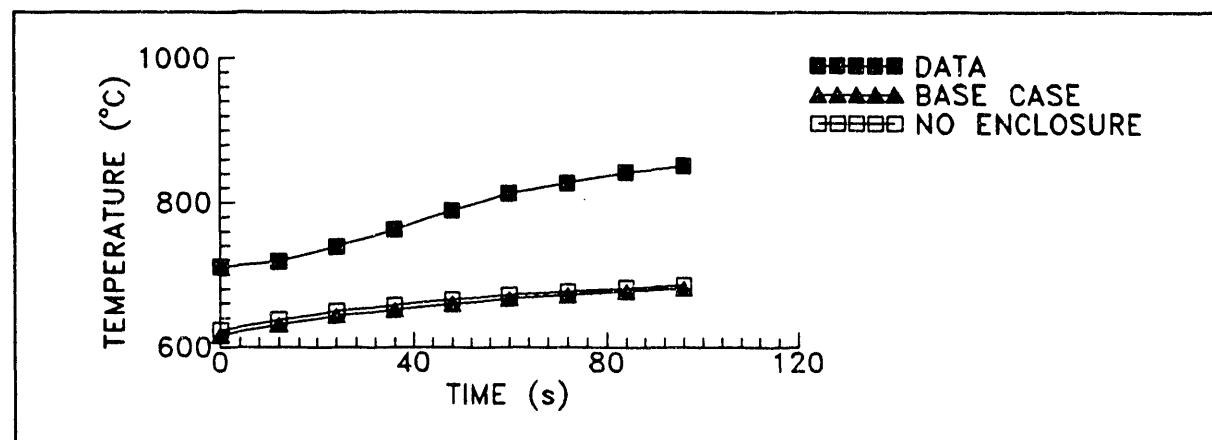
(c) bottom thermocouple location

Fig. 36. Model agreement for the case where enclosure radiation approximation was removed.
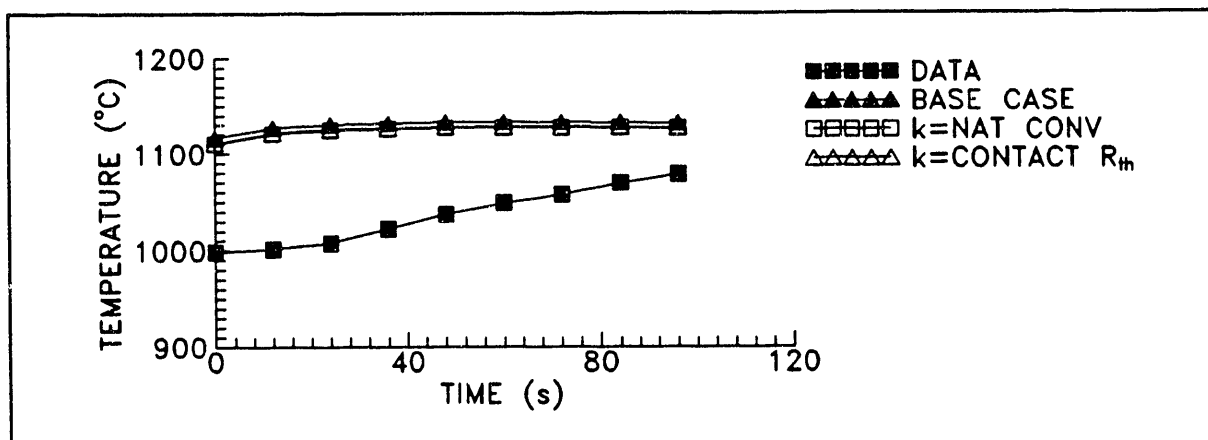
(a) top thermocouple location
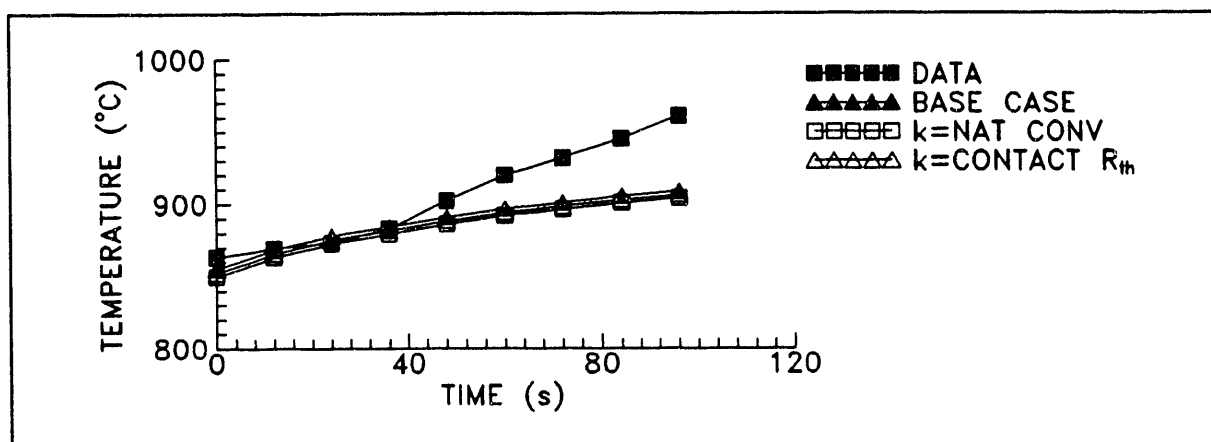
(b) middle thermocouple location
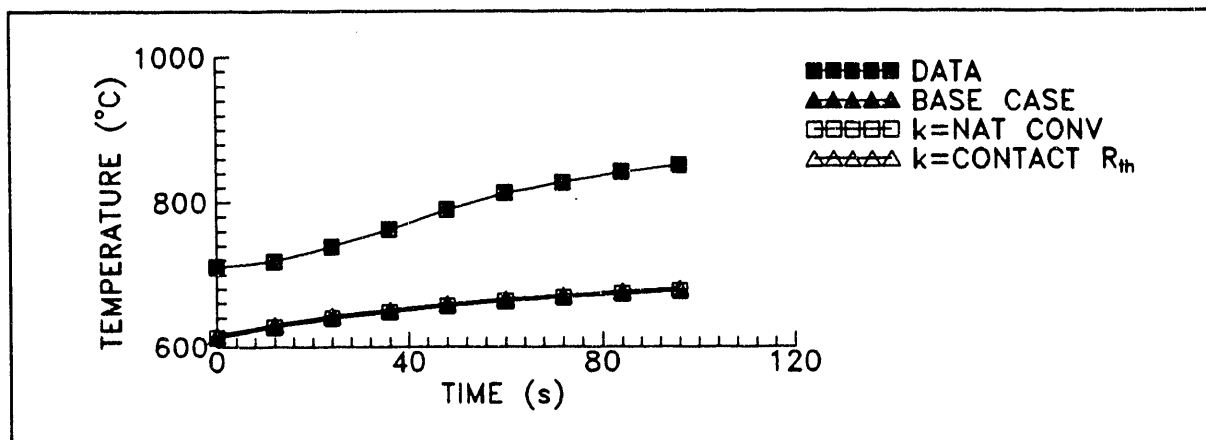
(c) bottom thermocouple location

Fig. 37. Model agreement for the cases where the solidified uranium-bookmold interfacial gap conductance was equal to the base-case liquid uranium natural convection heat transfer coefficient and thermal contact resistance.
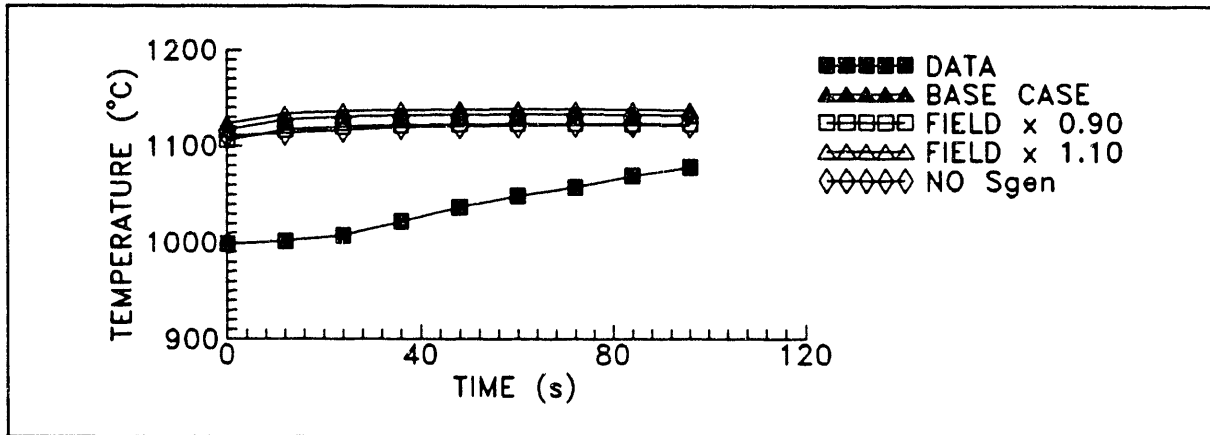
(a) top thermocouple location
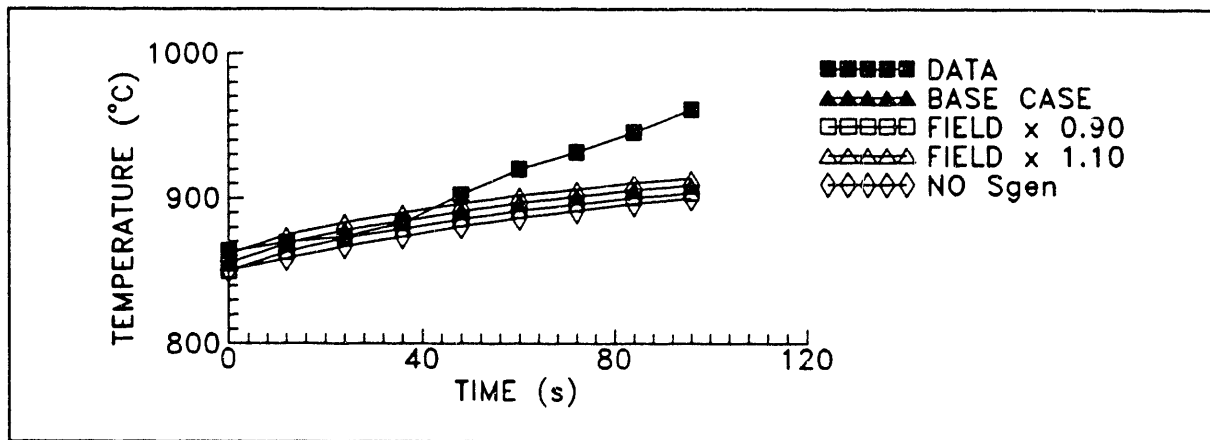
(b) middle thermocouple location
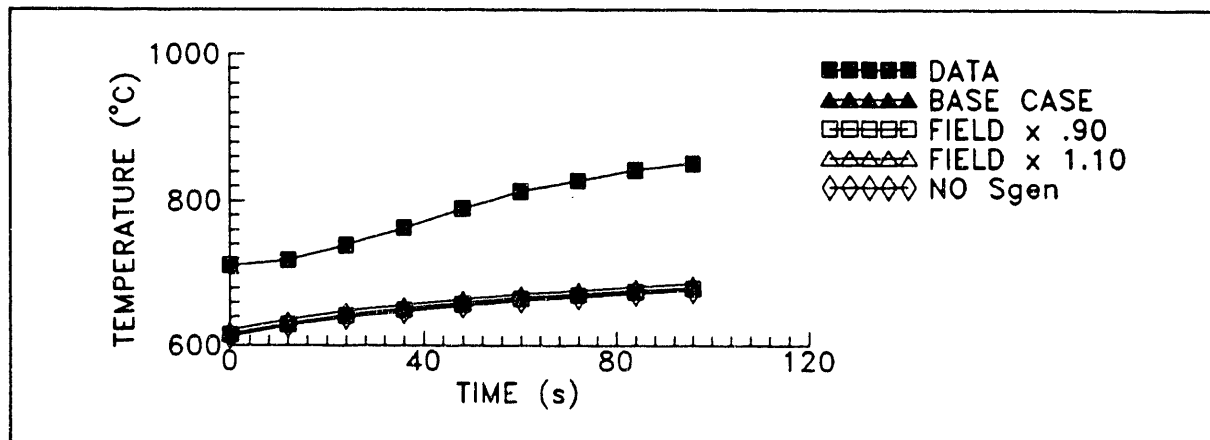
(c) bottom thermocouple location

Fig. 38. Model agreement for the cases where the magnetic field axial direction attenuation was varied by ±10% and where there was no internal heat generation during the solidification transient.
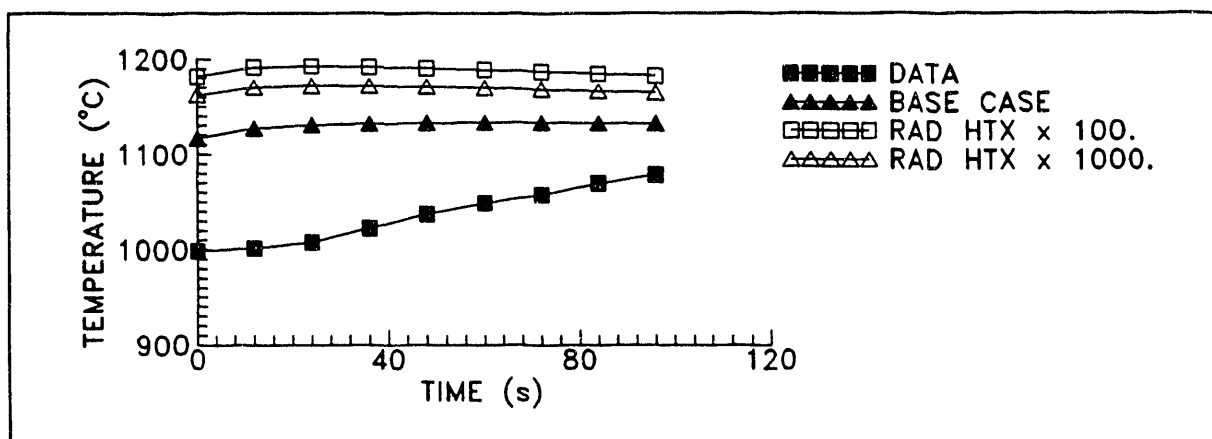
(a) top thermocouple location
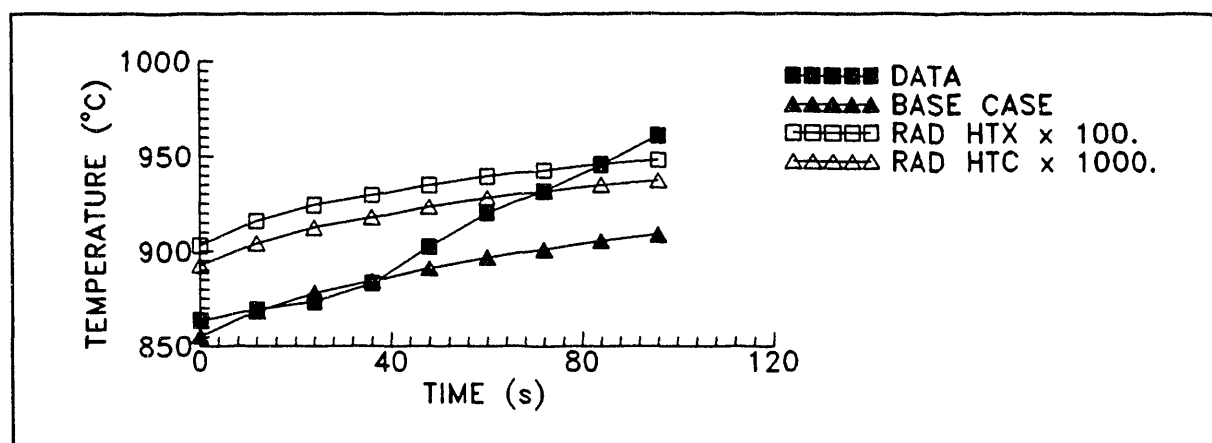
(b) middle thermocouple location

(c) bottom thermocouple location

Fig. 39. Model agreement for the cases where the radiation heat transfer coefficient between the vertical crucible walls and the Al_2O_3 shield was increased by factors of 100 and 1000.
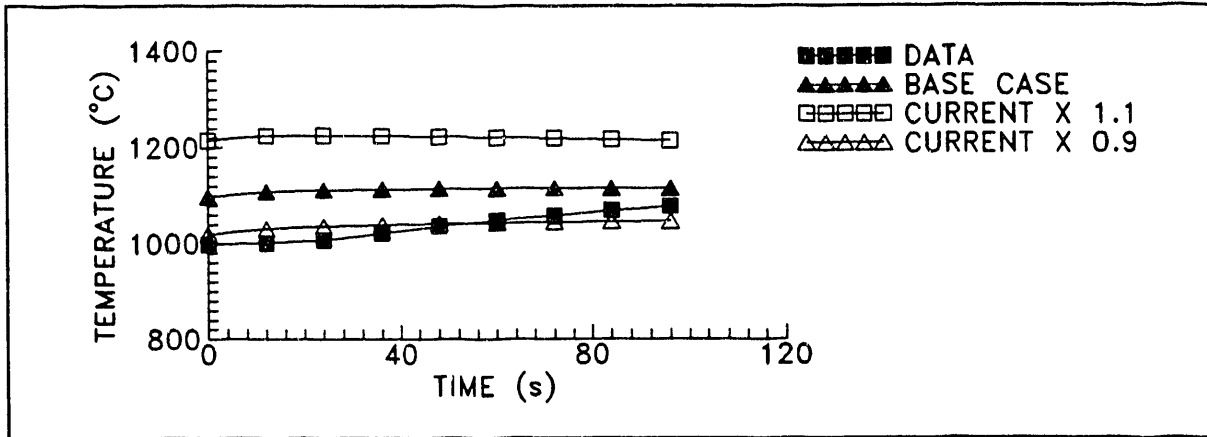
(a) top thermocouple location
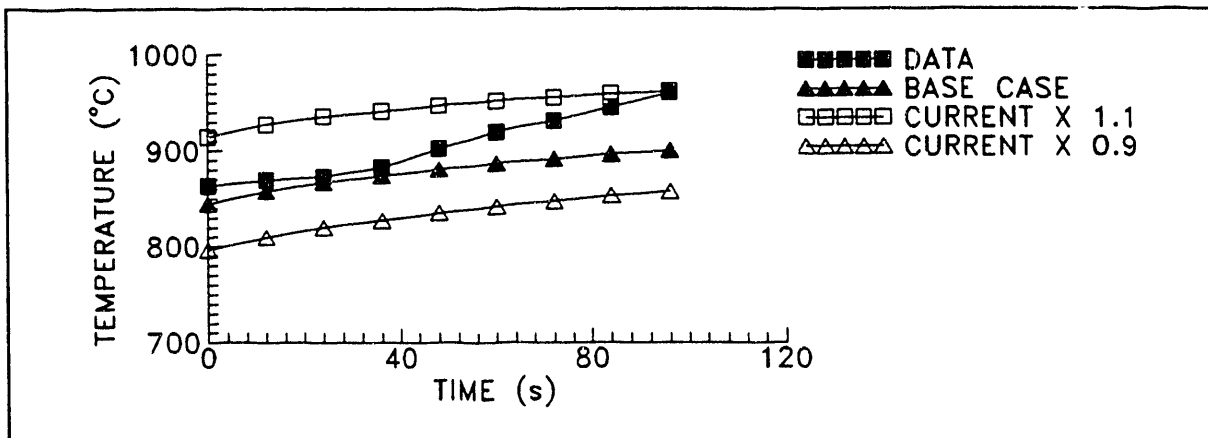
(b) middle thermocouple location
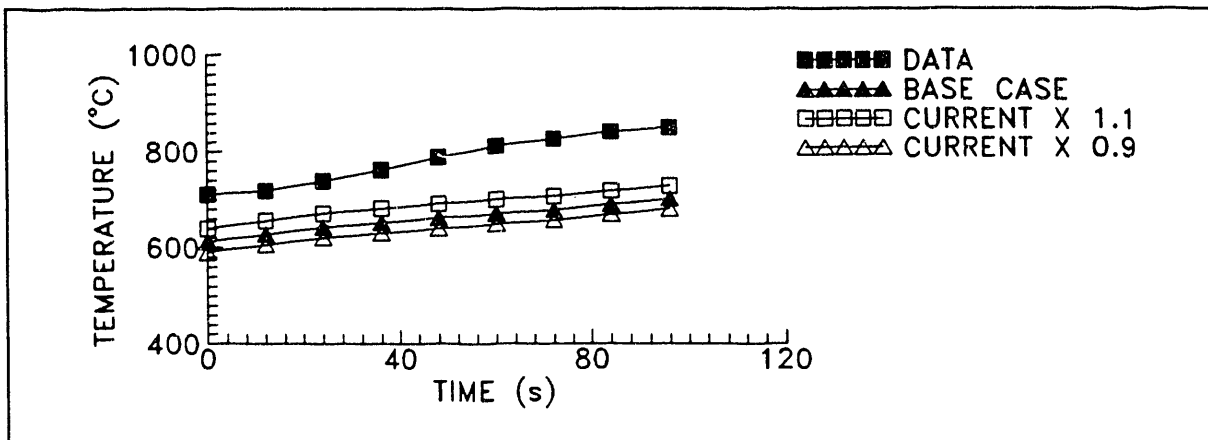
(c) bottom thermocouple location

Fig. 40. Model agreement for the cases where the heating coil current was varied by ±10 %.
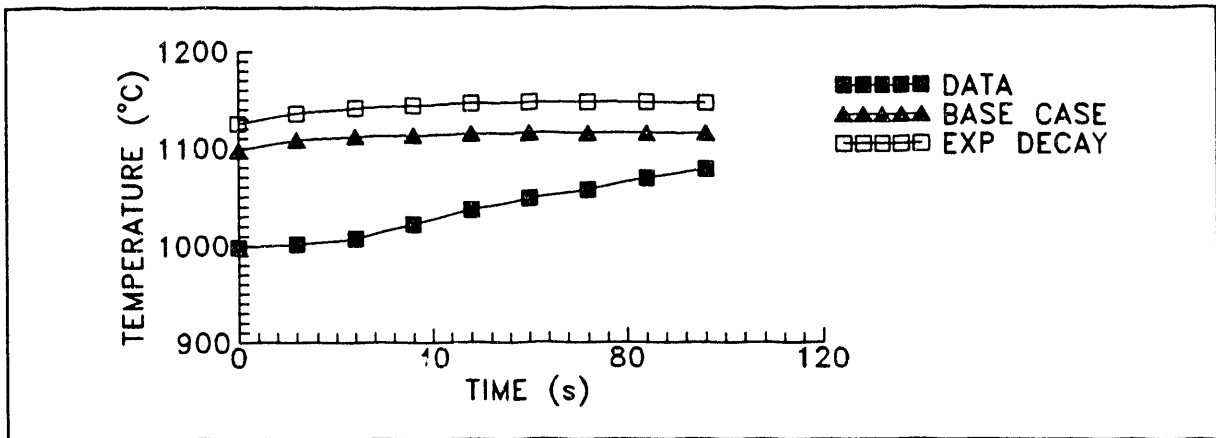
(a) top thermocouple location
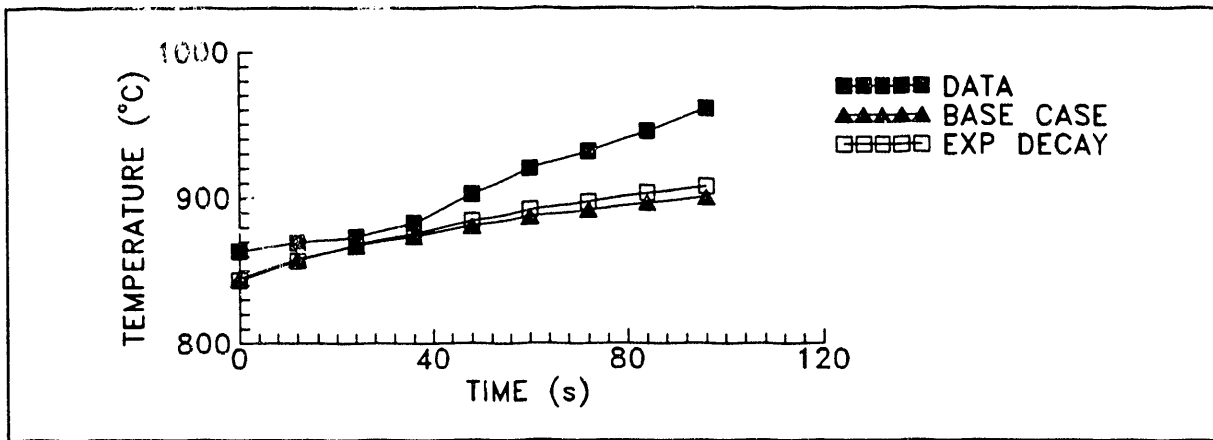
(b) middle thermocouple location
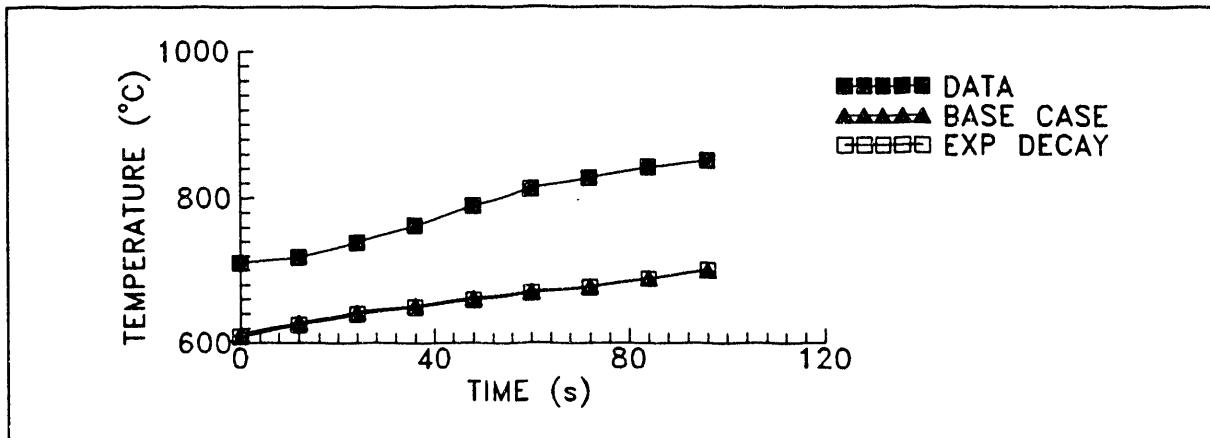
(c) bottom thermocouple location

Fig. 41. Model agreement for the cases where the induced power distribution had an exponential decay.
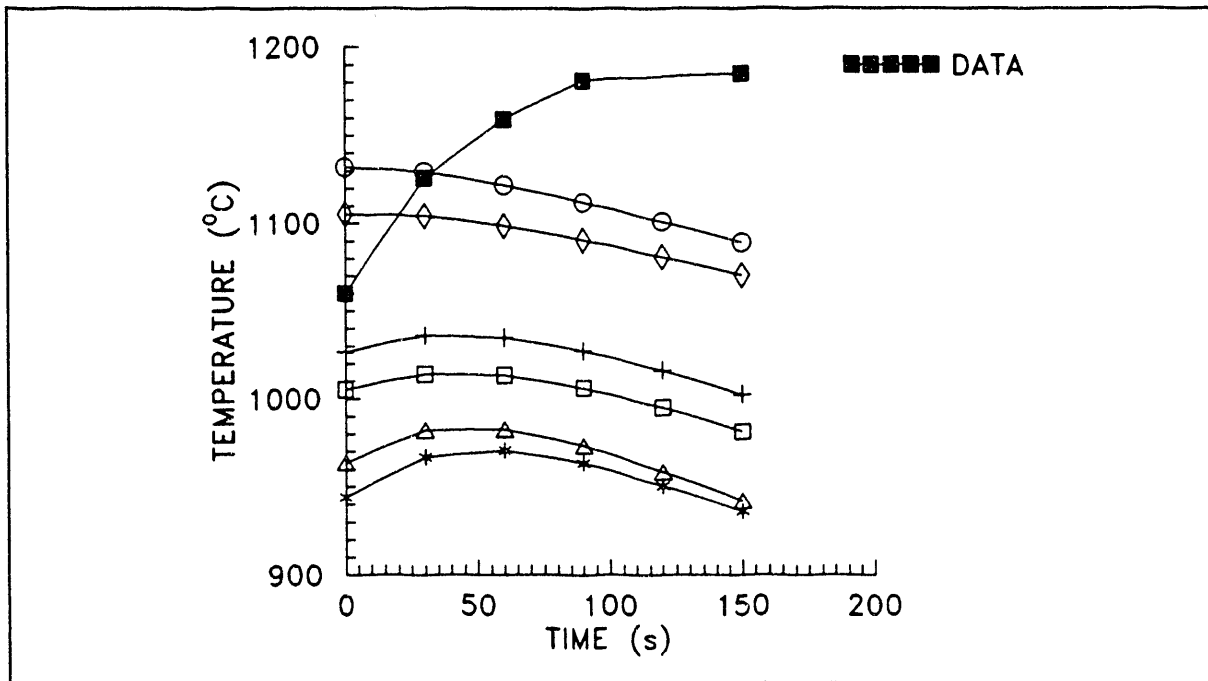
Fig. 42. Typical model agreement from the earlier sensitivity study for the middle thermocouple location for several combinations of pressure vessel wall temperature, contact resistance, water flow rate, and water inlet temperature.

2. The insensitivity to vertical contact resistances and the resistances due to cooling-water convective heat transfer coefficients is attributed to their relative magnitude compared with all the thermal resistances between the solidifying uranium and the temperature sinks, that is, liquid uranium convective heat transfer coefficient, material conduction, radiation heat transfer and/or thermal contact resistance between the casting assembly and the insulating shield, as well as between the shield and coils. Vertical contact resistances should be included in the second-phase model but only as accurately as the other contact resistances, and the forced convective heat transfer coefficient should be calculated with the same simple relationship used in this analysis and applied as a constant (wrt coil length) value boundary condition.

3. Removing induction heating during the early transient had a negligible effect on model agreement, and the result is believed to be real. It is conceivable, however, that some amount of prolonged induction heating or direct current (DC) magnetic field could be required to achieve the desired carbide transport. Thus, it would be prudent to include the mechanism in the second-phase model.

4. The observed insensitivity to gap conductance between solidified uranium and the bookmold is attributed to the fact that over the relatively short transient (approximately 100 s), only a fraction of the melt has solidified. Thus, only a small portion of the uranium's total surface area sees the interfacial conductance, too small an amount to influence the overall response. Because interfacial gap conductance has been identified as a prominent mechanism in the literature,[20] it should also be included in the second-phase model.

5. The negligible effect of removing the enclosure radiation heat transfer approximation is attributed to its relative crudeness. It did not include surface emissivities nor significant percentages of enclosure surface area. Again, because of its prominence in the literature, it should also be included in the second-phase model.

6. Changing the distribution of the induced power to an exponentially decaying function only slightly affected agreement at the top thermocouple location. It is noteworthy, however, that the fraction of heating coil current required to obtain the target melt temperature in the crucible dropped considerably. Whereas for most cases 40% more current was required than was estimated, changing the distribution to the more correct exponential decay resulted in only 18% excess current being required. From the perspective then of constructing an accurate stand-alone predictive second-phase model, the exponential distribution should be included.

Those mechanisms that had a prominent effect on thermocouple agreement and must therefore be accurately represented in the second-phase model were contact resistances, natural convection heat transfer coefficients, the value of the heat transfer coefficient between the vertical crucible wall and the insulating shield, and heating coil current. These results are believed to be real because specific effects resulting from changes in these variables are consistent with the physics of the problem.

1. Decreasing the thermal contact resistance between assembly components decreases the resistance to heat flow. Since steady-state thermal energy is internally generated, this reduction means the energy is more able to distribute itself among components. This manifests itself in smaller currents being required to give the same steady-state melt temperature in the crucible and lower steady-state and transient temperatures in the casting assembly. Similarly, increasing the contact resistance requires greater coil currents to achieve the same temperature in the crucible and gives larger overall temperatures.

2. Varying the liquid uranium natural convection heat transfer coefficient does not significantly affect steady-state temperatures but does influence the transient response. Within the context of this model, the convection coefficient represents a thermal resistance between the uranium and the local thermal sink. Decreasing the resistance by increasing the coefficient allows greater energy flows and higher overall temperatures. Increasing the resistance would, of course, have the opposite effect. The magnitude of the temperature change for a given variation is a function of the local *thermal environment* and will be discussed below.

3. Increasing the heat transfer coefficient between the crucible and insulating shield results in increased overall temperatures for both values examined. Increasing the rate of heat transfer from the crucible walls initially results in lower wall temperatures, and higher coil currents are required to compensate and maintain the desired uranium melt temperature. These increased currents cause the higher temperatures. The fact that the required current remains essentially the same (1.56 vs 1.58) for a large increase in heat transfer rate (1000 vs 100) is attributed to the relative size of the heat transfer coefficient/temperature difference product; increased heat transfer gives larger shield temperatures and smaller crucible/shield temperature differences, resulting in essentially the same total heat flow out of the crucible.

4. The effect of varying coil current is quite straightforward; increased amounts give higher rates of internal heat generation and correspondingly higher steady-state temperatures.

Note that the top and middle thermocouple locations experienced approximately the same change in temperature for a given change in current.

An additional observation is that for each of the prominent mechanisms the level of agreement varies between thermocouple locations and the transient response for each variation parallels the base-case response. This behavior is attributed to the location of the thermocouples relative to the casting assembly geometry and the heating coil magnetic field. These positions are illustrated in Fig. 43 and show that the thermal resistances surrounding each thermocouple vary with axial position.

1. The top location is bounded on the left by convection from the uranium and conduction through the bookmold; on the right by conduction through the bookmold, radiation heat transfer to the shield, and conduction through contact resistances to the upper end cap; on the top by conduction through the bookmold and conduction across contact resistances to the upper end cap and crucible; and on the bottom by conduction through the bookmold.

2. The middle location is bounded on the left by convection from the uranium and conduction through the bookmold; on the right by conduction through the bookmold and radiation heat transfer to the shield; on the top by conduction through the bookmold; and on the bottom by conduction through the bookmold.

3. The bottom location is bounded on the left by convection from the uranium and conduction through the base of the bookmold; on the right by conduction through the bookmold, conduction through contact resistances to the lower end cap, and radiation heat transfer to the pressure-vessel wall; on the top by conduction through the bookmold; and on the bottom by conduction through the bookmold and conduction through contact resistances to the lower end cap.

4. The lower boundary of the heating coil magnetic field is approximately located at the lower edge of the insulating shield. Thus, the bookmold region containing the bottom thermocouple is not internally heated.

5. Within the context of uranium regions being thermal sources, note that the position of the problem's source changes relative to the thermocouple locations between the steady-state and transient analyses. During steady state it is in the crucible, while during the transient analysis it is further down in the bookmold.

Because these localized *thermal environments* extend for several wall thicknesses into the width of the bookmold wall, it is believed they are responsible for the varying thermocouple agreement.

1. When coil current is varied the resulting temperature changes at the top and middle locations are about equal, but the change at the bottom is much smaller. Because the bottom thermocouple is outside the magnetic field, it is only heated by conduction from the internally heated regions. Thus, it is reasonable to expect smaller temperature changes at the bottom as thermal energy is diffused away from the hotter regions.

2. For the cases where contact resistances are varied, the magnitude of the steady-state temperature change from base-case values decreases from top to bottom with essentially no change at the bottom location; smaller currents are required for the lower resistance case and higher currents for the higher resistance case; middle temperatures for the lower resistance case are warmer than would be expected if only the coil current had been

changed; and middle temperatures for the higher resistance cases are cooler than would be expected if only the coil current had been changed. The varying temperatures at the middle location results from the value of the contact resistance; less gives more heat flow from the hot crucible region and warmer than expected temperatures in the cooler bookmold, whereas more resistance restricts heat flow from the hot crucible region, thus allowing localized energy within the bookmold wall to diffuse more and give lower than expected temperatures. The much lower temperature changes at the bottom location is again attributed to conduction effects from warmer regions.

3. When the liquid uranium natural convection heat transfer coefficient is varied, the steady-state temperatures are not affected, but the transient responses are and the magnitude of the change varies between thermocouple locations. During

Fig. 43. Thermocouple locations relative to the casting assembly geometry.

steady-state the liquid uranium is located in the crucible, and heat transfer to the thermocouples is a function of all the intervening thermal resistances. The insensitivity of the steady-state temperatures is attributed to the relative size of the natural convection coefficient. The size did not represent a significant fraction of all the resistances. During the transient analysis the uranium is located in the bookmold, and the relative size of the coefficient when compared with local conduction and radiation heat transfer at the exterior wall is such that it is a significant fraction of the total resistances. As the data in Fig. 35 show, the middle thermocouple's response is greater than either the top or bottom locations. The bookmold exterior wall in the vicinity of the middle thermocouple has a radiation heat transfer boundary condition, but the top and bottom locations have mixed radiation and conduction influences. When compared with these two classes of boundary conditions, the relative size of the convection coefficient (which is modeled as a constant along the interior bookmold surface) is such that it influences middle location response to a greater degree than either the top and bottom locations.

4. When the heat transfer rate between the crucible walls and insulating shield is varied, the resulting temperature change from base-case values increases for both heat transfer rates; the amount of the change for the top and middle locations is essentially equal; and the

temperature change for the bottom location is negligible. The equal temperature changes for the top and middle locations are attributed to the increased coil current. As we have seen, varying only the coil current gives equal temperature changes at these locations. The small change at the bottom location is again attributed to its location relative to the coil magnetic field and the diffusion of thermal energy away from the warmer regions.

This behavior indicates that an accurate representation of localized *thermal systems* is essential for improved thermocouple agreement. Macroscopically this means the second-phase model must contain an exact casting assembly geometry, as well as accurate mathematical models for natural convection heat transfer from the uranium, radiation heat transfer from exterior surfaces, and contact resistances between assembly components.

The second macroscopic trend observed for the four prominent thermal mechanisms is that the slope of their transient responses essentially parallels the base-case response, even when initial temperatures are different from base-case values. Because this trend is consistent for small and large initial temperature differences and because localized *thermal environments* strongly influence agreement, the behavior is attributed to the time-varying thermal resistances between the uranium and the two thermal sinks (i.e., the pressure-vessel wall and coil-cooling water). This result is interpreted as additional justification for requiring the second-phase model to have an exact physical representation and rigorous mathematical descriptions of the prominent mechanisms.

THERMAL MODEL MACROSCOPIC PERFORMANCE

Further insight into the physics of the problem was gained by examining base-case thermocouple agreement, uranium melt behavior, and casting assembly temperature distributions for the complete time period covered by the Run No. *892* experimental data. An additional reason for defining these data at this time is that they will serve as a benchmark for future model improvements. It is conceivable (and even likely) that past a point, continued model refinements will only affect thermocouple agreement and not the simulation of carbide transport. In the final analysis carbide transport and not thermocouple agreement is the subject of interest.

Base-case thermocouple agreement at the three thermocouple locations for the complete experimental transient is shown in Fig. 44. Melt behavior at 0, 60, 120, 180, 240, 300, 360, and 420 s into the transient is shown in Figs. 45−52 respectively. Each figure shows the bookmold uranium region from two perspectives. The left-hand side is from the plane of symmetry viewpoint; that is the same perspective as the left hand side of Fig. 21. The right-hand side shows the melt rotated approximately 180°; that is viewed from the bookmold surfaces immediately adjacent to the uranium. The color represents liquid and solid regions; red for those locations with temperatures above the melting point of 1133°C and blue for those below 1133°C. Temperature distributions for portions of the casting assembly at the same eight elapsed times are shown in Figs. 53−60. Each figure shows the uranium, bookmold, and end caps from the plane of symmetry viewpoint. The following observations are made.

1. Model agreement at each location during the extended period (i.e., past 100 s) basically parallels the experimental data but consistently has lower absolute temperatures. Again this is attributed to the incorrect modeling of time-dependent thermal mechanisms.

2. The uranium region completely solidifies between 6 and 7 min after pour and exhibits the overall directional solidification required for acceptable castings. However, there appears to be a slight meniscus at the solid-liquid boundary and it is not known at this point if it is real. It results from strictly thermal considerations: those portions of the uranium in contact with the bookmold experience higher rates of heat transfer due to its cooler temperature. It is conceivable that once CFD considerations are included the meniscus could disappear.

3. As it concerns temperature distributions in the casting assembly during a solidification transient, the largest gradient is in the Y direction, there are relatively small gradients in the X and Z directions, the upper portion of the assembly cools down during the transient while the lower portion heats up, and there is a significant temperature gradient along the height of the bookmold wall. The macroscopic energy flows are consistent with the physics of the problem and the structure of the base-case model. At steady-state the upper portion of the assembly is inside the heating coil and also contains the liquid uranium. The lower portion is outside the coil and can conduct to the firebrick. Thus, a strong axial direction gradient is to be expected. The macroscopic cooling trends in the assembly during the transient result from draining the uranium into the bookmold. This draining allows the crucible and upper-end cap to cool but causes the bookmold, lower-end cap, and firebrick to heat up. The most noteworthy results are the distributions in the bookmold. Specifically, the small X and Z direction gradients and the large Y direction gradient. The small X and Z gradients are attributed to the essentially uniform boundary conditions in those directions. These boundary conditions also influence the magnitude of the Y direction gradient. This particular gradient must be accurately

modeled for two reasons: it influences melt-behavior including carbide transport, and the value at the bottom of the bookmold influences the quality of the casting.[20]   It is conceivable that once enclosure radiation and accurate contact resistances are included, the uniformity will be lost. The problem will become more *two-dimensional*, and the Y-direction gradient will be severely affected.

Again, these results reinforce the need to model problem physics as accurately as possible.
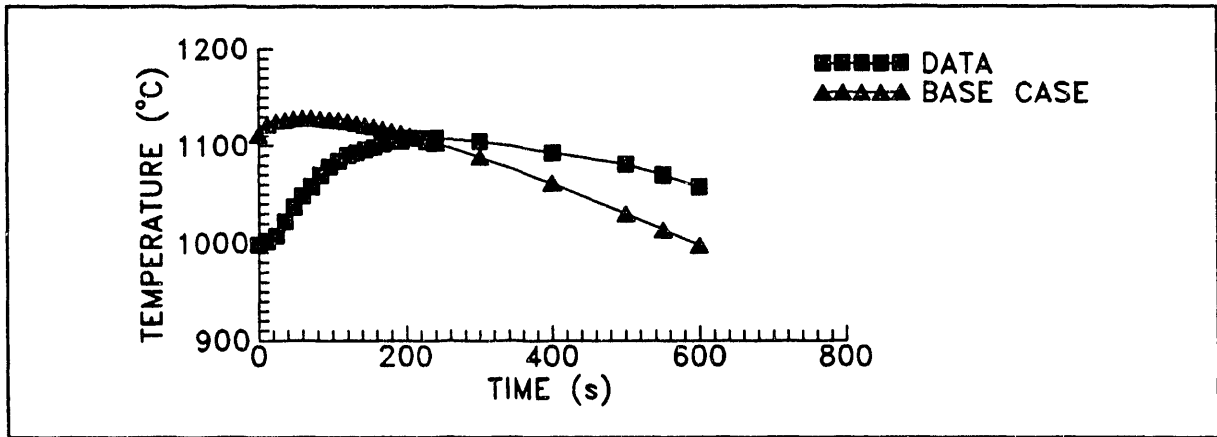
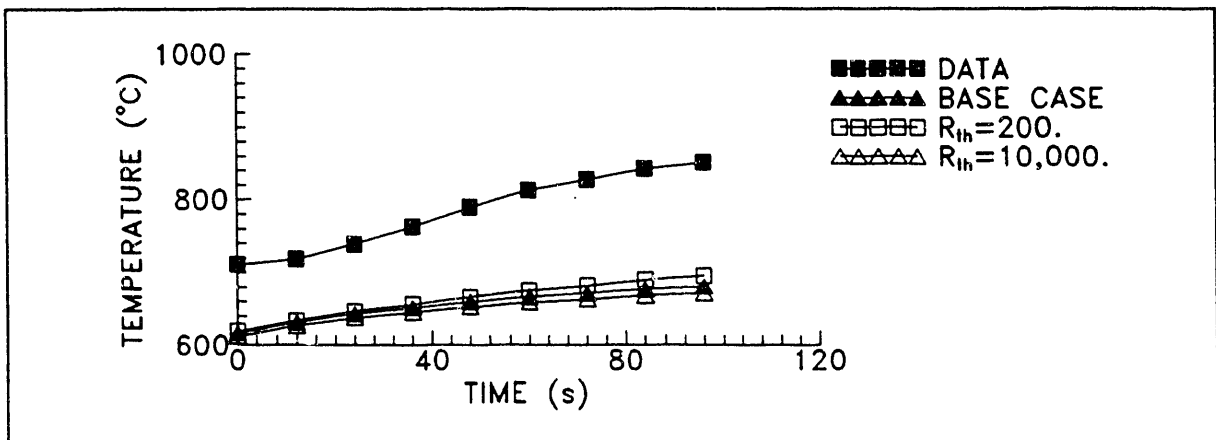(a) top thermocouple location
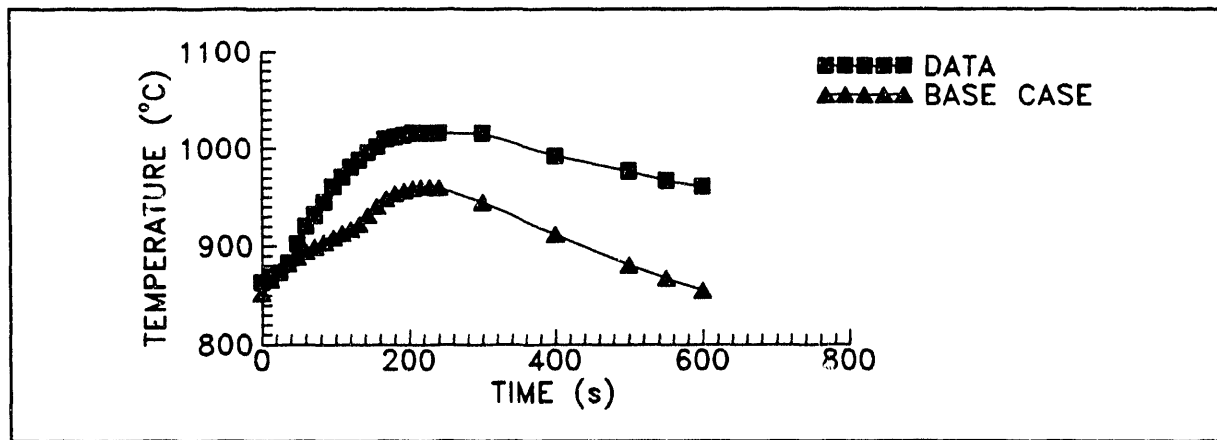
(b) middle thermocouple location
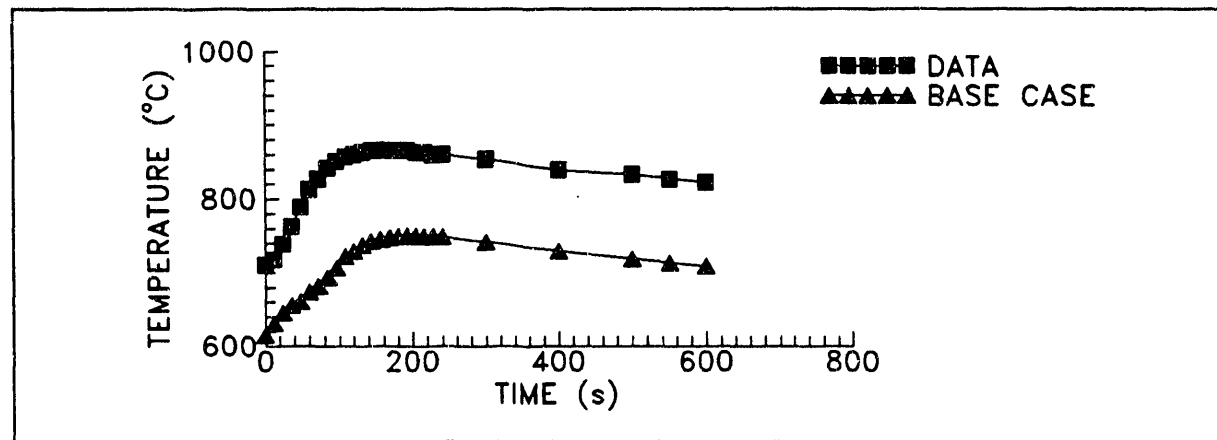
(c) bottom thermocouple location

Fig. 44. Base-case model agreement for the complete time period covered by experimental run 892.
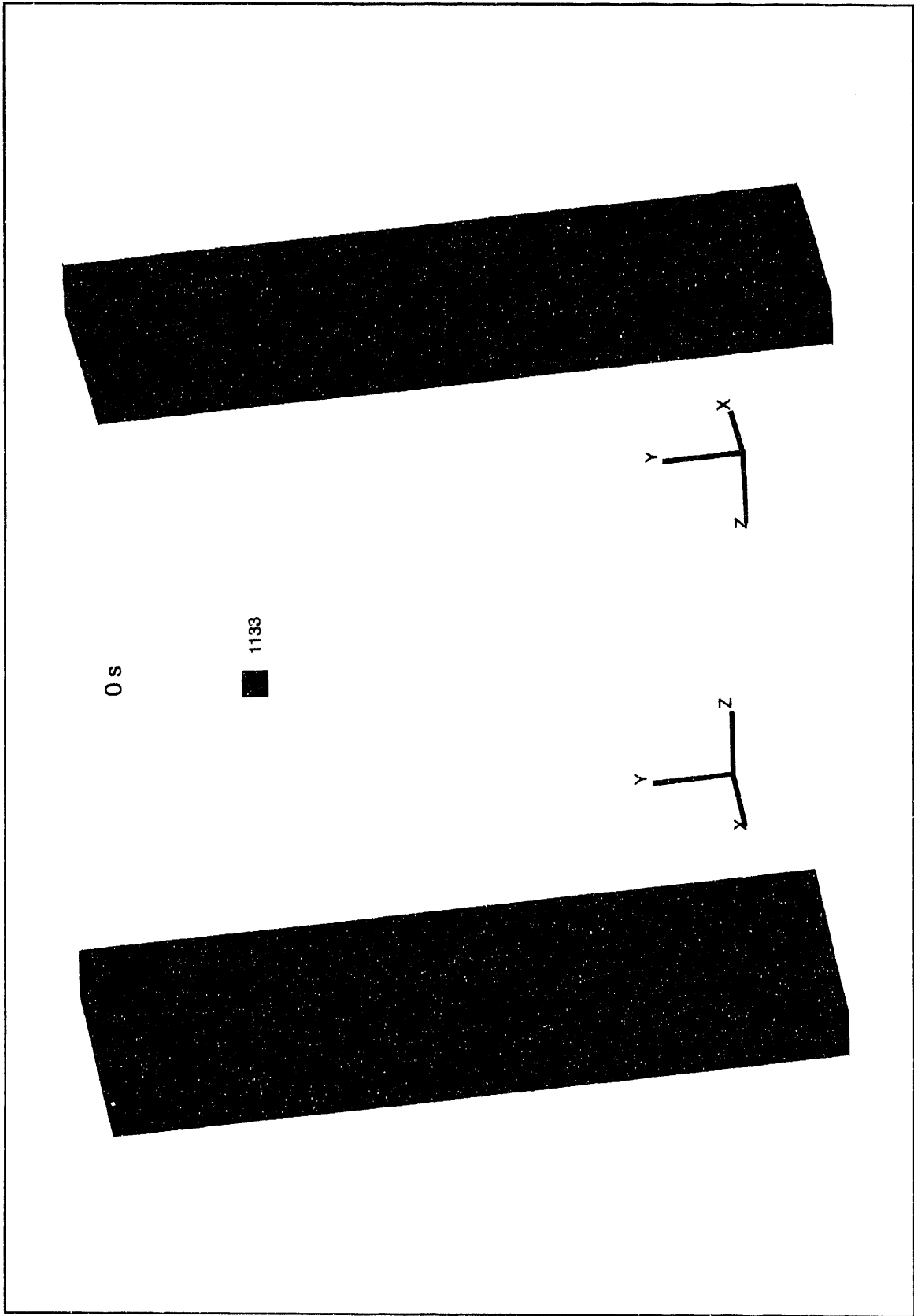
Fig. 45.   Uranium melt behavior at the beginning of the base-case solidification transient analysis.

60 s

1133
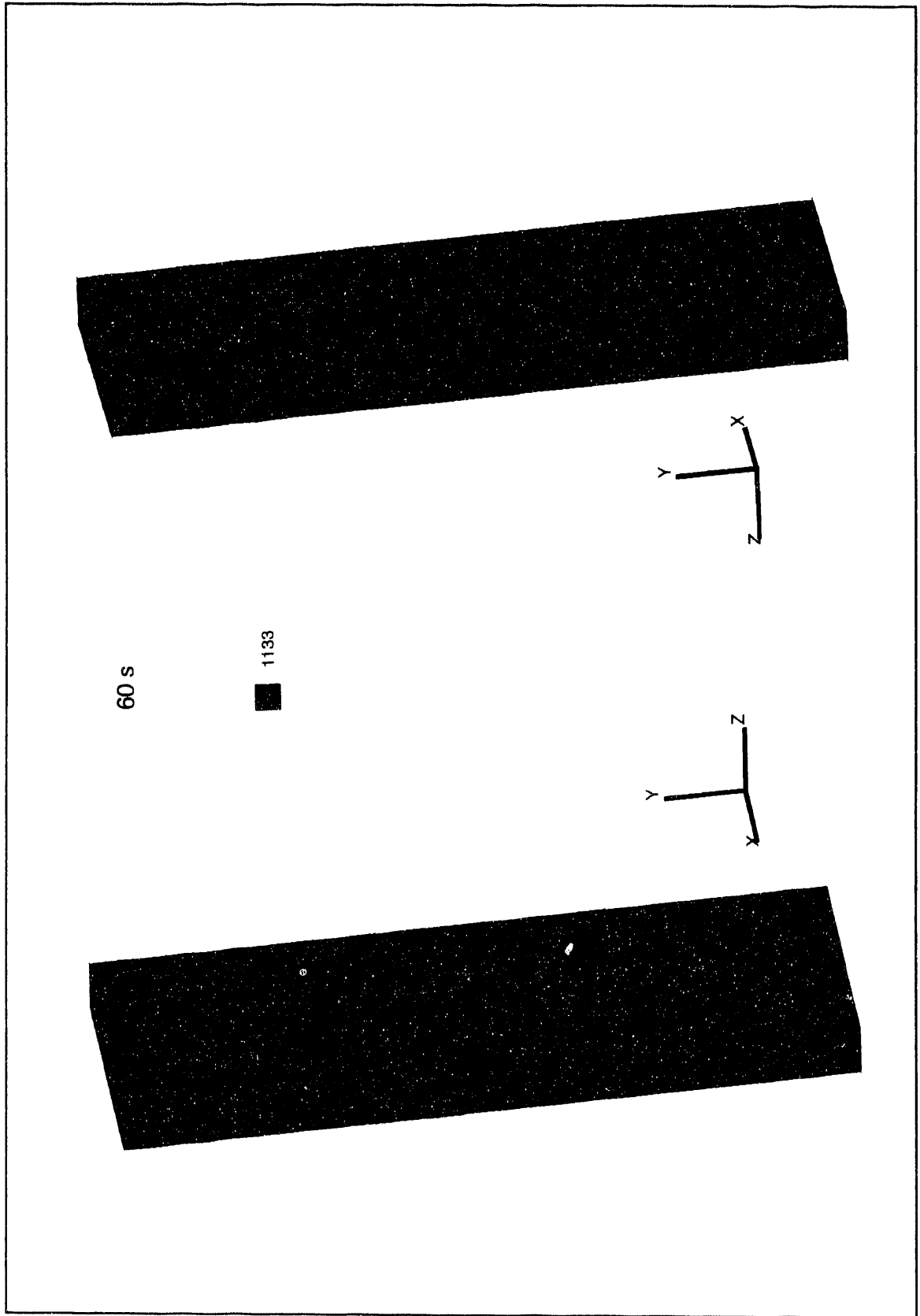
Fig. 46.   Uranium melt behavior 60 s into the base-case solidification analysis.
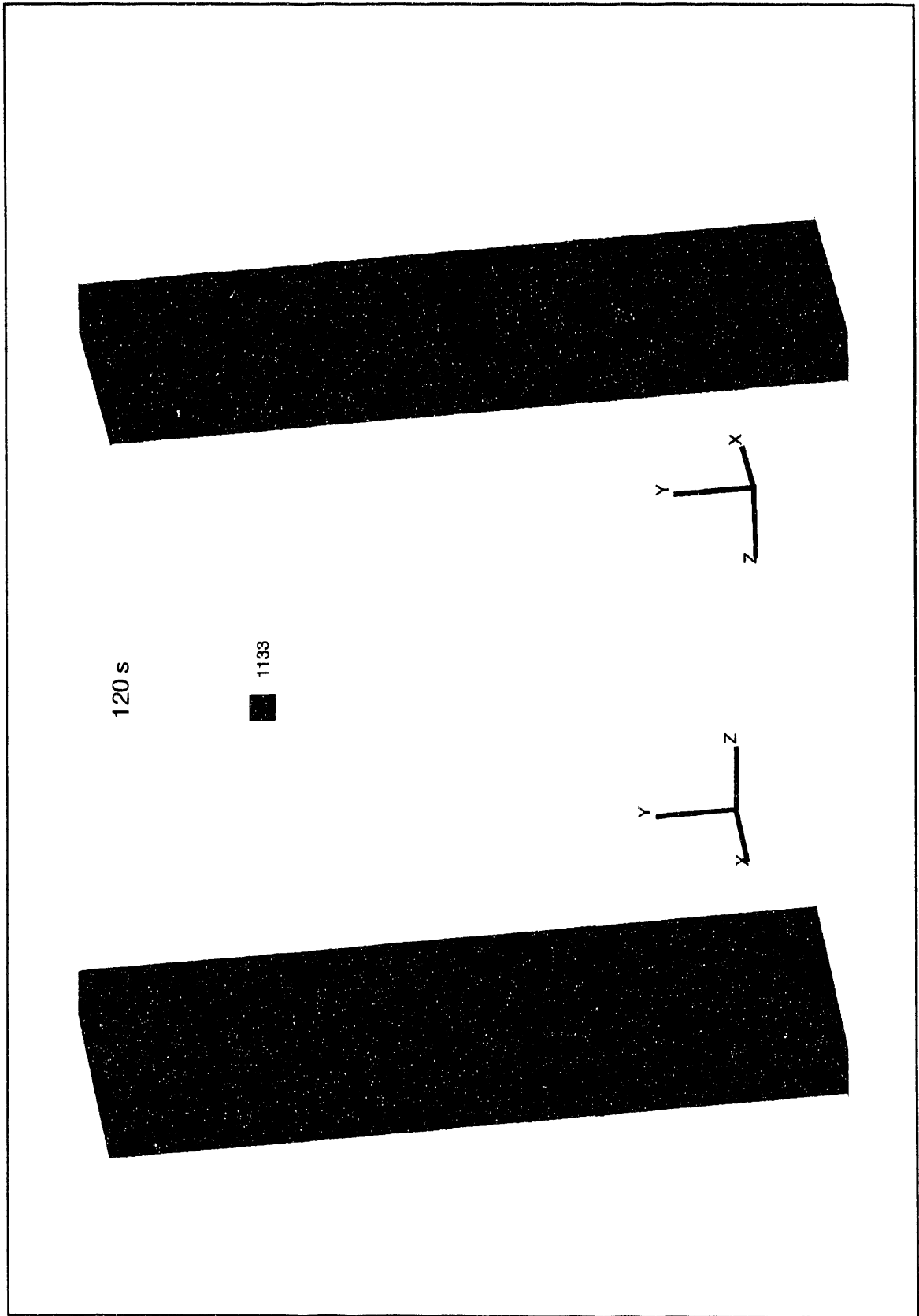
Fig. 47. Uranium melt behavior 120 s into the base-case solidification analysis.

180 s

1133
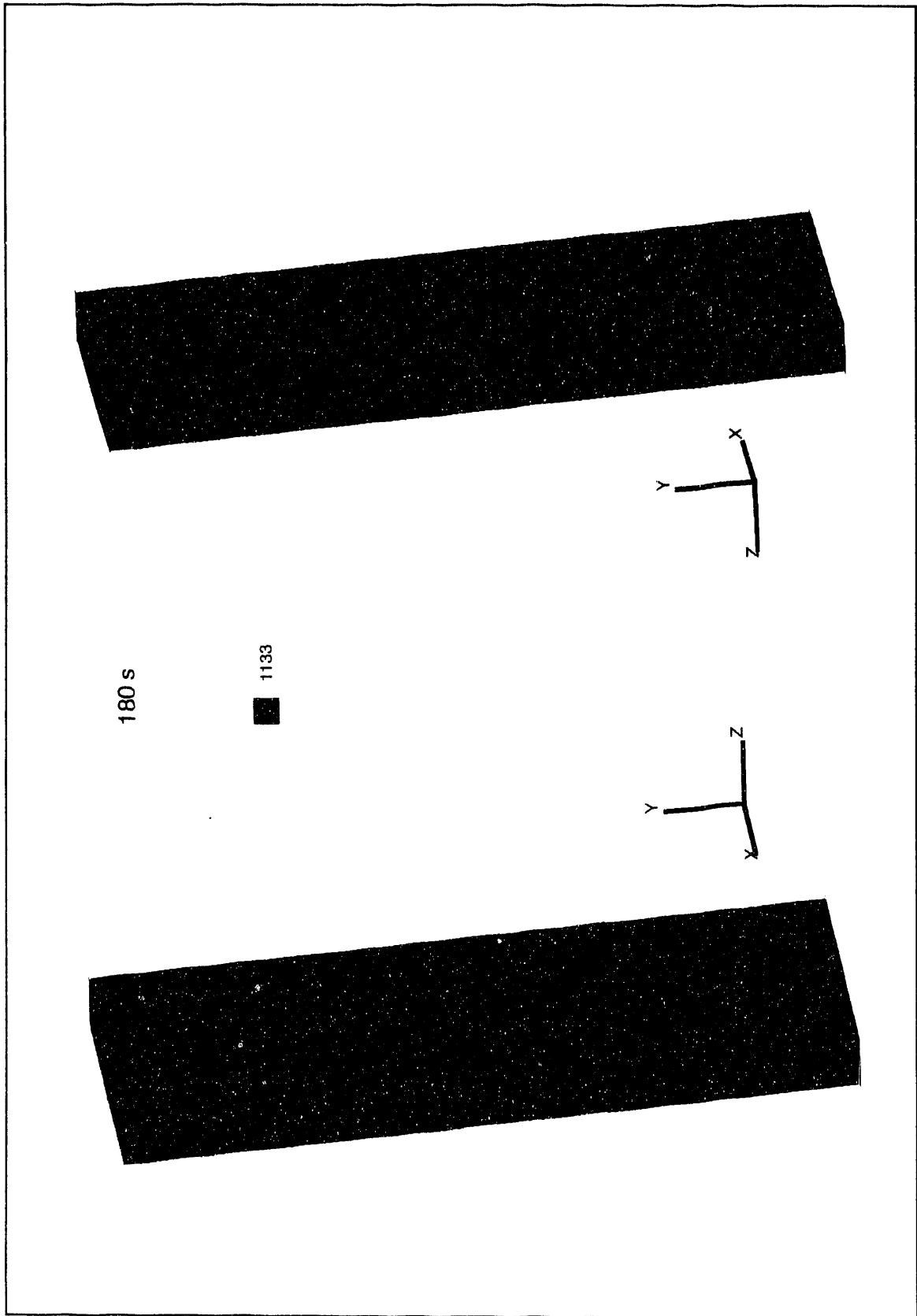
Fig. 48.   Uranium melt behavior 180 s into the base-case solidification analysis.

240 s

1133
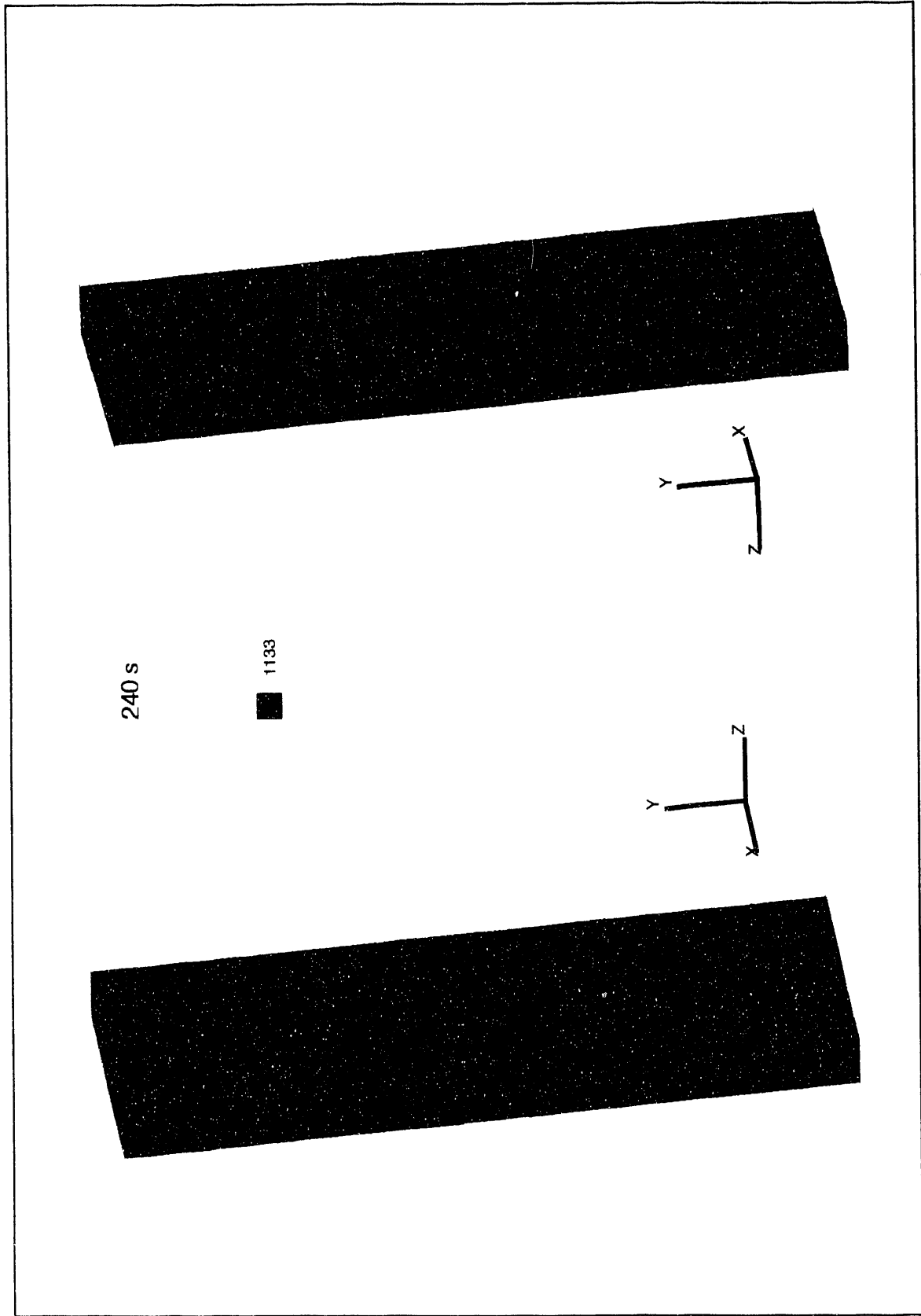
Fig. 49.   Uranium melt behavior 240 s into the base-case solidification analysis.
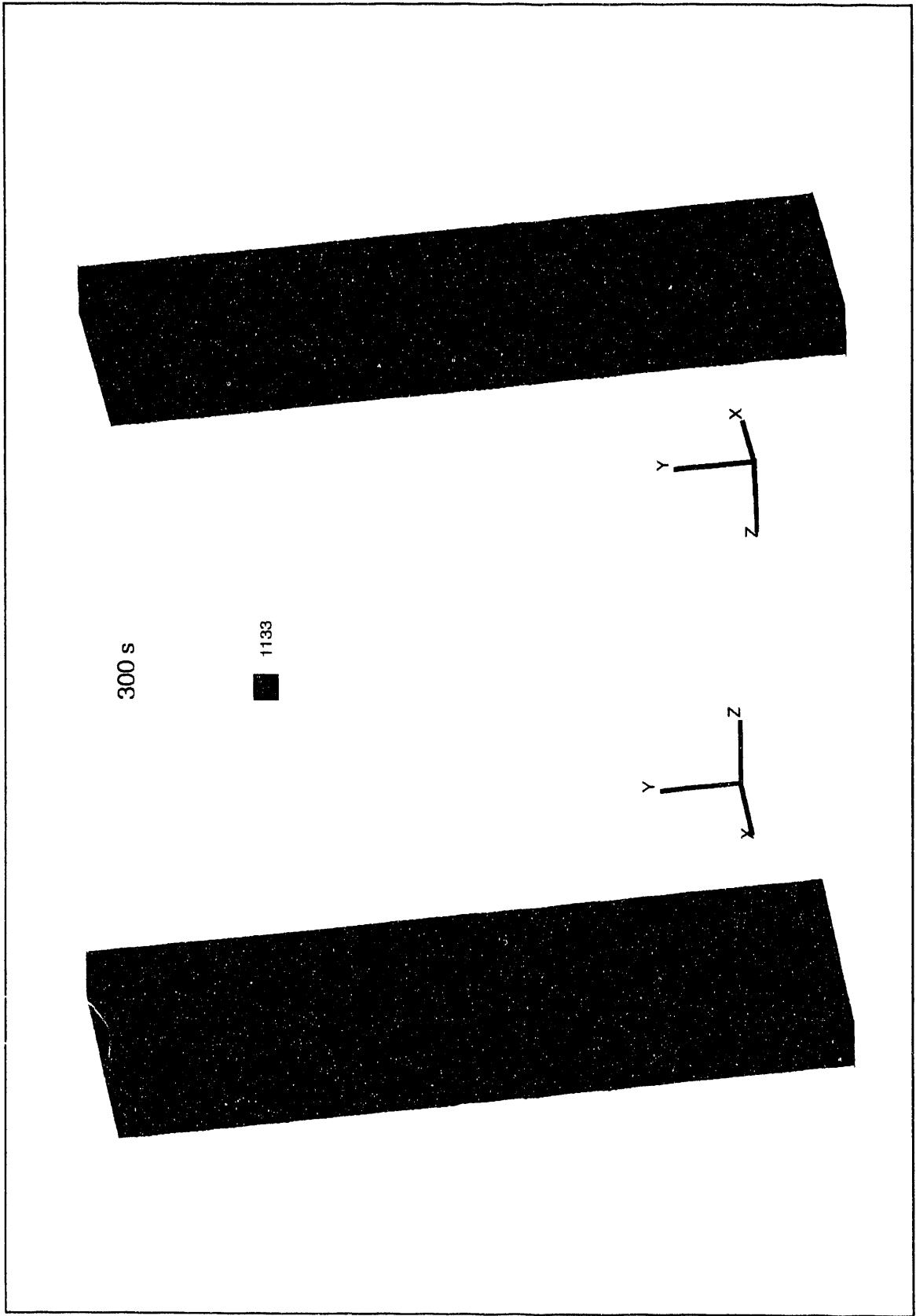
Fig. 50. Uranium melt behavior 300 s into the base-case solidification analysis.

360 s

1133
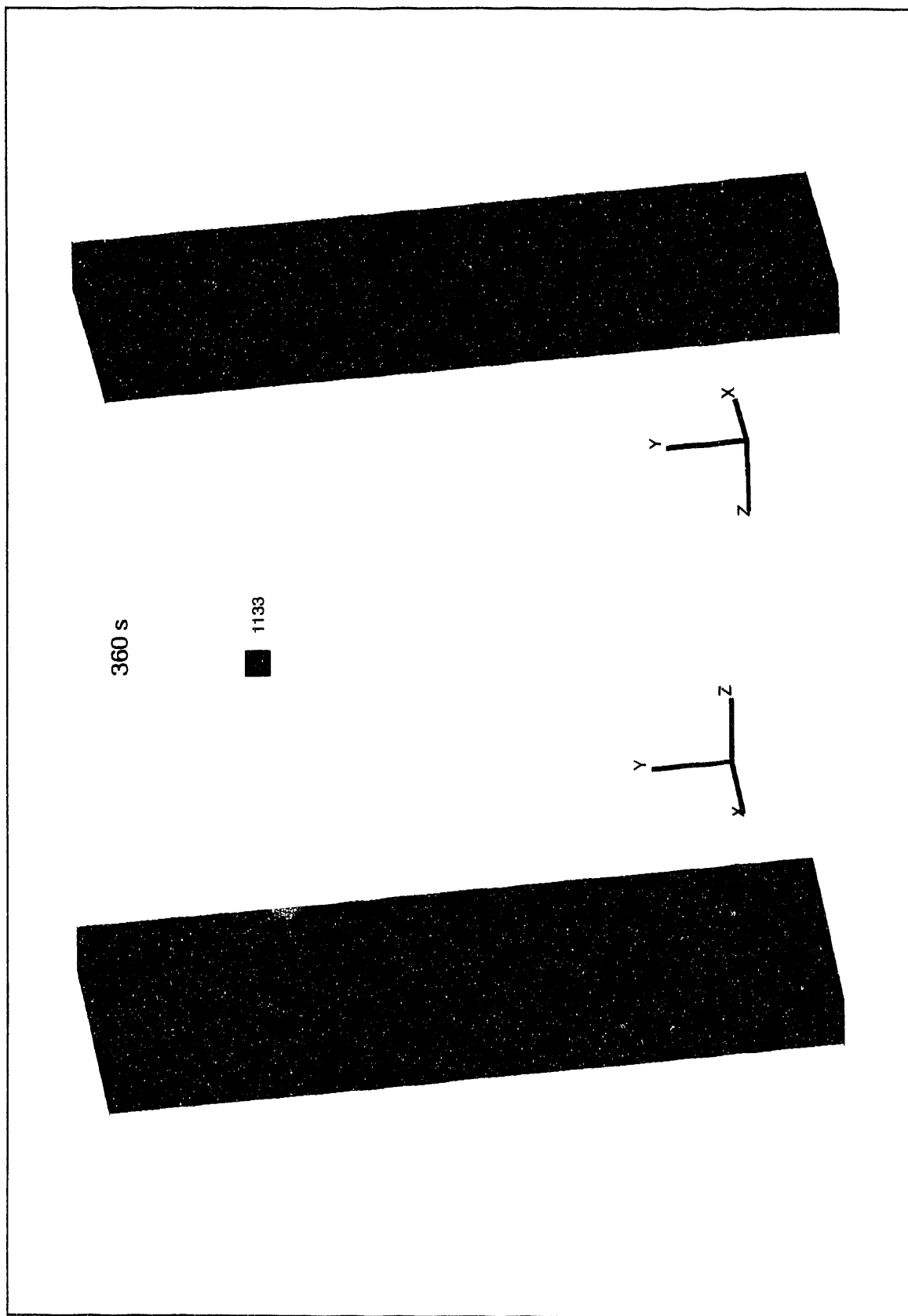
Fig. 51. Uranium melt behavior 360 s into the base-case solidification analysis.
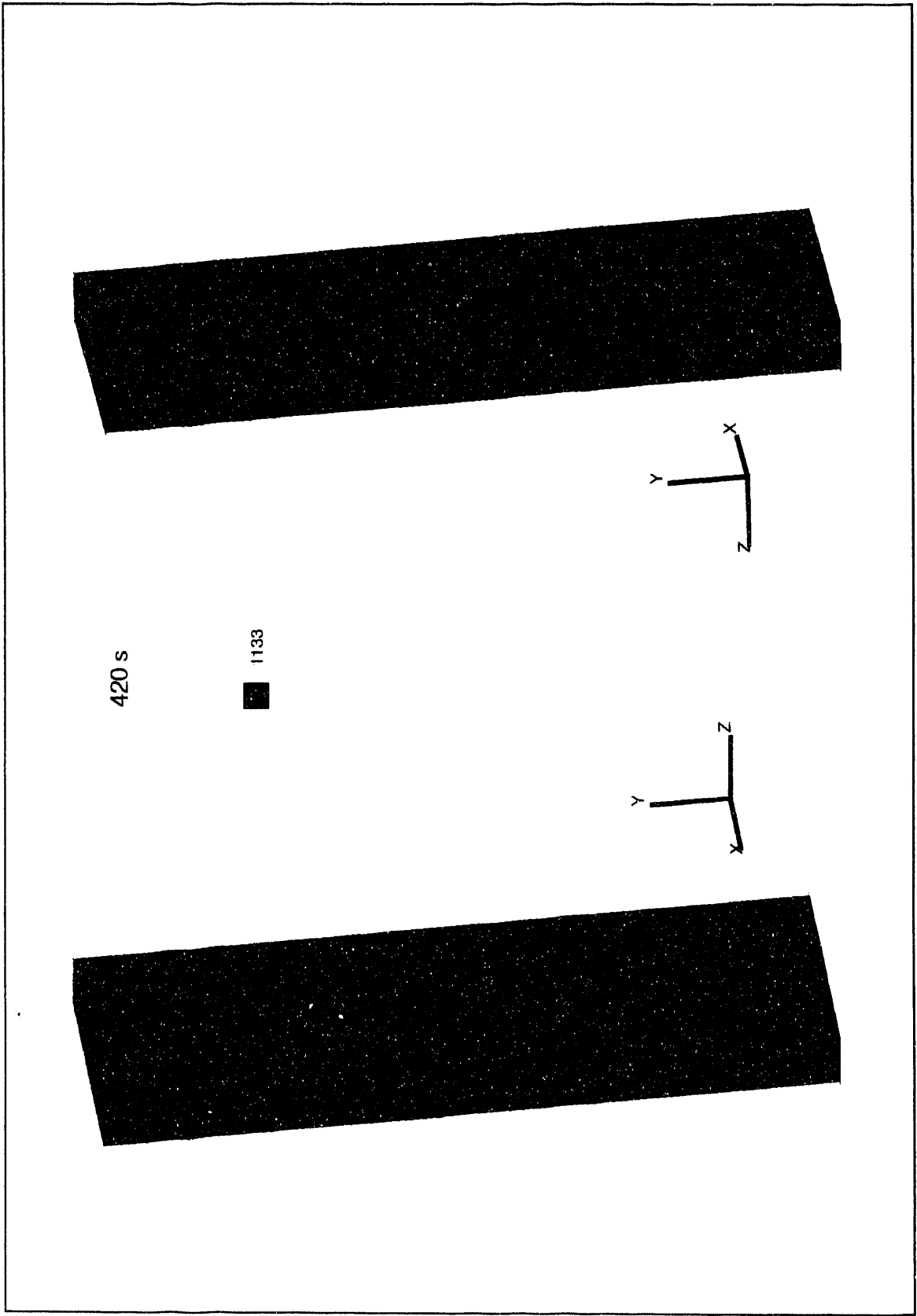
Fig. 52. Uranium melt behavior 420 s into the base-case solidification analysis.
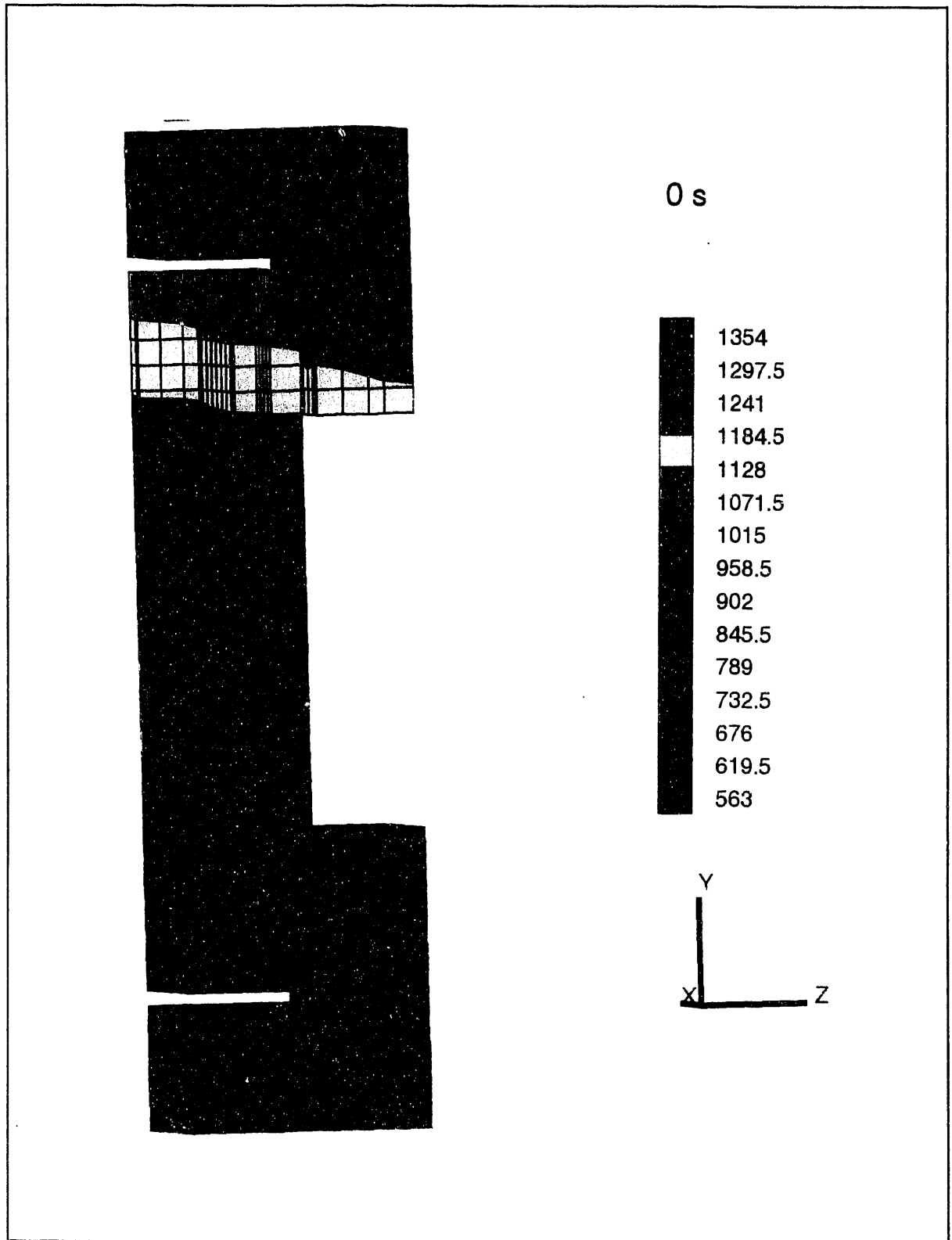
Fig. 53. Casting assembly temperature distribution at the beginning of the base-case solidification analysis.

60 s

	1354
	1297.5
	1241
	1184.5
	1128
	1071.5
	1015
	958.5
	902
	845.5
	789
	732.5
	676
	619.5
	563

Y

X   Z
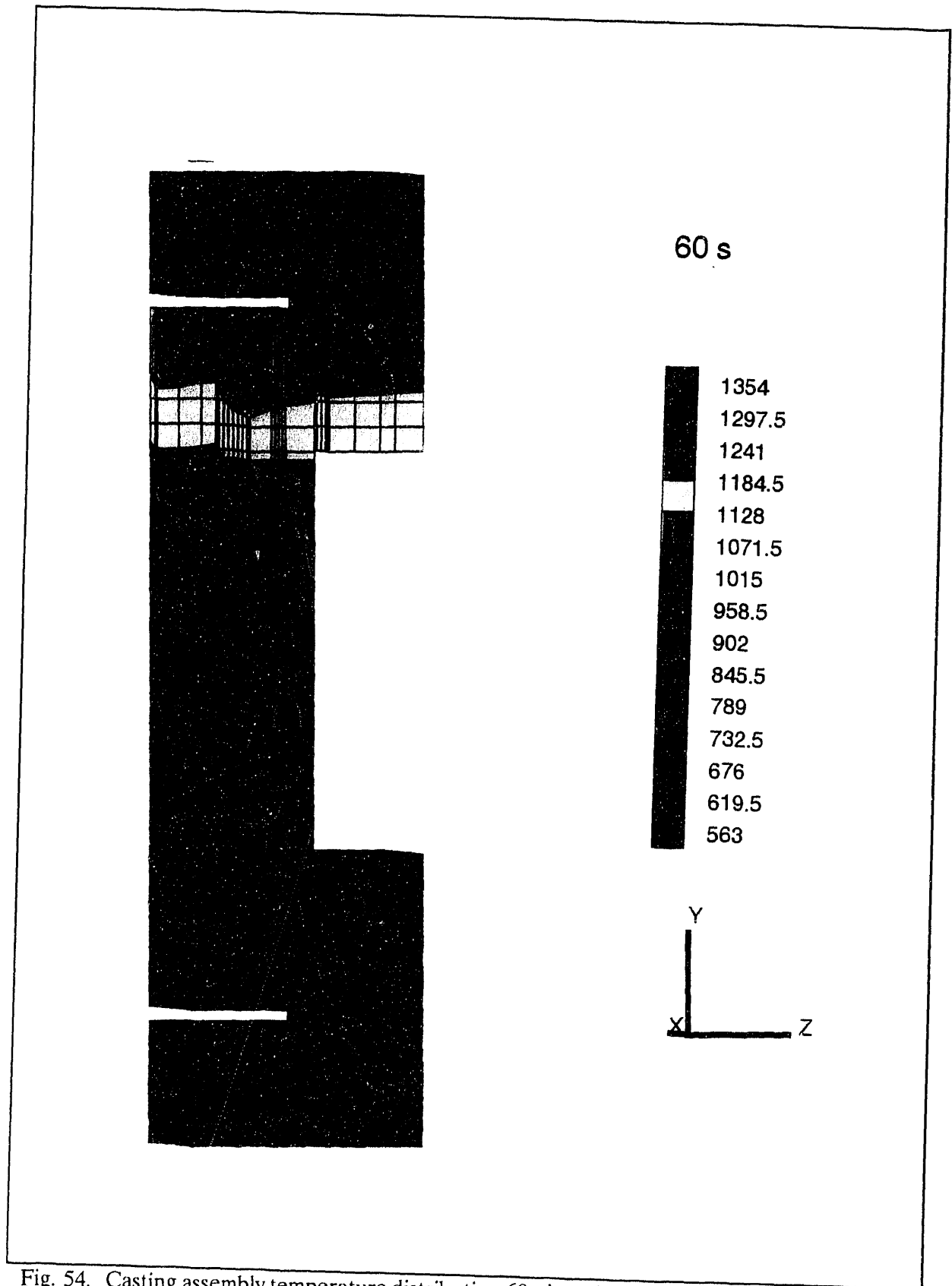
Fig. 54.   Casting assembly temperature distribution 60 s into the base-case solidification analysis.
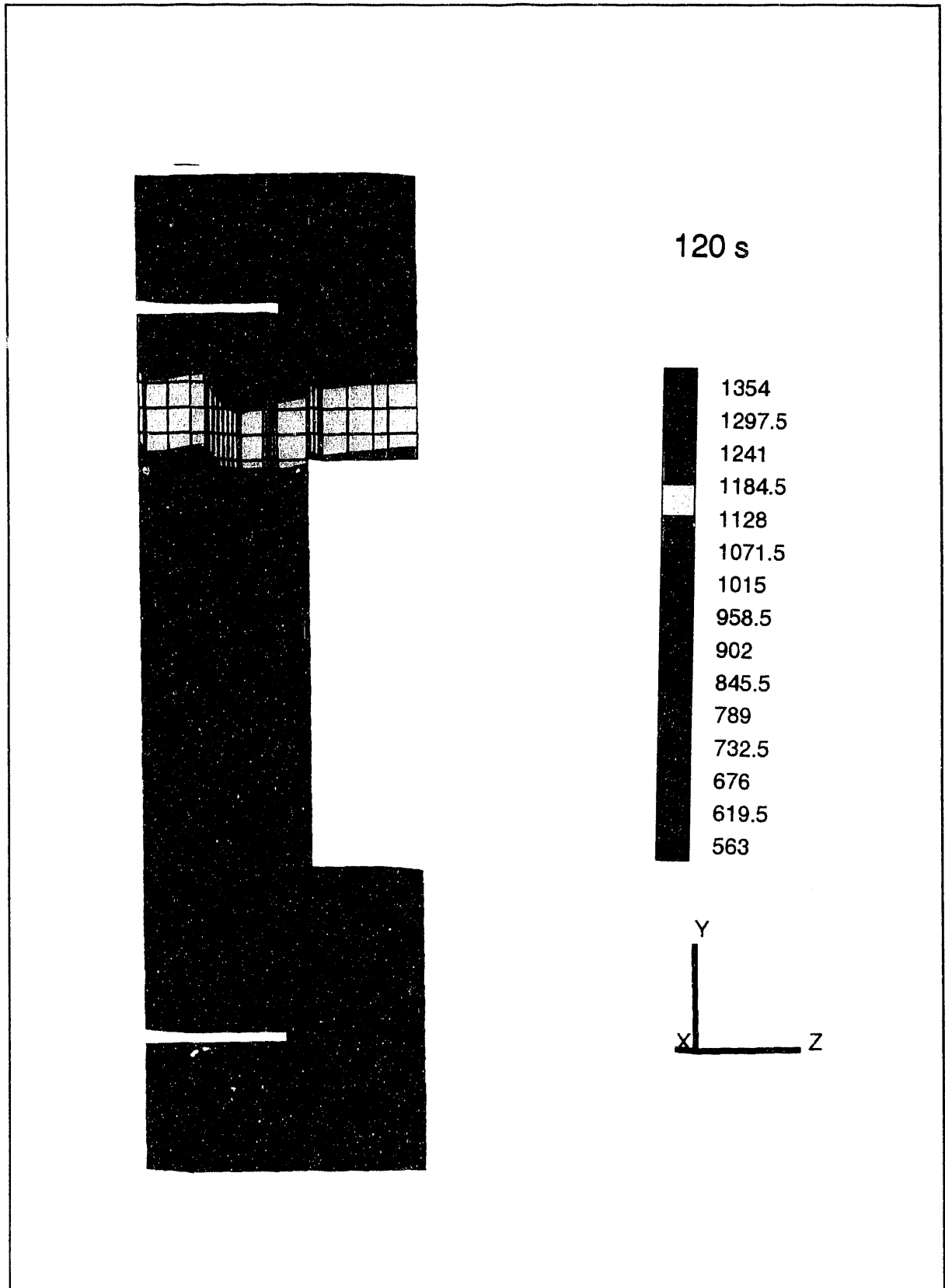
Fig. 55. Casting assembly temperature distribution 120 s into the base-case solidification analysis.

180 s

	1354
	1297.5
	1241
	1184.5
	1128
	1071.5
	1015
	958.5
	902
	845.5
	789
	732.5
	676
	619.5
	563
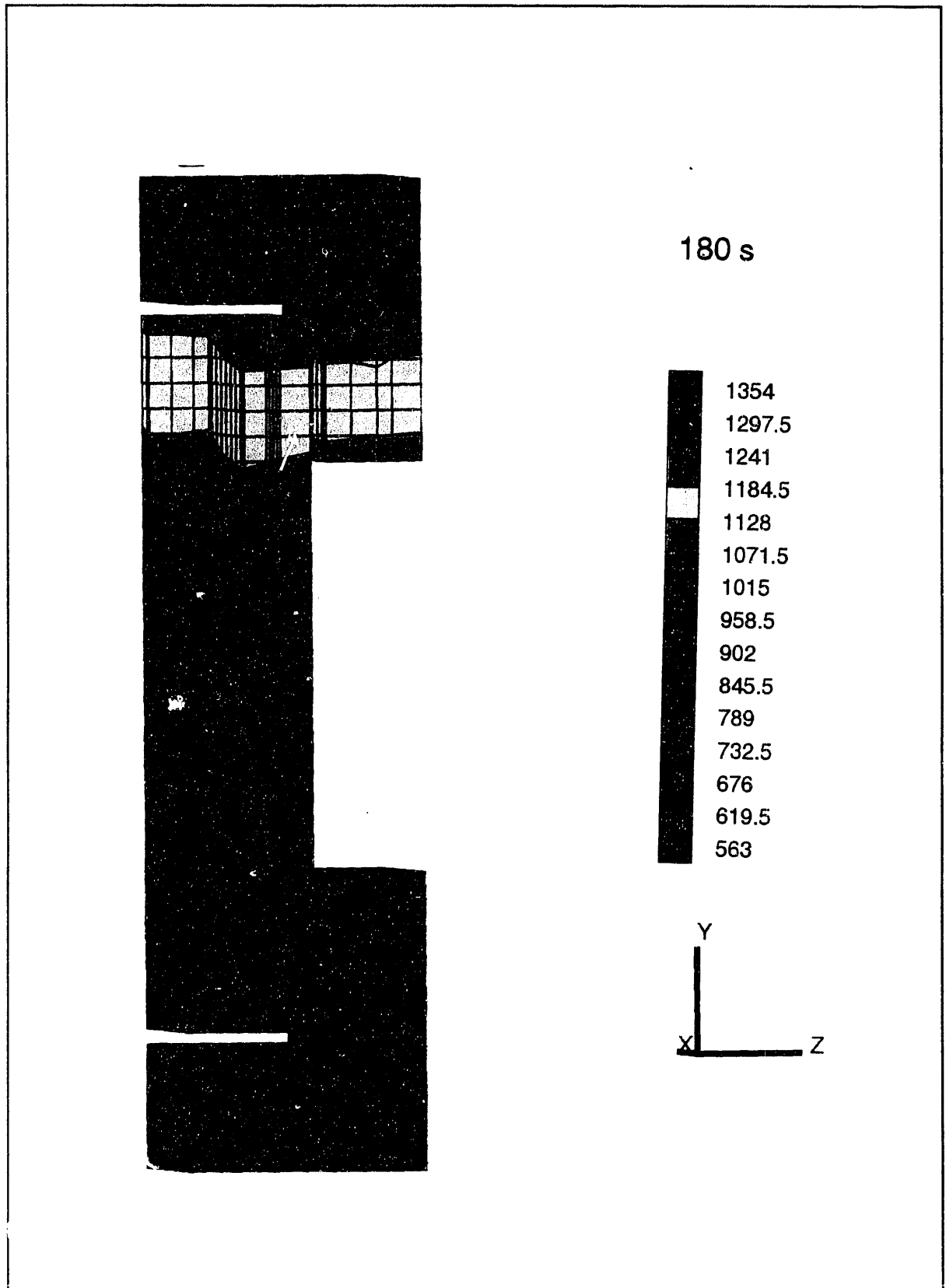
Fig. 56. Casting assembly temperature distribution 180 s into the base-case solidification analysis.

240 s

1354
1297.5
1241
1184.5
1128
1071.5
1015
958.5
902
845.5
789
732.5
676
619.5
563
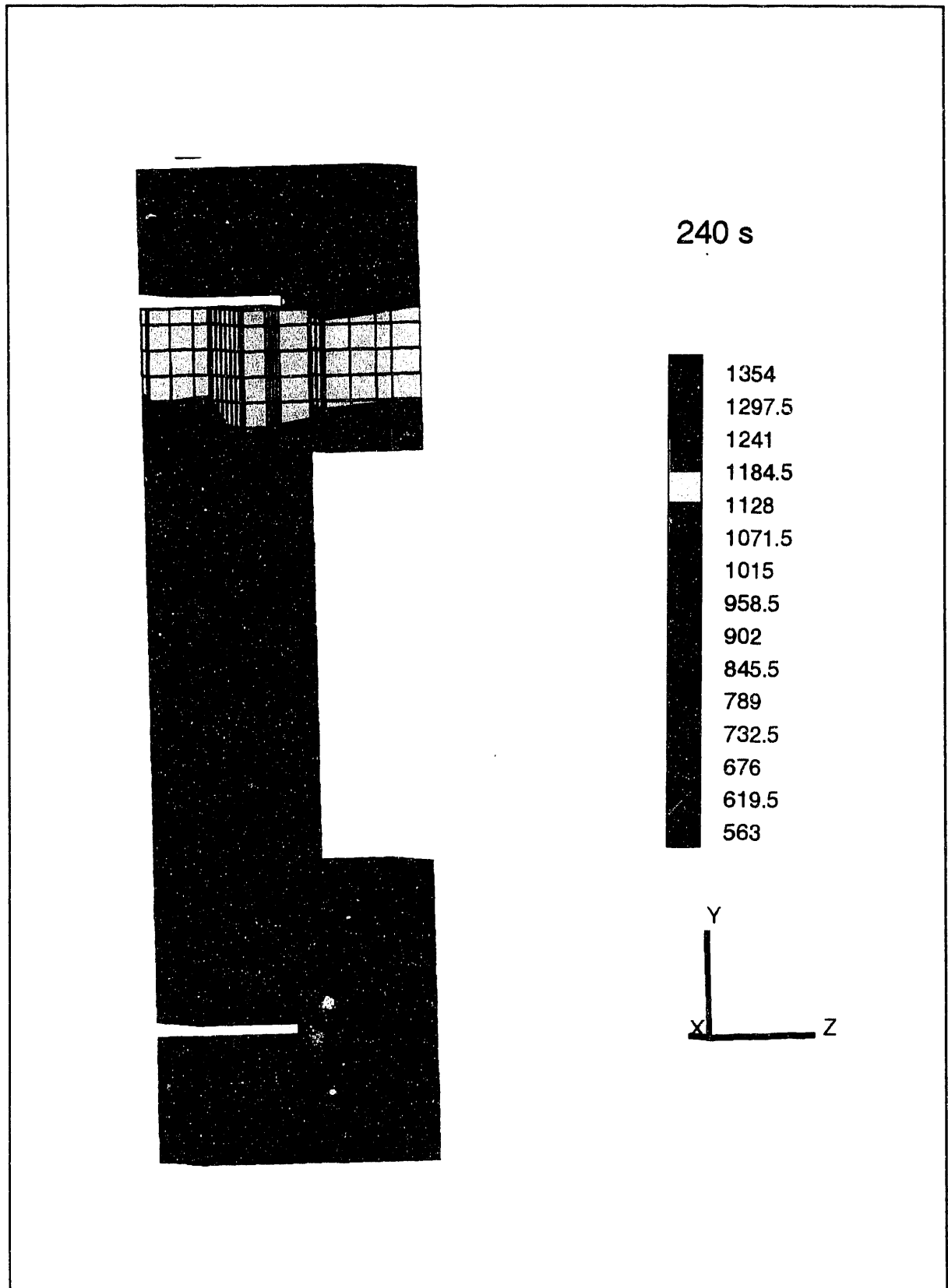
Fig. 57. Casting assembly temperature distribution 240 s into the base-case solidification analysis.
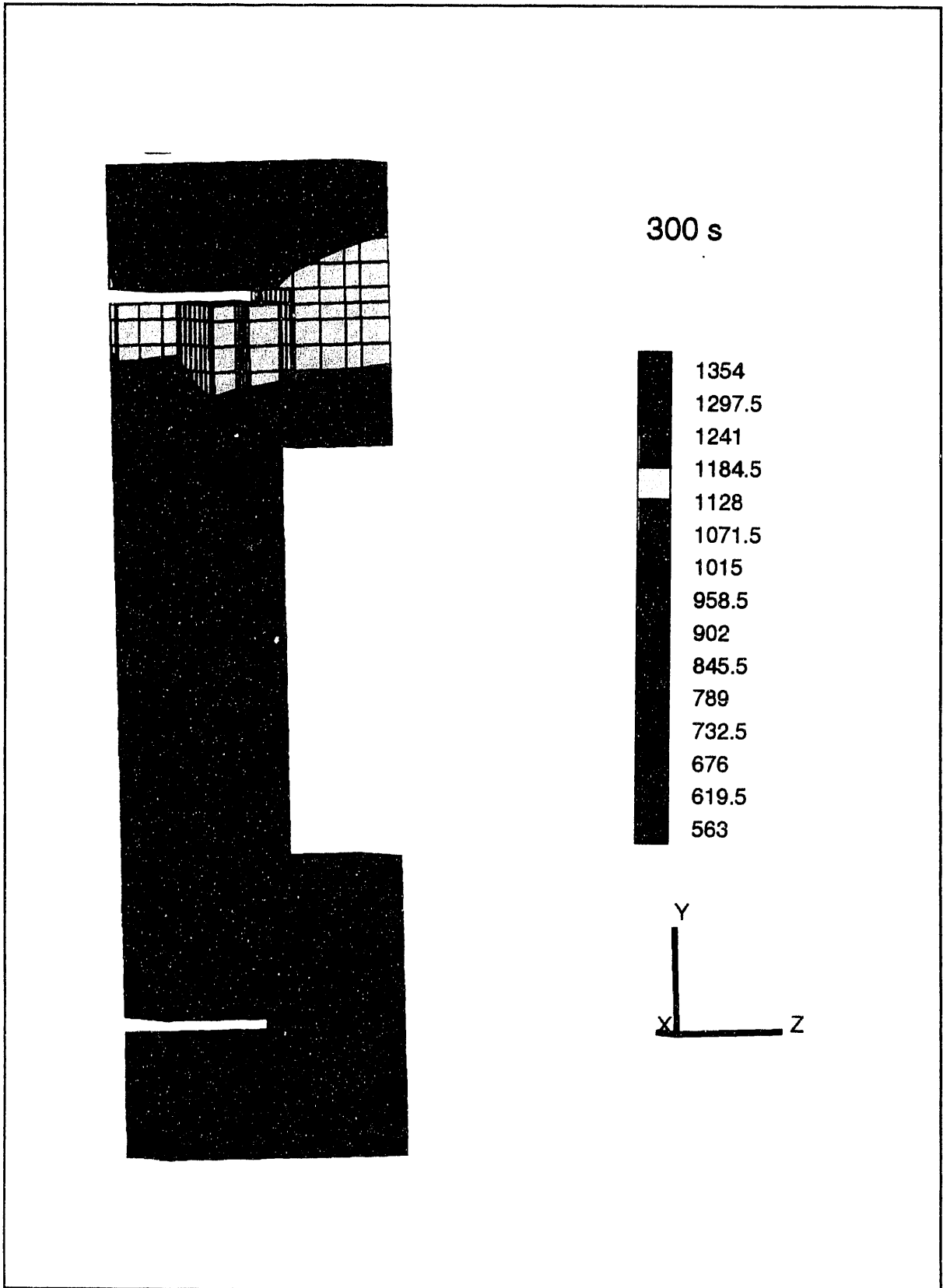
Fig. 58. Casting assembly temperature distribution 300 s into the base-case solidification analysis.

360 s

	1354
	1297.5
	1241
	1184.5
	1128
	1071.5
	1015
	958.5
	902
	845.5
	789
	732.5
	676
	619.5
	563

Fig. 59. Casting assembly temperature distribution 360 s into the base-case solidification analysis.

420's

	1354
	1297.5
	1241
	1184.5
	1128
	1071.5
	1015
	958.5
	902
	845.5
	789
	732.5
	676
	619.5
	563
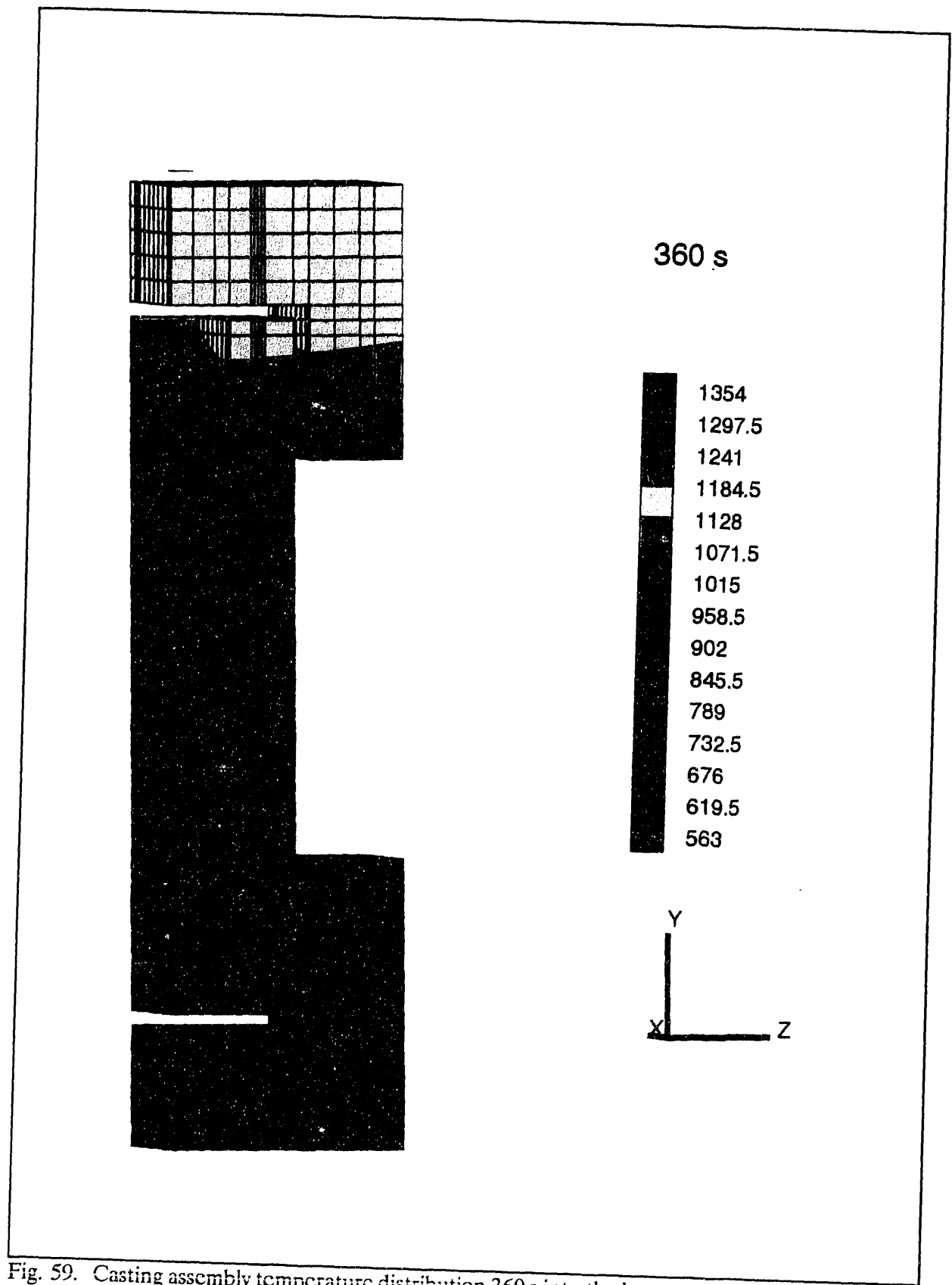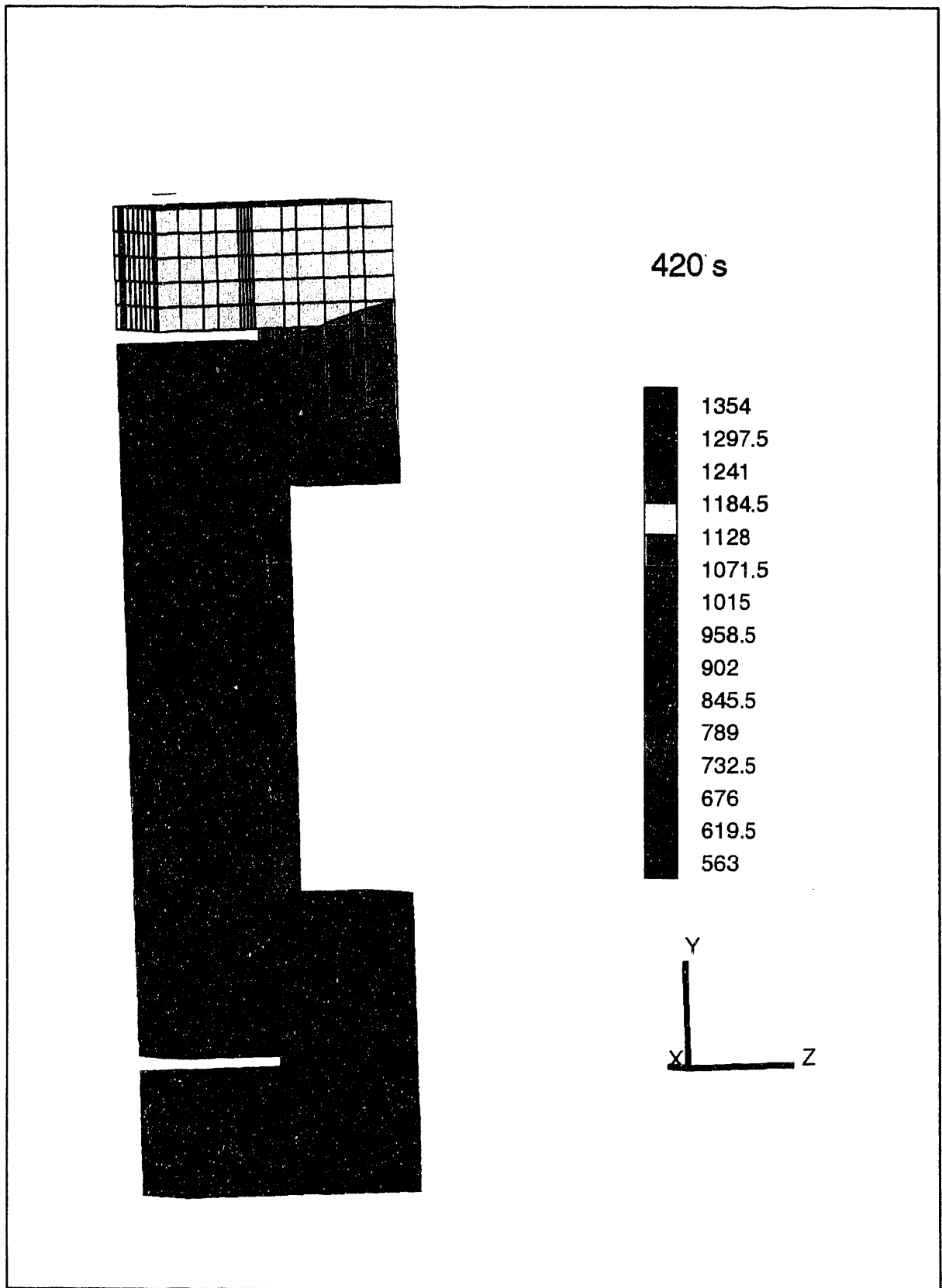
Fig. 60. Casting assembly temperature distribution 420 s into the base-case solidification analysis.

PHYSICAL MODEL SIMPLIFICATION

It was known that the second-generation studies would require a large number of computer runs to characterize carbide transport and examine the effect of casting assembly design changes. Economic considerations dictated the use of a physical model that was as simple as possible yet still gave meaningful agreement with experimental data. Accordingly, three simplifications to the base-case model were examined: removing the platinum thermocouple junctions and/or their insulating sheaths; eliminating portions of the firebrick base; and replacing the heater coil representation (i.e., the flat plates) with a boundary condition representative of the thermal resistances between the shield and cooling water.

To determine how much of the firebrick base could be removed, base-case transient temperatures at four locations in the X/Z plane were plotted for several different Y elevations. The goal was to find that elevation where temperatures were constant for the duration of the transient, preferably at ambient. All material below this point could then be eliminated and replaced with a constant temperature boundary condition. The four locations correspond to the corners of the base of the lower end cap and are illustrated in Fig. 61. The four Y elevations were the base of the lower end cap and 5.5, 15.5, and 25.5 cm into the firebrick. These temperature data are summarized in Figs. 62−65 and show that:

1. Temperatures do not become constant wrt time until 5.5 cm into the firebrick.

2. At each elevation there is a temperature difference between the set of nodes on the inside (i.e., Z = 0.) of the end cap and the outside set. This is attributed to the design of the casting assembly: the inside surfaces contact the bookmold containing the hot uranium, but the back side is separated from the bookmold by the thickness of the end cap. Thus, it is reasonable to expect cooler temperatures at the *insulated* locations on the back side of the end cap.

3. The absolute values of temperatures, as well as temperature differences between the inside

Fig. 61.   The set of X−Z plane monitored locations.

and outside locations, decrease with increasing distance into the firebrick, but at no elevation are they equal to ambient.

Note that all temperatures are greater than ambient. Experimental data had indicated constant temperatures approximately equal to ambient 15.24 cm into the firebrick. The higher calculated temperatures are attributed to the fact that the base was modeled as a single solid
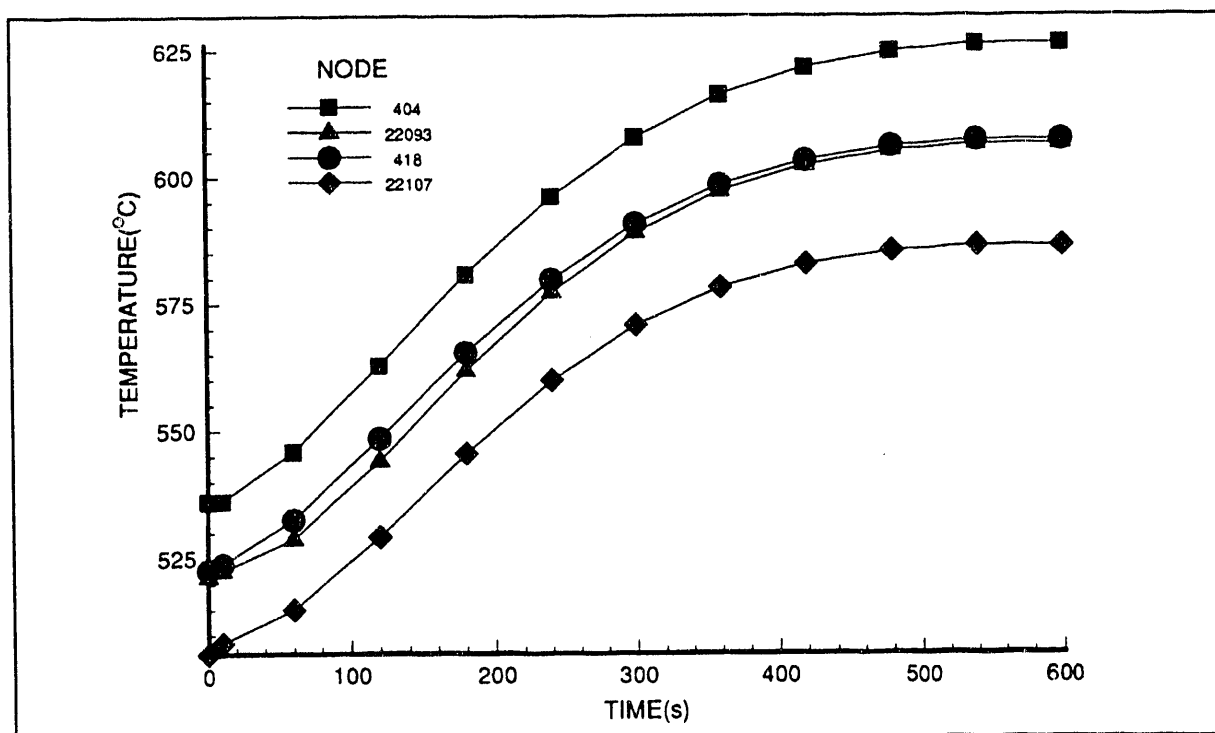
Fig. 62.   Temperature history of selected nodes at the base of the lower end cap.
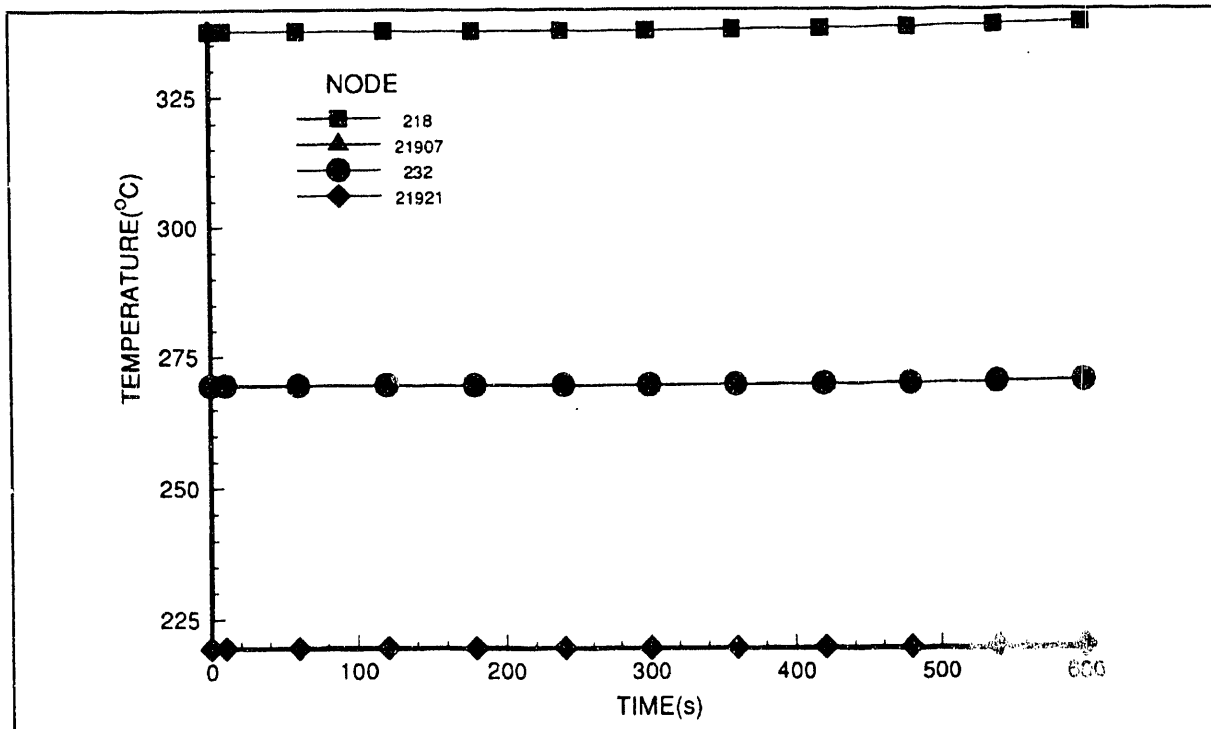
Fig. 63.   Temperature history of selected nodes at 5.5 cm into the firebrick base.
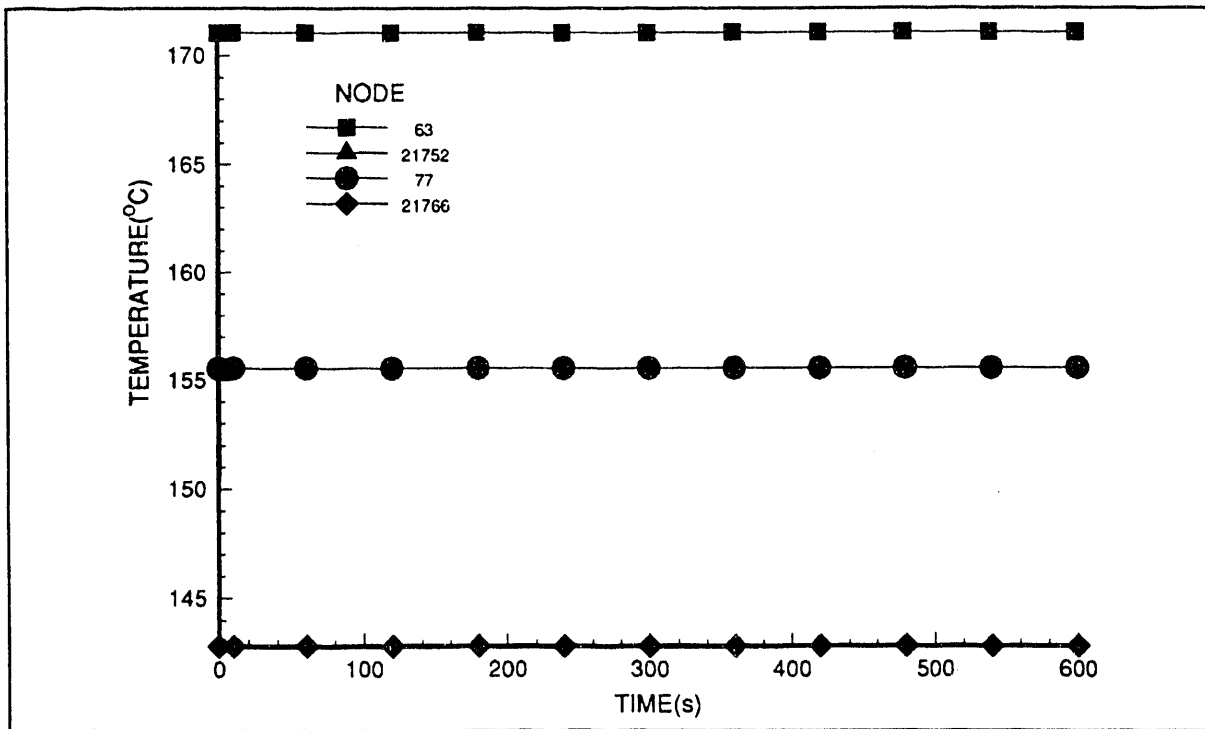
Fig. 64.   Temperature history of selected nodes at 15.5 cm into the firebrick base.
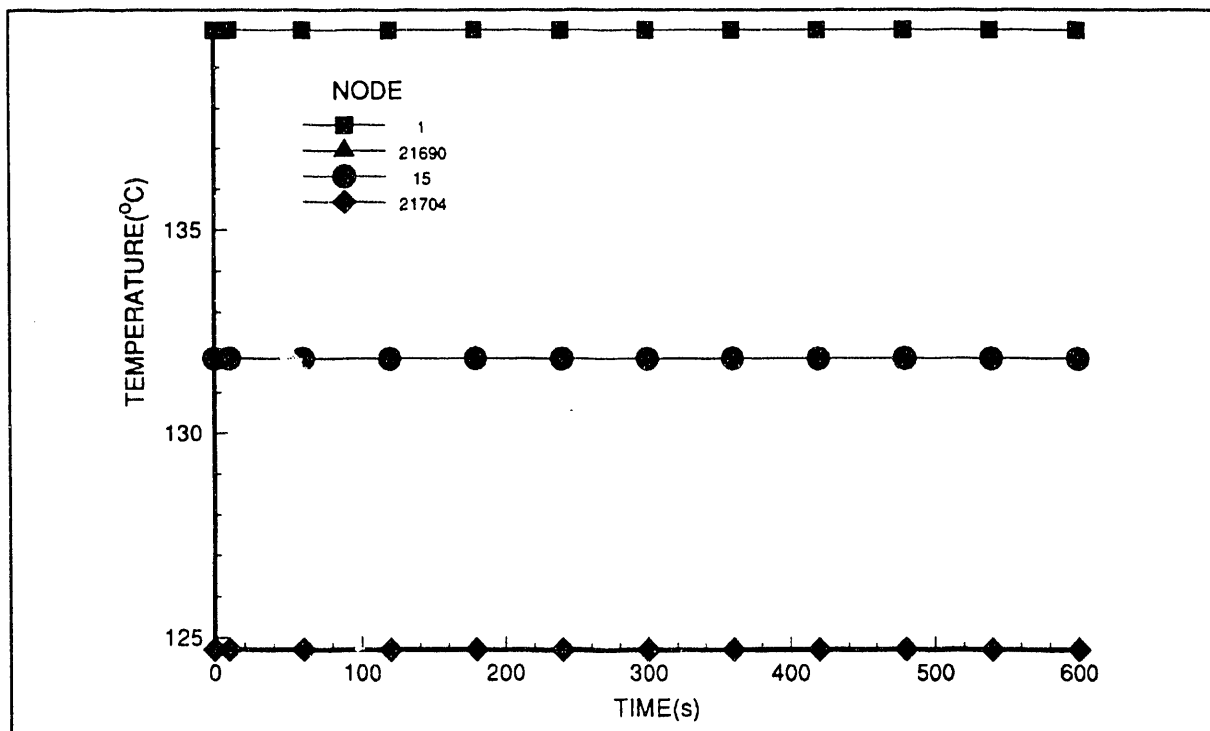
Fig. 65.   Temperature history of selected nodes at 25.5 cm into the firebrick base.

region when it is actually a loose stacking of several bricks. Thus, there were no void regions to impede conduction away from the casting assembly. It is also believed this is one of the reasons for the consistently low temperatures calculated for the bottom thermocouple location during the sensitivity studies. Based on these data and the belief that future melt temperatures are likely to be the same magnitude as Run No. 892, a case could be made for placing a constant-temperature boundary condition of approximately 275°C at 5.5 cm into the firebrick and then removing all material below that point. However, given the macroscopic result that all thermal mechanisms need to be included to some degree to obtain meaningful agreement, the most prudent action would be to model 15.24 cm of the actual stacking with its void spaces and place a constant temperature boundary condition of 25°C at the bottom of the stack.

To determine if the thermocouples and/or their insulating sheaths could be removed without adversely affecting model agreement, two configurations were examined: one where only the sheath was removed, and a second where the junction was removed as well. Model agreement for these two cases is summarized in Fig. 66 and shows that neither had a significant impact. The last potential simplification examined was to replace the flat plates with a radiation heat transfer coefficient applied to that portion of the insulating shield covered by the plates. Temperature data monitored during the sensitivity studies had indicated that the coils had an essentially constant temperature approximately equal to the cooling-water temperature. Accordingly, the boundary temperature for the new coefficient was made equal to the cooling-water temperature. Model agreement for this case is also summarized in Fig. 66 and shows that the simplification did not significantly effect agreement. It appears that both the thermocouple system and the heating coil approximation could be removed from the second-phase model without adversely effecting its accuracy. Removing the coil approximation, however, is conditional upon not altering the cooling-water flow rate during the solidification transient. The primary reason the plates could be replaced was that the plate temperature was essentially constant during the transient. If the water flow rate were to be significantly decreased or stopped, the coil temperature would vary with time, and this response would then have to be modeled to correctly calculate the energy leaving the casting assembly.
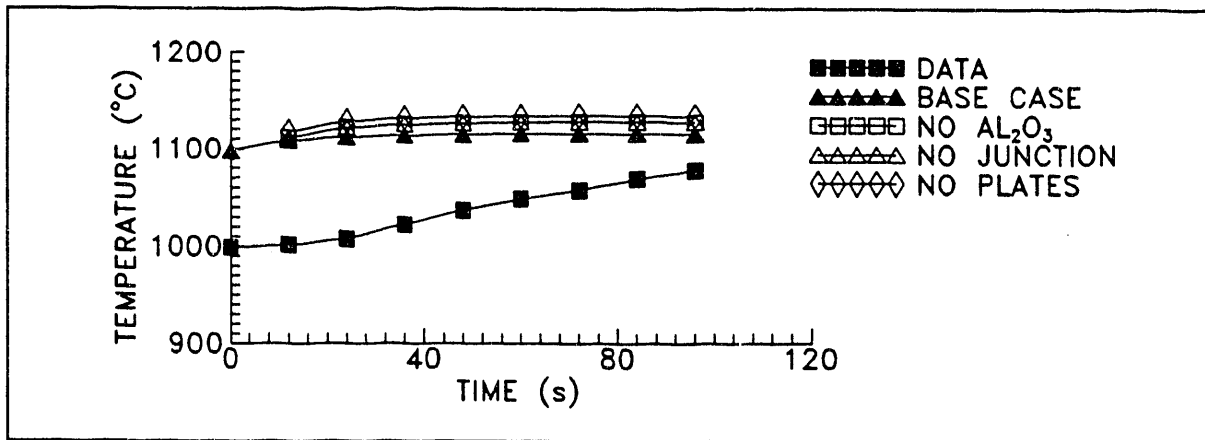
(a) top thermocouple location
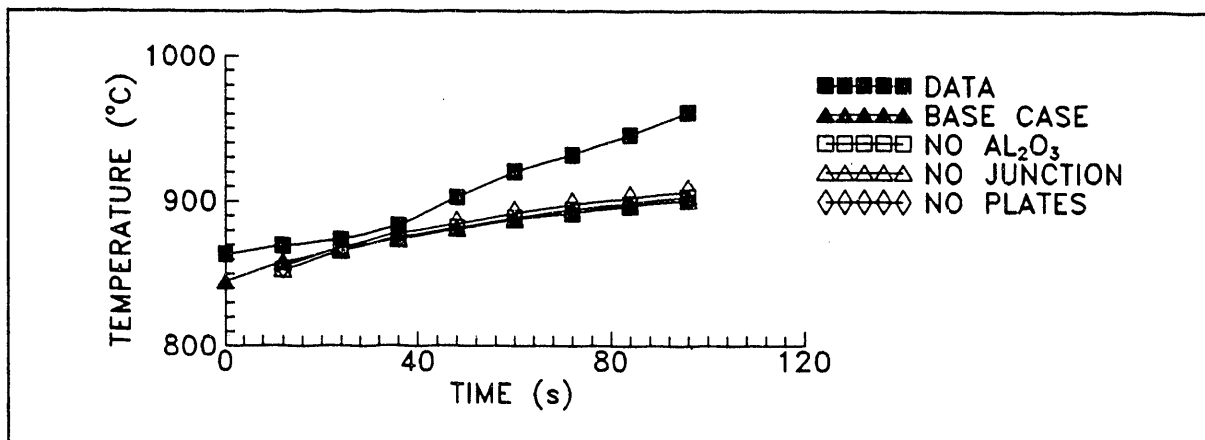
(b) middle thermocouple location
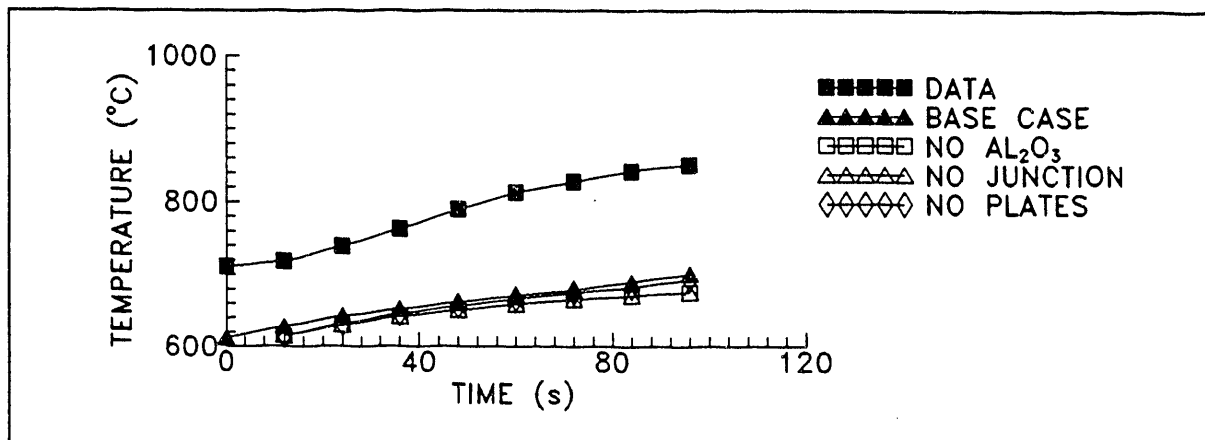
(c) bottom thermocouple location

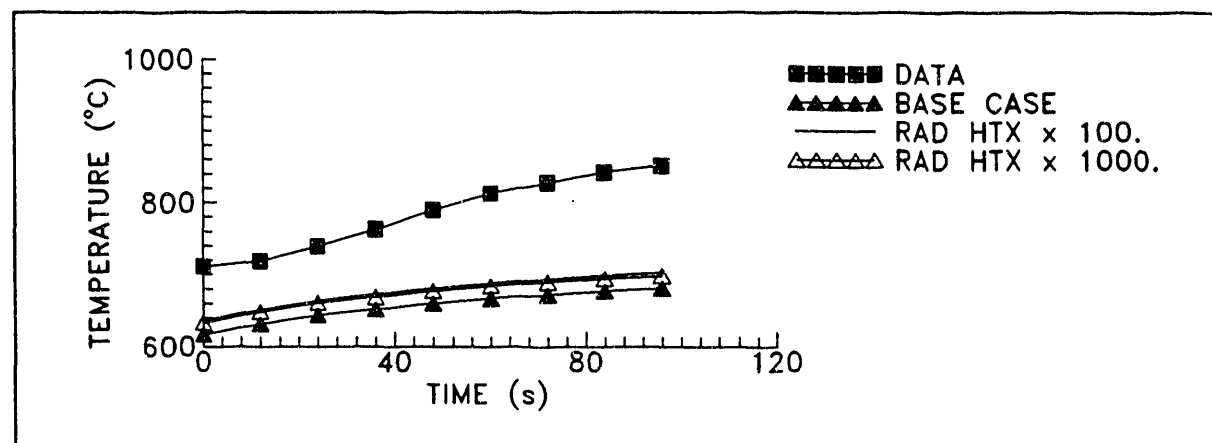Fig. 66. Model agreement for the thermocouple and flat plate simplification scenarios.

CONCLUSIONS AND RECOMMENDATIONS

Two macroscopic conclusions can be drawn from the results of the first-phase study concerning modeling heat transfer in the current laboratory scale casting assembly:

1. those convection/conduction/radiation heat transfer mechanisms that locally influence net heat flow through casting assembly components have a greater impact on model accuracy than the absolute values of sink temperatures and coil cooling water flow rates; and

2. although this subset of prominent mechanisms exists; all major assembly components, heat transfer mechanisms, and boundary conditions must be included to some degree to obtain meaningful agreement with experimental data.

Accordingly, the following recommendations are made to facilitate the planning and execution of the second-phase thermal studies.

1. The design of the vacuum-caster system should be modified to permit routine measurements of pressure vessel interior wall temperature, cooling-water flow rate, water inlet and outlet temperatures, and heating coil current.

2. The experimental casting procedure should be slightly modified to ensure that *thermally* consistent data are collected.

3. The second-phase thermal model should have the following macroscopic design features:

   a. a precise physical model exclusive of the heater coils;

   b. first-order accurate mathematical definitions for radiation heat transfer to the pressure vessel wall and between closely spaced components; and

   c. second-order accurate definitions for thermal contact resistances (including that between the crucible wall and insulating shield), liquid uranium natural convection heat transfer, interfacial gap conductance between the solidified uranium and bookmold, internal heat generation, and radiation enclosure heat transfer.

The following briefly discusses some of the details associated with implementing these recommendations.

The only measure of computational accuracy is a comparison between measured and calculated bookmold temperatures. Thus, accurate measurements are required for bookmold temperatures as well as for those data used to define initial and/or boundary conditions for the analyses. Within this context there are two areas of concern with the current experimental casting procedure: the execution of the procedure itself and the placement of the bookmold thermocouples. The current procedure should be modified as per the following guidelines to ensure that consistent *thermal* data are taken.

1. The single most important consideration is to establish a *thermal* steady state prior to pour. Currently the only criteria is a non-changing melt temperature for 30 min, and the coil current is continually reduced during this time period to achieve this condition. Steady state must be redefined to be *that condition where coil current, melt temperature, and bookmold temperatures have all remained unchanged for 30 min*.

2. It is also very important to coordinate the operation of the data recorder with the pour that is, define a *time 0* for the solidification analysis. To achieve this the data recorder

should be turned on very early in the melting phase and left on for the duration of the experiment, at least to the point where the caster is first backfilled with argon. Once the operators are satisfied that steady-state conditions exist (i.e., non-changing coil current and temperatures), the pour rod should be removed. The exact time the rod is removed should be recorded on the data sheet and a notation made on the strip chart.

3. In addition to the data currently taken by the operators, heating coil current, coil frequency, cooling water flow rate, and water inlet and outlet temperatures should also be recorded at steady-state conditions (i.e., just prior to the pour) as well as during the solidification portion of the experiment. These data should be recorded at the same time and with the same frequency as the bookmold temperatures. Also, it is especially important to continue to record coil current and frequency during and just after the pour, as well as the exact amount of time the power remains on after the pour rod has been removed.

4. When the caster is first backfilled with argon, the exact time the procedure was begun should be recorded on the data sheet and a notation made on the strip chart. In addition, the final pressure in the caster should also be noted on the data sheet.

There are two aspects of bookmold thermocouple placement that are of concern: location and installation. It is extremely important that the location of the three bookmold thermocouple junctions be well defined. Otherwise a comparison of measured and calculated temperatures cannot be made and it will not be possible to estimate the accuracy of the carbide transport calculations. The recommended locations have been previously documented,[28] but are summarized here as well for completeness. The locations were actually defined to achieve two goals: obtaining temperature data within the bookmold wall to help in establishing the accuracy of the solidification analyses, and obtaining temperature differences across assembly components to help in defining the magnitude of thermal contact resistances. Six locations are recommended: one each in the crucible and end caps, and three in a particular bookmold half-section. Figures 67–69 illustrate these locations in the upper end cap, lower end cap, and bookmold half-section respectively. When studying these figures, please note the following.

1. Each drawing shows a TOP, FRONT, and SIDE VIEW of a particular component with the thermocouple location(s) identified by a filled circle, letter, and complete set of dimensions.

2. Each drawing shows a REFERENCE CORNER. When the components are assembled, all of these corners must line up.

3. The bookmold drawing shows a specific half-section; the one that *wraps* around the other half-section.

4. The end cap drawings, and therefore the location of their REFERENCE CORNERS, are oriented as they would be in the assembled bookmold; that is, the slot in the bottom cap is visible in its TOP VIEW, but the slot in the upper end cap is not visible in its TOP VIEW.

5. *Vertical, horizontal, up, and down* are defined in the traditional sense; that is, with respect to the top, bottom and sides of a flat sheet of paper.

6. *Height* is defined as the vertical direction in the SIDE and FRONT VIEWS.

7. *Width* is defined as the vertical direction in the TOP VIEW and the horizontal direction in the FRONT VIEW.

8. *Depth* is defined as the horizontal direction in the SIDE and TOP VIEWS.

REFERENCE CORNER

3.125 in.

E

0.813 in.

TOP VIEW

0.250 in.

E

FRONT VIEW

3.125 in.

E

SIDE VIEW
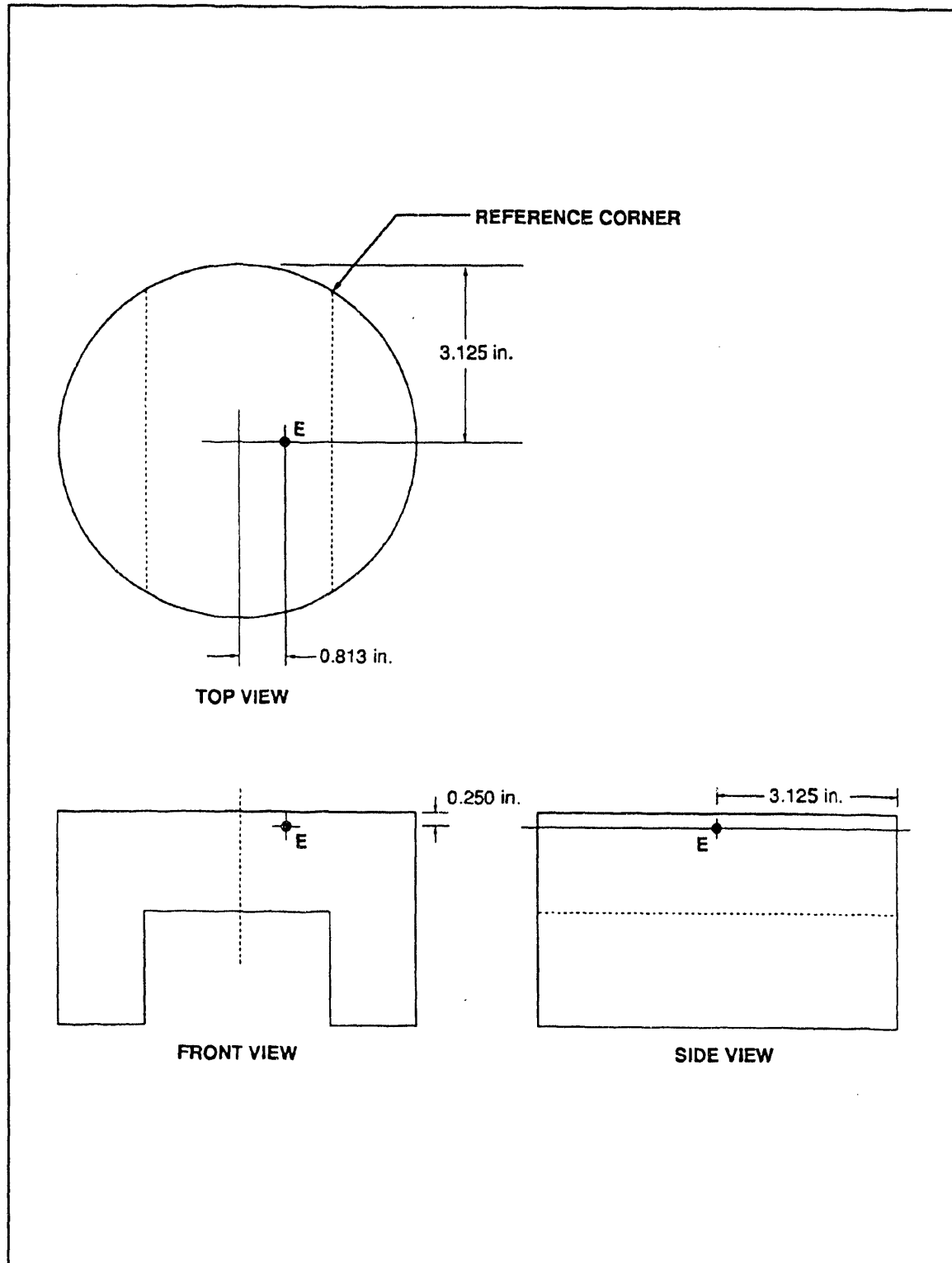
Fig. 67. Schematic illustration showing recommended thermocouple locations for upper end cap.

REFERENCE CORNER

3.125 in.

2.813 in.

D

0.420 in.

TOP VIEW

0.420 in.

D

1.500 in.

FRONT VIEW

3.125 in.

D

SIDE VIEW
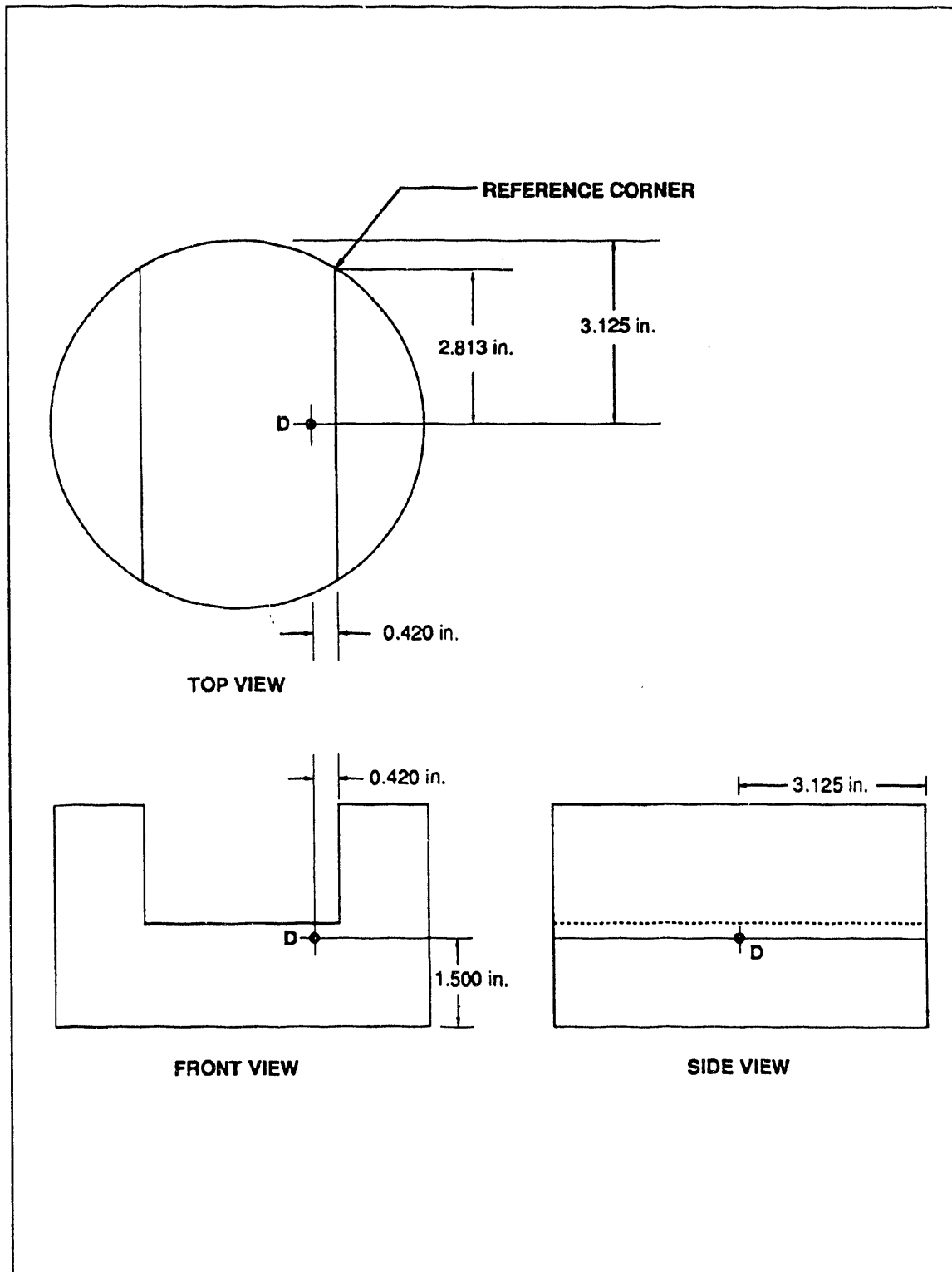
Fig. 68. Schematic illustration showing recommended thermocouple locations for the lower-end cap.

REFERENCE CORNER

0.420 in.

0.250 in.

C

1.532 in.

B

2.813 in.

A

TOP VIEW

2.813 in.

1.532 in.

0.420 in.

0.250 in.

C

C

8.053 in.

B

B

4.152 in.

A

0.250 in.

A

SIDE VIEW

FRONT VIEW
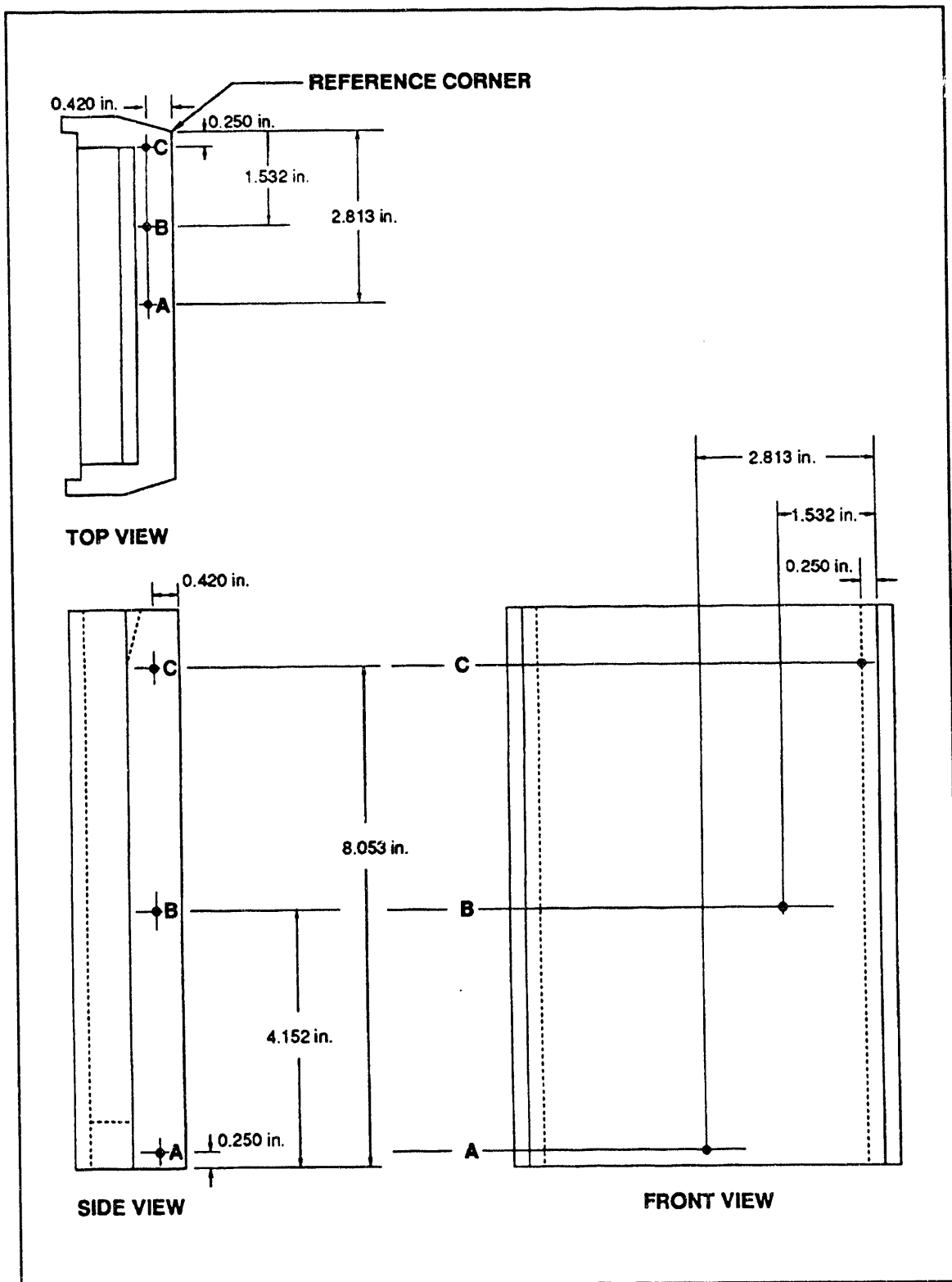
Fig. 69. Schematic illustration showing recommended thermocouple locations for the bookmold half-section.

The following verbal descriptions compliment and reinforce the illustrations. Thermocouples A, B, and C should all be placed in the center of the indicated wall; that is, at a distance equal to half the depth of the indicated wall. Thermocouple A should be placed at a point half way across the width of the section and 0.25 in. up from the bottom of the section. Thermocouple C should be placed 0.25 in. into the width of the section measured from the REFERENCE CORNER, and 7.303 in. from the bottom of the mold cavity. Since the bottom of the cavity is 0.75 in. from the bottom of the section, thermocouple C should be placed 8.053 in. up from the bottom of the section. Thermocouple B should be placed midway between thermocouples A and C in both the width and height of the section. Thermocouples A in the bookmold half-section and D in the lower end cap will be used to characterize the contact resistance between uncoated components. Thermocouple D must align with thermocouple A and be separated by a distance of 0.5 in. Its location, therefore, should be halfway into the width of the end cap, 0.42 in. to the right of the slot wall, and 1.5 in. up from the bottom of the cap. Thermocouple E in the upper end cap and the crucible thermocouple will be used to define contact resistances between coated carbon components and they should also be aligned, one over the other. The only placement criterion for Thermocouple E is that it should be separated from the thermocouple in the crucible by a distance of 0.5 in. Accordingly, its position should be half way into the width of the cap, midway between the centerline of the cap and the right hand wall of the slot, and 0.25 in. down from the top surface of the cap. The crucible thermocouple (not shown) should be positioned anywhere on a 0.813 in. radius measured from the center of the crucible and 0.25 in. into the bottom wall thickness. The 0.25 in. should be <u>measured from the bottom of the crucible; that is, from the surface that contacts the upper end cap</u>. Because of the crucible's uniform cylindrical geometry, it is not possible to define a REFERENCE CORNER. Accordingly, care should be taken during the assembly process to ensure these two thermocouples are properly aligned.

An additional concern is the actual installation of the thermocouples: specifically, the diameter of the holes that are drilled in the assembly components to accommodate the thermocouples. I have noticed that the diameter of the holes in the existing bookmold section is very much larger than the diameter of the thermocouple junction. Unless the leads are somehow mechanically secured (brazing or cementing is not recommended for this application), the junction will almost certainly move away from the end of the hole during a casting experiment. This, in turn, will introduce considerable uncertainty in the temperature measurements. The hole diameter should be approximately equal to the diameter of the insulating sheath on the thermocouple leads. This should permit friction to hold the junction in place.

A precise physical model will be required for the second-phase model as well as very accurate calculations for enclosure radiation heat transfer, liquid uranium natural convection heat transfer, thermal contact resistances, internal heat generation, and interfacial gap conductance. Considerable effort will be required to develop and execute these numerical capabilities.

The **PATRAN** family of integrated software will be the primary numerical tool used to construct and execute the second-phase physical model and calculate radiation heat transfer configuration factors. The **PATRAN Plus** module will be used to construct a 3-D, quarter symmetric finite-element mesh of the casting assembly. The **P/VIEWFACTOR** module will be used to calculate configuration factors for the crucible/crucible top, bookmold/upper end cap, and bookmold/Al_2O_3 shield radiation heat transfer *enclosures*. The **P/THERMAL** module will utilize the mesh and configuration factors to conduct the thermal analysis. These codes are currently available within Energy Systems and are among the most sophisticated commercially available programs for mesh generation and thermal analysis.

The effects of natural convection heat transfer within the crucible and bookmold buoyancy induced flow *enclosures* will be included via the technique used to iterate between the **PATRAN** and **FLOW-3D** codes. The **FLOW-3D** code will be used to study fluid motion and carbide transport, and inherent limitations in both **PATRAN** and **FLOW-3D** make it necessary to iterate between them to define a complete thermal-hydraulic solution. The iteration sequence that will be used is based on having each code supply boundary and initial conditions for its counterpart. To fix ideas consider the simplified steady-state buoyancy-driven flow system shown in Fig. 70. It consists of a vertical flat plate in an infinite, quiescent fluid at a constant temperature T_∞. The plate is heated from the exterior surface and is assumed to have a constant temperature. Velocity and thermal boundary layers develop along the height of the plate. Fluid velocities and temperature within the boundary layer, as well as the thickness of the layers, are a function of X and Y. At the edge of the boundary layer the fluid has a zero velocity and a temperature equal to ambient. Furthermore, the temperature of the interior wall (i.e., facing the uranium) is controlled by this flow system. However, the comparable system for an *enclosure* is considerably more complicated. The wall has a varying temperature along its height and the fluid outside the boundary layer is stratified; it has temperatures greater than ambient and non-zero velocities. Also, as previously explained, each wall comprising the enclosure has similar systems and they all interfere with each other. Now, **FLOW-3D** can calculate the stratified conditions at all locations within the enclosure but cannot calculate the complicated heat fluxes at the exterior surface of the enclosure. **PATRAN** can easily calculate conditions at the exterior wall given temperatures at the interior wall but cannot model the stratified conditions within the liquid uranium. Accordingly, the iteration sequence is conceptualized as follows.

Fig. 70. Simplified buoyancy-driven flow system showing velocity and thermal boundary layers.

1. The **PATRAN** physical model will initially include a simple phase-change uranium region within the bookmold and Eqs. (5) and (6) will be used to calculate a value for the heat transfer coefficient at the interior wall. A solidification analysis will then be run that will produce transient temperatures at a mid-plane in each of the bookmold walls.

2.   **FLOW-3D** will use this information as boundary conditions for a fluids analysis that will calculate temperatures at the bookmold interior surfaces as a function of the buoyancy-induced flow system described above.

3.   The phase-change region will be removed from the **PATRAN** model and replaced with a specified temperature boundary condition defined from the **FLOW-3D** results. The solidification analysis will then be repeated and the resulting mid-plane wall temperatures again supplied to **FLOW-3D**.

4.   These temperature iterations will continue until differences between successive values have become acceptably small. At this point a complete thermal-hydraulic solution will have been defined.

Thermal contact resistances between assembly components will be calculated using the following engineering correlation:[29]

$$U = 1.0 + \cfrac{BC}{K \tan^{-1}\left[\left(\dfrac{1.0}{C}\right)\sqrt{1.0 - \left(\dfrac{1.0}{U}\right)} - 1.0\right]} \ .$$

(20)

The conductance number, U, is defined as

$$U = \frac{u\delta}{k_f} \ ,$$

(21)

where

   δ = effective gap thickness between surfaces and can be approximated using:
   $\delta = 3.56\,(\ell_1 + \ell_2)$ for $(\ell_1 + \ell_2) < 7\mu m$
   $\delta = 0.46\,(\ell_1 + \ell_2)$ for $(\ell_1 + \ell_2) > 7\mu m$
   k_f = effective thermal conductivity of the fluid in the void spaces of the contact joint.

The effective conductivity for a liquid is simply its thermal conductivity. When the fluid is a gas transparent to thermal radiation, k_f is defined as

$$k_f = \cfrac{k_{g,0}}{1.0 + \left[\cfrac{8\gamma\eta L_m\left(a_1 + a_2 - a_1 a_2\right)}{\delta P_r a_1 a_2 (\gamma + 1.0)}\right]} + \frac{4\sigma\delta\epsilon_1\epsilon_2 T_m^3}{\epsilon_1 + \epsilon_2 - \epsilon_1\epsilon_2} \ .$$

(22)

For our problem, where contact occurs in a vacuum, energy exchange across voids occurs only by radiation heat transfer. Thus, Eq. (22) reduces to

$$k_f = \frac{4\sigma\delta\epsilon_1\epsilon_2 T_m^3}{\epsilon_1 + \epsilon_2 - \epsilon_1\epsilon_2} \ .$$

(23)

The constriction number of a contact joint, C, is defined as

$$C = \sqrt{\frac{P}{M}} \quad . \tag{24}$$

The conductivity number of a contact joint, K, is the ratio of the effective fluid conductivity to the harmonic mean of the material conductivities and is defined as

$$K = k_f \left(\frac{k_1 + k_2}{2k_1 k_2} \right) . \tag{25}$$

The gap number of a contact joint, B, is defined as the ratio of the effective void thickness to the radius of the contact element and can be approximated using

$$B = 0.335 C^\Psi, \quad \text{where} \quad \Psi = 0.315 \left(\frac{\sqrt{A}}{\delta} \right)^{0.137} . \tag{26}$$

There are three noteworthy considerations associated with incorporating Eq. (20) into the second-phase model: a solution procedure, defining surface roughness and hardness, and estimating contact pressures within the casting assembly as well as between the crucible wall and the Al_2O_3 insulating shield.

1. Equation (20) is transcendental and, therefore, requires an iterative solution procedure. Furthermore, temperature-dependent values for hardness and thermal conductivity as well as position dependent contact pressures are required. Because it would be inefficient to perform these calculations at run-time, a stand-alone FORTRAN program will be written to solve Eq. (20) as a function of temperature for each desired location (i.e., Z position) in the casting assembly. The resulting discrete data will then be input to the **P/THERMAL** model.

2. Surface roughness and Meyer hardness measurements for each assembly component are required. To my knowledge these data are not currently available and should be defined as soon as possible for the following locations:

    a. the underside of the crucible and its exterior wall;
    b. those portions of the upper end cap that contact the crucible and the bookmold;
    c. those portions of the bookmold that contact the upper and lower end caps;
    d. the firebrick; and
    e. the Al_2O_3 insulating shield.

    The actual casting assembly and firebrick should be used for the measurements, and those surfaces normally coated with yttrium-oxide should have a fresh application. Also, some estimate of the change in hardness with temperature should be made, a direct measurement if possible or a generic relationship from the literature.

3. Defining contact pressures has the potential to be quite complicated. As a first approximation for joints with a horizontal orientation, the weights of the individual

components above a joint can be used to estimate pressure. Thus, accurate weights of each component will be required. For those bookmold-end cap joints with a vertical orientation, a direct measurement of forces will be required. One possible procedure is to secure the upper end cap to a fixture, seat the bookmold, and then apply a force to the bookmold (either extra weights or a measured downward pull) until it unseats. The combined weights of the bookmold and the additional force could then be used to estimate the contact pressure. All of these values, however, could be significantly altered by thermal distortion of the casting assembly at the high temperatures encountered during a casting experiment. This effect must be defined if only qualitatively. Accordingly, the **ADINA** stress analysis computer program will be used to calculate the deformations. Thus, accurate dimensions for each assembly component will also be required. **ADINA** is currently in use within Energy Systems, can utilize a **PATRAN** mesh, and there are experienced personnel within the Technical Applications Engineering Department to help expedite the calculations.

The effective conductance between the crucible wall and insulating shield will also be approximated using Eq. (20). The **ADINA** code will be used to estimate the thermal growth (and therefore contact pressure) for the two components.

Internal heat generation will also have to be calculated independently of the second-phase model and then input as discrete data. Because of the complicated casting assembly-induction heater geometry, it will be necessary to solve the electromagnetic field governing equations (i.e., Maxwell's equations) directly. The Computing and Telecommunication Division does not have the necessary computer program to make this calculation, but the capability will soon exist within Energy Systems. Engineering Division is in the process of acquiring the **EMAS** code from the MacNeal-Schwendler Corporation. **EMAS** is a general analysis program for calculating electromagnetic fields in three dimensions using a finite-element solution procedure. This code should be more than adequate for our needs. One advantage of **EMAS** is that it can utilize a **PATRAN** mesh, thus reducing the total amount of time needed to construct and execute a case. We have spoken with the individual responsible for acquiring **EMAS**, and he has agreed to allow us access to the code. A great deal of properties and experimental data will be required to execute **EMAS**, and, except for heating coil current, the information should be readily available.

Defining a value for the interfacial conductance between the solidified uranium and bookmold could also require a considerable numerical effort. The literature[30,31] indicates that the mechanisms controlling the formation, growth, and thermal conductance of a gap are quite involved.

1.   A vertical[‡] gap will develop only after a sufficiently thick solid skin has formed around the melt permitting it to shrink away from the mold wall, which is simultaneously expanding because of its sudden exposure to the hot liquid metal.

2.   The transient gap size will vary as a function of the coefficients of expansion of the metal and mold and will eventually shrink to (essentially) zero as they cool.

3.   Typically the gap is too small for natural convection heat transfer and too large for contact resistance effects (i.e., those fluid-solid interactions represented by

---

‡ It is assumed that heat transfer between the bottom of the solidified melt and the mold can be calculated using Eq. (20).

accommodation coefficients). Thus, energy transfer across a gap will be by conduction through any gas that might be present and radiation heat transfer.

It is not clear if this entire sequence applies to our problem. Specifically, during the time it takes the uranium to completely solidify (which is our current focus), is the differential expansion such that radiation heat transfer is the only mechanism or do contact resistance effects become significant? This question can only be accurately answered experimentally and/or numerically, and it is not clear at this time if such an effort is warranted. Accordingly, vertical gap conductances will be calculated in the second-phase model assuming only radiation heat transfer. As a part of the model verification process, we will examine the model's sensitivity to changes in this value and then make a determination as how to proceed. If an extremely accurate value is required to achieve meaningful thermocouple agreement, it is likely that a series of minor solidification experiments and/or numerical studies using ADINA will be necessary. In any event, the implementation of the conductance mechanism within the model will also be modified. Recall that in the first-phase study the value was applied to individual nodes once the uranium at that location had solidified. In the second-phase model the conductance will only be applied after all of the uranium has solidified. Given the highly directional solidification in the current casting assembly, it is unlikely that a skin will form before the melt has completely solidified. Furthermore, it will be assumed that once the gap forms, its behavior for the remainder of the analysis is such that only radiation heat transfer occurs. It should be understood that if the scope of the analyses changes to include very long times, a numerical study of differential metal-mold expansion using ADINA might be required.

An additional category of information required to support the second-phase studies is experimental casting data. At least one consistent set of data, including direct measurements of heating coil current and cooling water temperature rise, will be needed during the model construction phase. As we have previously discussed, the current test procedure will have to be slightly modified to ensure that consistent *thermal* data are taken.

As can be seen, a great deal of data collection and preprocessing of input data will be required to conduct the second-phase thermal studies. This includes, but is not necessarily limited to,

1. modifying the vacuum-caster's instrumentation and conducting at least one casting experiment;
2. measuring surface roughness, Meyer hardness, and contact pressures of casting assembly components;
3. preparing input and executing EMAS as well as reading results into the P/THERMAL input file;
4. constructing a FORTRAN program to calculate contact resistances as a function of measured contact pressure data and temperature dependent material properties, and then reading results into the P/THERMAL input file;
5. calculating radiation heat transfer configuration factors using P/VIEWFACTOR and reading results into the P/THERMAL input file;
6. preparing input and executing ADINA as well as reading the results into the contact resistance program; and
7. constructing a FORTRAN program to read FLOW-3D results into the P/THERMAL input file.

Now, completing these tasks before developing the **P/THERMAL** model will almost certainly cause the July target for the first **P/THERMAL - FLOW-3D** iteration to slip. To prevent this, I propose to combine the construction and verification phases into discrete steps which have been designed to demonstrate the feasibility of a **P/THERMAL - FLOW-3D** iteration by the end of July. Once this has been accomplished, the remainder of the numerical/informational infrastructure required to support routine transport studies will then be developed. These steps are summarized below.

1. The efforts to construct the **P/THERMAL** model, conduct a casting experiment, measure surface characteristics and contact pressures, and define weights and dimensions of assembly components will begin immediately.

2. Steady-state and transient **P/THERMAL** models will be constructed. The models will contain uranium regions in the crucible and bookmold and will have the following macroscopic features.

    a. Natural convection heat transfer within the liquid uranium will be approximated with the same technique as was used for the first-phase study.

    b. Enclosure radiation heat transfer will be accurately calculated using configuration factors from **P/VIEWFACTOR**.

    c. Temperature-dependent contact resistances will be specified for each contact joint using predefined discrete data. Rather than run the **ADINA** code at this point, values will be approximated using Eq. (20), the measured surface characteristic, and contact pressure data. Specifically, the combined weights of assembly components will be used for horizontal joints and the *measured forces* will be used for vertical joints. As explained, a stand-alone FORTRAN program will have to be written to solve Eq. (20).

    d. Constant (i.e., not a function of time) internal heat generation rates for each affected node will be approximated with the same basic technique as was utilized for the first-phase study. The **EMAS** code will not be run at this point.

    e. Interfacial gap conductance will be accurately calculated as described above (i.e., radiation heat transfer between neighbor nodes once the entire melt has solidified).

    f. The conductance between the crucible wall and the Al_2O_3 insulating shield will be approximated assuming only radiation heat transfer.

    g. A specified heat flux boundary condition will be defined for that portion of the insulating shield normally covered by the heating coils. The value will be approximated assuming a 2°C temperature rise in the cooling water.

3. These simplified models will be verified and a nominal transient response defined. FORTRAN programs will then be written to read selected **FLOW-3D** output temperatures into **P/THERMAL** and write selected **P/THERMAL** temperatures to a data file for use by **FLOW-3D**. The uranium regions will then be removed from the **P/THERMAL** models and replaced with specified temperature boundary conditions and one complete **P/THERMAL/FLOW-3D** iteration will be completed. These tasks will be completed by the end of July 1992.

4. T e **EMAS** code will be executed to define accurate values for internal heat generation. The data will be read into **P/THERMAL**, replacing the simplified values.

5. The **ADINA** code will be run to define the contact pressure between the crucible wall and insulating shield as well as examine the effect of thermal growth on the contact resistances between assembly components.

6. Experimental data will be used to redefine the specified heat flux boundary condition on the insulating shield.

7. P/THERMAL - FLOW-3D will then be rerun and the results compared to experimental thermocouple data. An abbreviated sensitivity study will also be conducted to establish macroscopic accuracy limits for P/THERMAL. This will be accomplished by characterizing thermocouple agreement for nominal changes in certain prominent variables. The specific variables are those used to calculate macroscopic mechanisms (e.g., radiation heat transfer) but which have a natural variability (i.e., uncertainty) associated with their typical values. These include, but are not limited to, surface emissivity, material roughness and hardness, and electrical resistivity. One last caveat: the intent of the study is to quantify accuracy and not identify a single variable that could be used to calibrate the model. However, should it become apparent that such a dominant variable exists and the value needed to force agreement is physically real, some small amount of additional analyses might be required to formalize the calibration effort.

At this point, all of the properties data and numerical tools needed to support the second-phase thermal studies will be available, and carbide transport studies will begin. It should be understood that the combined thermal, hydraulic, and metallurgical problem is extremely complex. As such, it is unrealistic at this time to attempt to define a detailed action plan. This constraint results from the nature of the problem. For any development effort that seeks to define cause and effect for an actual engineering system, it is typically not possible to predefine the exact sequence of steps that will be taken. At any point in time the focus of current activities, as well as the perception of what is a potentially productive future activity, are functions of the current level of technical understanding. As cause and effect become better defined and understanding matures, the execution sequence must change to accommodate the new knowledge. Within this environment the most efficient procedure is to have a well-defined goal and a reasonable starting point. This is the approach that will be taken. The macroscopic goal of the second-phase studies is to understand transport physics to the degree required to specify those casting assembly design and/or casting procedure changes needed to force the carbide contaminants to migrate and remain at the top of the billet. These specifications will be the major deliverable of the second-phase studies. The near-term modeling tasks have been designed to accurately quantify fundamental carbide transport mechanisms within the current casting assembly during a complete casting sequence. Specifically, they will confirm the assumption that pouring completely mixes the carbide contaminants, define the effect of pouring on initial temperature distribution within the casting assembly, and characterize carbide transport in the crucible during steady state and in the bookmold during solidification. Once these results are clearly understood, a second set of analyses will be defined and executed which will ultimately produce the design and/or process modifications.

As it concerns the combined P/THERMAL - FLOW-3D studies, there is one final category of information that will have to be defined. To accurately characterize carbide transport it will be necessary to understand *solidus-liquidus* effects on carbide formation and transport. The most useful tool for defining these effects appears to be a U-C-Hf phase diagram. Thus, it will also be necessary to generate this information as a part of the second-phase studies.

ACKNOWLEDGMENTS

REFERENCES

1. G. Mackiewicz-Ludtka, W. C. Pullen, C. A. Henderson, W. Chu, and M. W. Wendel, *Carbon Reduction in Uranium Alloys Utilizing Hafnium Additions*, YDV-980, Martin Marietta Energy Systems, Inc., Oak Ridge Y-12 Plant, August 1990.

2. K. W. Childs, *HEATING 7.1 Users Manual*, K/CSD/TM-96, Martin Marietta Energy Systems, Inc., Oak Ridge K-25 Site, July 1991.

3. W. Chu and M. W. Wendel, Oak Ridge K-25 Site, letter to G. Mackiewicz-Ludtka, *Summary of U_6Nb Solidification Model Results*, Oak Ridge Y-12 Plant, December 15, 1989.

4. M. W. Wendel, Oak Ridge K-25 Site, letter to G. Mackiewicz-Ludtka, *Update of Uranium Alloy Solidification-in-a-book-mold Analysis*, Oak Ridge Y-12 Plant, May 31, 1990.

5. *Handbook of Tables for Applied Engineering Science*, Table 1-113, p. 180.

6. Y. S. Touloukian, R. W. Powell, Y. C. Ho, and P. G. Klemens, *Thermophysical Properties of Matter, Vol. 1, Thermal Conductivity Metallic Element and Alloys*, IFI/Plenum, New York, 1970.

7. Y. S. Touloukian, R. W. Powell, Y. C. Ho, and P. G. Klemens, *Thermophysical Properties of Matter, Vol. 2, Thermal Conductivity Non-Metallic Solids*, IFI/Plenum, New York, 1970.

8. Y. S. Touloukian and E. H. Buyco, *Thermophysical Properties of Matter, Vol. 4, Specific Heat Metallic Elements and Alloys*, IFI/Plenum, New York, 1970.

9. Y. S. Touloukian and E. H. Buyco, *Thermophysical Properties of Matter, Vol. 5, Specific Heat Non-Metallic Solids*, IFI/Plenum, New York, 1970.

10. J. P. Holman, *Heat Transfer*, Fifth Edition, McGraw-Hill, New York, 1981.

11. G. H. Llewellyn, G. A. Aramayo, M. Siman-Tov, K. W. Childs, and G. M. Ludtka, *Computer Simulation of Immersion Quenching of Uranium − 0.75 wt Titanium Alloy Cylinders*, Y-2355, Martin Marietta Energy Systems, Inc., Oak Ridge Y-12 Plant, June 1986.

12. R. N. Mulford and R. I. Sheldon, "Density and Heat Capacity of Liquid Uranium at High Temperatures," *J. Nucl. Mater.*, 154, 268−275 (1988).

13. C. T. Ewing, B. E. Walker, J. A. Grand, and R. R. Miller, "Thermal Conductivity of Metals," *Chem. Eng. Progr. Symp. Ser.*, 20, (53) 19−24, (1957).

14. *Metals Reference Handbook*, fifth ed., Butterworths, 1976.

15. D. Ofte, "The Viscosities of Liquid Uranium, Gold, and Lead, *J. Nucl. Mater.* 22, 28−32 (1967).

REFERENCES (continued)

16. A. F. Grens and A. P. Levitt, "The Spectral Emissivity and Total Normal Emissivity of Commercial Graphites at Elevated Temperatures," *Proceedings of the 5th Annual Conference on Carbon*, Vol. 2, pp. 639–646, 1963.

17. P. Moore, unpublished communication to P. T. Williams, *Emissivity of Liquid Uranium*, Oak Ridge Y-12 Plant, February 16, 1983.

18. Y. S. Touloukian and D. P. DeWitt, *Thermophysical Properties of Matter, Vol. 7, Thermal Radiative Properties Metallic Elements and Alloys*, IFI/Plenum, New York, 1972.

19. Y. S. Touloukian and D. P. DeWitt, *Thermophysical Properties of Matter, Vol. 8, Thermal Radiative Properties Non-Metallic Solids*, IFI/Plenum, New York, 1972.

20. A. D. Rollett and H. D. Lewis, "Casting Simulation in Vacuum Induction Melting," *Trans. Am. Foundrymen's Society*, 94, 349–372 (1986).

21. K. J. Jackson, *Vacuum-Induction Melting, Refining, and Casting of Uranium and its Alloys*, RFP-4186 UC-704 MATERIALS DOE/OSTI--500 (Interim 3), Rockwell International, Aerospace Operations, Rocky Flats Plant, Golden, Col., October 1989.

22. J. D. Lavers and P. P. Biringer, "An Improved Method of Calculating the Power Generated in an Inductively Heated Load," *Conference Record of 1971 Tenth Biennial IEEE Conference on Electric Process Heating in Industry*, pp. 44–50, April 1971.

23. N. W. McLachlan, *Bessel Functions for Engineers*, 2nd Edition, Clarendon Press, Oxford, 1955.

24. E. May, *Industrial High Frequency Electric Power*, John Wiley and Sons, New York, 1950.

25. R. P. Tye, ed. *Thermal Conductivity, Volume 2*, Academic Press, New York, 1969.

26. P. Hunley, Oak Ridge Y-12 Plant, personal communications to M. J. Taylor, Oak Ridge K-25 Site, 1991.

27. G. Mackiewicz-Ludtka and M. J. Taylor, *Utilizing Analytic Modeling to Optimize Carbon Reduction During Casting of Uranium*, Y/DV-1108, Martin Marietta Energy Systems, Inc., Oak Ridge Y-12 Plant, September 1991.

28. M. J. Taylor, Oak Ridge K-25 Site, letter to G. M. Ludtka, *Proposed Thermocouple Locations for the U-Nb Bookmold Assembly*, Oak Ridge Y-12 Plant, October 19, 1990.

29. T. N. Vezirogula, "Correlation of Thermal Contact Conductance Experimental Results," *Prog. Astron. Aero*, 20, Academic Press, New York (1967).

REFERENCES (continued)

30. B. P. Winter et al., "Volumetric Shrinkage and Gap Formation During Solidification of Copper-Base Alloys," *Trans. Am. Foundrymen's Societ* **91**, 81–88 (1983).

31. C. Y. Ho and R. D. Pehlke, "Transient Methods for Determiniation of Metal-Mold Interfacial Heat Transfer." *Trans. Am. Foundrymen's Society*, **91**, 689–698 (1983).

APPENDIX A

PROGRAM LISTINGS:

HEATING 7.1 BASE-CASE STEADY-STATE AND TRANSIENT INPUT FILES AND USER-SUPPLIED SUBROUTINES

```
options
maxpts=36000,maxcp=3500,maxpbt=2900
gml's hfc prob/3d/steady state/complete geom+gaps/props&bc's=f(t)/
********************************************************************
*
*   this heating file is for gail ludtka's 1.5' bookmold thermal analysis
*   problem. file name is "h7ss.in" and is stored in the hfc/base
*   directory on the workstations.  its purpose is to conduct the second
*   set of sensitivity studies prior to the accuracy/improvement portion
*   of the problem.
*
*   most basic problem units are w, j, m, kg, and c.
*   properties units are:
*   a.  thermal conductivity = w/m-k
*   b.  specific heat = j/kg-k
*   c.  density = kg/m3
*   d.  heats of transformation and fusion = j/kg-k
*   e.  internal heat generation = w/m3
*   f.  viscosity = mns/m2
*   g.  stef/boltz = 5.67e-08 w/m2-deg4
*
********************************************************************

20000 6 0.0 1
1 0 0 0 0

regions
*bookmold
1 1 0.0000   0.0650  0.0445  0.0636  0.0000  0.0198
2 1    0        0      38       0       0       0
2 1 0.00635  0.0650  0.0636  0.0953  0.1200  0.0198  0.0414
2 1    0        0       0       0       0       0
3 1 0.00635  0.0650  0.0953  0.1200  0.1906  0.0198  0.0414
2 1    0        0       0       0       0      24
4 1 0.00635  0.0650  0.1200  0.1906  0.2273  0.0198  0.0414
2 1    0        0       0       0       0       0
5 1 0.00635  0.0650  0.1906  0.2273  0.0198  0.0414
2 1    0        0       0       0       0
6 1 0.0000   0.0650  0.2273  0.2731  0.0198  0.0414
2 1    0        0       0       0       0
7 1 0.0650   0.0778  0.0636  0.0953  0.0000  0.0414
2 1    0       26       0       0       0       0
8 1 0.0650   0.0778  0.1200  0.1906  0.0000  0.0414
2 1    0        0       0       0       0
9 1 0.0650   0.0778  0.1906  0.2273  0.0000  0.0414
2 1    0        0       0       0       0
10 1 0.0650  0.0778  0.2273  0.2731  0.0000  0.0414
2 1    0        0       0       0       0
*liquid/solid uranium & these dimensions will change for
*different size charges.
11 2 0.0000  0.0600  0.0686  0.2681  0.0000  0.0148
1 0    0        0       0       0       0
*gap between liquid/solid uranium & top end cap
*(old hot top) & these dimensions will change for different
*size charges
12 0 0.0000  0.0600  0.2681  0.2781  0.0000  0.0148
0 0    0        0       0       0
*lower end cap
13 8 0.0000  0.0778  0.0000  0.0395  0.0000  0.0464
2 1    0       25       0       0       0
14 8 0.0000  0.0778  0.0000  0.0953  0.0464  0.0778
2 1    0       25       0      24       0      25
*upper end cap
15 8 0.0000  0.0650  0.2781  0.3176  0.0000  0.0198
2 1    0        0      39       0       0
16 8 0.0000  0.0778  0.2273  0.2781  0.0464  0.0778
2 1    0       24       0       0
*firebrick insulation/multiple regions to allow varying
*node spacing so as to reduce the total number of nodes
*in the model
17 6 0.0000  0.0778 -0.0550 -0.0050  0.0000  0.0778
6 0    0        0       0       0
18 6 0.0000  0.1068 -0.0550 -0.0050  0.1068  0.1468
6 0    0        0       4       0
19 6 0.0000  0.1068 -0.0550 -0.0050  0.1468  0.2268
6 0    0        0       4       0
20 6 0.0000  0.1068 -0.0550 -0.0050  0.2268  0.2550
6 0    0        0       4       0
21 6 0.1068  0.1468 -0.0550 -0.0050  0.0000  0.1068
6 0    0        0       0       0
22 6 0.1068  0.1468 -0.0550 -0.0050  0.1068  0.1468
```

Fig. A1. Listing of base-case HEATING steady-state input file.

```
 6 0    0       0   0        0  0       0
23 6  0.1068  0.1468   0  -0.0550  0  0.1468  0.2268
 6 0    0       0   0        0  0       0
24 6  0.1068  0.1468   0  -0.0550  0  0.2268  0.2550
 6 0    0       0   0        0  0       0
25 6  0.1468  0.2268   0  -0.0550  4  0.0000  0.1068
 6 0    0       0   0        0  0       0
26 6  0.1468  0.2268   0  -0.0550  0  0.1068  0.1468
 6 0    0       0   0        0  0       0
27 6  0.1468  0.2268   0  -0.0550  0  0.1468  0.2268
 6 0    0       0   0        0  0       0
28 6  0.1468  0.2268   0  -0.0550  0  0.2268  0.2550
 6 0    0       0   0        0  0       0
29 6  0.2268  0.2550   0  -0.0550  4  0.0000  0.1068
 6 0    0       0   0        0  0       0
30 6  0.2268  0.2550   0  -0.0550  4  0.1068  0.1468
 6 0    0       0   0        0  0       0
31 6  0.2268  0.2550   0  -0.0550  4  0.1468  0.2268
 6 0    0       0   0        0  0       0
32 6  0.2268  0.2550   0  -0.0550  4  0.2268  0.2550
 6 0    0       0   0        0  0       0
33 6  0.0000  0.1068   0  -0.1550  0  0.0000  0.1068
 6 0    0       0   0        0  0       0
34 6  0.0000  0.1068   0  -0.1550  0  0.1068  0.1468
 6 0    0       0   0        0  0       0
35 6  0.0000  0.1068   0  -0.1550  0  0.1468  0.2268
 6 0    0       0   0        0  0       0
36 6  0.0000  0.1068   0  -0.1550  0  0.2268  0.2550
 6 0    0       0   0        0  0       0
37 6  0.1068  0.1468   0  -0.1550  0  0.0000  0.1068
 6 0    0       0   0        0  0       0
38 6  0.1068  0.1468   0  -0.1550  0  0.1068  0.1468
 6 0    0       0   0        0  0       0
39 6  0.1068  0.1468   0  -0.1550  0  0.1468  0.2268
 6 0    0       0   0        0  0       0
40 6  0.1068  0.1468   0  -0.1550  0  0.2268  0.2550
 6 0    0       0   0        0  0       0
41 6  0.1468  0.2268   0  -0.1550  4  0.0000  0.1068
 6 0    0       0   0        0  0       0
42 6  0.1468  0.2268   0  -0.1550  0  0.1068  0.1468

 6 0    0       0   0        0        0  0       0
43 6  0.1468  0.2268   0  -0.1550  -0.0550  0  0.1468  0.2268
 6 0    0       0   0        0        0  0       0
44 6  0.1468  0.2268   0  -0.1550  -0.0550  0  0.2268  0.2550
 6 0    0       0   0        0        0  0       0
45 6  0.2268  0.2550   0  -0.1550  -0.0550  4  0.0000  0.1068
 6 0    0       0   0        0        0  0       0
46 6  0.2268  0.2550   4  -0.1550  -0.0550  0  0.1068  0.1468
 6 0    0       0   0        0        0  0       0
47 6  0.2268  0.2550   4  -0.1550  -0.0550  0  0.1468  0.2268
 6 0    0       0   0        0        0  0       0
48 6  0.2268  0.2550   4  -0.1550  -0.0550  4  0.2268  0.2550
 6 0    0       0   0        0        0  0       0
49 6  0.0000  0.1068   0  -0.2550  -0.1550  0  0.0000  0.1068
 6 0    0       0   0        0        0  0       0
50 6  0.0000  0.1068   0  -0.2550  -0.1550  0  0.1068  0.1468
 6 0    0       0   0        0        0  0       0
51 6  0.0000  0.1068   0  -0.2550  -0.1550  0  0.1468  0.2268
 6 0    0       0   0        0        0  0       0
52 6  0.0000  0.1068   0  -0.2550  -0.1550  4  0.2268  0.2550
 6 0    0       0   0        0        0  0       0
53 6  0.1068  0.1468   0  -0.2550  -0.1550  0  0.0000  0.1068
 6 0    0       0   0        0        0  0       0
54 6  0.1068  0.1468   0  -0.2550  -0.1550  0  0.1068  0.1468
 6 0    0       0   0        0        0  0       0
55 6  0.1068  0.1468   0  -0.2550  -0.1550  0  0.1468  0.2268
 6 0    0       0   0        0        0  0       0
56 6  0.1068  0.1468   0  -0.2550  -0.1550  4  0.2268  0.2550
 6 0    0       0   0        0        0  0       0
57 6  0.1468  0.2268   0  -0.2550  -0.1550  0  0.0000  0.1068
 6 0    0       0   0        0        0  0       0
58 6  0.1468  0.2268   0  -0.2550  -0.1550  0  0.1068  0.1468
 6 0    0       0   0        0        0  0       0
59 6  0.1468  0.2268   0  -0.2550  -0.1550  0  0.1468  0.2268
 6 0    0       0   0        0        0  0       0
60 6  0.1468  0.2268   0  -0.2550  -0.1550  4  0.2268  0.2550
 6 0    0       0   0        0        0  0       0
61 6  0.2268  0.2550   0  -0.2550  -0.1550  0  0.0000  0.1068
 6 0    0       0   0        0        0  0       0
62 6  0.2268  0.2550   0  -0.2550  -0.1550  0  0.1068  0.1468
```

Fig. A1. Listing of base-case HEATING steady-state input file (continued).

```
6 0     0       0       0        0       0       0
63 6  0.2268  0.2550  -0.2550  -0.1550  0.1468  0.2268
6 0     0       4       0        0       0
64 6  0.2268  0.2550  -0.2550  -0.1550  0.2268  0.2550
6 0     0       4       0        0       4
*gaps between lower end cap & bookmold
65 0  0.0000  0.0778  0.0395  0.0445  0.0000  0.0414
0 0     0       0       21      21      0       0
66 0  0.0000  0.0778  0.0445  0.0953  0.0414  0.0464
0 0     0       0       0       0       15      15
*gaps between liquid/solid uranium - bookmold & these
*will change for different size charges
67 0  0.0600  0.0650  0.0686  0.2681  0.0000  0.0148
0 0     0       0       0       0       0
68 0  0.0000  0.0600  0.0686  0.2681  0.0148  0.0198
0 0     0       0       0       0       0
69 0  0.0000  0.0600  0.0636  0.0686  0.0000  0.0148
0 0     0       0       0       0       0
*gaps between bookmold & upper end cap
70 0  0.0000  0.0650  0.2731  0.2781  0.0198  0.0414
0 0     0       20      20      0       0
71 0  0.0650  0.0778  0.2731  0.2781  0.0000  0.0414
0 0     0       20      20      0       0
72 0  0.0000  0.0778  0.2273  0.2731  0.0414  0.0464
0 0     0       0       0       15      15
*gap between lower end cap & firebrick
73 0  0.0000  0.0778  -0.005  0.0000  0.0000  0.0778
0 0     0       22      22      0       0
*crucible
75 1  0.0000  0.06827  0.3226  0.3480  0.00000  0.06827
2 1     0       0       0        0       0
76 1  0.0000  0.0778  0.3480  0.43403  0.06827  0.0778
2 1     0       0       0        0       0
77 1  0.06827  0.0778  0.2273  0.43403  0.0000  0.06827
2 1     0       0       0        0       0
*solid/liquid uranium and these dimensions will change for
*different size charges
78 3  0.0000  0.06327  0.3530  0.41013  0.0000  0.06327
1 0     0       0       0        0
*gaps between solid/liquid uranium - crucible & these will

*change for different size charges
79 0  0.00000  0.06327  0.3480  0.3530  0.00000  0.06327
0 0     0        0        12      12      0        0
80 0  0.00000  0.06327  0.41013  0.43903  0.00000  0.06327
0 0     0        0        29       29       0        0
81 0  0.06327  0.06827  0.3530  0.41013  0.00000  0.06327
0 0     13       13       0       0        0
82 0  0.00000  0.06327  0.3530  0.41013  0.06327  0.06827
0 0     0        0        0       0        13       13
*crucible top(made from al2o3)
83 4  0.3000  0.06827  0.43903  0.44853  0.0000  0.06827
2 0     0       0        2        0        0
*gaps between crucible & crucible top
84 0  0.00000  0.0778  0.43403  0.43903  0.06827  0.0778
0 0     0        0       15       15       0        0
85 0  0.06827  0.0778  0.43403  0.43903  0.0000  0.06827
0 0     0        0       15       15       0
*lower region of al2o3 shield
86 4  0.00000  0.08280  0.1200  0.1850  0.08280  0.0923
3 0     0        0        30      0       30
87 4  0.08280  0.09230  0.1200  0.1850  0.00000  0.0923
4 0     0        30       30      0       30
*region of al2o3 shield adjacent to heater coils
88 4  0.00000  0.08280  0.1850  0.4200  0.08280  0.0923
3 0     0        0        0       0        0
89 4  0.08280  0.09230  0.1850  0.4200  0.00000  0.0923
4 0     0        0        0       0        0
*upper region of al2o3 shield
90 4  0.00000  0.08280  0.4200  0.4450  0.08280  0.0923
3 0     0        0        30      0       30
91 4  0.08280  0.09230  0.4200  0.4450  0.00000  0.0923
4 0     0        30       30      0       30
*gaps between bookmold & shield
92 0  0.0000  0.07780  0.3480  0.43403  0.0778  0.08280
0 0     0       0        0       31       31
93 0  0.0778  0.08280  0.3480  0.43403  0.0000  0.07780
0 0     31      31       0       0        0
*gaps between shield & heater coils
94 0  0.0000  0.09230  0.1850  0.4200  0.0923  0.0973
0 0     0       0        0       35       35
```

Fig. A1 Listing of base-case HEATING steady-state input file (continued).

```
95 0 0.0923 0.09730 0.1850 0.4200 0.0000 0.0923
0 0  35  35  0  0  0  0
*representation for first set of heater coil plates
96 5 0.0000 0.09730  0.1850 0.4200 0.0973 0.098951
5 2  0  0  5  5  0  5
97 5 0.0973 0.098951 0.1850 0.4200 0.0000 0.098951
5 2  0  5  5  5  0  5
*gap between upper end cap & crucible
98 0 0.0000 0.0778 0.3176 0.3226 0.0000 0.0778
0 0  0  0  19  19  0  0
*additions to region #17 to permit consistent boundary
*conditions
99 6 0.0000 0.0778  -0.0550 -0.0050 0.0778 0.098951
6 0  0  0  0  4  0  0
100 6 0.0778 0.098951 -0.0550 -0.0050 0.0000 0.098951
6 0  0  0  0  4  0  0
*additions to region #8 to permit consistent boundary
*conditions on bookmold
101 1 0.0650 0.0778 0.0953 0.1200 0.0000 0.0414
2 1  0  26  0  0  24
*gaps to permit radiation heat transfer between bookmold
*& shield in that y space between lower edge of shield and
*bottom of top end cap
102 0 0.0 0.0778 0.1200 0.2273 0.0414 0.08280
0 0  0  0  0  34  34
*modification to gap region #93 to permit correct boundary conditions
103 0 0.0778 0.08280 0.1200 0.2273 0.0000 0.0414
0 0  34  34  0  0  0
*more modifications to region #17 to permit consistent boundary
*conditions
104 6 0.000000 0.098951 -0.0550 -0.0050 0.098951 0.1068
6 0  0  0  4  0  0
105 6 0.098951 0.106800 -0.0550 -0.0050 0.000000 0.1068
6 0  0  0  4  0  0
*representation for second set of heater coil plates
106 5 0.0000 0.0973  0.1850 0.4200 0.1200 0.121650
5 2  0  0  5  5  5  3
107 5 0.1200 0.121650 0.1850 0.4200 0.0000 0.098951
5 2  5  3  5  5  0  0
*modifications to bookmold regions to permit modeling of tc's

108 1 0.0 0.006350 0.06360 0.09530 0.031570 0.0414
2 1  0  0  0  0  0
109 1 0.0 0.006350 0.09530 0.12000 0.031570 0.0414
2 1  0  0  0  0  1
110 1 0.0 0.006350 0.12000 0.19060 0.031570 0.0414
2 1  0  0  0  0  0
111 1 0.0 0.006350 0.19060 0.22730 0.031570 0.0414
2 1  0  0  0  0  0
112 1 0.0 0.006350 0.06360 0.22730 0.01980 0.027081
2 1  0  0  0  0  0
113 1 0.0 0.006350 0.06360 0.08671 0.027081 0.031570
2 1  0  0  0  0  0
114 9 0.0 0.006350 0.08671 0.087828 0.028203 0.030448
2 0  0  0  0  0
115 9 0.0 0.006350 0.08671 0.091195 0.027081 0.028203
2 0  0  0  0  0
116 9 0.0 0.006350 0.090073 0.091195 0.028203 0.030448
2 0  0  0  0  0
117 9 0.0 0.006350 0.08671 0.091195 0.030448 0.031570
2 0  0  0  0  0
118 1 0.0 0.006350 0.091195 0.153386 0.027081 0.031570
2 1  0  0  0  0
119 9 0.0 0.006350 0.153386 0.15451 0.028203 0.030448
2 0  0  0  0  0
120 9 0.0 0.006350 0.153386 0.157875 0.027081 0.028203
2 0  0  0  0  0
121 9 0.0 0.006350 0.15675 0.157875 0.028203 0.030448
2 0  0  0  0  0
122 9 0.0 0.006350 0.153386 0.157875 0.030448 0.031570
2 0  0  0  0  0
123 1 0.0 0.006350 0.157875 0.220056 0.027081 0.031570
2 1  0  0  0  0
124 9 0.0 0.006350 0.220056 0.221178 0.028203 0.030448
2 0  0  0  0  0
125 9 0.0 0.006350 0.220056 0.22454 0.027081 0.028203
2 0  0  0  0  0
126 9 0.0 0.006350 0.22342 0.22454 0.028203 0.030448
2 0  0  0  0  0
127 9 0.0 0.006350 0.220056 0.22454 0.030448 0.031570
2 0  0  0  0  0
```

Fig. A1. Listing of base-case HEATING steady-state input file (continued).

106

```
128  1  0.0  0.006350  0.22454  0.227300  0.027081  0.031570
2 1     0    0         0        0         0         0
129  9  0.0  0.0015875 0.087828 0.090073  0.028203  0.030448
2 0     0    0         0        0         0         0
130  7  0.0015875 0.0047625 0.087828 0.090073 0.028203 0.030448
2 1     0    0         0        0         0         0
131  9  0.0047625 0.006350 0.087828 0.090073 0.028203 0.030448
2 0     0    0         0        0         0         0
132  9  0.0  0.0015875 0.15451 0.15675 0.028203 0.030448
2 0     0    0         0        0         0         0
133  7  0.0015875 0.0047625 0.15451 0.15675 0.028203 0.030448
2 1     0    0         0        0         0         0
134  9  0.0047625 0.006350 0.15451 0.15675 0.028203 0.030448
2 0     0    0         0        0         0         0
135  9  0.0  0.0015875 0.221178 0.22342 0.028203 0.030448
2 0     0    0         0        0         0         0
136  7  0.0015875 0.0047625 0.221178 0.22342 0.028203 0.030448
2 1     0    0         0        0         0         0
137  9  0.0047625 0.006350 0.221178 0.22342 0.028203 0.030448
2 0     0    0         0        0         0         0
*gap regions between copper flat plates
138  0  0.0  0.0973  0.1850  0.4200  0.098951  0.1200
0 0     0    0       11      11
139  9  0.098951  0.1200  0.1850  0.4200  0.0  0.098951
0 0     11      11      0       0       0
*modifications to gap region #93 to permit more accurate boundary
*conditions
140  0  0.0778  0.08280  0.2273  0.2781  0.0  0.0778
0 0     34      34       0       0       0
*modifications to gap region #92 to permit more accurate boundary
*conditions
141  0  0.0  0.0778  0.2273  0.3176  0.0778  0.08280
0 0     0    0       33      33
*modifications to gap regions 92 and 93 to permit more accurate
*boundary conditions
142  0  0.0778  0.08280  0.3176  0.3480  0.0  0.0778
0 0     32      32       0       0       0
143  0  0.0  0.0778  0.3176  0.3480  0.0778  0.08280
0 0     0    0       32       32
*modifications to regions 140 to permit more accurate boundary


*conditions
144  0  0.0778  0.08280  0.2781  0.3176  0.0  0.0778
0 0     33      33       0       0       0
*modifications to region #1 to permit more accurate boundary
*conditions
145  1  0.0  0.0650  0.0445  0.0636  0.0198  0.0414
2 1     0    0       0       0       0       0
146  1  0.0650  0.0778  0.0445  0.0636  0.0  0.0414
2 1     0    26      0       0       0       0
*modifications to region #15 to permit more accurate boundary
*conditions
147  8  0.0  0.0778  0.2781  0.3176  0.0198  0.0778
2 1     0    0       0       0       0       0
152  8  0.0650  0.0778  0.2781  0.3176  0.0  0.0198
2 1     0    0       0       0       0       0
*modifications to region #75 to permit more accurate boundary
*conditions
148  1  0.0  0.0778  0.3226  0.3480  0.06827  0.0778
2 1     0    0       0       0       0       0
149  1  0.06827  0.0778  0.3226  0.3480  0.0  0.06827
2 1     0    0       0       0       0       0
*modifications to region #83 to permit more accurate boundary
*conditions
150  4  0.0  0.0778  0.43903  0.44853  0.06827  0.0778
2 0     0    0       0        2        0       0
151  4  0.06827  0.0778  0.43903  0.44853  0.0  0.06827
2 0     0    0       0        2        0       0
materials
*
*  1 = atj carbon:  constant density but temp dependent km and cp.  applied
*                   to all carbon regions except end caps.
*  2 = unalloyed:  temp dependent km,cp,and density.  density function
*     uranium      has two values, 1 for t .lt. tmelt and 1 for t .ge.
*                  tmelt.  values used for each are averages. km and cp
*                  are accurately defined for both for liquid and solid
*                  temperatures.
*  3 = unalloyed:  constant cp but temp dependent km and density.
*     liquid
*     uranium
*  4 = al2o3:     constant density but temp dependent km and cp.  applied
```

Fig. A1. Listing of base-case HEATING steady-state input file (continued).

```
*       to all al2o3 regions except to sheaths.
* 5 = copper:   constant density but temp dependent km and cp. also
*       density has been adjusted to compensate for actual Ao
*       .ne. modeled Ao.
*
* 6 = firebrick:  constant properties.  used "burnt fireclay brick".
* 7 = platinum:  constant density but temp dependent km and cp. also
*       density has been adjusted to compensate for actual Ao
*       .ne. modeled Ao.
*
* 8 = atj carbon:  constant density which has been adjusted to compensate
*       for modeled volume not equal to actual volume, but actual
*       temp depen km and cp. applied to end caps.
* 9 = al2o3:   constant density which has been adjusted to compensate
*       for modeled volume not equal to actual volume.  applied
*       to thermocouple sheaths.
*
1 carbn 1   1730.0 1   -1 0  -2 0
2 urans 1   1     1   -3 -19 -4 1
661.0 20.1e+03 769.0 12.3e+03 1132.0 38.72e+03
3 uranl 1   1    198.4 -5 -18  0 0
4 al2o3 1   811.2  1   -6 0  -7 0
5 coper 1   1.899e+04  1   -8 0  -9 0
6 fbrik 1.04 2000.0 960.0  0 0   0 0
7 pltnm 1   3.421e+04  1   -20 0  -21
8 carbn 1   1902.3 1   -1 0  -2 0
9 al2o3 1   376.8  1   -6 0  -7 0
initial temperatures
*
*these temperature definitions are used for the initial debugging of the
*input file.  accordingly, they are most crude.  during an actual analysis,
*transient initial temperatures will be taken from the results of a steady
*state run using heating's "restart" option.  in all cases, the uranium region
*#1 should allways contain the desired melt temperature.
*  1 = uranium region and is constant
*  2 = carbon regions and varies with y only
*  3 = al2o3 shield with thin dimension in z direction.  varies with y & z
*  4 = al2o3 shield with thin dimension in x direction.  varies with y & x
*  5 = copper regions and is constant
*  6 = firebrick and varies with y only
1 1375.0
2 1.00 0 -10 0
```

```
3 1.0 0 -22 -23
4 1.0 -24 -22 0
5 30.0
6 1.00 0 -11 0
heat generations
1 1.41 0 0 0 2 0
2 1.41 0 0 0 2 0
boundary conditions
*
*  1 = type 1:  surf-bound for carbon via rad htx only
*       coeff is constant & bound temp is constant
*
*  2 = type 1:  surf-bound for al2o3 via rad htx only
*       coeff is func of temp & bound temp is constant
*
*  3 = type 1:  surf-bound for copper via rad htx only
*       coeff is func of temp & bound temp is constant
*       ment for exterior of copper tube.
*
*  4 = type 1:  surf-bound for firebrick via rad htx only and
*       coeffs constant & bound temp is constant
*
*  5 = type 1:  surf-bound for copper via convection and is constant
*  6 = type 3:  surf-surf for uranium to carbon via rad htx only
*       coeff is constant
*
*  7 = type 3:  surf-surf for carbon to carbon via rad htx only
*       coeff is constant
*
*  8 = type 3:  surf-surf for carbon to firebrick via rad htx only
*       coeff is constant
*
*  9 = type 3:  surf-surf for carbon to al2o3 via rad htx only
*       coeff is func of temp
*
* 10 = type 3:  surf-surf for al2o3 to copper via rad htx only
*       coeff is func of temp.  this formulation is an extreme
*       approximation and might have to be modified later in the
*       analysis.  also h has been adjusted to compensate for
*       actual Ao .ne. modeled Ao.
*
* 11 = type 3:  surf-surf for pseudo conduction between copper flat plates
*       and is applied to gap regions 138 and 139.
*
* 12 = type 3:  surf-surf for natural convection from bottom of crucible
*       and is applied to gap region # 79.
*
* 13 = type 3:  surf-surf for natural convection from vertical walls of
*       crucible and is applied to gap regions 81 & 82.
*
* 14 = type 3:  surf-surf for natural convection from bottom/vertical walls
*       of bookmold and is applied to gap regions 67, 68, and 69.
*
```

Fig. A1. Listing of base-case HEATING steady-state input file (continued).

```
*   requires user supplied subroutine
* 15 = type 3: surf-surf to simulate sliding fit between bookmold and end
*            caps and is applied gap regions 66 and 72.
* 16 = type 3: surf-surf to simulate sliding fit between bookmold and
*            shield and is applied to gap regions 92 and 93.
* 17 = type 3: surf-surf to simulate sliding fit between shield and heater
*            coils and is applied to gap regions 94 and 95.
* 18 = type 3: surf-surf to simulate contact resistance between crucible and
*            and crucible top. applied to gap regions 84 and 85.
* 19 = type 3: surf-surf to simulate contact resistance between crucible
*            and upper end cap and is applied to gap region 98.
* 20 = type 3: surf-surf to simulate contact resistance between upper end ca
*            and bookmold. applied to gap regions 70 and 71.
* 21 = type 3: surf-surf to simulate contact resistance between bookmold and
*            lower end cap. applied to gap region 65.
* 22 = type 3: surf-surf to simulate contact resistance between lower end
*            cap and firebrick. applied to gap region 73.
* 23 = type 3: surf-surf between molten uranium and al2o3.applied to gap
*            region #80.
* 24 = type 1: surf-boundary via rad htx.  constant coefficient. Boundary
*            temperature calculated in BNDTMP subroutine.  applied to:
*            1.  upper z face of regions 3 & 101
*            2.  upper y face of region 14 & 16
* 25 = type 1: surf-boundary via rad htx.  constant coefficient. Boundary
*            temperature calculated in BNDTMP subroutine. applied to
*            upper z face of region 14, upper x face of 14, and upper
*            x face of 13. also the h has been adjusted to compensate
*            for actual Ao .ne. modeled Ao.
* 26 = type 1: surf-boundary via rad htx.  constant coefficient.Boundary
*            temperature is calculated in BNDTMP subroutine.  applied to
*            upper x face of regions 1, 7, 13, and 101.
* 27 = type 3: surf to surf to simulate sliding fit between bookmold and
*            shield and is applied across gap regions 142 and 143.  also
*            the h has been adjusted to compensate for actual Ao .ne.
*            modeled Ao.
* 28 = type 3:  surf to surf to simulate radiation heat transfer between
*            upper end cap and shield and is applied to gap region 144.
*            also the h has been modified to compensate for actual Ao
*            .ne. modeled Ao.
* 29 = type 3:  surf to surf to simulate radiation heat transfer between
```

```
*            molten uranium and al2o3 crucible cover.  coefficient is
*            a function of temperature.
* 30 = type 1: surf to boundary for radiation heat transfer between al2o3
*            shield and pv wall.  coefficient is a function of temperature
*            and has been adjusted for Ao, actual .ne. Ao, modeled.
* 31 = type 3: surf-surf to simulate rad htx between al2o3 and crucible
*            vertical walls.  calculated in user supplied subroutine
*            to permit proper temp depen for surface emissivity.
* 32 = type 3:  surf-surf to simulate rad htx between crucible bottom
*            vertical walls and al2o3.  calculated in user supplied
*            subroutine to permit proper temp depen for surface
*            emissivity and value has been adjusted for actual Ao .ne.
*            modeled Ao.
* 33 = type 3:  surf-surf to simulate rad htx between top end cap and
*            al2o3.  value calculated in user supplied subroutine
*            to permit proper temp depen for surface emissivity and
*            value has been adjusted for actual Ao .ne. modeled Ao.
* 34 = type 3:  surf-surf to permit rad htx between bookmold and
*            al2o3.  value calculated in user supplied subroutine
*            to permit proper temp depen for surface emissivity.
* 35 = type 3:  surf-surf to simulate rad htx between al2o3 and copper
*            coils.  value calculated in user supplied subroutine
*            to permit proper temp depen for surface emissivity and
*            value has been adjusted for actual Ao .ne. modeled Ao.
* 36 = type 1:  surf to boundary to simulate radiation heat transfer
*            between crucible bottom and crucible top.
* 37 = type 1:  surf to boundary for radiation heat transfer between
*            crucible top and curicible bottom
* 38 = type 1:  surf to boundary to simulate radiation heat transfer
*            between bookmold bottom and lower surface of upper end
*            cap
* 39 = type 1:  surf to boundary to simulate radiation heat transfer
*            between lower surface of upper end cap and bookmold
*            bottom
*
1 1 43.0
0. 4.536e-08
2 1 43.0
0. 4.3659e-08  0  0  0  2
0 -12
```

Fig. A1. Listing of base-case HEATING steady-state input file (continued).

```
0. 1.9845e-08 0 0 0 2          2.0e+03
0 -13                          21 3 0
4 1 43.0                       2.0e+03
0. 4.2525e-08                  22 3 0
5 1 1. 0 0 -25                 2.0e+03
1.293e+04 0 0 0 0              23 3 0
6 3 0                          0.0 1.09e-08
0. 1.92026e-08                 24 1 1.0 3 0 0 0
7 3 0                          0.0 4.536e-08
0. 3.78e-08                    25 1 1.0 3 0 0 0
8 3 0                          0.0 3.661e-08
0. 3.5811e-08                  26 1 1.0 3 0 0 0
9 3 0                          0.0 4.536e-08
0. 3.6611e-08 0 0 0 2          27 3 0
0 -15                          0.0 3.273e-08
10 3 0                         28 3 0
0. 3.2e-08 0 0 0 2             0.0 2.95e-08
0 -16                          29 3 0
11 3 0                         0.0 1.8891e-08 0 0 0 2
50.e+03                        0 -26
12 3 0                         30 1 43.0
0. 0. 1.557e+04 0.25           0.0 7.7713e-08 0 0 0 2
13 3 0                         0 -12
0. 0. 4.215e+03 0.25           31 3 0
14 3 0                         0.0 1.0 0 0 0 2
1. 0 0 0 0 2                   0 4
1 0 0 0 0 0                    32 3 0
15 3 0                         0.0 1.0 0 0 0 2
2.0e+03                        0 4
16 3 0                         33 3 0
0.0 3.6611e-08 0 0 0 2         0.0 1.0 0 0 0 2
0 -27                          0 4
17 3 0                         34 3 0
2.0e+03                        0.0 1.0 0 0 0 2
18 3 0                         0 4
3.0 0 0 0 0 2                  35 3 0
-1                             0.0 1.0 0 0 0 2
19 3 0                         0 4
2.0e+03                        36 1 1.0 3
20 3 0                         0.0 1.0 0 0 0 2
```

Fig. A1. Listing of base-case HEATING steady-state input file (continued).

```
0 4
37 1 1.0 3
0.0 1.0 0 0 0 2
0 4
38 1 1.0 3
0.0 2.4192e-08
39 1 1.0 3
0.0 2.4192e-08
*
*   when conducting mesh refinement studies, the fine grid
*   line entries defined below must not be changed.  they represent
*   (basically) gaps which are quite small and do not need more than 1
*   fine grid line.
*       xgrid: positions #
*       ygrid: positions #
*       zgrid: positions #
xgrid
0.0 0.0015875 0.003175 0.0047625 0.006350 0.0600 0.06327
@0.0650 0.06827 0.0778 0.08280 0.09230 0.09730 0.098951
@0.1068 0.1200 0.121650 0.1468 0.2268 0.2550
1 1 1 1 6 1 1 1 1 1 1 1 1 1 2 1 3 4 1
ygrid
-.2550 -.1550 -.0550 -.005 0.0 .0395 .0445 .0636
@0.0686 .08671 .087828 .08895 .090073 .091195 .0953
@.1200 .153386 .15451 .15563 .15675 .157875 .1850 .1906
@.220056 .221178 .2223 .22342 .22454 .2273 .2681 .2731
@ .2781 .3176 .32260 .3480 .3530 .40513 .41013 .4200 .43403
@ .43903 .4450 0.44853
2 5 5 1 5 1 2 1 2 1 1 1 1 1 1 4 1 1 1 1 1 3 1
@4 1 1 1 1 5 1 1 5 1 3 1 6 1 2 2 1 1 1
zgrid
0.0 0.0148 0.0198 0.027081 0.028203 0.029325 0.030448 0.031570
@0.0414 0.0464 0.06327 0.06827 0.0778 0.08280 0.09230 0.0973
@0.098951 0.1068 0.1200 0.121650 0.1468 0.22680 0.25500
2 1 1 1 1 1 1 2 1 1 1 1 1 1 1 1 3 4 4
tabular functions
*
*   1 = temp depen km for carbon
*   2 = temp depen cp for carbon
*   3 = temp depen km for solid&liquid uranium
*   4 = temp depen cp for solid&liquid uranium
*   5 = temp depen km for liquid uranium
*   6 = temp depen km for al2o3
*   7 = temp depen cp for al2o3
*   8 = temp depen km for copper
*   9 = temp depen cp for copper
*   10 = y direction variation for carbon initial temps
*   11 = y direction variation for firebrick initial temps
*   12 = temp depen hr in bc#2
*   13 = temp depen hr in bc#3
*   14 = temp depen hr in bc#5
*   15 = temp depen hr in bc#9
*   16 = temp depen hr in bc#10
*   17 = temp depen hr in bc#13
*   18 = temp depen density for liquid uranium in crucible
*   19 = temp depen density for solid/liq uranium in bookmold
*   20 = temp depen km for platinum
*   21 = temp depen cp for platinum
*   22 = y direction variation for al2o3 initial temps
*   23 = z direction variation for al2o3 shield initial temps with
*        thin dimension in the z direction
*   24 = x direction variation for al2o3 shield initial temps with
*        thin dimension in the x direction
*   25 = y direction variation of cooling water temperature
*   26 = temp dependent h in bc#29
*   27 = temp dependent h in bc#16
1
27.0 129.0 77.0 124.0 127.0 118.0 227.0 106.0 327.0 95.0
@427.0 85.0 527.0 77.0 627.0 70.0 727.0 64.0 927.0 55.0
@1127.0 49.0 1327.0 45.0 1527.0 42.0 1727.0 40.0 1927.0 38.0
@2127.0 36.0 2327.0 35.0 2527.0 33.0 2727.0 31.0 2927.0 28.0
2
27.0 921.0 127. 1130.4 227. 1256.0 327. 1465.4 427.0 1549.1
@527.0 1632.9 627.0 1716.6 727.0 1758.5 1727.0 2051.5 2727.0
@2135.3
3
27. 27.6 77. 28.6 127. 29.6 227. 31.7 327.0 34.0 427.0 36.4
@527. 38.8 627.0 41.3 727. 43.9 827.0 46.3 927.0 49.0 1027.0
@50.0 1132.6 55.0 1133.6 56.0 1227.0 60.58 1477.0 67.03 1727.0
@72.56
4
```

Fig. A1. Listing of base-case HEATING steady-state input file (continued).

```
27.0 117.23 127.0 125.60 227.0 138.16 327.0 150.72 427.0 163.3
@527.0 167.47 627. 188. 727.0 205.15 827.0 209.34 927.0 234.5
@1132.6 293.08 1133.6 200.5 1800.0 200.5
5
1133.6 56.0 1227.0 60.58 1477.0 67.03 1727.0 72.56
6
27.0 36.0 77.0 30.7 127.0 26.4 227.0 20.2 327.0 15.8 427.0
@12.6 527.0 10.4 627.0 8.9 727.0 7.85 827.0 7.10 927.0
@6.55 1027. 6.13 1127. 5.83 1227. 5.66 1327. 5.56 1427. 5.54
@1527.0 5.59 1627.0 5.74 1727.0 6.0 1827.0 6.44
7
27.0 628.02 127.0 921.1 227.0 1046.7 327.0 1130.4 427.0 1172.3
@527.0 1214.2 627.0 1256.0 1827.0 1339.8
8
27.0 398.0 127.0 394. 227. 392. 327. 388. 427.0 377.0 527.0
@371.0 627.0 364.0 727.0 357.0 827.0 350.0 927.0 342.0 1027.0
@334.0
9
27.0 381.0 1027.0 460.5
10
0.0 506. 0.08895 700. 0.15563 870.0 0.2223 1000.0 0.2781 1200.0
@0.40513 1200. 0.40613 1000. 0.43403 1000.0 0.43903 800. 0.44853
@750.
11
-0.2550 25.0 -0.1270 28.0 0.0 506.0
12
127.0 1.0 1327.0 0.442
13
27.0 1.0 127.0 1.057 227.0 1.1143 327.0 1.2571 427.0 1.3429
@527.0 1.5714 927.0 2.857
14
27.0 1.0 127. 1.056 227. 1.1i2 327. 1.2513 427. 1.335 527.
@1.555 927.0 2.7643
15
127.0 1.0 1327.0 0.4213
16
127.0 1.0 1327.0 1.176
17
127.0 1.0 1327.0 1.176
18

1133. 17270. 1200. 17220. 1300. 17050. 1400. 16880. 1500. 16710.
19
27.0 18400. 1132. 18400. 1133. 17050. 1500. 17050.
20
27. 71.4 127. 71.6 227. 72.2 327.73. 427. 74.1 527. 75.5
@627. 77. 727. 78.6 827. 80.5 927. 82.6 1027. 84.8 1127. 87.1
@1227. 89.6 1327. 92.1 1427. 94.7
21
27. 125.6 127. 128.59 227. 131.58 327. 134.57 427. 137.56 527.
@140.55 627. 143.54 727. 146.54 827. 149.53 927. 152.52 1027.
@155.51 1127. 158.50 1227. 161.49 1327. 164.48 1427. 167.47
22
.1200 700.0 0.4450 1100.0
23
0.08280 1.0 0.09230 0.5
24
0.08280 1.0 0.09230 0.5
25
.1850 24.0 .4200 30.0
26
127.0 1.0 1327.0 0.64634
27
127.0 1.0 1327.0 0.4213
analytical functions
1

2

3

4

nodes monitored
*1st entry is printout per time and remaining entries are node numbers. They
*are, respectively:
* top tc, middle tc, bottom tc, uranium melt in crucible, & nominal copper tube
1 10724 10492 10330 14479 26784
steady state
1 3000 1.0e-06 1.9 10
%
```

Fig. A1. Listing of base-case HEATING steady-state input file (continued).

```
options
maxpts=36000,maxcp=3500,maxpbt=2900
gml's hfc prob/3d/trans/complete geom+gaps/props&bc's=f(t)/
****************************************************************
*
*    this heating input file is for gail ludtke's 1.5" bookmold thermal
*    analysis problem.  file name is "h7trans.in" and is stored in the hfc/base
*    directory on the workstations.  its purpose is to conduct the second set
*    of sensitivity studies prior to the accuracy improvememnt portion
*    of the problem.
*
*    most basic problem units are w, j, m, kg, and c.
*    properties units are:
*    a.  thermal conductivity = w/m-k
*    b.  specific heat = j/kg-k
*    c.  density = kg/m3
*    d.  heats of transformation and fusion = j/kg-k
*    e.  internal heat generation = w/m3
*    f.  viscosity = mns/m2
*    g.  stef/boltz = 5.67e-08 w/m2-deg4
*
****************************************************************
180000 6 0.0 1
1 0 0 0 0
regions
*bookmold
1 1  0.0000  0.0650  0.0445  0.0636  0.0000  0.0198
2 1    0       0       0       0       0       0
2 1  0.00635 0.0650  0.0636  0.0953  0.0198  0.0414
2 1    0       0       0       0       0       0
3 1  0.00635 0.0650  0.0953  0.1200  0.0198  0.0414
2 1    0       0       0       0       0      24
4 1  0.00635 0.0650  0.1200  0.1906  0.0198  0.0414
2 1    0       0       0       0       0       0
5 1  0.00635 0.0650  0.1906  0.2273  0.0198  0.0414
2 1    0       0       0       0       0       0
6 1  0.0000  0.0650  0.2273  0.2731  0.0198  0.0414
2 1    0       0       0       0       0       0
7 1  0.0650  0.0778  0.0636  0.0953  0.0000  0.0414
2 1    0      26       0       0       0       0
8 1  0.0650  0.0778  0.1200  0.1906  0.0000  0.0414
2 1    0       0       0       0       0       0
9 1  0.0650  0.0778  0.1906  0.2273  0.0000  0.0414
2 1    0       0       0       0       0       0
10 1 0.0650  0.0778  0.2273  0.2731  0.0000  0.0414
2 1    0       0       0       0       0       0
*liquid/solid uranium & these dimensions will change
*for different size charges.
11 2 0.0000  0.0600  0.0686  0.2681  0.0000  0.0148
1 0    0       0       0       0       0       0
*gap between liquid/solid uranium & top end cap
*(old hot top) & these dimensions will change for different
*size charges.
12 0 0.0000  0.0600  0.2681  0.2781  0.0000  0.0148
0 0    0       0       6       6       0       0
*lower end cap
13 8 0.0000  0.0778  0.0000  0.0395  0.0000  0.0464
2 1    0      25       0       0       0       0
14 8 0.0000  0.0778  0.0000  0.0953  0.0464  0.0778
2 1    0      25       0      24       0      25
*upper end cap
15 8 0.0000  0.0650  0.2781  0.3176  0.0000  0.0198
2 0    0       0       0       0       0       0
16 8 0.0000  0.0778  0.2273  0.2781  0.0464  0.0778
2 0    0      24       0       0       0       0
*firebrick insulation/multiple regions to allow varying
*node spacing so as to reduce the total number of nodes
*in the model
17 6 0.0000  0.0778 -0.0550 -0.0050  0.0000  0.0778
6 0    0       0       0       0       0       0
18 6 0.0000  0.1068 -0.0550 -0.0050  0.1068  0.1468
6 0    0       0       4       0       0       0
19 6 0.0000  0.1068 -0.0550 -0.0050  0.1468  0.2268
6 0    0       0       4       0       0       0
20 6 0.0000  0.1068 -0.0550 -0.0050  0.2268  0.2550
6 0    0       0       4       0       4       0
21 6 0.1068  0.1468 -0.0550 -0.0050  0.0000  0.1068
6 0    0       0       4       0       0       0
22 6 0.1068  0.1468 -0.0550 -0.0050  0.1068  0.1468
```

Fig. A2. Listing of base-case HEATING transient input file.

```
6  0
23 6  0.1068  0.1468  0  -0.0550  -0.0050  0.1468  0.2268
6  0
24 6  0.1068  0.1468  0  -0.0550  -0.0050  0.2268  0.2550
6  0
25 6  0.1468  0.2268  4  -0.0550  -0.0050  0.0000  0.1068
6  0
26 6  0.1468  0.2268  0  -0.0550  -0.0050  0.1068  0.1468
6  0
27 6  0.1468  0.2268  0  -0.0550  -0.0050  0.1468  0.2268
6  0
28 6  0.1468  0.2268  0  -0.0550  -0.0050  0.2268  0.2550
6  0
29 6  0.2268  0.2550  4  -0.0550  -0.0050  0.0000  0.1068
6  0
30 6  0.2268  0.2550  0  -0.0550  -0.0050  0.1068  0.1468
6  0
31 6  0.2268  0.2550  0  -0.0550  -0.0050  0.1468  0.2268
6  0
32 6  0.2268  0.2550  0  -0.0550  -0.0050  0.2268  0.2550
6  0
33 6  0.0000  0.1068  4  -0.1550  -0.0550  0.0000  0.1068
6  0
34 6  0.0000  0.1068  0  -0.1550  -0.0550  0.1068  0.1468
6  0
35 6  0.0000  0.1068  0  -0.1550  -0.0550  0.1468  0.2268
6  0
36 6  0.0000  0.1068  0  -0.1550  -0.0550  0.2268  0.2550
6  0
37 6  0.1068  0.1468  4  -0.1550  -0.0550  0.0000  0.1068
6  0
38 6  0.1068  0.1468  0  -0.1550  -0.0550  0.1068  0.1468
6  0
39 6  0.1068  0.1468  0  -0.1550  -0.0550  0.1468  0.2268
6  0
40 6  0.1068  0.1468  0  -0.1550  -0.0550  0.2268  0.2550
6  0
41 6  0.1468  0.2268  4  -0.1550  -0.0550  0.0000  0.1068
6  0
42 6  0.1468  0.2268  0  -0.1550  -0.0550  0.1068  0.1468

6  0
43 6  0.1468  0.2268  0  -0.1550  -0.0550  0.1468  0.2268
6  0
44 6  0.1468  0.2268  0  -0.1550  -0.0550  0.2268  0.2550
6  0
45 6  0.2268  0.2550  4  -0.1550  -0.0550  0.0000  0.1068
6  0
46 6  0.2268  0.2550  0  -0.1550  -0.0550  0.1068  0.1468
6  0
47 6  0.2268  0.2550  0  -0.1550  -0.0550  0.1468  0.2268
6  0
48 6  0.2268  0.2550  0  -0.1550  -0.0550  0.2268  0.2550
6  0
49 6  0.0000  0.1068  4  -0.2550  -0.1550  0.0000  0.1068
6  0
50 6  0.0000  0.1068  0  -0.2550  -0.1550  0.1068  0.1468
6  0
51 6  0.0000  0.1068  0  -0.2550  -0.1550  0.1468  0.2268
6  0
52 6  0.0000  0.1068  0  -0.2550  -0.1550  0.2268  0.2550
6  0
53 6  0.1068  0.1468  4  -0.2550  -0.1550  0.0000  0.1068
6  0
54 6  0.1068  0.1468  0  -0.2550  -0.1550  0.1068  0.1468
6  0
55 6  0.1068  0.1468  0  -0.2550  -0.1550  0.1468  0.2268
6  0
56 6  0.1068  0.1468  0  -0.2550  -0.1550  0.2268  0.2550
6  0
57 6  0.1468  0.2268  4  -0.2550  -0.1550  0.0000  0.1068
6  0
58 6  0.1468  0.2268  0  -0.2550  -0.1550  0.1068  0.1468
6  0
59 6  0.1468  0.2268  0  -0.2550  -0.1550  0.1468  0.2268
6  0
60 6  0.1468  0.2268  0  -0.2550  -0.1550  0.2268  0.2550
6  0
61 6  0.2268  0.2550  4  -0.2550  -0.1550  0.0000  0.1068
6  0
62 6  0.2268  0.2550  0  -0.2550  -0.1550  0.1068  0.1468
```

Fig. A2. Listing of base-case HEATING transient input file (continued).

```
6 0    0      4      0      0      0      0
63 6  0.2268 0.2550 -0.2550 -0.1550 0.1468 0.2268
6 0    0      4      0      0      0      0
64 6  0.2268 0.2550 -0.2550 -0.1550 0.2268 0.2550
6 0    0      4      0      0      0      4
*gaps between lower end cap & bookmold
65 0  0.0000 0.0778 0.0395 0.0445 0.0000 0.0414
0 0    0      0     21     21      0      0
66 0  0.0000 0.0778 0.0445 0.0953 0.0414 0.0464
0 0    0      0      0      0     15     15
*gaps between liquid/solid uranium & bookmold and these
*dimensions will change for different size charges
67 0  0.0600 0.0650 0.0886 0.2681 0.0000 0.0148
0 0   14     14      0      0      0      0
68 0  0.0000 0.0600 0.0686 0.2681 0.0148 0.0198
0 ?    0      0      0     14     14
69 0  0.0000 0.0600 0.0636 0.0686 0.0000 0.0148
0 0    0      0     14     14      0      0
*gaps between bookmold & upper end cap
70 0  0.0000 0.0650 0.2731 0.2781 0.0198 0.0414
0 0    0     20     20      0      0
71 0  0.0650 0.0778 0.2731 0.2781 0.0000 0.0414
0 0    0     20     20      0      0
72 0  0.0000 0.0778 0.2273 0.2731 0.0414 0.0464
0 0    0      0      0     15     15
*gap between lower end cap & firebrick
73 0  0.0000 0.0778 -0.005 0.0000 0.0000 0.0778
0 0    0     22     22      0      0
*crucible
75 1  0.0000 0.06827 0.3226 0.3480 0.00000 0.06827
2 1    0      0     36      0      0      0
76 1  0.0000 0.0778 0.3480 0.43403 0.06827 0.0778
2 1    0      0      0      0      0      0
77 1  0.06827 0.0778 0.3480 0.43403 0.0000 0.06827
2 1    0      0      0      0      0      0
*solid/liquid uranium and these dimensions will change for
*different size charges
78 3  0.0000 0.06327 0.3530 0.41013 0.0000 0.06327
1 0    0      0      0      0      0      0
```

```
79 0  0.00000 0.06327 0.3480 0.3530 0.00000 0.06327
0 0    0      0      0      0      0      0
80 0  0.00000 0.06327 0.41013 0.43903 0.00000 0.06327
0 0    0      0      0      0      0      0
81 0  0.06327 0.06927 0.3530 0.41013 0.00000 0.06327
0 0    0      0      0      0      0      0
82 0  0.00000 0.06327 0.3530 0.41013 0.06327 0.06827
0 0    0      0      0      0      0      0
*crucible top(made from al2o3)
83 4  0.0000 0.06827 0.43903 0.44853 0.0000 0.06827
2 0    0     37      2      0      0
*gaps between crucible & crucible top
84 0  0.00000 0.0778 0.43403 0.43903 0.06827 0.0778
0 0    0     15     15      0      0
85 0  0.06827 0.0778 0.43403 0.43903 0.0000 0.06827
0 ?    0     15     15      0
*lower region of al2o3 shield
86 4  0.00000 0.08280 0.1290 0.1850 0.09280 0.0923
3 0    0     30      0      0     30
87 4  0.08280 0.09230 0.1200 0.1850 0.00000 0.0923
4 0    0     30     30      0     30
*region of al2o3 shield adjacent to heater coils
88 4  0.00000 0.08280 0.1850 0.4200 0.08280 0.0923
3 0    0      0      0      0      0
89 4  0.08280 0.09230 0.1850 0.4200 0.00000 0.0923
4 0    0      0      0      0      0
*upper region of al2o3 shield
90 4  0.00000 0.08280 0.4200 0.4450 0.08280 0.0923
3 0    0      0     30      0     30
91 4  0.08280 0.09230 0.4200 0.4450 0.00000 0.0923
4 0    0     30     30      0     30
*gaps between bookmold & shield
92 0  0.0000 0.07780 0.3480 0.43403 0.0778 0.08280
0 0    0      0      0     31     31
93 0  0.0778 0.08280 0.3480 0.43403 0.0000 0.07780
0 0   31     31      0      0      0
*gaps between shield & heater coils
94 0  0.0000 0.09230 0.1850 0.4200 0.0923 0.0973
0 0    0      0      0     35     35
```

Fig. A2. Listing of base-case HEATING transient input file (continued).

```
0 0    35   35   0    0    0    0    0
*representation for first set of heater coil plates
96 5 0.0000 0.09730  0.1850 0.4200 0.0973 0.098951
5 2    0    0    5    5    5    0    5
97 5 0.0973 0.098951 0.1850 0.4200 0.0000 0.098951
5 2    0    5    5    5    0    5
*gap between upper end cap & crucible
98 0 0.0000 0.0778 0.3176 0.3226 0.0000 0.0778
0 0    0    0    19   19   0    0
*additions to region #17 to permit consistent boundary
*conditions
99 6 0.0000 0.0778  -0.0550 -0.0050 0.0778 0.098951
6 0    0    0    0    4    0    0
100 6 0.0778 0.098951 -0.0550 -0.0050 0.0000 0.098951
6 0    0    0    0    4    0    0
*additions to region #8 to permit consistent boundary
*conditions on bookmold
101 1 0.0650 0.0778 0.0953 0.1200 0.0000 0.0414
2 1    0    26   0    0    0    24
*gaps to permit radiation heat transfer between bookmold
*& shield in that y space between lower edge of shield and
*bottom of top end cap
102 0 0.0 0.0778 0.1200 0.2273 0.0414 0.08280
0 0    0    0    0    34   34
*modification to region #93 to permit correct boundary conditions
103 0 0.0778 0.08280 0.1200 0.2273 0.0000 0.0414
0 0    34   34   0    0    0    0
*more modifications to region #17 to permit consistent boundary
*conditions
104 6 0.000000 0.098951 -0.0550 -0.0050 0.098951 0.1068
6 0    0    0    0    4    0    0
105 6 0.098951 0.106800 -0.0550 -0.0050 0.000000 0.1068
6 0    0    0    0    4    0    0
*representation for second set of heater coil plates
106 5 0.0000 0.0973 0.1850 0.4200 0.1200 0.121650
5 2    0    0    5    5    5    3
107 5 0.1200 0.121650 0.1850 0.4200 0.0000 0.098951
5 2    5    3    5    5    0    0
*modifications to bookmold regions to permit modeling of tc's
108 1 0.0 0.006350 0.06360 0.09530 0.031570 0.0414
2 1   0    0    0    0    0    0
109 1 0.0 0.006350 0.09530 0.12000 0.031570 0.0414
2 1   0    0    0    0    0    1
110 1 0.0 0.006350 0.12000 0.19060 0.031570 0.0414
2 1   0    0    0    0    0    0
111 1 0.0 0.006350 0.19060 0.22730 0.031570 0.0414
2 1   0    0    0    0    0    0
112 1 0.0 0.006350 0.06360 0.22730 0.01980 0.027081
2 1   0    0    0    0    0    0
113 1 0.0 0.006350 0.06360 0.08671 0.027081 0.031570
2 1   0    0    0    0    0    0
114 9 0.0 0.006350 0.08671 0.087828 0.028203 0.030448
2 0   0    0    0    0    0    0
115 9 0.0 0.006350 0.08671 0.091195 0.027081 0.028203
2 0   0    0    0    0    0    0
116 9 0.0 0.006350 0.090073 0.091195 0.028203 0.030448
2 0   0    0    0    0    0    0
117 9 0.0 0.006350 0.08671 0.091195 0.030448 0.031570
2 0   0    26   0    0    0    24
118 1 0.0 0.006350 0.091195 0.153386 0.027081 0.031570
2 1   0    0    0    0    0    0
119 9 0.0 0.006350 0.153386 0.15451 0.028203 0.030448
2 0   0    0    0    0    0    0
120 9 0.0 0.006350 0.153386 0.157875 0.027081 0.028203
2 0   0    0    0    0    0    0
121 9 0.0 0.006350 0.15675 0.157875 0.028203 0.030448
2 0   0    0    0    0    0    0
122 9 0.0 0.006350 0.153386 0.157875 0.030448 0.031570
2 0   0    0    0    0    0    0
123 1 0.0 0.006350 0.157875 0.220056 0.027081 0.031570
2 1   0    0    0    0    0    0
124 9 0.0 0.006350 0.220056 0.221178 0.028203 0.030448
2 0   0    0    0    0    0    0
125 9 0.0 0.006350 0.220056 0.22454 0.027081 0.028203
2 0   0    0    0    0    0    0
126 9 0.0 0.006350 0.22342 0.22454 0.028203 0.030448
2 0   0    0    0    0    0    0
127 9 0.0 0.006350 0.220056 0.22454 0.030448 0.031570
2 0   0    0    0    0    0    0
128 1 0.0 0.006350 0.22454 0.227300 0.027081 0.031570
```

Fig. A2. Listing of base-case HEATING transient input file (continued).

```
2 1      0        0         0        0        0         0
129 9 0.0 0.0015875 0.087828 0.090073 0.028203 0.030448
2 0      0        0         0        0        0
130 7 0.0015875 0.0047625 0.087828 0.090073 0.028203 0.030448
2 1      0        0         0        0        0
131 9 0.0047625 0.006350 0.087828 0.090073 0.028203 0.030448
2 0      0        0         0        0        0
132 9 0.0 0.0015875 0.15451 0.15675 0.028203 0.030448
2 0      0        0         0        0
133 7 0.0015875 0.0047625 0.15451 0.15675 0.028203 0.030448
2 1      0        0         0        0        0
134 9 0.0047625 0.006350 0.15451 0.15675 0.028203 0.030448
2 0      0        0         0        0
135 9 0.0 0.0015875 0.221178 0.22342 0.028203 0.030448
2 0      0        0         0        0
136 7 0.0015875 0.0047625 0.221178 0.22342 0.028203 0.030448
2 1      0        0         0        0        0
137 9 0.0047625 0.006350 0.221178 0.22342 0.028203 0.030448
2 0      0        0         0        0
*gap regions between copper flat plates
138 0 0.0 0.0973 0.1850 0.4200 0.098951 0.1200
0 0     0        0        11       11
139 0 0.098951 0.1200 0.1850 0.4200 0.0 0.098951
0 0    11       11        0        0
*modifications to gap region #93 to permit more accurate boundary
*conditions
140 0 0.0778 0.08280 0.2273 0.2781 0.0 0.0778
0 0    34      34        0        0        0
*modifications to gap region #92 to permit more accurate boundary
*conditions
141 0 0.0 0.0778 0.2273 0.3176 0.0778 0.08280
0 0    0        0        33       33
*modifications to regions 140 to permit more accurate boundary
*conditions
144 0 0.0778 0.08280 0.2781 0.3176 0.0 0.0778
0 0    33      33        0        0        0
*modifications to gap regions 92 and 93 to permit more accurate
*boundary conditions
142 0 0.0778 0.08280 0.3176 0.3480 0.0 0.0778
0 0    32      32        0        0        0


143 0 0.0 0.0778 0.3176 0.3480 0.0778 0.08280
0 0    0        0        32       32
*modifications to region #1 to permit more accurate boundary
*conditions
145 1 0.0 0.0650 0.0445 0.0636 0.0198 0.0414
2 1    0        0        0        0        0
146 1 0.0650 0.0778 0.0445 0.0636 0.0 0.0414
2 1    0       26        0        0        0
*modifications to region #15 to permit more accurate boundary
*conditions
147 8 0.0 0.0778 0.2781 0.3176 0.0198 0.0778
2 1    0        0        0        0        0
152 8 0.0650 0.0778 0.2781 0.3176 0.0 0.0198
2 1    0        0        0        0        0
*modifications to region #75 to permit more accurate boundary
*conditions
148 1 0.0 0.0778 0.3226 0.3480 0.06827 0.0778
2 1    0        0        0        0        0
149 1 0.06827 0.0778 0.3226 0.3480 0.0 0.06827
2 1    0        0        0        0        0
*modifications to region #83 to permit more accurate boundary
*conditions
150 4 0.0 0.0778 0.43903 0.44853 0.06827 0.0778
2 0    0        0        2        0        0
151 4 0.06827 0.0778 0.43903 0.44853 0.0 0.06827
2 0    0        0        2        0        0
materials
*
*   1 = atj carbon:  constant density but temp dependent km and cp.  applied
*                    to all carbon regions except end caps.
*   2 = unalloyed:   temp dependent km,cp, and density.  density function
*       uranium      has two values, 1 for t .lt. tmelt and 1 for t .ge.
*                    tmelt.  values used for each are averages.  but km and cp
*                    are accurately defined for both for liquid and solid
*                    temperatures.
*   3 = unalloyed:   constant cp but temp dependent km and density.
*       liquid
*       uranium
*   4 = al2o3:       constant density but temp dependent km and cp.  applied
*                    to all al2o3 regions except tc sheaths.
```

Fig. A2. Listing of base-case HEATING transient input file (continued).

```
* 5 = copper:    constant density but temp dependent km and cp. also density
*                has been adjusted to compensate for actual Ao .ne. modeled
*                Ao.
*
* 6 = firebrick:  constant properties. used "burnt fireclay brick".
* 7 = platinum:   constant density but temp dependent km and cp. also density
*                 density has been adjusted to compensate for actual Ao .ne.
*                 modeled Ao.
*
* 8 = atj carbon: constant density which has been adjusted to compensate
*                 for modeled volume not equal to actual volume, but actual
*                 temp depen km and cp. applied to end caps.
* 9 = al2o3:      constant density which has been adjusted to compensate
*                 for modeled volume not equal to actual volume. applied
*                 to thermocouple sheaths.
1 carbn 1    1730.0  1      -1 0    -2 0
2 urans 1    1       1      -3 -19 -4 1
661.0 20.1e+03 769.0 12.3e+03 1132.0 38.72e+03
3 uranl 1        198.4 -5 -18  0 0
4 al2o3 1    811.2   1      -6 0 -7 0
5 coper 1    1.899e+04  1   -8 0 -9 0
6 fbrik 1.04 2000.0 960.0   0 0 0 0,
7 pltnm 1    3.421e+04  1   -20 0 -21
8 carbn 1    1920.3  1      -1 0 -2 0
9 al2o3 1    376.8   1      -6 0 -7 0
initial temperatures
*these temperature definitions are used for the initial debugging of the
*input file. accordingly, they are most crude. during an actual analysis,
*transient initial temperatures will be taken from the results of a steady
*state run using heating's "restart" option. in all cases, the uranium region
*#1 should allways contain the desired melt temperature.
*   1 = uranium region and is constant
*   2 = carbon regions and varies with y only
*   3 = al2o3 shield with thin dimension in z direction.  varies with y & z
*   4 = al2o3 shield with thin dimension in x direction.  varies with y & x
*   5 = copper regions and is constant
*   6 = firebrick and varies with y only
1 1375.0
2 1.00 0 -10 0
3 1.0 0 -22 -23
4 1.0 -24 -22

5 30.0
6 1.00 0 -11 0
heat generations
1 1.41 -26 0 0 2 0
2 1.41 -26 0 0 2 0
boundary conditions
*
*  1 = type 1:  surf-bound for carbon via rad htx only
*               coeff is constant & bound temp constant
*  2 = type 1:  surf-bound for al2o3 via rad htx only
*               coeff is func of temp & bound temp constant
*  3 = type 1:  surf-bound for copper via rad htx only
*               coeff is func of temp & bound temp constant
*               ment for exterior of copper tube.
*  4 = type 1:  surf-bound for firebrick via rad htx only and
*               coeffis constant & bound temp constant
*  5 = type 1:  surf-bound for copper via convection and is constant
*  6 = type 3:  surf-surf for uranium to carbon via rad htx only
*               coeff is constant
*  7 = type 3:  surf-surf for carbon to carbon via rad htx only
*               coeff is constant
*  8 = type 3:  surf-surf for carbon to firebrick via rad htx only
*               coeff is constant
*  9 = type 3:  surf-surf for carbon to al2o3 via rad htx only
*               coeff is func of temp
* 10 = type 3:  surf-surf for al2o3 to copper via rad htx only
*               coeff is func of temp.  this formulation is an extreme
*               approximation and might have to be modified later in the
*               analysis.  also h has been adjusted to compensate for
*               actual Ao .ne. modeled Ao.
* 11 = type 3:  surf-surf for pseudo conduction between copper flat plates
* 12 = type 3:  surf-surf for natural convection from bottom of crucible
*               and is applied to gap region # 79.
* 13 = type 3:  surf-surf for natural convection from vertical walls of
*               crucible and is applied to gap regions 81 & 82.
* 14 = type 3:  surf-surf for natural convection from bottom/vertical walls
*               of bookmold and is applied to gap regions67, 68, and 69.
*               requires user supplied subroutine
* 15 = type 3:  surf-surf to simulate sliding fit between bookmold and end
*               caps and is applied gap regions 66 and 72.
```

Fig. A2. Listing of base-case HEATING transient input file (continued).

```
* 16 = type 3: surf-surf to simulate sliding fit between bookmold and
*          shield and is applied to gap regions 92 and 93.
* 17 = type 3: surf-surf to simulate sliding fit between shield and heater
*          coils and is applied to gap regions 94 and 95.
* 18 = type 3: surf-surf to simulate contact resistance between crucible and
*          and crucible top. applied to gap regions 84 and 85.
* 19 = type 3: surf-surf to simulate contact resistance between crucible
*          and upper end cap and is applied to gap region 98.
* 20 = type 3: surf-surf to simulate contact resistance between upper end ca
*          and bookmold. applied to gap regions 70 and 71.
* 21 = type 3: surf-surf to simulate contact resistance between bookmold and
*          lower end cap. applied to gap region 65.
* 22 = type 3: surf-surf to simulate contact resistance between lower end
*          cap and firebrick. applied to gap region 73.
* 23 = type 3: surf-surf between molten uranium and al2o3. applied to gap
*          region 80
* 24 = type 1: surf-boundary via rad htx.  constant coefficient. Boundary
*          temperature is calculated in BNDTMP subroutine.  applied to
*          1.  upper z face of regions 3 and 101
*          2.  upper y face of region 14 and 16
* 25 = type 1: surf-boundary vis rad htx.  constant coefficient. Boundary
*          temperature is calculated in BNDTMP subroutine.  applied to
*          upper z face of region 14, upper x face of 14, and upper x
*          face of 13.  also the h has been adjusted to compensate for
*          actual Ao .ne. modeled Ao.
* 26 = type 1: surf-boundary via rad htx.  constant coefficientr. Boundary
*          temperaure calculated in BNDTMP subroutine.  applied to upper
*          x face of regions 1, 7, 13, and 101.
* 27 = type 3: surf to surf to simulate sliding fit between bookmold and
*          shield and is applied across gap regions 142 and 143.  also
*          the h has been adjusted to compensate for actual Ao .ne.
*          modeled Ao.
* 28 = type 3: surf to surf to simulate radiation heat transfer between
*          upper end cap and shield and is applied across gap region
*          144.  also the h has been adjusted to compensate for actual
*          Ao .ne. modeled Ao.
* 29 = type 3: surf to surf to simulate radiation heat transfer between
*          molten uranium and al2o3 crucible cover.  coefficient is a
*          function of temperature.
* 30 = type 1: surf to boundary for radiation heat transfer between al2o3
```

```
*          shield and pv wall.  coefficient is a function of temperature
*          and value has been adjusted for actual Ao .ne. modeled Ao.
* 31 = type 3: surf-surf to simulate rad htx between al2o3 and crucible
*          vertical walls.  calculated in user supplied subroutine
*          to permit proper temp depen for surface emissivity.
* 32 = type 3: surf-surf to simulate rad htx between crucible bottom
*          vertical walls and al2o3.  calculated in user supplied
*          subroutine to permit proper temp depen for surface
*          emissivity and value has been adjusted for actual Ao .ne.
*          modeled Ao.
* 33 = type 3: surf-surf to simulate rad htx between top end cap and
*          al2o3.  value calculated in user supplied subroutine
*          to permit proper temp depen for surface emissivity and
*          value has been adjusted for actual Ao .ne. modeled Ao.
* 34 = type 3: surf-surf to permit rad htx between bookmold and
*          al2o3.  value calculated in user supplied subroutine
*          to permit proper temp depen for surface emissivity.
* 35 = type 3: surf-surf to simulate rad htx between al2o3 and copper
*          coils.  value calculated in user supplied subroutine
*          to permit proper temp depen for surface emissivity and
*          value has been adjusted for actual Ao .ne. modeled Ao.
* 36 = type 1: surf to boundary to simulate radiation heat transfer
*          between crucible bottom and crucible top.
* 37 = type 1: surf to boundary for radiation heat transfer between
*          crucible top and curicible bottom
* 38 = type 1: surf to boundary to simulate radiation heat transfer
*          between bookmold bottom and lower surface of upper end
*          cap
* 39 = type 1: surf to boundary to simulate radiation heat transfer
*          between lower surface of upper end cap and bookmold
*          bottom
*
1 1 43.0
0. 4.536e-08
2 1 43.0
0. 4.3659e-08  0  0  0  2
0 -12
3 1 43.0
0. 1.9845e-08  0  0  0  2
0 -13
```

Fig. A2. Listing of base-case HEATING transient input file (continued).

```
4  1  43.0
0.  4.2525e-08
5  1  24.0  0  0  0  0
1.293e+04  0  0  0  0
6  3  0
0.  1.92026e-08
7  3  0
0.  3.78e-08
8  3  0
0.  3.5811e-08
9  3  0
0.  3.6611e-08  0  0  0  2
0  -15
10  3  0
0.  3.2e-08  0  0  0  2
0  -16
11  3  0
50.e+03
12  3  0
0.  0.  1.557e+04  0.25
13  3  0
0.  0.  4.215e+03  0.25
14  3  0
1.  0  0  0  0  2
1  0  0  0  0  0
15  3  0
2.0e+03
16  3  0
0.0  3.6611e-08  0  0  0  2
0  -28
17  3  0
2.0e+03
18  3  0
3.0  0  0  0  0  2
-1
19  3  0
2.0e+03
20  3  0
2.0e+03
21  3  0

2.0e+03
22  3  0
2.0e+03
23  3  0
0.0  1.09e-08
24  1  1.0  3  0  0  0
0.0  4.536e-08
25  1  1.0  3  0  0  0
0.0  3.661e-08
26  1  1.0  3  0  0  0
0.0  4.536e-08
27  3  0
0.0  3.273e-08
28  3  0
0.0  2.95e-08
29  3  0
0.0  1.8891e-08  0  0  0  2
0  -27
30  1  43.0
0.0  7.7713e-08  0  0  0  2
0  -12
31  3  0
0.0  1.0  0  0  0  2
0  4
32  3  0
0.0  1.0  0  0  0  2
0  4
33  3  0
0.0  1.0  0  0  0  2
0  4
34  3  0
0.0  1.0  0  0  0  2
0  4
35  3  0
0.0  1.0  0  0  0  2
0  4
36  1  1.0  3
0.0  1.0  0  0  0  2
0  4
37  1  1.0  3
```

Fig. A2. Listing of base-case HEATING transient input file (continued).

```
0.0 1.0 0 0 0 0 2
0 4
38 1 1.0 3
0.0 2.4192e-08
39 1 1.0 3
0.0 2.4192e-08
*   when conducting mesh refinement studies, the fine grid
*   line entries defined below must not be changed.  they represent
*   (basically) gaps which are quite small and do not need more than 1
*   fine grid line.
*       xgrid: positions #
*       ygrid: positions #
*       zgrid: positions #
xgrid
0.0 0.0015875 0.003175 0.0047625 0.006350 0.0600 0.06327
@0.0650 0.06827 0.0778 0.08280 0.09230 0.09730 0.098951
@0.1068 0.1200 0.121650 0.1468 0.2268 0.2550
1 1 1 1 6 1 1 1 1 1 1 1 1 2 1 3 4 1
ygrid
-0.2550 -0.1550 -0.0550 -0.005 0.0 0.0395 0.0445 0.0636
@0.0686 0.08671 0.087828 0.08895 0.090073 0.091195 0.0953
@0.1200 0.153386 0.15451 0.15563 0.15675 0.157875 0.1850 0.1906
@0.220056 0.221178 0.2223 0.22342 0.22454 0.2273 0.2681 0.2731
@0.2781 0.3176 0.3226 0.3480 0.3530 0.40513 0.41013 0.4200
@0.43403 0.43903 0.4450 0.44853
2 5 5 1 5 1 2 1 2 1 1 1 1 1 1 4 1 1 1 1 3 1
@4 1 1 1 1 5 1 1 5 1 3 1 6 1 2 2 1 1 1
zgrid
0.0 0.0148 0.0198 0.027081 0.028203 0.029325 0.030448 0.031570
@0.0414 0.0464 0.06327 0.06827 0.0778 0.08280 0.09230 0.0973
@0.098951 0.1068 0.1200 0.121650 0.1468 0.2268 0.2550
2 1 1 1 1 1 1 1 2 1 1 1 1 1 1 1 1 3 4 4
tabular functions
*
*   1 = temp depen km for carbon
*   2 = temp depen cp for carbon
*   3 = temp depen km for solid&liquid uranium
*   4 = temp depen cp for solid&liquid uranium
*   5 = temp depen km for liquid uranium
*   6 = temp depen km for al2o3
*   7 = temp depen cp for al2o3
*   8 = temp depen km for copper
*   9 = temp depen cp for copper
*  10 = y direction variation for carbon initial temps
*  11 = y direction variation for firebrick initial temps
*  12 = temp depen hr in bc#2
*  13 = temp depen hr in bc#3
*  14 = temp depen hr in bc#5
*  15 = temp depen hr in bc#9
*  16 = temp depen hr in bc#10
*  17 = temp depen hr in bc#13
*  18 = temp depen density for liquid uranium in crucible
*  19 = temp depen density for solid/liq uranium in bookmold
*  20 = temp depen km for platinum
*  21 = temp depen cp for platinum
*  22 = y direction variation for al2o3 initial temps
*  23 = z direction variation for al2o3 shield initial temps with
*       thin dimension in z direction
*  24 = x direction variation for al2o3 shield initial temps with
*       thin dimension in x direction
*  25 = y direction variation for cooling water temperature
*  26 = time dependence for internal heat generation
*  27 = temp dependent h in bc#29
*  28 = temp dependent h in bc#16
1
27.0 129.0 77.0 124.0 127.0 118.0 227.0 106.0 327.0 95.0
@427.0 85.0 527.0 77.0 627.0 70.0 727.0 64.0 927.0 55.0
@1127.0 49.0 1327.0 45.0 1527.0 42.0 1727.0 40.0 1927.0 38.0
@2127.0 36.0 2327.0 35.0 2527.0 33.0 2727.0 31.0 2927.0 28.0
2
27.0 921.0 127. 1130.4 227. 1256.0 327.0 1465.4 427.0 1549.1
@527.0 1632.9 627.0 1716.6 727.0 1758.5 1727.0 2051.5 2727.0
@2135.3
3
27. 27.6 77. 28.6 127. 29.6 227. 31.7 327.0 34.0 427.0 36.4
@527. 38.8 627.0 41.3 727. 43.9 827.0 46.3 927.0 49.0 1027.0
@50.0 1132.6 55.0 1133.6 56.0 1227.0 60.58 1477.0 67.03 1727.0
@72.56
4
27.0 117.23 127.0 125.60 227.0 138.16 327.0 150.72 427.0 163.3
```

Fig. A2. Listing of base-case HEATING transient input file (continued).

```
@1.555 927.0 2.7643
15
127.0 1.0 1327.0 0.4213
16
127.0 1.0 1327.0 1.176
17
127.0 1.0 1327.0 1.176
18
1133. 17270. 1200.0 17220. 1300. 17050. 1400. 16880. 1500. 16710.
19
27. 18400. 1132. 18400. 1133. 17050. 1500. 17050.
20
27. 71.4 127. 71.6 227. 72.2 327. 73. 427. 74.1 527. 75.5
@627. 77. 727. 78.6 827. 80.5 927. 82.6 1027. 84.8 1127. 87.1
@1227. 89.6 1327. 92.1 1427. 94.7
21
27. 125.6 127. 128.59 227. 131.58 327. 134.57 427. 137.56 527.
@140.55 627. 143.54 727. 146.54 827. 149.53 927. 152.52 1027.
@155.51 1127. 158.50 1227. 161.49 1327. 164.48 1427. 167.47
22
.1200 700. .4450 1100.
23
.08280 1.0 .09230 0.5
24
0.08280 1.0 0.09230 0.5
25
.1850 24. .4200 25.
26
0.0 1.0 15.0 1.0 15.05 0.0 40000 0.0
27
127.0 1.0 1327.0 0.64634
28
127.0 1.0 1327.0 0.4213
analytical functions
1

2

3

4
printout times
0.0 1.0 5.0 10.0 30.0 60.0 90.0 96.0
*120.0 150.0 180.0 210.0 240.0 270.0 300.0 330.0 360.0
*0.0 2 4 6 8 10 12 14 16 18 20 22 24 26 28 30 32 34 36
*@38 40 42 44 46 48 50 52 54 56 58 60 62 64 66 68 70 72
*@74 76 78 80 82 84 86 88 90 92 94 96 98 100 102 104 106
*@108 110 112 114 116 118 120 122 124 126 128 130 132 134
*@136 138 140 142 144 146 148 150 152 154 156 158 160 162
*@164 166 168 170 172 174 176 178 180
nodes monitored
*1st entry is printout per time and remaining entries are node numbers.
*They are, respectively:
*top tc, middle tc, nottom tc, uranium melt in crucible, & nominal copper tube
100 10724 10492 10330 14479 26784
transient
1 96.0
2.1e-05 1000 10
%
```

Fig. A2. Listing of base-case HEATING transient input file (continued).

122

```
c
c
c     this collection of user supplied subroutines was developed for
c     use with HEATING for the carbon reduction problem.  they allow:
c     1.  the heat transfer coefficient across the slodifying uranium to
c         be varied as a function of the temperature of the uranium.  for
c         t .ge. tmelt, a natural conduction coefficient is assigned.
c         for t.lt.tmelt, an effective conductance is assigned representative
c         of the shrinkage that occurs during solidification, and
c     2.  position dependent internal heat generation.
c     3.  boundary temperature as a function of al2o3 temperatures and pvw
c         temputures.
c
c
c     subroutine umontr(c,ic,lc)
c
c
c     Subroutine UMONTR allows the user access to any of the variably
c     dimensioned arrays at the end of each iteration for steady state
c     calculations or at the end of each time level for transient
c     calculations by adding one or more of the labeled commons /MON???/
c     from HEATN7.
c     initially call from HEATN7.
c     Called from SSSOR, DIRSOL, SSCGRD, TRANEX, and TRANIM at the
c     beginnig of each solution and at end of each iteration or time
c     step.
c     USRPRT called from SUMARY at output times.
c
c
      implicit double precision (a-h,o-z)
      dimension        c(1),nodes24(77),nodes26(55)
      integer      ic(1)
      logical      lc(1)
      common /monreg/ noreg,matl,mats,intem,its,ngen,ngens,nregbc,
     .nregdm,iregdi
      common /monmat/ imatna,icondu,idenst,isphea,ixd,ixc,ixk,ixt,ixtp,
     .mat,ncontp,ndentp,nsphtp,munch,mcp
      common /monint/ intm,nitpos,itempi
      common /monhgn/ lgen0,iggen,lptmf,iqhgnu,lqhgnn,ngn,ngnfcn
      common /monbdc/ nbdtp,nbytyp,nbytfn,nbtpos,ibhflg,nbctim,nbctem,
```

```
     .ibytem,ibcdef,iqbndu,iqbndn,itdum,itdum0,itdum1,ipdbtp,npdbtb,
     . npdbti,npdbtn
      common /mongrd/ ir,ith,iz,irg,ithg,izg,ndrg,ndthg,ndzg
      common /monstr/ nanalt,nparm,ie,larg,ival,ntbprs,nteb,lhival,
     . loval,lprtim,nds
      common /monrpt/ it1,it2,icdlis,ivglis,ismrcv,ismvg,id,iu,iaa,it3,
     . it4,idiag,lh,neqnod
      common /monipt/ nb,nnb,npt,nvg,ntpi,ntpj,ntpk,mreg,nt1,nblist,
     . nns,nslist,nglist,npdbtp,ludcap,ludcon,ludgen,ludpro,itixtp
      common /moncon/ nnc,nclist,nbnnc,lcnlis,n1tmp,n2tmp,nbctmp
      common /monpc / islcap,ix1,nphsch,npclst
      common /prbtyp/ nt     , ngeom , ntype , nset , kf    , idegre
      common /transt/ tim    , ftime , deltat, ktmfct, netpex, ktrans
      common /stuff/ tivs1(179),tivs2(180),tivs3(131),tivl1(179),
     *tivl2(180),tivl3(131),tlhs(33),tlhl(33)
      common /betsy/ solidk,iv1,iv2,iv3,ttot,hmax,tmelt,
     *ivs1(179),ivs2(180),ivs3(131),ivl1(179),ivl2(180),ivl3(131),
     *lhs(33),lhl(33)
      common/bounds/tavg24,tavg26,tpvw,tb36,tb37,tb38,tb39
      common/barb/t31a,t32a,t33a,t34a,t35a,t35cu,ta3637
      data nodes24/23483,23485,23487,23489,23491,23493,23495,
     *23517,23519,23521,23523,23525,23527,23529,23551,23553,
     *23555,23557,23559,23561,23563,23585,23587,23589,23591,
     *23593,23595,23597,23619,23621,23623,23625,23627,23629,
     *23631,23653,23655,23657,23659,23661,23663,23665,23691,
     *23693,23695,23697,23699,23701,23703,23735,23737,
     *23739,23741,23743,23745,23775,23777,23779,23781,23783,
     *23785,23787,23817,23819,23821,23823,23825,23827,23829,
     *23859,23861,23863,23865,23867,23869,23871/
      data nodes26/665,697,729,761,793,825,3861,3893,3925,
     *3957,3989,4021,7113,7147,7181,7215,7249,7283,10403,
     *10437,10471,10505,10539,10573,13693,13727,13761,13795,
     *13829,13863,16968,16972,16976,16980,16984,16988,19628,
     *19632,19636,19640,19642,19646,19650,22348,22352,22356,
     *22360,22364,22368,24933,24967,25001,25035,25069,25103/
      data i24/77/,i26/55/
      logical    ltrans
c
c     logic to assign temperatures of boundary nodes
c     for gaps around liquid-solid uranium
```

Fig. A3. Listing of base-case HEATING user supplied subroutines.

```
c
      do 100 i=1,iv1
      icnt=(it1+(ivs1(i)-1))
      icnt=(it1+(ivi1(i)-1))
      tivs1(i)=c(icnt)
100   tivi1(i)=c(icnt)
      do 200 i=1,iv2
      icnt=(it1+(ivs2(i)-1))
      icnt=(it1+(ivi2(i)-1))
      tivs2(i)=c(icnt)
200   tivi2(i)=c(icnt)
      do 300 i=1,iv3
      icnt=(it1+(ivs3(i)-1))
      icnt=(it1+(ivi3(i)-1))
      tivs3(i)=c(icnt)
300   tivi3(i)=c(icnt)
      do 400 i=1,hmax
      icnt=(it1+(ihs(i)-1))
      icnt=(it1+(ihl(i)-1))
      tihs(i)=c(icnt)
400   tihl(i)=c(icnt)
c
c     logic to define temperatures of values in
c     al2o3 shield for use in defining boundary
c     conditions. first step is to define al2o3
c     node temps for bc#24 and take their average
      tpvw=c(itdum)
      sum=0.0
      do 10 i=1,i24
      icnt=it1+(nodes24(i)-1)
10    sum=sum+c(icnt)
      tavg24=sum/i24
c
c     define al2o3 node temperatures for bc#26
c     and take their average
c
      sum=0.0
      do 20 i=1,i26
      icnt=it1+(nodes26(i)-1)
20    sum=sum+c(icnt)
      tavg26=sum/i26
c
c     logic to define temperature pairs for
c     gap-gap radiation bc's # 31,32,33,34, and
c     35.
c
      t31a=c(it1+(24350-1))
      t32a=c(it1+(24203-1))
      t33a=c(it1+(24119-1))
      t34a=c(it1+(23644-1))
      t35a=c(it1+(25470-1))
      t35cu=c(it1+(26718-1))
c
c     logic for boundary temperatures for bc's
c     #36,37,38,and 39
c
      tb36=c(it1+(11332-1))
      tb37=c(it1+(11127-1))
      tb38=c(it1+(2761-1))
      tb39=c(it1+(2129-1))
      ta3637=tb36
9999  return
      entry usrprt(c,ic,lc)
      return
      end
c
c
c
c
      subroutine convtn(rvalue,r,th,z,tim,ten,value,number,n,arg,val,
     *ntbprs,ntab,hival,loval)
c
c     this subroutine identifies the orientation of the current node and
c     then assigns a value for the heat transfer coefficient based on the
c     temperature of the liquid uranium at that point.
c
      implicit double precision (a-h,o-z)
      common/iounit/iecho,ihstry,imatlb,in,io,iplot,iplot0,icmvrg,iconn
      dimension arg(1),val(1)
```

Fig. A3. Listing of base-case HEATING user supplied subroutines (continued).

```fortran
      common/betsy/solidk,iv1,iv2,iv3,itot,hmax,tmelt,ivs1(179),
     *ivs2(180),ivs3(131),ivl1(179),ivl2(180),ivl3(131),ihs(33),
     *ihl(33)
      common/stuff/tivs1(179),tivs2(180),tivs3(131),tivl1(179),
     *tivl2(180),tivl3(131),tihs(33),tihl(33)
c
c     program logic
c
      do 100 i=1,iv1
      if(n.eq.ivs1(i).or.n.eq. ivl1(i))then
      ts=tivs1(i)
      tl=tivl1(i)
      go to 1000
      else
      go to 100
      end if
100   continue
      do 200 i=1,iv2
      if(n.eq.ivs2(i).or.n.eq. ivl2(i))then
      ts=tivs2(i)
      tl=tivl2(i)
      go to 1000
      else
      go to 200
      end if
200   continue
      do 300 i=1,iv3
      if(n.eq.ivs3(i).or.n.eq. ivl3(i))then
      ts=tivs3(i)
      tl=tivl3(i)
      go to 1000
      else
      go to 300
      end if
300   continue
      do 400 i=1,hmax
      if(n.eq.ihs(i).or.n.eq.ihl(i)) then
      ts=tihs(i)
      tl=tihl(i)
      go to 1500

      else
      go to 400
      end if
400   continue
      write(io,5000)n
      stop
c
c     logic for vertical plate coefficient
c
1000  if(tl.lt.tmelt)then
      rvalue=solidk
      else
      dt=dabs(tl-ts)
      h=1.5778e+(.4*(dt**.25)
      rvalue=h/dt
      endif
      go to 9999
c
c     logic for horizontal plate coefficient
c
1500  if(tl.lt.tmelt)then
      rvalue=solidk
      else
      dt=dabs(tl-ts)
      h=1.595e+04*(dt**.25)
      rvalue=h/dt
      endif
9999  return
c
c     format statements for this routine
c
5000  format(10x,'///DANGER,DANGER, WILL ROBINSON!!'/
     *10x,'CONVTN could not identify node # ',i5/10x,
     *'Execution terminated.')
      end
c
c
c
c
c
```

Fig. A3.   Listing of base-case HEATING user supplied subroutines (continued).

```fortran
      subroutine heatgn(rvalue,r,th,z,tim,tsn,value,number,n,arg,val,
     . ntbprs,ntab,hival,loval)
c*********************************************************************
c
c this routine calculates internal heat generation for the carbon casting
c assembly and copper flat plates.
c
c when it is referenced, this subroutine must be supplied by the user to
c evaluate the user-supplied function defining the volumetric heat
c generation rate.  this parameter may be time-, temperature- and/or
c position-dependent.
c
c note: the heat generation rate is calculated as
c            q = f(r,th,z,tsn) * g(tim)
c      this subroutine may be called first to calculate the
c      factor f.  then, this routine is called from the solution
c      algorithm to update the time-dependent factor g of
c      the heat generation rate.  when this factor is updated, only
c      tim, number, and value are defined where value = 1.0.
c      the two calls may be identified by the value of n.
c      in the first call, n contains the number of the node whose
c      heat generation rate is being evaluated.  in the second
c      call, n is set to zero.
c
c the variables in the argument list are defined in the following table.
c (y) indicates that the variable has been defined when this subroutine
c is called.  (n) indicates it has not been defined.
c
c variable  type     definition
c rvalue    real     value of the user-supplied function
c                    evaluating the volumetric heat generation
c                    rate (this value must be computed by this
c                    routine). (n)
c                    name of variable in calling sequence - gen.
c r         real     x or r coordinate of node n. (y)
c th        real     y or theta coordinate of node n. (y)
c z         real     z or phi coordinate of node n. (y)
c tim       real     time at which parameter is to be
c                    evaluated. (y)
c tsn       real     temperature at which parameter is to be
c                    evaluated. (y)
c value     real     constant value of the parameter which
c                    appears on its respective input card (g) if
c                    it is non-zero.
c                    if it is zero, value contains 1.0. (y)
c                    name of variable in calling sequence -
c                    gen0(ngn).
c number    integer  index of parameter being evaluated. (y)
c                    name of variable in calling sequence - ngn.
c n         integer  node number. (y)
c arg,val   real     arrays containing the independent and
c                    dependent values for tabular functions,
c                    respectively. only used in calls to table.
c
c*********************************************************************
c
      implicit double precision (a-h,o-z)
      dimension   arg(1), val(1)
      common /iounit/ iecho, ihstry, imatlb, in   , io   , iplot ,
     .                iplot0, icrvrg, iconn
      data a0/0.7845/,a1/0.1262/,a2/-0.4752/,a3/0.02667/,tol/1.0e-08/,
     . debug/0.0/
      rvalue=0.0
c
c determine if carbon or copper region is being defined and then
c route to appropriate logic
c
      if(r.gt..09.or.z.gt..09) then
      rvalue=4.938e+01*(value**2)
      go to 9999
      else
      go to 50
      end if
   50 if(th.gt..47875.or.th.lt..12625) then
      go to 9999
      else
      zhat=dabs(th-.3025)/0.1175
      hrat=a0+a1*zhat+a2*(zhat**2)+a3*(zhat**3)
```

Fig. A3. Listing of base-case HEATING user supplied subroutines (continued).

```
      if(hrat.lt.0.0)hrat=0.0e+00
c
c     determine appropriate vertical region.  multiple
c     logic checks are required because of double precision
c     considerations
c
      if(th.gt..3480.and.th.lt..47875) go to 100
      tol1=dabs(th-.3480)
      tol2=dabs(th-.47875)
      if(tol1.lt.tol.or.tol2.lt.tol) go to 100
      if(th.gt..3226.and.th.lt..3480)  go to 200
      tol1=dabs(th-.3226)
      if(tol1.lt.tol) go to 200
      if(th.gt..2781.and.th.lt..3176)  go to 300
      tol1=dabs(th-.2781)
      tol2=dabs(th-.3176)
      if(tol1.lt.tol.or.tol2.lt.tol) go to 300
      if(th.gt..2273.and.th.lt..2781)  go to 400
      tol1=dabs(th-.2273)
      if(tol1.lt.tol) go to 400
      if(th.gt..12625.and.th.lt..2273) go to 500
      tol1=dabs(th-.12625)
      if(tol1.lt.tol) go to 500
      go to 600
      end if
c
c     logic for crucible walls
c
100   rvalue= 5.088e+06*hrat*(value**2)
      go to 9999
c
c     logic for crucible bottom
c
200   c1=4.116e+06*hrat*(value**2)
      if(r.gt..0636.and.r.lt..0778)rvalue=c1
      tol1=dabs(r-.0636)
      tol2=dabs(r-.0778)
      if(tol1.lt.tol.or.tol2.lt.tol)rvalue=c1
      if(z.gt..0636.and.z.lt..0778.and.r.lt..0636)rvalue=c1
      tol1=dabs(z-.0636)

      tol2=dabs(z-.0778)
      if(tol1.lt.tol.and.r.lt..0636)rvalue=c1
      if(tol2.lt.tol.and.r.lt..0636)rvalue=c1
      go to 9999
c
c     logic for top end cap/horizontal
c
300   c1=4.122e+06*hrat*(value**2)
      if(r.gt..0636.and.r.lt..0778)rvalue=c1
      tol1=dabs(r-.0636)
      tol2=dabs(r-.0778)
      if(tol1.lt.tol.or.tol2.lt.tol)rvalue=c1
      if(z.gt..0636.and.z.lt..0778.and.r.lt..0636)rvalue=c1
      tol1=dabs(z-.0636)
      tol2=dabs(z-.0778)
      if(tol1.lt.tol.and.r.lt..0636)rvalue=c1
      if(tol2.lt.tol.and.r.lt..0636)rvalue=c1
      go to 9999
c
c     logic for top end cap/vertical
c
400   c1=5.0775e+06*hrat*(value**2)
      if(z.gt..0636.and.z.lt..0778) rvalue=c1
      tol1=dabs(z-.0636)
      tol2=dabs(z-.0778)
      if(tol1.lt.tol.or.tol2.lt.tol)rvalue=c1
      go to 9999
c
c     logic for bookmold
c
500   c1=4.446e+06*hrat*(value**2)
      if(r.gt..0650.and.r.lt..0778)rvalue=c1
      tol1=dabs(r-.0650)
      tol2=dabs(r-.0778)
      if(tol1.lt.tol.or.tol2.lt.tol)rvalue=c1
      if(z.gt..0272.and.z.lt..0414.and.r.lt..0650)rvalue=c1
      tol1=dabs(z-.0272)
      tol2=dabs(z-.0414)
      if(tol1.lt.tol.and.r.lt..0650)rvalue=c1
      if(tol2.lt.tol.and.r.lt..0650)rvalue=c1
```

Fig. A3. Listing of base-case HEATING user supplied subroutines (continued).

```fortran
      subroutine bndtmp(rvalue,r,th,z,tim,tsn,value,number,n,arg,val,
     . ntbprs,ntab,hival,loval)
c   **************************************************************
c
c   when it is referenced, this subroutine must be supplied by the user to
c   evaluate the user-supplied function defining the boundary temperature.
c
c this parameter may be time-dependent and/or position-dependent.
c the variables in the argument list are defined in the following table.
c (y) indicates that the variable has been defined when this subroutine
c is called.  (n) indicates it has not been defined.
c
c   variable  type    definition
c   rvalue    real    value of the user-supplied function
c                     evaluating the boundary temperature (this
c                     value must be computed by this routine). (n)
c                     name of variable in calling sequence –
c                     tdum(i).
c
c   r         real    x or r coordinate of node n. (y)
c   th        real    y or theta coordinate of node n. (y)
c   z         real    z or phi coordinate of node n. (y)
c   tim       real    time at which parameter is to be
c                     evaluated. (y)
c   tsn       real    temperature at which parameter is to be
c                     evaluated. (n)
c   value     real    constant value of the parameter which
c                     appears on its respective input card (b1) if
c                     it is non-zero.
c                     if it is zero, value contains 1.0. (y)
c   number    integer index of parameter being evaluated. (y)
c                     name of variable in calling sequence - nbdtp
c                     bytemp(nbdtp).
c   n         integer node number. (n)
c   arg,val   real    arrays containing the independent and
c                     dependent values for tabular functions,
c                     respectively.  only used in calls to table.
c
c **********************************************************************
c
      implicit double precision(a-h,o-z)
      common/bounds/tavg24,tavg26,tpvw,tb36,tb37,tb38,tb39
      if(number.eq.24)rvalue=tavg24
      if(number.eq.25)rvalue=.50*tavg24+.5*tpvw
      if(number.eq.26)rvalue=.25*tavg26+.75*tpvw
          if(number.eq.36)rvalue=tb36
          if(number.eq.37)rvalue=tb37

      tol1 = dabs(z-.0272)
      tol2 = dabs(z-.0414)
      if(tol1.lt.tol.and.r.lt..0650)rvalue=c1
      if(tol2.lt.tol.and.r.lt..0650)rvalue=c1
      go to 9999
c
c   write statement for routine problem
c
600   write(io,5000)n,th
      stop
c
c   debugging write statement
c
9999  if(rvalue.gt.0.0.and.debug.gt.0.0) then
      write(io,5010)n,r,th,z,rvalue
      else
      if(debug.gt.0.0) write(io,5020)n,r,th,z
      end if
      return
c
c   format statements for this routine
c
5000  format(10x,'////DANGER, DANGER WILL ROBINSON !',/
     ' .10X,'HEATGN logic cannot route node number ',i6,
     ' @ Y = ',e30,20)
5010  format(i6,4e15.9)
5020  format(i6,3e15.9,5x,'NOT ASSIGNED')
      end
c
c
c
c
c
```

Fig. A3. Listing of base-case HEATING user supplied subroutines (continued).

128

```
c        if(number.eq.38)rvalue=tb38
c        if(number.eq.39)rvalue=tb39
c
         return
         end
c
c
c
c        subroutine radltn(rvalue,r,th,z,tim,tsn,value,number,n,arg,val,
c       .ntbprs,ntab,hival,loval)
c *****************************************************
c
c  when it is referenced, this subroutine must be supplied by the user to
c  evaluate the user-supplied function defining the coefficient for
c  radiative heat transfer.  this parameter may be time- and/or
c  temperature-dependent.
c  the variables in the argument list are defined in the following table.
c  (y) indicates that the variable has been defined when this subroutine
c  is called.  (n) indicates it has not been defined.
c
c  variable  type   definition
c  rvalue    real   value of the user-supplied function
c                   evaluating the coefficient for radiative
c                   heat transfer (this value must be computed
c                   by this routine). (n)
c                   name of variable in calling sequence -
c                   bhrad1.
c
c  r         real   x or r coordinate of node n. (y)
c  th        real   y or theta coordinate of node n. (y)
c  z         real   z or phi coordinate of node n. (y)
c  tim       real   time at which parameter is to be
c                   evaluated. (y)
c  tsn       real   temperature at which parameter is to be
c                   evaluated. (y)
c  value     real   constant value of the parameter which
c                   appears on its respective input card (b2) if
c                   it is non-zero.
c                   if it is zero, value contains 1.0. (y)
c                   name of variable in calling sequence -
```

```
c        bhrad(nbdtp).
c  number  integer  index of parameter being evaluated. (y)
c                   name of variable in calling sequence - nbdtp
c  n       integer  node number. (y)
c  arg,val real     arrays containing the independent and
c                   dependent values for tabular functions,
c                   respectively.  only used in calls to table.
c
c *****************************************************
c
c        implicit double precision (a-h,o-z)
         common/barb/t31a,t32a,t33a,t34a,t35a,t35cu,te3637
         common/iounit/iecho,ihstry,imatlb,in,io,iplot,
        *iplot0,icnvrg,iconn
c
c        begin program logic. define either carbon or copper
c        surface emissivity
c
         if(number.lt.31.or.number.gt.37) go to 9000
         if(number.gt.35)goto 3000
         if(number.le.34) emis1=0.8
         if(number.eq.35) then
         emis1=0.3092*dexp(0.118d-02*t35cu)
         if(t35cu.le.127.) emis1=0.35
         if(t35cu.ge.927.)then emis1=1.0
         endif
c
c        define al2o3 surface emissivity
c
         if(number.eq.31)then
         tmp=t31a
         aoadj=1.0
         elseif(number.eq.32)then
         tmp=t32a
         aoadj=0.894
         elseif(number.eq.33)then
         tmp=t33a
         aoadj=0.807
         elseif(number.eq.34)then
```

Fig. A3. Listing of base-case HEATING user supplied subroutines (continued).

```
          tmp=t34a
          aoadj=1.0
        else
          tmp=t35a
          aoadj=1.78
        endif
        emis2=-0.3583d-03*tmp+0.8155
        if(tmp.le.127.)emis2=0.77
        if(tmp.ge.1327.)emis2=0.34
        denom=(1./emis1 + 1./emis2 -1.0)
        rvalue=((emis1*emis2*5.67d-08)/denom)*aoadj
        go to 9999
 3000   emis1=0.8
        emis2=-0.3583d-03*ta3637+0.8155
        if(ta3637.le.127.)emis2=0.77
        if(ta3637.gt.1327.)emis2=0.34
        denom=(1./emis1 + 1./emis2 - 1.)
        rvalue=(emis1*emis2*5.67d-08)/denom
        go to 9999
 9000   write(io,5000)number
        stop
 9999   return
c
c       format statements for this routine
c
 5000   format(10x,///'DANGER,DANGER, WILL ROBINSON!!!'/
       *10x,'RADITN could not identify bc# ',i3/
       *10x,'Execution terminated.')
        end
c
c
c
c
c       block data bmt
c
c       basic information that needs to be initialized in order to calculate
c       uranium melt boundary conditions as a function of temperature.
c
        implicit double precision (a-h,o-z)
```

```
        common/betsy/rolidk,iv1,iv2,iv3,itct,hmax,tmelt,ivsi(179),
       *tvs2(180),tvs3(131),lvt1(179),lvt2(180),lvt3(131),lhe(33),lhf(33)
        data iv1/179/,iv2/180/,iv3/131/,itot/490/,inmax/33/,
       *tmelt/1133./,solidk/0.5e+03/
        data ivs1/5955,5934,5913,5892,5871,5850,5829,5808,5787,5766,
       *5745,
       *5724,5703,5682,5661,5640,5623,5606,5589,5572,5555,5538,5521,
       *5504,5487,5470,5453,5436,5423,5408,5393,5378,5363,5348,5333,
       *5956,5935,5914,5893,5872,5851,5830,5809,5788,5767,5746,5725,
       *5704,5683,5662,5641,5624,5607,5590,5573,5556,5539,5522,5505,
       *5488,5471,5454,5439,5424,5409,5394,5379,5364,5349,5334,5957,
       *5936,5915,5894,5873,5852,5831,5810,5789,5768,5747,5726,5705,
       *5684,5663,5642,5625,5608,5591,5574,5557,5540,5523,5506,5489,
       *5472,5455,5440,5425,5410,5395,5380,5365,5350,5335,5958,5937,
       *5916,5895,5874,5853,5832,5811,5790,5769,5748,5727,5706,5685,
       *5664,5643,5626,5609,5592,5575,5558,5541,5524,5507,5490,5473,
       *5456,5441,5426,5411,5396,5381,5366,5351,5336,5959,5938,5917,
       *5896,5875,5854,5833,5812,5791,5770,5749,5728,5707,5686,5665,
       *5644,5627,5610,5593,5576,5559,5542,5525,5508,5491,5474,5457,
       *5442,5427,5412,5397,5382,5367,5352,5337,5960,5939,5918,5897/
        data ivs2/
       *5876,5855,5834,5813,5792,5771,5750,5729,5708,5687,5666,5645,
       *5628,5611,5594,5577,5560,5543,5526,5509,5492,5475,5458,5443,
       *5428,5413,5398,5383,5368,5353,5338,5961,5940,5919,5898,5877,
       *5856,5835,5814,5793,5772,5751,5730,5709,5688,5667,5646,5629,
       *5612,5595,5578,5561,5544,5527,5510,5493,5476,5459,5444,5429,
       *5414,5399,5384,5369,5354,5339,5962,5941,5920,5899,5878,5857,
       *5836,5815,5794,5773,5752,5731,5710,5689,5668,5647,5630,5613,
       *5596,5579,5562,5545,5528,5511,5494,5477,5460,5445,5430,5415,
       *5400,5385,5370,5355,5340,5963,5942,5921,5900,5879,5858,5837,
       *5816,5795,5774,5753,5732,5711,5690,5669,5648,5631,5614,5597,
       *5580,5563,5546,5529,5512,5495,5478,5461,5446,5431,5416,5401,
       *5386,5371,5356,5341,5964,5943,5922,5901,5880,5859,5838,5817,
       *5796,5775,5754,5733,5712,5691,5670,5649,5632,5615,5598,5581,
       *5564,5547,5530,5513,5496,5479,5462,5447,5432,5417,5402,5387,
       *5372,5357,5342,5965,5944,5923,5902,5881,5860,5839,5818,5797/
        data ivs3/
       *5776,5755,5734,5713,5692,5671,5650,5633,5616,5599,5582,5565,
       *5548,5531,5514,5497,5480,5463,5446,5433,5418,5403,5388,5373,
       *5358,5343,3746,2148, 550,3760,2162, 564,3774,2176, 578,3788,
```

Fig. A3. Listing of base-case HEATING user supplied subroutines (continued).

```
*2190, 592,3802,2204, 606,3816,2218, 620,3830,2232, 634,3844,
*2246, 648,3858,2260, 662,3874,2276, 678,3890,2292, 694,3906,
*2308, 710,3922,2324, 726,3938,2340, 742,3954,2356, 758,3970,
*2372, 774,3986,2388, 790,4002,2404, 806,4018,2420, 822,4034,
*2436, 838,4054,2456, 858,4074,2476, 878,4094,2496, 898,4114,
*2516, 918,4134,2536, 938,4154,2556, 958,4174,2576, 978,4194,
*2596, 998,4214,2616,1018,4234,2636,1038,4254,2656,1058,4274,
*2676,1078,4294,2696,1098,4314,2716,1118,4334,2736,1138/
data ivl1/4323,4303,4283,4263,4243,4223,4203,4183,4163,4143,
*4123,4103,4083,4063,4043,4023,4007,3991,3975,3959,3943,3927,
*3911,3895,3879,3863,3847,3833,3819,3805,3791,3777,3763,3749,
*3735,4324,4304,4284,4264,4244,4224,4204,4184,4164,4144,4124,
*4104,4084,4064,4044,4024,4008,3992,3976,3960,3944,3928,3912,
*3896,3880,3864,3848,3834,3820,3806,3792,3778,3764,3750,3736,
*4325,4305,4285,4265,4245,4225,4205,4185,4165,4145,4125,4105,
*4085,4065,4045,4025,4009,3993,3977,3961,3945,3929,3913,3897,
*3881,3865,3849,3835,3821,3807,3793,3779,3765,3751,3737,4326,
*4306,4286,4266,4246,4226,4206,4186,4166,4146,4126,4106,4086,
*4066,4046,4026,4010,3994,3978,3962,3946,3930,3914,3898,3882,
*3866,3850,3836,3822,3808,3794,3780,3766,3752,3738,4327,4307,
*4287,4267,4247,4227,4207,4187,4167,4147,4127,4107,4087,4067,
*4047,4027,4011,3995,3979,3963,3947,3931,3915,3899,3883,3867,
*3851,3837,3823,3809,3795,3781,3767,3753,3739,4328,4308,4288,
*4268/
data ivl2/
*4248,4228,4208,4188,4168,4148,4128,4108,4088,4068,4048,
*4028,4012,3996,3980,3964,3948,3932,3916,3900,3884,3868,3852,
*3838,3824,3810,3796,3782,3768,3754,3740,4329,4309,4289,4269,
*4249,4229,4209,4189,4169,4149,4129,4109,4089,4069,4049,4029,
*4013,3997,3981,3965,3949,3933,3917,3901,3885,3869,3853,3839,
*3825,3811,3797,3783,3769,3755,3741,4330,4310,4290,4270,4250,
*4230,4210,4190,4170,4150,4130,4110,4090,4070,4050,4030,4014,
*3998,3982,3966,3950,3934,3918,3902,3886,3870,3854,3840,3826,
*3812,3798,3784,3770,3756,3742,4331,4311,4291,4271,4251,4231,
*4211,4191,4171,4151,4131,4111,4091,4071,4051,4031,4015,3999,
*3983,3967,3951,3935,3919,3903,3887,3871,3855,3841,3827,3813,
*3799,3785,3771,3757,3743,4332,4312,4292,4272,4252,4232,4212,
*4192,4172,4152,4132,4112,4092,4072,4052,4032,4016,4000,3984,
*3968,3952,3936,3920,3904,3888,3872,3856,3842,3828,3814,3800,
*3786,3772,3758,3744,4333,4313,4293,4253,4233,4213,4193.

*4173/
data ivl3/
*4153,4133,4113,4093,4073,4053,4033,4017,4001,3985,3969,
*3953,3937,3921,3905,3889,3873,3857,3843,3829,3815,3801,3787,
*3773,3759,3745,3745,2147, 549,3759,2161, 563,3773,2175, 577,
*3787,2189, 591,3801,2203, 605,3815,2217, 619,3829,2231, 633,
*3843,2245, 647,3857,2259, 661,3873,2275, 677,3889,2291, 693,
*3905,2307, 709,3921,2323, 725,3937,2339, 741,3953,2355, 757,
*3969,2371, 773,3985,2387, 789,4001,2403, 805,4017,2419, 821,
*4033,2435, 837,4053,2455, 857,4073,2475, 877,4093,2495, 897,
*4113,2515, 917,4133,2535, 937,4153,2555, 957,4173,2575, 977,
*4193,2595, 997,4213,2615,1017,4233,2635,1037,4253,2655,1057,
*4273,2675,1077,4293,2695,1097,4313,2715,1117,4333,2735,1137/
data ihs/ 3720,2122, 524,3721,2123, 525,3722,2124, 526,3723,
*2125, 527,3724,2126, 528,3725,2127, 529,3726,2128, 530,3727,
*2129, 531,3728,2130, 532,3729,2131, 533,3730,2132, 534/
data ihl/ 3735,2137, 539,3736,2138, 540,3737,2139, 541,3738,
*2140, 542,3739,2141, 543,3740,2142, 544,3741,2143, 545,3742,
*2144, 546,3743,2145, 547,3744,2146, 548,3745,2147, 549/
end
```

Fig. A3. Listing of base-case HEATING user supplied subroutines (continued).

INTERNAL DISTRIBUTION

1.	A. M. Ammons	18.	S. H. Park
2.	R. L. Beatty	19.	A. S. Quist
3.	E. L. Bird	20.	R. C. Riepe
4.	K. W. Childs	21-22.	C. H. Shappert
5.	J. S. Crowell	23-27.	M. J. Taylor
6.	G. E. Giles	28.	J. J. Tomlinson
7.	J. R. Kirkpatrick	29.	M. W. Wendel
8.	T. G. Kollie	30.	G. E. Whitesides/R. P. Leinius/
9.	D. J. Lott		Applied Technology Library
10-13.	G. Mackiewicz-Ludtka	31.	P. T. Williams
14.	G. M. Ludtka	32.	Applied Technology Library
15.	W. G. Northcutt, Jr.	33.	Central Research Library
16.	M. Olszewski	34.	Laboratory Records
17.	J. E. Park	35.	K-25 Site Records (RC)

EXTERNAL DISTRIBUTION

36-47. Office of Scientific and Technical Information, P.O. Box 62, Oak Ridge, TN 37831.

131

DATE
FILMED

2 /22/ 93